WIND-DRIVEN DESERTIFICATION:

PROCESS MODELING, REMOTE MONITORING, AND FORECASTING

Thesis By

Gregory S. Okin

In Partial Fulfillment of the Requirements

for the Degree of

Doctor of Philosophy

California Institute of Technology

Pasadena, California

2001

(Submitted October 13, 2000)

ABSTRACT

Arid and semiarid landscapes comprise nearly a third of the Earth's total land surface. These areas are coming under increasing land use pressures. Despite their low productivity these lands are not barren. Rather, they consist of fragile ecosystems vulnerable to anthropogenic disturbance.

The purpose of this thesis is threefold: (I) to develop and test a process model of wind-driven desertification, (II) to evaluate next-generation process-relevant remote monitoring strategies for use in arid and semiarid regions, and (III) to identify elements for effective management of the world's drylands.

In developing the process model of wind-driven desertification in arid and semiarid lands, field, remote sensing, and modeling observations from a degraded Mojave Desert shrubland are used. This model focuses on aeolian removal and transport of dust, sand, and litter as the primary mechanisms of degradation: killing plants by burial and abrasion, interrupting natural processes of nutrient accumulation, and allowing the loss of soil resources by abiotic transport. This model is tested in field sampling experiments at two sites and is extended by Fourier Transform and geostatistical analysis of high-resolution imagery from one site.

Next, the use of hyperspectral remote sensing data is evaluated as a substantive input to dryland remote monitoring strategies. In particular, the efficacy of spectral mixture analysis (SMA) in discriminating vegetation and soil types and determining vegetation cover is investigated. The results indicate that hyperspectral data may be less useful than often thought in determining vegetation parameters. Its usefulness in

determining soil parameters, however, may be leveraged by developing simple multispectral classification tools that can be used to monitor desertification.

Finally, the elements required for effective monitoring and management of arid and semiarid lands are discussed. Several large-scale multi-site field experiments are proposed to clarify the role of wind as a landscape and degradation process in drylands. The role of remote sensing in monitoring the world's drylands is discussed in terms of optimal remote sensing platform characteristics and surface phenomena which may be monitored in order to identify areas at risk of desertification. A desertification indicator is proposed that unifies consideration of environmental and human variables.

ACKNOWLEDGMENTS

First, I'd like to acknowledge Bruce Murray for advising this thesis and mentoring me throughout my five years at Caltech. Were it not for his interest in this problem as well as the broader drivers and impacts of desertification, this thesis definitely would not have been what it is.

Throughout my time at Caltech, I've had several very positive interactions with other scientists interested in biogeochemistry and Earth systems science. In particular, my personal and professional interactions with Bill Schlesinger have been extremely rewarding. I look forward to an ongoing relationship. Many thanks also to George Rossman for advising one of my propositions and being willing to discuss environmental, scientific, and administrative issues at the drop of a hat. Many thanks also to Joe Kirschvink for taking me to Morocco and South Africa and providing the opportunity to dramatically change my perspective on the cost of land degradation. The members of the Caltech faculty for whom I had the pleasure of TAing have also dramatically impacted my impressions of teaching in the Earth sciences: Bruce Murray, Gerry Wasserburg, George Rossman, Bill Schlesinger, Andy Andreae, and John Eiler. Jim Morgan and Mike Hoffman in Environmental Engineering have also provided advise, insight, and resources for which I am grateful.

Funding for this thesis project was provided by a series of grants from NASA and JPL. Many thanks to Diane Wickland and Tony Janetos for providing the resources to

allow it to proceed. Many thanks also to Dave Curkendall and Ron Blom for helping me obtain continuing, if stop-gap, funds. Much work was also completed with help from the Caltech President's Fund, and I thank Vince McCoy and Terry Cole for advocating and sponsoring the joint Caltech/UCSB/JPL supercomputing project as well as Dave Curkendall and Dar Roberts for their interest and support. Of course, many thanks also to the AVIRIS folks at JPL. Without the support of Rob Green, especially, I would never have been able to proceed with hyperspectral analysis. To Jessica Faust, Betina Pavri, Chris Chovitt, and Orlesa Williams I extend hearty thanks.

Dave Curkendall and the JPL supercomputing group were great to work with on the President's Fund work. Thanks to Herb Siegel, Jim Collier, and Craig Miller. On this and other projects, many thanks to Dar Roberts and Tom Painter for providing tools as well as insight. Also at JPL, Ron Blom, Dianne Newman, and Nevin Bryant, JoBea Way have provided much needed information as well as guidance.

Thanks to reviewers of my manuscripts, including the anonymous reviewers. In particular, I would like to thank Norm Meek, Dale Gillette, Oliver Chadwick, Greg Asner, Nick Lancaster, and Stuart Phinn.

In helping with the work I did at Jornada, I would like to thank first Dale Gillette for providing scientific as well as practical insights, a really interesting problem, and a continuing personal and scientific relationship. Other folks at the Jornada experimental range including John Anderson, Barbara Nolen, and Curtis Monger have greatly aided in my work there.

Also helping in very practical ways were the many Caltech undergrads that helped throughout my time at Caltech: Mike Tice, Sam Bauknight, Christie Edwards, Matt

Bachmann, and Jacob Lacouture.

How to thank the many people in the Division who have helped in very substantial ways? Jim O'Donnell is the greatest librarian in the world as far as I am concerned. He and Susan Leising have helped me find the most obscure things I could think of without raising an eyebrow. My work here would have been a hundred times harder if not for their excellent contributions. The staff in the planetary science office have proved helpful on inumerable occasions. They have also proven to be wonderful to sit and shoot the breeze with. Thanks to Kay Campbell, Irma Black, Tammie Henderson, Susan Powell, Joyce Campbell, and Vilia Zmuidzinas. The members of the Division staff have also been tremendously kind and helpful. I would especially like to acknowledge Jean Grinols, Carolyn Porter, and Donna Sackett.

Last but definitely not least, many thanks to my friends and family. To Mom for her interest, Dad for his interest and support. To BJ for, well, everything a brother could possibly ask for, way too numerous to mention. To Tom and Harold for their love and continuing support. Jim, Annmarie, and Kathy for their friendship. To my friends in the Division: Ro, Nathan, Ronit, Emily, Magali, Julia, Sarah, Sujoy and others. Finally, especially to Patrick and Danny as well as the members of the Ojai Valley Dharma center for their wisdom, generosity, genuine hearts, community, and love.

May whatever merit derived from this thesis contribute to the welfare of all beings until all have attained enlightenment.

TABLE OF CONTENTS

CHAPTER 2: DEGRADATION OF SANDY ARID SHRUBLAND ENVIRONMENTS: OBSERVATIONS, PROCESS MODELING, AND MANAGEMENT IMPLICATIONS

CHAPTER 3: DESERTIFICATION IN AN ARID SHRUBLAND IN THE OUTHWESTERN UNITED STATES: PROCESS MODELING AND VALIDATION

CHAPTER 6: THE ROLE OF OPTICAL REMOTE SENSING IN DRYLAND MONITORING

APPENDIX D: DUST EMISSION AND NUTRIENT LOSSES FROM SEMIARID GRASSLANDS: RELATION TO CLIMATE CHANGE AND DESERTIFICATION

TABLE OF FIGURES

TABLE OF TABLES

CHAPTER 1

INTRODUCTION

Arid and semiarid landscapes exist on every continent of the world, and comprise nearly a third of the total land surface of the globe. These areas are coming under increasing land use pressures ranging from agribusiness and suburbanization to subsistence farming and pastoralism. Despite their low productivity these lands are not barren. Rather, they consist of fragile ecosystems vulnerable to anthropogenic disturbance.

Desertification, defined by the 1994 United Nations (UN) Convention to Combat Desertification (CCD) as the "degradation of land in arid, semi-arid, and dry sub-humid areas caused primarily by human activities and climatic variations," is a global phenomenon. According to the CCD, "over 250 million people are directly affected by desertification. In addition, some one thousand million (or one billion) people in over one hundred countries are at risk. These people include many of the world's poorest, most marginalized, and politically weak citizens" (see http://www.unccd.int for more information). The CCD provides for scientific and technical exchange to combat desertification and to promote sustainable land use in arid and semiarid environments. The gravity of the desertification problem is supported by a vast and growing literature in which the problems of arid and semiarid land degradation are reported. Desertification and related problems have been reported in the scientific literature in, at least, the United

States, Mexico, Brazil, Argentina, Spain, Greece, Morocco, Egypt, the Sudan, Ethiopia, Mali, Kenya, Tanzania, Namibia, Botswana, South Africa, Israel, Jordan, Saudi Arabia, Qatar, Kuwait, Iraq, India, China, Tibet, and Australia.

No matter where it manifests, desertification around the world has may be defined in a more specific and informative manner than that used by the UN above. For the purposes of this thesis, desertification will be defined as the "temporally continuous reduction or spatial redistribution of net primary productivity in arid and semiarid environments." This definition is derived from the discussion by Schlesinger *et al.* (1990) of the biological and biogeochemical feedbacks in global desertification.

THE POTENTIAL COST OF INACTION

Most of the countries in which desertification is a problem are developing nations. Unlike richer countries where the productivity losses in one area can be offset by productivity gains in another, the developing nations cannot afford to waste land. In these countries, and in broad regions where desertification is a problem (Africa, the Middle East, Northern China, the Indian Subcontinent), loss of productivity through land degradation is grave indeed (Pinstrup-Andersen and Pandya-Lorch, 1998), and can be exacerbated by widespread poverty and population growth (Barbier, 1997; Bongaarts, 1996; Grepperud, 1996; Lado, 1999).

Sustainable agricultural development is necessary to feed populations and to promote economic stability in developing nations (Lanz, 1996; Pinstrup-Andersen and Pandya-Lorch, 1998). Without the stability engendered by reliable agricultural output,

developing nations cannot develop the industries or infrastructure required to partake in the global economy and create prosperity for its citizens. Likewise, if a nation is forced to devote human and financial resources to combat past land degradation, less is available to invest in sustainable agriculture, infrastructure, governmental institutions, industry, and the education of its populace. A negative feedback therefore exists in which nations experiencing widespread declining productivity due to land degradation have fewer resources to commit to economic growth (Homer-Dixon, 1999). Declining economic productivity, in turn, prohibits adequate development of sustainable agricultural and economic growth. Lack of environmental reliability makes a developing nation or a region unattractive to international capital and such a region thereby misses further opportunities for economic growth (Biswas, 1998; Zhang and Markusen, 1997).

Nations with a large proportion of their territory in arid and semiarid regions are vulnerable to a wide range of threats to the health and security of their populations. Health threats such as malnourishment, famine, and disease can exist during environmental failure or drought exacerbated by inadequate infrastructure and appropriate agriculture. This pattern is abundantly clear in recurring famines and associated disease epidemics in the Horn of Africa (Broad and Agrawala, 2000). Local and regional security are likewise threatened as populations expand out of degraded lands and cross traditional tribal, ethnic, or political boundaries (Babu and Hassan, 1995; Gleditsch, 1998; Hauge and Ellingsen, 1998; Homer-Dixon, 1999; Lanz, 1996; Westing, 1994).

In his book, *Environment, Scarcity, and Conflict*, Thomas F. Homer-Dixon argues that scarcity of environmental resources, due in part to land degradation, also

"often acts as a deep underlying stressor of social systems" (p. 81, Homer-Dixon, 1999). In particular, Homer-Dixon arguments that environmental scarcity can weaken the institution of the state, and "as the state weakens, the social balance of power can shift in favor of groups challenging state authority" (p. 103, Homer-Dixon, 1999).

In turn, the international community often pays a price for regional conflicts, drought, and land degradation in the form of deployment of peacekeeping troops, famine relief, or food aid. Conflicts caused by weakened state institutions and exacerbated by environmental scarcity are particularly concerning:

> Conflicts generated partly by environmental scarcity, although perhaps not as conspicuous or dramatic as interstate wars, can nonetheless have serious indirect effects on the international community. The changing nature of the international system—heightened economic interdependence, easier long-distance travel, and increased access to arms—makes previously insignificant regions of interest to policymakers. Crises in small countries, such as Haiti, often create serious foreign policy difficulties for developed countries, and large and significant countries—including Pakistan, China, India, and Indonesia—are not immune to these severe stresses that environmental scarcity generates. Major civil violence within states can affect external trade relations, cause refugee flows, and produce humanitarian disasters that call upon the military and financial resources of developed countries and international organizations (p. 180, Homer-Dixon, 1999).

Thus, land degradation in particular and environmental scarcity in general are therefore

global problems that affect citizens from all nations. The large area and the growing number of people affected by land degradation in already-marginal arid and semiarid areas strongly suggests that the drivers and effects of desertification cannot be ignored.

Significant nations such as China and India, each with large proportions in arid and semiarid regions, should give us pause. Each year, the population of these nations grow and to meet increasing food demands, these nations must cultivate new lands. Since most of the best arable lands are already under cultivation, or have been incorporated into urban areas near the coast, this agricultural expansion tends to invade increasingly marginal lands in arid and semiarid regions. This inevitably leads to land degradation (see a recent article in the New York Times available at: www.nytimes.com/library/world/asia/073000china-farmers.html) and a further need for agricultural expansion onto lands unsuitable for this purpose. As these nations' food requirements increase and their ability to grow food decreases, there is a high probability that their food and land shortages will have dramatic effects on the global stage.

Closer to home, the Dust Bowl in the 1930's affected large areas of the semiarid Great Plains. Most Americans are familiar with footage and anecdotes from this period including failed crops, tremendous wind erosion, and food shortages. This environmental disaster worsened prospects for American farmers during the Great Depression, forcing many of them to abandon their lands. As a result, millions of Americans were forced to migrate with few or no possessions to states such as California. The Dust Bowl was a desertification event induced both by climate and unsound agricultural practices that presented an enormous political and economic strain on this country. There is no reason that this event could not be repeated in the United States or elsewhere in the near future.

The developed nations, with resources to commit to research, development, and environmental monitoring technologies have a vital role to play in enabling sustainable environmental growth worldwide. Basic and applied scientific research can help stem desertification (Thomas, 1997) but science alone will not be able to succeed in this goal. Indeed, no single individual or organization will be able to independently pursue every avenue to combating desertification. Instead, a network of academic researchers, regional planners, corporations, non-governmental organizations, local to national government, and individual land users must work together to remediate and where possible, avoid land degradation before irreversible damage has occurred.

Any modern program aimed at understanding and eventually limiting desertification must take several interconnected elements into account:

(1) Process Modeling,

(2) Field Observation,

(3) Remote Observation and Monitoring,

(4) Management and Planning, and

(5) Implementation.

Process modeling and field observation are clearly scientific endeavors. Remote observation and monitoring must be informed by field-tested process models in order to guide these observations and to put them in their proper context. Land management and planning and land-use implementation are not traditional scientific roles, but need to be informed by process models and field or remote observations in order to determine the areas at greatest risk of degradation, best strategies for remediation, and the effectiveness of anti-desertification measures. Thus, scientific process modeling provides information

from which the principal metrics of land degradation and recovery can be derived.

ORGANIZATION OF THE THESIS

This thesis is in three parts reflecting its threefold purpose: (I) to develop and test a process model of wind-driven desertification, (II) to evaluate next-generation process-relevant remote monitoring strategies for use in arid and semiarid regions, and (III) to identify further requirements for effective management for the worlds drylands.

Part I of the thesis, in which the processes of desertification are considered, is in three chapters. Chapter 2 is dedicated to the development and extrapolation of a new process model for wind-driven anthropogenic desertification in arid shrublands and provides the integral concepts for the rest of the thesis. Chapter 3 tests this model using soil chemical analyses. Chapter 4 examines the role of wind in landscape development in arid and semiarid regions using high spatial-resolution aerial photography. Chapters 2 and 3 are in press (*Journal of Arid Environments* and *Land Degradation*, a peer-reviewed book of papers from the 1999 COMLAND conference on land degradation, respectively). Chapter 4 has been accepted for publication in the *Journal of Geophysical Research-Atmospheres*.

Part II, in which remote sensing tools for dryland monitoring are evaluated, is in two chapters. Chapter 5 is dedicated to establishing practical limits on the retrieval of vegetation information from hyperspectral remote sensing data in arid and semiarid environments. The potential utility of hyperspectral remote sensing in enhancing multispectral (Landsat-class) remote sensing is also discussed. Chapter 5 is in press in

Remote Sensing of Environment. In Chapter 6, the prospects for and challenges of using remote sensing in effective dryland monitoring are discussed.

Part III of this thesis is in one chapter. Chapter 7 clearly identifies obstacles on the road to sustainable land use in arid and semiarid areas and outlines approaches to overcoming them. In particular, future work on wind-driven desertification process

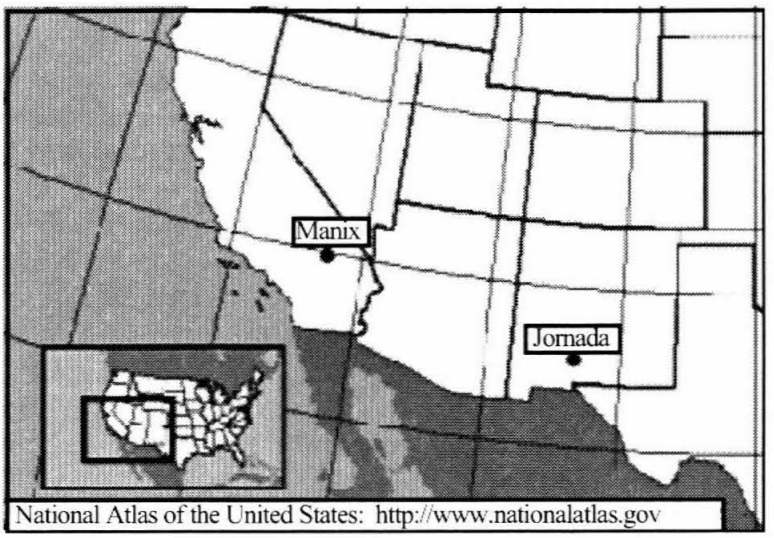

Figure 1-1. Map showing the location of the Manix and Jornada Basins.

modeling, remote monitoring of desertification, and desertification forecasting are outlined.

HISTORY AND FEATURES OF PRINCIPAL STUDY SITES

Two study sites are discussed in detail in this thesis: the Manix Basin of Southeastern California and the Jornada del Muerto Basin in south-central New Mexico (Figure 1-1). The history and features of these sites are provided here in order to avoid

redundant expostulation in subsequent chapters.

The Manix Basin, San Bernardino County, California

The Manix Basin is in the Mojave Desert, about 25 miles ENE of Barstow in southeastern California (centered around 34°56.5' N 116°41.5' W at an elevation of about 540 m). The basin has an area of 40,700 ha and was the site of ancient Lake Manix which existed during the peak pluvial episode of the last glaciation and drained through Afton Canyon to the east (Meek, 1989; Smith and Street-Perrott, 1983). Much of the basin is filled with lacustrine, fluvial, and deltaic sediments capped by weak armoring (Meek, 1990). There is clear evidence of pre-modern wind erosion, indicating that wind erosion, transport, and deposition have long been important geological processes in the area (Evans, 1962).

The modern climate of the Manix Basin is arid with the average annual precipitation of 10 cm falling mostly in the winter, although there can be significant summer precipitation in some years (Table 1) (National Climate Data Center, 1997). The average annual temperature is 19.6°C, the average winter temperature is 9.1°C, and the average summer temperature is 31.4°C (Meek, 1990). The average wind speed at the airport in Daggett is 5.5 m/s at a height of 6.1 m and is typically out of the west (National Climate Data Center, 1993).

The vegetation in undisturbed areas of the basin is dominated by an association of *Larrea tridentata* (creosotebush) and *Ambrosia dumosa* (burro brush) with minor occurrence of *Atriplex polycarpa* (saltbush), *Atriplex hymenelytra* (desert holly), *Atriplex canescens* (four-winged saltbush), *Ephedra californica* (Mormon tea), and *Opuntia spp.*

(cactus family). *Prosopis glandulosa* (mesquite) occurs in some areas of the basin. Areas that have been disturbed directly by human activity are dominated by *A. polycarpa* with total cover often greater than that in undisturbed desert. *Schismus*, an exotic annual grass, is ubiquitous, but grass cover varies significantly with yearly precipitation.

There has been extensive human activity in the Manix Basin with several phases of agricultural activity utilizing groundwater recharged by the Mojave River, which carries runoff from the San Bernardino Mountains to the south-southwest (Tugel and Woodruff, 1978). The basin was used for dryland farming in the 1800s (Tugel and Woodruff, 1978). Limited irrigated farming started in the basin in 1902 with the acreage of irrigated land increasing sharply after World War II (Tugel and Woodruff, 1978). Today alfalfa hay is the major agricultural product. In the Coyote Dry Lake sub-basin, square flood-irrigated fields and abandoned flood irrigation equipment are seen in early Landsat images. After the mid-1970s, central-pivot agriculture became the dominant form of land use in the area, but many fields have now been abandoned throughout the northern part of the basin due to increasing costs of pumping groundwater to the surface for agriculture (Ray, 1995).

The Jornada Del Muerto Basin, Doña Ana County, New Mexico

The Jornada del Muerto basin lies approximately 30 km northeast of Las Cruces, NM, in the Chihuahuan Desert ecosystem. It is bounded by the San Andres Mountains on the east and by the Rio Grande Valley and the Fra Cristobal-Caballo Mountain complex on the west. Elevation above sea level varies from 1180 to 1360 m. The Jornada Plain consists of unconsolidated Pleistocene detritus. This alluvial fill from the nearby

mountains is 100 m thick in places and the aggradation process is still active. Coarser materials are found near foothills along the eastern part of the study area. The topography of the study area consists of gently rolling to nearly level uplands, interspersed with swales and old lake beds (Buffington and Herbel, 1965).

The climate of the area is characterized by cold winters and hot summers and displays a bimodal precipitation distribution. Winter precipitation usually occurs as low-intensity rains or occasionally as snow and contributes to the greening of shrub species in the basin in the early spring. Summer monsoonal precipitation, usually in the form of patchy, but intense, afternoon thunderstorms, is responsible for the late-summer greening of grasses. The average annual precipitation between 1915 and 1962 in the basin was 230 mm, with 52% falling between July 1 and September 30 (Paulsen and Ares, 1962). The average maximum temperature is highest in June, when it averages 36°C, and lowest in January, when it averages 13°C (Buffington and Herbel, 1965).

The principal grass species in the study area are *Scleropogon brevifolius* (burrograss), several species of *Aristida*, and *Hilaria mutica* (tobosa grass) while major shrubs are *Larrea tridentata Prosopis glandulosa*, *Florensia cernua*. Soils in the basin are quite complex but generally range from clay loams to loamy fine sands, with some areas being sandy or gravelly (Soil Conservation Service, 1980).

The Jornada Basin is an area of intense research as part of the Jornada Long Term Ecological Research (LTER) program of the National Science Foundation. The primary reason for the broad scientific interest in the Jornada Basin is because it is the premier site in which widespread conversion of grassland communities to shrublands over the past 100 years (Buffington & Herbel 1965; Bahre 1991) has been studied. Grazing and

other anthropogenic disturbances are commonly invoked to explain this trend (Bahre and Shelton 1993). Extensive work on soil structure and plant community composition at the Jornada LTER site and the adjacent New Mexico State University (NMSU) Ranch strongly supports this hypothesis (Schlesinger *et al.* 1990).

PART I

PROCESS MODELING

Process modeling forms the basis of any attempt to understand desertification or to enhance sustainable land use in arid and semiarid environments. Process models identify and integrate basic insights into landscape function and structure. In Part I, the role of wind as a desertification process is considered. Chapter 2 is dedicated to the development and extrapolation of a new process model for wind-driven anthropogenic desertification in arid shrublands and provides the integral concepts for the rest of the thesis. Chapter 3 tests this model using soil chemical analyses. Chapter 4 examines the role of wind in landscape development in arid and semiarid regions using high spatial-resolution aerial photography.

CHAPTER 2

DEGRADATION OF SANDY ARID SHRUBLAND ENVIRONMENTS: OBSERVATIONS, PROCESS MODELING, AND MANAGEMENT IMPLICATIONS

(*This chapter is in press in Journal of Arid Environments.*)

1. INTRODUCTION

The Manix Basin in the Mojave Desert of southeastern California is the site of ancient Lake Manix (Buwalda, 1914; Dohrenwend *et al.*, 1991; Meek, 1989, 1990). Far from being a unique geological setting, the fine-grained lacustrine sediments in the Basin are part of the Pleistocene legacy shared by depressions throughout the entire Basin and Range and Mojave provinces (Smith and Street-Perrott, 1983). Morrison (1991a; 1991b) has reported that "nearly all closed or formerly closed basins in the Great Basin have ancient strandlines marked by lacustrine bars, spits, embankments, terraces, deltas, and wave-cut cliffs at elevations well above the playas or permanent lakes of today." The lacustrine sediments of Pleistocene age that form the floors of these basins share qualities that make them amenable for agriculture and other human activities: very low slopes, little or no relief, subsurface water resources, and fine-grained sediments suitable for farming or other activities. The intersection of the human uses of Pleistocene paleolakes

with their geological history creates opportunities for land degradation much greater than typically recognized.

Wind erosion in the Mojave Desert is the principal mechanism of land degradation. Agriculture, urban development, military maneuvers, pipeline, road and powerline construction and recreational vehicles all destroy vegetation cover and expose the soil to wind erosion (Sharifi *et al.*, 1999). These activities can result in increased dust emissions, blowing sand, and damage of native vegetation.

Although the processes of arid land degradation have been well established elsewhere in the Southwestern U.S. (see for example, Schlesinger *et al.*, 1990), no published process model exists for shrubland degradation in Mojave Desert or other shrublands. In this chapter, I report on the importance of human-induced wind erosion in initiating and propagating land degradation in the Manix Basin of the Mojave Desert. Based on these observations, I develop a new model of wind-driven desertification in sandy arid shrublands.

Arid land degradation has received significant attention in the technical and popular media over the past several decades. Much of this interest has been practical in nature because: (1) desertification is widespread throughout the southwestern United States and globally (Dregne, 1995; Khalaf and Al-Ajmi, 1993; Mabbutt and Floret, 1980; Verstraete and Schwartz, 1991; Walker, 1982; Warren and Hutchinson, 1984); (2) it has severe financial and societal consequences including property damage, increased health and safety hazards, and decreased agricultural productivity (Bach, 1998; Bowden *et al.*, 1974; Clements *et al.*, 1963; Fryrear, 1981; Hyers and Marcus, 1981; Leathers, 1981; Leys and McTainsh, 1994); and (3) some forms of desertification are irremediable on

human timescales at reasonable cost (Dregne, 1995; Whitford, 1992). The increasing use of desert shrublands by humans for habitation, agriculture, industry, and recreation increases the amount of arid land directly impacted (Verstraete and Schwartz, 1991). Thus it is important to understand the processes of arid land degradation in these environments. Improved process understanding will allow improved identification of areas at heightened risk of desertification before serious damage has occurred.

2. METHODS

In this study a series of Landsat Multispectral Scanner (MSS) and Airborne Visible Infrared Imaging Spectrometer (AVIRIS) images from the Manix Basin from 1979, 1982, 1985, 1988, 1997, and 1998 were used in order to identify areas of blowing sand associated with central-pivot agriculture in the Basin. AVIRIS images taken from a NASA ER-2 aircraft flying at 20-km altitude measure the total upwelling spectral radiance in 224 bands from 400 to 2500 nm in 20-m ground pixels. Landsat MSS measures upwelling radiation in four visible-near infrared broad multispectral bands in 80-m ground pixels. Geographical information about the extent and locations of blowing sand were the object of the remote sensing analysis. Simple spatial information is readily available from uncalibrated remote sensing images. Therefore, no attempt was made to calibrate the images or correct for atmospheric scattering. The images were incorporated into a geographical information system.

A series of field trips between 1996 and 1999 were taken to the Manix Basin in order to verify remote-based observations of sand blow-outs. In 1998 and 1999,

perennial vegetation cover was estimated at several sites in the Manix Basin by measuring individual plant diameters in circular plots with 5-m radii (12 replicates each) and assuming full, circular shrub canopies.

Finally, a quantitative assessment of observed wind erosion and deposition rates was undertaken in order to link observed phenomena with physical and mathematical wind erosion models.

3. RESULTS AND DISCUSSION

3.1 Remote Observations from the Manix Basin

The Landsat MSS and AVIRIS images clearly indicates the growth of sand blow-outs downwind of abandoned agricultural fields in the Manix Basin (Figure 2-1). Deposition of sand downwind of the fields is a progressive process, with sand plumes lengthening in each successive image. No regrowth of perennial vegetation was observed in these sand plumes. Thus, the occasional darkening of the sand blow-outs is inferred to be due to annual vegetation related to winter rainfall. Annual cover can be relatively high in wet years, but seldom lasts through the spring and summer months.

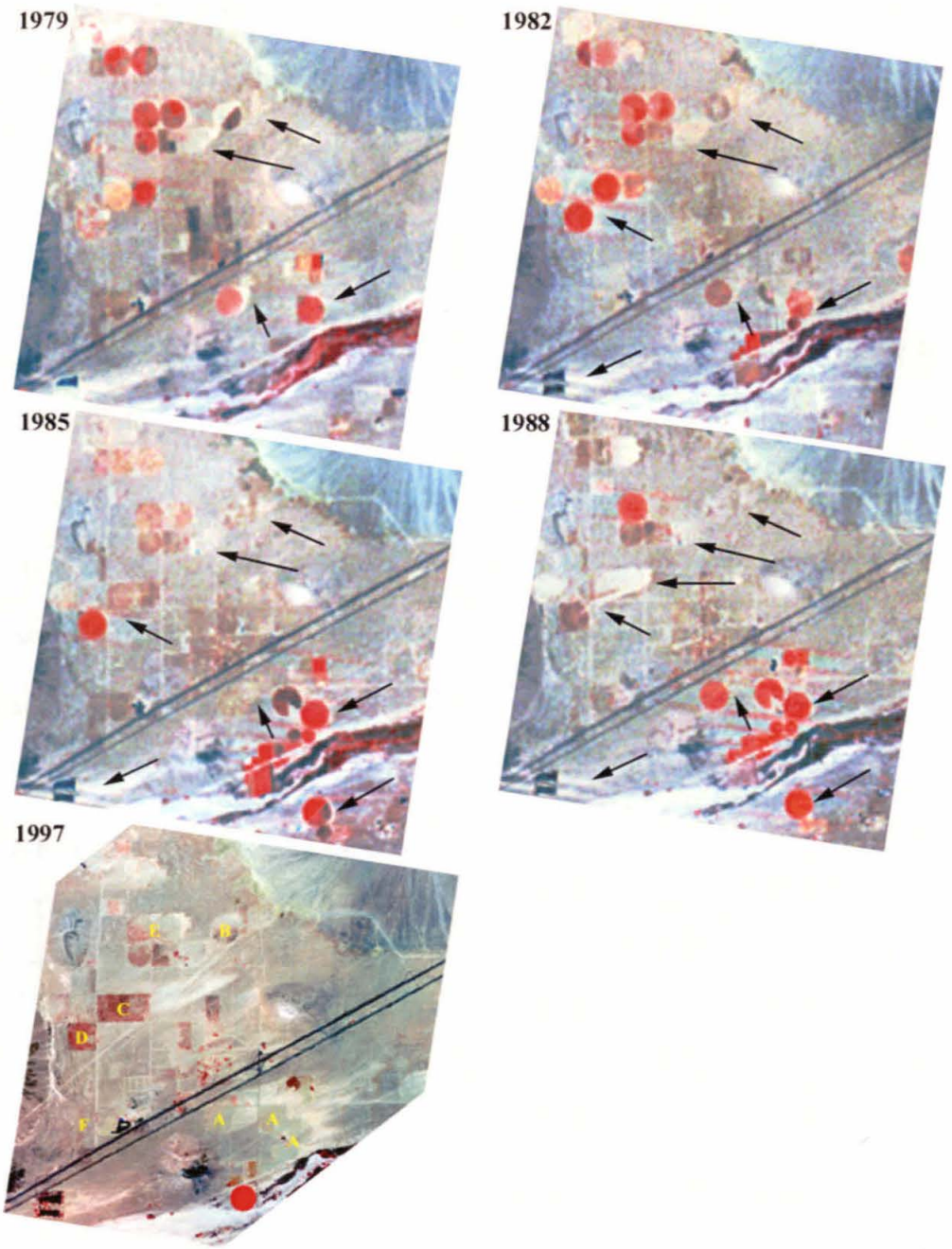

Figure 2-1. 1979-1988: Landsat Multispectral Scanner (MSS) images of the Manix Basin. Red is MSS band 4 (800-1100 nm), green is MSS band 2 (600-700 nm), and blue is MSS band 1 (500-600 nm). Interstate 15 goes diagonally through the center of the images. North is up and active fields appear bright red in these images. The wind blows from west to east across the basin causing sand blow outs to appear as bright areas east of fields. Arrows indicate the progressive appearance of sand mobilized off of agricultural fields. **1997**: An Airborne Visible Infrared Imaging Spectrometer (AVIRIS) image of the same area taken in 1997, and processed to display colors in the same way as in the MSS images. The relative sharpness of this image is due to the higher spatial resolution of the AVIRIS instrument. The dark-red Area **C** consists of two fields covered with *A. polycarpa* while Area A is an abandoned field with very little shrub cover. Both areas exhibit dramatic sand blow outs downwind.

Anthropogenic disturbance in the Manix Basin may be separated into two types: direct and indirect. Direct anthropogenic disturbance refers to human activities and the consequences of those activities in the area in which they were performed. This includes the actual fields, roads, pastures, corrals, trails, and so on that are affected by land use practices. Indirect disturbance refers to the consequences of direct disturbance in areas not directly disturbed. Both direct and indirect disturbance are extensive in the Manix Basin, and that they are coupled by wind erosion and redeposition of wind-blown sediment.

Ray (1995) has reported that in 1985 agriculture in the Manix Basin reached its greatest extent with 37 active central-pivot irrigated fields accounting for 3062 ha of land in cultivation. Agricultural activity in the Basin has decreased in the last decade. Thus,

Table 2-1. Direct and indirect disturbance for some selected fields in the Manix Basin.

Location	Total time cultivated	Time since abandonment	Soil Texture	Area subject to direct disturbance	Area subject to indirect disturbance	Indirect/Direct
See Figure 1	years	years		hectares	hectares	(area ratio)
A	> 7	< 10	Sand/Loamy Sand	185	518	2.8
B	1	26	Sand/Loamy Sand	62	109	1.8
C	5	15, 17	Sand	182	241	1.3
D	6	11	Loamy Sand	79	91	1.2
E	6 to 8	10, 14	Loamy Sand	124	33	0.3

at least 3000 ha of land have been directly disturbed in the Manix Basin. In an analysis of 1998 AVIRIS data, the relative areas of direct and indirect disturbance in the form of sand blow-outs, for some of the fields in the Manix Basin were identified (Table 2-1). Analysis was carried out by summing the area of pixels in sand blow-outs downwind of each field. There is no clear relationship between time of abandonment nor of cultivation

with the magnitude of indirect disturbance. All fields were located in soils with sandy or loamy sand soils, the dominant soil textures in the Basin (Tugel and Woodruff, 1978).

Sand may be blown several kilometers beyond the downwind boundary of a field and therefore the area of indirect disturbance can exceed the directly disturbed area by several-fold. With 3,000 ha of land directly disturbed in the Basin, 3,000 to 9,000 ha of land may be expected to be indirectly disturbed by agriculture. This sums to 6,000 to 12,000 ha total disturbance or 15% to 30% of the total Basin floor area, and approximately 23% to 45% of the non-playa area of the Basin. Other disturbances, such as housing developments and roads are also present in the Basin, while large areas of the Basin are taken up by the Coyote and Troy playas. Anthropogenic degradation appears to have a major impact on land quality and status in the Manix Basin.

3.2 Field Observations in the Manix Basin

3.2.1 Direct Disturbance

Before the fields of the Manix Basin could be cultivated they were cleared of vegetation. Vegetation cover shelters the soil from the erosive force of the wind by: (1) reducing the force of the wind near the ground, (2) by extracting momentum above the surface (Wolfe and Nickling, 1993), and (3) by trapping soil particles in transport (Lancaster and Baas, 1998). Tillage destroys fragile surface armors, thereby reducing the threshold shear velocity (Gillette, 1988; Gillette *et al.*, 1980; López, 1998; Tegen and Fung, 1995). Vegetation removal and soil cultivation therefore have the combined effect of dramatically increasing soil erodibility in the Manix Basin (as seen in Figure 2-1).

Mechanical agriculture itself visibly mobilizes dust and sand on windy days and ensures that the soil surface is exposed for at least part of the year. Active fields, therefore, become sustained sources of material for aeolian transport immediately upon clearing.

The magnitude of deflation associated with wind erosion of agricultural fields in the Manix Basin is difficult to quantify. However, in one agricultural field abandoned about 30 years ago (Figure 2-1, Area F), wind erosion has led to an average deflation rate of more than 1.5 cm per year, as evidenced by wind excavation of buried irrigation pipes. These pipes provide a rare field constraint on deflation, as the vertical feeder sections were once flush with the ground.

Areas that have been cleared of vegetation and then abandoned follow one of two principal trajectories with respect to their vegetative cover. Areas may be recolonized principally by *A. polycarpa*, a perennial shrub, and annual exotic grasses such as *Schismus*. Perennial vegetation cover estimates from various sites in the Manix Basin are shown in Table 2-2. There is 8 to 30 percent cover of *A. polycarpa* on abandoned fields, compared to 5 to 7 percent cover, in undisturbed areas dominated by *L. tridentata*. In some cases, only the upwind portions of abandoned fields support a low cover of *A. polycarpa*, even after a decade or more of disuse. Fetch, and therefore mass transport rate of the wind, is lowest here, minimizing plant abrasion and seed removal. These fields have only been abandoned for at most 30 years, and are nowhere near the 65 years that Carpenter *et al.* (1986) estimate for a creosote bush scrub community to approach climax conditions nor the several hundred years estimated by Vasek *et al.* (1975). Stylinski and Allen (1999) have suggested that in arid shrublands, altered stable states can occur if a community is pushed beyond its threshold of resilience by anthropogenic

disturbance. The dramatic differences between abandoned agricultural fields and undisturbed desert in the Manix Basin after several decades certainly argue for centuries for recovery, if it happens at all.

Some of the abandoned fields in the Manix Basin do not support any native

Table 2-2. Percent cover by species in undisturbed desert compared with areas on abandoned central-pivot agriculture fields. Abandoned fields fall into two distinct cover classes: some fields have almost no cover while others have a high cover of *Atriplex polycarpa.*

	Undisturbed	On-Field (Low Cover)	On-Field (High Cover)
Larrea tridentata	4.8%	0.8%	0.0%
Ambrosia dumosa	1.1%	0.4%	0.0%
Atriplex polycarpa	0.8%	8.3%	32.5%
Total Fractional Cover	6.7%	9.5%	32.5%

Plant counts were carried out in February, 1998 and April, 1999 in 5-m radius circles. The "Undisturbed" plant cover data represent three sites with 12, 4, and 12 replicates, respectively. The "On-Field (low cover)" data represent two sites with 12 replicates.

perennial vegetation, even after a decade or more of disuse. This may be explained by: (1) transport of sand by wind over the exposed soil surface killing young seedlings, and/or (2) absence of climatic or soil conditions suitable for plant germination (Lovich and Bainbridge, 1999). In an experiment aimed at restoring Mojave Desert farmland by seeding native plants in order to reduce dust emissions, Grantz *et al.* (1998) found *A. canescens* could be established in areas without deep sand. However, "this revegetation was achieved in an anomalous year with above average and late rainfall that eliminated early competition from annual species and later fostered abundant shrub growth. This success was not reproducible in more normal years." Thus, natural germination of native perennial vegetation on abandoned fields may be rare, explaining the lack of cover on some abandoned fields in the Manix Basin. The importance of germination conditions highlights the dramatic role of interannual climate variability and long-term regional

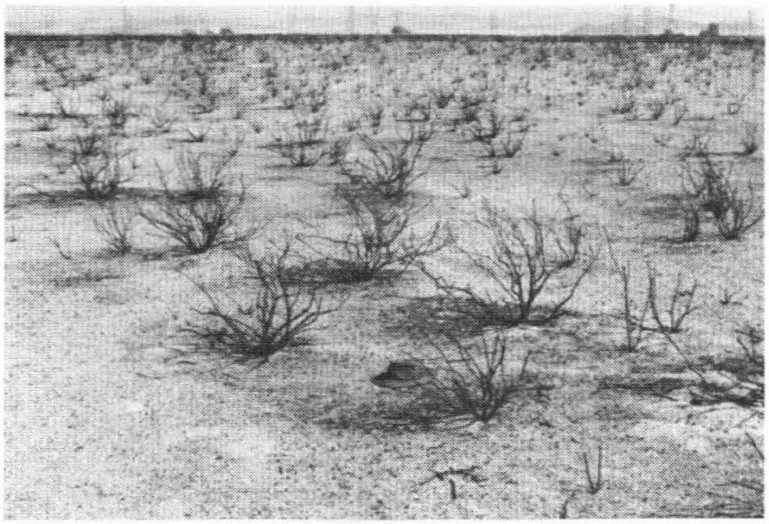

Figure 2-2. Photograph taken in an abandoned field in the Manix Basin after a fire in the summer of 1998 showing the response of highly disturbed areas to fire. Prior to the fire, this abandoned field had been covered with approximately 30% cover of *A. polycarpa*. Most individuals in the path of the fire in the area of high *A. polycarpa* cover were killed as shown here. Nearby, in adjacent undisturbed desert, only the annual grasses burned and perennial plant mortality was low.

climatic conditions on the response of these ecosystems to human disturbance. Bare fields in the Manix Basin may be expected to take much longer than the vegetated fields to approach climax conditions.

Once fields are abandoned, they serve as sources of wind-borne sediment at least until a deflationary soil pavement is re-established or the soils are crusted (López, 1998). Landsat MSS and AVIRIS images in Figure 2-1 depict the mobilization of sand from abandoned agricultural fields in the Manix Basin. Area C, which appears as dark red in the 1997 AVIRIS image, is a set of two fields abandoned in the early 1980s according to Landsat images of the basin from 1973 to 1992; Area A was abandoned in 1988 (Ray, 1995). Areas downwind of both fields show significant sand encroachment even though Area A has almost no cover and C has relatively high (~30%) *A. polycarpa* cover. Thus, even after regrowth of *A. polycarpa*, abandoned fields remain sources of aeolian sand. High *A. polycarpa* cover may increase roughness length and decrease boundary layer

Figure 2-3. Photograph taken downwind of an abandoned field in the Manix Basin in the spring of 1998 displaying evidence of active sand movement (sand ripples) and plant mortality. The plants in the foreground are *L. tridentata* and *A. dumosa* individuals that have been buried, abraded and ultimately killed by the encroaching sands.

velocity, but once the soil crust was removed, these soils clearly remained highly wind-erodible.

A notable consequence of the trajectory that areas of direct disturbance follow is their potential response to fire. Lovich and Bainbridge (1999) have reported a 10-year average of 175 fires in the Mojave and Colorado deserts of California that affected an average of 10,927 ha annually. Besides this, there are no published definitive studies of fire return intervals or typical areas burned in individual fires in the Mojave Desert. Nonetheless, it is clear that fire has only recently become a factor in shaping the structure and dynamics of plant communities in the Mojave Desert. Prior to European colonization of North America, limited biomass, large intershrub spacing, low combustibility of some native plants and sparse ground cover to support and propagate combustion are thought to have led to very low fire frequencies (Lovich and Bainbridge, 1999). The recent proliferation of exotic annual plants has increased the fuel load and fire frequencies in

many ecosystems around the world have increased in recent years (Lovich and Bainbridge, 1999).

A fire in the Manix Basin that occurred in June, 1998, showed that areas of high *A. polycarpa* cover have different fire responses than undisturbed areas or abandoned areas of direct disturbance with little or no vegetation regrowth. After the 1998 Manix Basin fire, mortality of nearly all shrubs on an *A. polycarpa*-covered abandoned field was observed. The same burn extended through a nearby undisturbed area dominated by *L. tridentata* and *A. dumosa*. Here, the fire killed few shrubs and was only sustained as a ground fire in areas with a dense cover of exotic annual grasses. A fire in an abandoned field covered with *A. polycarpa*, therefore, re-exposes the soil surface to wind erosion while a fire in an undisturbed area has little effect on the landscape (Figure 2-2). Therefore, disturbed areas that are subsequently burned are likely to have much longer times to recovery than their unburned neighbors, both due to fire mortality and the enhanced vulnerability of burnt landscapes to wind erosion.

3.2.2 Indirect Disturbance

Indirect disturbance in the Manix Basin primarily takes the form of redeposition of wind-borne sediments onto previously undisturbed adjacent lands. Three types of material are removed from abandoned agricultural fields by wind erosion: saltation-sized particles, suspension-size particles, and organic litter. Removal of all three contributes to indirect disturbance. Saltation of larger particles results in their redeposition wherever wind velocities drop, typically in adjacent, downwind vegetated areas or in the lee of plants growing on the field itself.

The encroachment of blowing sand into adjacent shrublands has dramatic consequences for the landscape. Field observations indicate that blowing sand abrades plants, resulting in leaf stripping and damage to the cambium and therefore to the plant's ability to distribute and use water. Young plants are especially vulnerable to the effect of blowing sand because they lack woody tissue. This results in the suppression of revegetation in bare areas and the loss of vegetation on adjacent lands. Nitrogen-fixing microbial communities and cryptobiotic crusts are buried by sand, reducing inputs of nitrogen to the soil (Belnap *et al.*, 1993; Evans and Belnap, 1999).

Blowing sand creates dunes in the wind-shadows of plants. Inspection reveals that these dunes typically have coarser texture than the material from which they were derived, a result of the progressive removal of fines in a continual process of winnowing (Gibbens *et al.*, 1983; Hennessy *et al.*, 1986; Lyles and Tatarko, 1986). Dunes can grow and coalesce resulting in: 1) burial of large plants not able to grow fast enough to keep up with dune growth, 2) burial of all vegetation including very young shrubs in inter-shrub spaces, and 3) complete blanketing of the soil surface by sand. The persistence of branches and twigs from buried or abraded vegetation decreases the erodibility of the surface (Figure 2-3). Since new vegetation growth is inhibited by blowing sand, the ability of vegetation to stem erosion is limited.

3.2.3 Anthropogenic Additions

Chemical fertilizers or other soil amendments are often added to agricultural fields to increase productivity or soil workability. Inorganic salts also may be added inadvertently to the soil as irrigation water evaporates. Wind erosion of soil from an area

of direct disturbance may be accompanied by dispersal of these soil additives across the landscape. The dispersal of salts by wind onto adjacent undisturbed areas may contribute to the decreased plant growth on these areas by increasing osmolyte concentrations in soil solutions. In Chapter 3, I find that Cl^-, SO_4^{-2}, and Na^+ are significantly elevated on and downwind of an abandoned field in the Manix Basin relative to the upwind as salts have spread with the moving sands. On the field, Cl^-, SO_4^{-2}, and Na^+ accumulated at average rates of approximately 9.9, 30, and 29%/year, respectively over seven years. This represents a dramatic addition of ions to the soil, which may limit the use of these areas for extended agriculture or influence the recovery of agricultural fields after abandonment.

Soil additives (including nitrate and phosphate) act as chemical tracers of mass flux and determine the relative effects of physical abrasion and nutrient loss in propagating desertification in arid shrublands. In Chapter 3 I report significantly elevated concentrations of plant-available N and P on and downwind of an abandoned field in the Manix Basin. Fertilizer has been broadcast across the landscape as the soil from the field has been transported by wind. Despite elevated nutrient concentrations on the abandoned agricultural field at Manix, the absence of shrubs on this field indicates that recolonization of fields by native shrubs after their abandonment is not simply related to nutrient content of the soils, but is dependant more on germination conditions as suggested by Grantz *et al.* (1998). The area immediately downwind of the fertilized field has seen an increase in plant mortality and not a bloom in response to increased nutrient concentrations. This indicates that abrasion and burial of vegetation may dictate a landscape's response to wind erosion, especially in years without favorable germination

conditions.

3.3 Quantitative Assessment

Using published threshold shear velocities and equations for the flux of wind-borne sediments, I conclude that observed deflation rates at the Manix basin are reasonable in light of literature values and theoretical considerations. The quantitative assessment provides insight into the magnitude of deflation, redeposition of saltation-sized particles, and emission of nutrient-laden dust.

Wind erosion and transport processes have been reviewed many times in the literature (see for example Greeley and Iversen, 1985, Table 2.5). Here, the analysis of Bagnold (1941) will be followed because it is still prevalent in the modern literature of aeolian transport and because it provides a simple method for determining the magnitude of sand transport. From momentum considerations and simplifying assumptions about the path of saltating grains, Bagnold derived a relationship for the horizontal mass flux of saltating grains integrated over all heights:

$$q = C\sqrt{\frac{d}{D}}\frac{\rho_a}{g}U_*^3, \tag{1}$$

where q is the horizontal mass flux in g cm^{-1} s^{-1}, U_* is the shear velocity, d is the grain diameter of the sand in question, D is the grain diameter of a standard 0.25-mm sand, ρ_a is density of air, g is the acceleration due to gravity, and C is 1.8 for a naturally graded sand. Assuming that $d = D$, Bagnold's equation simplifies to

$$q = 1.5 \times 10^{-9}\left(U - U_t\right)^3, \tag{2}$$

where U is the wind velocity and U_t is the threshold wind velocity measured at 1 m

height. U and U_t are related to shear velocity, U_*, and threshold shear velocity, U_{*t}, respectively, by Bagnold's formula:

$$U_Z = \frac{U_*}{k} \ln\left(\frac{z}{z_o}\right), \tag{3}$$

where U_z is wind speed at height z, k is von Karmann's constant taken to be 0.4, and z_o is the roughness length (Bagnold, 1941).

Shao and Raupach (1993) have shown from energetic considerations that vertical dust flux due to suspension, F, in mass per area per unit time is linearly related to q. Based on this, Gillette *et al.* (1997) have obtained a value for F/q of 5.4 x 10^{-4} m^{-1} from wind tunnel experiments, which is of the order of that for sandier soils (Gillette, 1977; Gillette *et al.*, 1997; Shao and Raupach, 1993) and therefore applicable here.

For a field with cross-wind diameter, x, and area, A:

$$\Delta\tau_{saltation} = \frac{q}{\rho_B}\frac{x}{A}, \tag{4}$$

where ρ_B is the bulk density of the soil and rate of deflation due to saltation, $\Delta\tau_{saltation}$, is expressed as cm yr^{-1}. The deflation rate due to saltation is given by:

$$\Delta\tau_{suspension} = \left(F/q\right)\frac{q}{\rho_B}. \tag{5}$$

ρ_B is taken to be 1.25 Mg m^{-3} for a dry, medium-texture mineral soil (Brady and Weil, 1999), x is taken to be 750 m, and $A = \frac{\pi}{4}x^2$ for a circular field. A/x is equivalent to erosive fetch. The total average mass rate of erosion is:

$$Q_{Total} = q\left(\frac{x}{A}\right) + F \approx q\left(\frac{x}{A}\right), \tag{6}$$

and the total deflation rate (in cm yr^{-1}) is given approximately by:

$$\Delta\tau_{Total} = \Delta\tau_{Saltation} + \Delta\tau_{Suspension} = \frac{q}{\rho_B}\left(\frac{x}{A} + F/q\right), \quad (7)$$

where the mass flux due to saltation, q, depends on a detailed wind record, z_o, and U_{*t} by Equations (2) and (3).

The threshold shear velocity required to account theoretically for $\Delta\tau_{Total}$ = 1.5 cm/yr in the Manix Basin was found iteratively using Equation (7), Gillette *et al.*'s (1997) value for F/q (5.4 x 10^{-4} m^{-1}), Gillette *et al.'s* (1980) values of z_o (0.04 cm is the average of values reported by for non-playa, uncrusted soil), and the wind conditions at Daggett Airport in the Manix Basin (collected hourly since 1961). U_{*t} was found to be 103 cm/s, well within the bounds of reported values for arid agricultural soils of 20-132 cm/s (Gillette, 1988). These results indicate that empirically-understood processes can account for observations in the Manix Basin and therefore that it is reasonable to invoke these processes to drive indirect disturbance in the conceptual model developed here.

The value q = 8.56 Mg m^{-1} yr^{-1} calculated from U_{*t} = 103 cm/s by Equation (2) implies that the equivalent of 10^8 - 10^9 sand grains saltate through each meter of width per year. In fact, considering that the majority of wind erosion occurs during storms of a few days in duration, this constitutes an extremely concentrated attack on vegetation which is capable of overwhelming plants' self-healing capabilities.

The effect of abrasion acts in tandem with redeposition and dune formation to compromise vegetation in adjacent downwind areas. The total volume, V in m^3 yr^{-1}, of soil moved by saltation off of an abandoned agricultural field is given by:

$$V = \frac{qx}{\rho_B} T, \quad (8)$$

where T is the time in years before the re-establishment of an armored surface. If the density of the soil is approximately the same after redeposition downwind, volume is conserved and the average depth of burial is given by V/A_b, where A_b is the area buried by the mobilized sand, which can be estimated from remote sensing imagery. Area C in the Manix Basin (Figure 2-1, Table 2-1) has been abandoned for 16 years and has a 241-ha sand plume downwind. Using the value of q calculated above, the average depth of this sand plume is approximately 6.8 cm. However, mobilized sand usually accumulates in the wake of plants, leading to dunes larger than the average depth of burial. In the Manix Basins dunes greater than one meter in height are present. There is currently no theory for determining dune height based on flux measurements or calculations.

Using Gillette *et al.*'s (1997) value for F/q, and reasonable values for x/A, $q(x/A)$ should always be greater than F, indicating that sand mobilization is more important as a wind erosion process than dust emission in terms of mass loss. However, dust emission represents the permanent removal of material from the regional ecosystem due to its potential for long-range transport. Nutrients, especially P, are often concentrated on small particles in soils (Avnimelech and McHenry, 1984; Leys and McTainsh, 1994). Assuming constant suspension flux, the removal of nutrient i from the bulk soil at time t may be written as:

$$F_i^d(t) = C_i^d(t)F, \tag{9}$$

where $C_i^d(t)$ is the concentration of soil nutrient i on the emitted dust and has units of mass of nutrient per mass dust. $F_i^d(t)$, therefore, is in units of mass of nutrient i lost per unit area per unit time. The mass per unit area of soil in a layer of depth, D, is:

$$M^D = \rho_B D, \tag{10}$$

and therefore, the reservoir of nutrients in this layer is $C_i^s(t)M^D$, where $C_i^s(t)$ is the concentration of nutrient i in the soil.

Conservation of mass gives:

$$M_i^{s,D}(t + \mathrm{d}t) - M_i^{s,D}(t) = C_i^d(t)F\mathrm{d}t, \tag{11}$$

where $M_i^{s,D}(t)$ is the mass of nutrient i at time t in a layer of soil of depth, D. Under the approximation that M^D is constant with time, divide Equation (10) by M^D yielding:

$$C_i^{s,D}(t + \mathrm{d}t) - C_i^{s,D}(t) \approx C_i^d(t)\frac{F}{M^D}\mathrm{d}t, \tag{12}$$

where $C_i^{s,D}(t)$is the concentration of nutrient i at time t in a layer of soil of depth, D. The ratio of $C_i^d(t)$ to $C_i^{s,D}(t)$ is assumed to be a constant, k_i, that is analogous to a chemical fractionation factor for nutrient i between dust and the bulk soil.

Rearranging Equation (11) yields:

$$\frac{\mathrm{d}C_i^s}{\mathrm{d}t} \approx -k_i\frac{F}{\rho_B D}C_i^s. \tag{13}$$

Therefore, the time for the concentration of nutrient i in a layer of soil of depth D to drop by $1/e$ times its original value is given by t_i^D:

$$t_i^D = \frac{\rho_B D}{k_i F} = \frac{t^D}{k_i}, \tag{14}$$

where t^D is the time it takes to completely excavate a layer of depth D with a mass flux rate equal to F. For D = 0.05 m (a typical sampling depth), F = 4.62 kg m^{-2} yr^{-1} (at U_{*t} = 103 cm/s) and bulk density of 1.25 Mg m^{-3}, t^D is approximately 14 years. Reported values of nitrogen enrichment for dust relative to soil, k_N, in Australian arid zone soils are on order of 10 (Carter *et al.*, 1999; Leys and McTainsh, 1994), though Larney *et al.* (1998) have reported values as low as 1.1. Thus, t_i^D may be as low as a few years.

Available N and P concentration at a site in the Jornada Basin reported in Chapter 3 indicate an 80% net loss of available N and a 70% net loss of plant-available P in the eight years since the establishment of the site. Thus, the *e*-folding times of N and P, t_N^D and t_P^D, in this surface soil undergoing active deflation and aerosol emission are inferred to be approximately 5-10 years. Wind erosion, therefore, impacts soil fertility in areas of both direct and indirect disturbance on short timescales. This has dramatic implications for nutrient availability in disturbed areas, especially for seed germination in surface soils where the degree of nutrient depletion will be greatest.

4. CONCLUSIONS

4.1 Anthropogenic Desertification Of Arid Shrublands

Extensive remote sensing, field, and quantitative assessment of arid land degradation in the Manix Basin leads us to conclude that in arid shrublands direct anthropogenic disturbance resulting in the destruction of soil crusts and vegetation cover can cause indirect disturbance of adjacent areas by initiating the disintegration of islands of fertility. Figure 2-4 illustrates a proposed model for the degradation of arid shrublands based on these observations. The inferred sequence can be visualized as:

(1) Transport of sand off of disturbances resulting in deflation of the disturbed surface.

(2) Mobilization of dust and plant litter by wind, depleting the soils of nutrients in areas of direct disturbance.

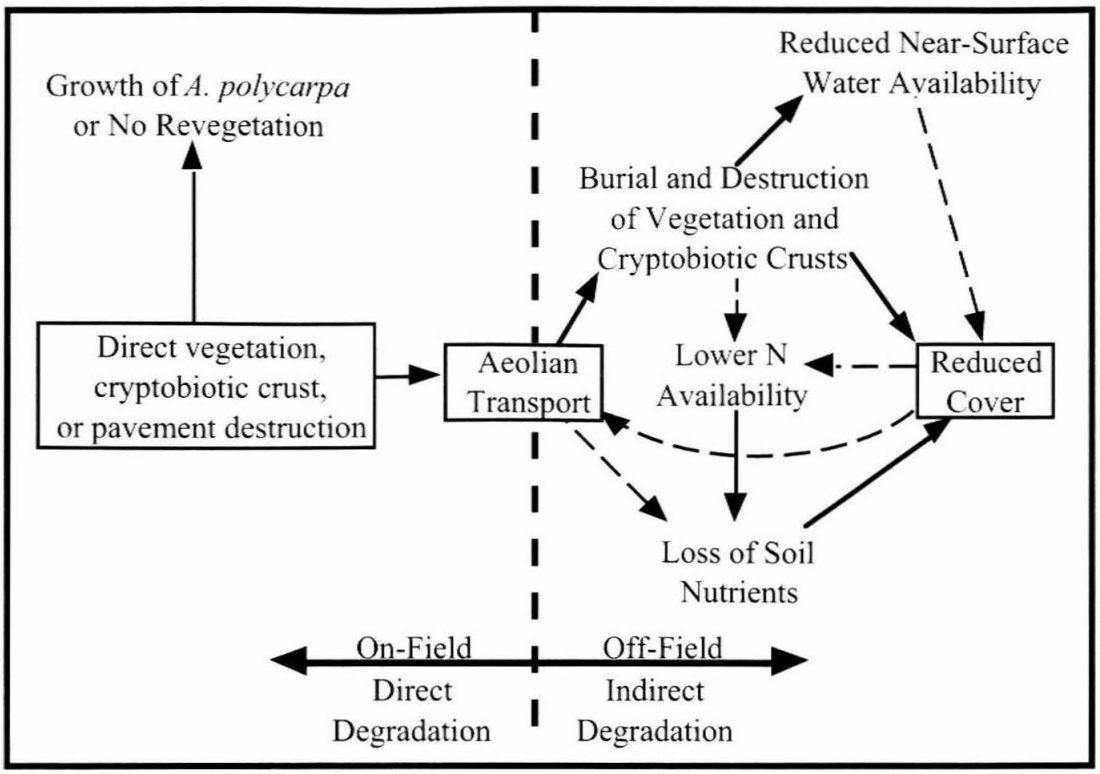

Figure 2-4. Process model for shrubland degradation developed from observations at the Manix Basin, California. Direct disturbance through vegetation, crust, or pavement destruction drives aeolian transport which leads to indirect degradation in the form of reduced cover in adjacent areas.

(3) Damage to and burial of plants by saltating sand in adjacent downwind areas.

(4) Reduction of vegetation cover downwind, leading to an expanding area in which wind removes dust and litter material, depleting the soils of nutrients.

A feedback threshold may be reached when these mechanisms act to dramatically reduce shrub cover in previously undisturbed areas. The accessibility of this threshold is related to allogenic changes in regional climate and interannual variability: reduced precipitation or increased temperature may exacerbate landscape vulnerability and cooler, wetter conditions may aid amelioration.

4.2 Nutrient Relations and Soil Resources

Shrubs are the loci of nutrient accumulation and represent islands of fertility in shrubland ecosystems (Schlesinger *et al.*, 1990; 1996). How then does wind erosion affect soil resources in degraded shrublands?

Nutrient removal from islands of fertility has three main mechanisms: 1) physical removal of litter and organic matter by the wind, 2) wind suspension of dust particles with high concentrations of plant nutrients (Leys and McTainsh, 1994), and 3) retarded accumulation of organic N due to increased surface and air temperatures (Post *et al.*, 1985). In areas of indirect disturbance, the mantle of winnowed dune sand may lead to decreased fertility of the surface soil, which is vital for seedling establishment. Areas of direct disturbance which are the sources for dune sand will also become less fertile through preferential removal of fines by wind. Removal of litter beneath shrubs limits the future availability of organic N and C to plants (Lyles and Tatarko, 1986; Schlesinger and Pilmanis, 1998).

Islands of fertility associated with shrubs normally are sites for recolonization by seedlings (Schlesinger and Pilmanis, 1998). These young plants are more vulnerable to sand abrasion and burial than their mature predecessors and their establishment may be limited. In many areas adjacent to abandoned agricultural fields in the Manix Basin, shrub sites are generally not recolonized and become areas of soil nutrient removal, effectively dismantling the islands of fertility. Schlesinger and Pilmanis (1998) have reviewed field experiments in which shrubs have been removed by cutting, herbicides or fire. These studies show variable rates of soil degradation, but in each case, "a loss of the

local biogeochemical cycle associated with shrubs has allowed physical processes to disperse soil nutrients across the landscape." Thus, the progressive reduction in fertility acts in tandem with the mechanical action of sand to further decrease shrub cover which, in turn, increases the susceptibility of the land to wind erosion. The permanent removal of suspension-sized particles from the soil by wind erosion results in a change of the soil texture, which may also reduce soil binding properties, resulting in increased wind erodibility.

In a study aimed at determining the effect of wind erosion on nutrient availability, available N and P were measured in soils at a disturbed site in the Jornada LTER site in south-central New Mexico (Chapter 3). These results indicated that surface soils upwind of the disturbance are richer in available N and P than those from downwind. Assuming that the soils from the upwind transect are considered representative of the original condition throughout the study sit, an 80% net loss of available N and a 70% net loss of plant-available P has occurred from the soils blown off of the disturbed area. In addition, the site itself lost nearly 94% of its available N and nearly 79% of its plant-available P. Similar results have been reported by Leys and McTainsh (1994) in Australia.

The nutrient cycle may be further disrupted when soil microbial communities are buried or destroyed by blown sand, minimizing their ability to fix atmospheric nitrogen and add it to the nutrient reservoir of the soil. The burial of cryptobiotic crusts also reduces their ability to enhance infiltration of water leading to decreased near-surface soil moisture (Belnap, 1995; Belnap *et al.*, 1993).

It has been suggested by Gibbens *et al.* (1983), Lyles and Tatarko (1986), Hennessy *et al.* (1986), and Leys and McTainsh (1994) that permanent removal of

suspension-size particles from the soil by wind erosion may reduce water-holding and cation-exchange capacities. This may result in less water in the surface soil, marginalizing the water balance of desert shrubs and increasing their susceptibility to drought and climate change. On short timescales, this may be particularly important for the establishment of annual exotic grasses. In wet years, these grasses form a carpet that reduces the susceptibility of soils to wind erosion (Lancaster and Baas, 1998). In dry years, decreased near-surface soil moisture makes the landscape more vulnerable to wind erosion. Dust storm frequency has been correlated with reduced soil moisture, indicating that soil erosion and nutrient removal are accelerated by decreased soil moisture (Brazel and Nickling, 1987).

4.3 Lessons for Land Managers

Several aspects of the arid shrubland degradation observed at the Manix Basin can provide lessons for land management in these environments. Wind erosion is the principal mechanism of degradation in arid shrublands on basin floors. The main consequences of land degradation are therefore:

1) Sand blasting of vegetation and equipment

2) Burial of vegetation and equipment

3) Dust emissions leading to decreased nutrient availability, cation exchange capacity, water holding capacity, and atmospheric pollution.

For virgin lands not already converted to human uses, if possible, arid shrublands with sandy wind-erodible soils should not be used for many activities. These are

extremely fragile lands the degradation of which could easily upset marginal economic gains from their cultivation or make recreation and habitation impossible. Furthermore, human disturbance of arid shrubland landscapes may prelude successional processes, resulting in permanent landscape change. Where development is deemed necessary, planning must precede plowing. A principal consideration must be the wind erodibility of soils. In the United States, county-wide soil surveys typically provide information on soil texture. Soils of sandy or loamy sand textures, even when covered by a thin layer of protective crust (deflationary crust, desert pavement, or cryptobiotic crusts), are very vulnerable to wind erosion. Activities that break up soil crusts and destroy vegetation are best avoided. High-risk activities include agriculture, grazing, ORV recreation, and military training. Roads, when necessary, should be situated to minimize the area of wind-erodible soils affected. The location of natural wind breaks such as trees, hills, and mountains should also be used to determine the location of planned developments.

For land already under cultivation or used for recreational purposes, technological and logistical methods for minimizing the effects of wind erosion in local vegetation, crops, and infrastructure should be implemented. Equipment, sheds, and other buildings should be situated upwind of fields so that they are not sandblasted or buried. Fields, likewise, should not be situated such that one is close to and downwind of another, or else sand eroded from one will be deposited on another. In the extremely sandy western lowlands of the Cape Province, South Africa, Talbot (1947) has observed that maintaining uncultivated areas between fields may stem wind erosion and keep redeposition of sand from occurring in undesirable places. Other wind breaks, preferably indigenous plants which do not need to be watered after establishment, will also help

stem erosion. Attempts must be made to maintain vegetation on fields. In light of this, nitrogen-fixing cover crops may be planted to minimize erosion and add nitrogen when tilled back into the soil. Fallow periods, especially in the windiest time of the year, should be avoided, and cover crops planted instead. Fertilizers may need to be added every few years, when significant nutrient loss is detected and when nitrogen-fixing cover crops are not sufficient to renew the soil resources. When abandoned, fields should be planted with a final, long-lived perennial indigenous cover that will help minimize wind erosion for years to come, and will allow natural succession processes to take place.

Novel techniques may provide the best opportunities for sustainable management of arid shrublands. Yearly monitoring of soil nitrogen and phosphorous in order to identify times or places where dust emission has significantly depleted the soil of nutrients is desirable. Where possible, use should be made of remote sensing and precision farming technologies to ascertain soil condition and to respond appropriately. Carter *et al.* (1999) have reported success in stemming erosion and improving soil condition by adding clays of sub-soil origin to sandy soils of Western Australia. These and other techniques could be used to dramatically improve the sustainability of agriculture in arid lands.

Past agriculture in the Manix Basin is a good example of unregulated and unmanaged human activities for short-term gain leading to long-term loss of value. As farming in the Basin became less profitable, farmers simply abandoned the land to natural degradation processes without implementing long-term remediation strategies. A principal lesson from this area, therefore, is that policy mandates and financial incentives need to be put in place to promote soil conservation initiatives during land-use and to

require restoration of the landscape after cultivation stops. Efforts at remediation do not need to focus on restoring the environment to its pristine condition, although this is preferable. Instead, they can focus on halting or slowing soil erosion by planting long-lived, native, and perennial shrubs that will partially protect the surface. Funds for post-agriculture remediation should be earmarked before cultivation begins, and must be considered a part of the cost of doing business in vulnerable lands. In this way, remediation becomes the responsibility of the short-term land-user and not someone else's long-term problem.

4.4 Regional Drivers and Effects

In addition to the increasing intensity of human disturbance, arid lands are affected by changes in regional climate. The 1980s and 1990s—the decades in which large areas of the Manix Basin were abandoned from agriculture and in which the greatest land degradation has been seen—were neither unusually windy nor dry. The annual average wind speed for the period 1961 to 1990 was 5.5 m/s, identical to the period of 1980-1989 (National Climate Data Center, 1993). Annual precipitation was only slightly higher between 1970 and 1990 than for the period 1941 to 1997 (Table 2-3). When the decadal-scale regional climate in the Manix Basin shifts to a windier or drier period, the area affected by nutrient loss and aeolian sand mobilization can be expected to increase dramatically.

There has been much discussion about the relative importance of human versus indirect climate drivers of desertification. Both can have a dramatic impact on a

Table 2-3. Average precipitation (cm) by season at Daggett Airport. Source: National Climate Data Center, U.S. Precipitation by State, California: http://www.ncdc.noaa.gov/ol/climate/online/coop-precip.html.

	Jan-Mar	Apr-Jun	Jul-Sept	Oct-Dec	Annual
1944-1997	3.7	0.9	2.9	2.4	10.0
1980-1989	4.5	1.1	3.1	3.1	12.7
1990-1997	6.0	0.3	2.8	2.0	11.1

landscape (Brown *et al.*, 1997; Schlesinger *et al.*, 1990). Climate change may either increase or decrease anthropogenic effects on a landscape. For example, during wetter than average years, the presence of annual grasses at covers greater than about 15% halts wind erosion, and increased soil moisture leads to higher threshold shear velocities (Brazel and Nickling, 1987; Lancaster and Baas, 1998). In drier than average years, threshold shear velocity may be lower due to decreased soil moisture, and annual cover is greatly reduced leading to accelerated degradation. In the northern Mojave Desert, Schultz and Ostler (1993) have reported a dramatic decrease in total plant cover after only 4 years of drought. Clearly, resistance to climate-induced changes is dependent on the degree of anthropogenic disturbance and vice-versa. Thus, regional decadal-scale climate conditions may be expected to dramatically influence the rate of arid shrubland degradation.

4.5 Extrapolation to Other Areas

In the process model developed from observations in the Pleistocene paleolake Manix, the primary driving mechanism is the aeolian mobilization of sand, dust, and litter

material initiated by anthropogenic disturbance of the surface crust and vegetation cover. Any process that destroys the surface crust in an arid or semiarid shrubland and increases the boundary layer velocity over a soil with saltation- and suspension-size particles will result in the progressive devegetation of the downwind area. Thus the new model developed here can be extended to apply to any arid or semiarid shrubland with a source of wind-erodable material.

4.5.1 Other Land Forms in the Arid Southwest

Any arid shrubland with a source of wind-erodable, fine-grained material at the surface may be susceptible to anthropogenic degradation. This study of the Manix Basin indicates that arid shrublands on Pleistocene paleolake beds are especially susceptible to anthropogenic degradation. Pleistocene lacustrine deposits are common in basins throughout the arid southwestern United States, where large, shallow pluvial lakes existed during the Last Glacial Maximum (Morrison, 1991a, b; Smith and Street-Perrott, 1983). Closed basins that were once Pleistocene lakes exist in many now-arid areas throughout the globe. The degradation observed in the Manix Basin is an example which can be applied to similar geological environments globally. Many of these areas have qualities that make them amenable for human use, such as very low slopes, little or no relief, subsurface water resources, and fine-grained sediments suitable for farming or other activities. Thus, the areas of greatest potential use are also susceptible to serious degradation.

The armored soils of desert bajadas—defined as broad, gently inclined alluvial surfaces extending from the base of mountain ranges to inland basins—may also be

susceptible to human-induced degradation. Although these soils are typically too gravelly or steep to be used for agriculture, these landforms may be wind erodible when disturbed by human activities. When present, the soil armor has been argued to develop through the "born at the top" model of McFadden *et al.* (1987), wherein fine, wind-mobilized particles are trapped by surface cobbles that float atop the accumulation of fine-grained material. Removal of the very stable desert pavement therefore exposes a layer of extremely wind-erodable wind-derived material, sometimes meters thick. Anthropogenic disturbance in these areas is likely to have profound consequences. Certainly, "born at the top" pavements downwind of areas of active dunes will be at high risk of degradation should the cover of protective pebbles be disturbed. Other soils of aeolian origin, including stabilized dunelands, will similarly be susceptible to anthropogenic degradation of the type discussed here.

Cryptobiotic soil crusts—communities of cyanobacteria, lichens, and mosses—are found throughout the world's deserts. These crusts bind fine soil particles by linked cyanobacterial fibers which protect the soil from wind erosion. Belnap (1995), Williams *et al.* (1995), and Marticorena *et al.* (1997) have suggested that the presence of cryptobiotic crusts dramatically decreases wind and water erosion. When disturbed, cryptobiotic crusts lose most of their protective qualities allowing mobilization of the underlying mineral soils. Shrubland areas with widespread cryptobiotic crusts are thus also vulnerable to progressive degradation should human activities disturb these fragile soil crusts.

4.6 Global Implications

The problem of wind-induced land degradation is not limited to southwestern United States. Greater use of mechanized agriculture in arid regions throughout the world as well as other land use demands is increasing the amount of arid and semiarid shrublands brought into cultivation or under human influence (see, for example, Kasusya, 1998; Khalaf, 1989; Khalaf and Al-Ajmi, 1993; Khresat *et al.*, 1998; Koch and El Baz, 1998; Luk, 1983; Mitchell *et al.*, 1998; Zha and Gao, 1997). This trend, linked with political/economic instability or the marginal and water-limited nature of arid land agriculture, makes sustainable arid region agriculture especially challenging.

Nations with a large proportion of their territory situated in arid environments with wind-erodible soils are particularly vulnerable to the consequences of land degradation. Great care needs to be employed in the responsible stewardship of these lands to promote sustainable agricultural, economic, and social development.

5. SUMMARY

Aeolian mobilization of dust, sand, and litter triggered by anthropogenic disturbance contributes to the destruction of islands of fertility by killing shrubs through burial and abrasion. This interrupts nutrient-accumulation processes and allows the loss of soil resources by abiotic transport processes. The resulting reduction of vegetation cover, in turn, increases susceptibility to wind erosion.

Land degradation processes necessarily exist in the context of regional climate and can either be bolstered or hindered by climatic conditions and changes, a fact that makes the rate of degradation ultimately climate-related. The process model developed here suggests various remediation techniques to halt shrubland degradation, but ultimately indicates that human use of landscapes susceptible to wind erosion should be avoided where possible.

In the face of largely unsustainable socioeconomic factors, the vulnerability of arid lands to degradation argues for development of linked degradation process models and monitoring strategies in order to minimize environmental damage and to promote sustainable management of human activities in arid lands. The dramatic landscape changes that accompany arid shrubland degradation can be monitored using present and future remote sensing techniques and technologies. When informed by process models such as the one presented here, remote monitoring tools may be used in the future to identify areas at risk of runaway degradation before large areas are adversely affected.

Globally, degradation of already-marginal arid lands represents a dramatic threat to local populations, food resources, and regional stability. Presently (2000) the United Nations Convention to Combat Desertification is before the United States Senate for ratification. This treaty provides for scientific and technical exchange to combat desertification. The processes of arid land degradation must be understood, effective monitoring techniques developed, and effective remediation and management techniques implemented to avoid costly and prolonged environmental crises. The model presented here represents a small step in attaining these goals.

CHAPTER 3

DESERTIFICATION IN AN ARID SHRUBLAND IN THE SOUTHWESTERN UNITED STATES: PROCESS MODELING AND VALIDATION

(*This chapter is in press in* Land Degradation, *Kluwer Scientific Publishing, Boston, MA.)*

1. INTRODUCTION

The Earth's expanding population is pressing into previously sparsely-inhabited regions. As a result the world's drylands, comprising nearly a third of the total land surface, are coming under increasing land use pressures. Despite their low vegetative productivity, these lands are not barren. Rather, they consist of fragile ecosystems vulnerable to anthropogenic disturbance in which degradation is often irremediable on human timescales. Any successful management plan or attempt at remediation must be firmly rooted in an understanding of natural arid zone processes and the way in which they are perturbed by human activities.

Observations in the deserts of the southwestern U.S. and elsewhere indicate that human destruction of soil crusts and removal of vegetation lead to a progressive, expanding degradation (Bach, 1998; Bowden *et al.*, 1974; Campbell, 1972; Fryrear, 1981; Hyers and Marcus, 1981; Khalaf and Al-Ajmi, 1993; Ray, 1995; Spitzer, 1993; Wilshire, 1980). Indirect disturbance of arid lands adjacent to areas of direct disturbance

can extend far beyond those initially disturbed. Severe financial and societal consequences can result including property damage, increased health and safety hazards, and decreased agricultural productivity (Bach, 1998; Bowden *et al.*, 1974; Clements *et al.*, 1963; Fryrear, 1981; Hyers and Marcus, 1981; Leathers, 1981).

The purpose of this study is to present soil chemical analyses and remote sensing observations which are designed to test the model hypothesis presented here. Chemical species are used to trace material transport from two severely disturbed sites in the American Southwest, and to probe the loss of N and P through dust emission. Remote sensing data provide temporal and spatial information about the extent of indirect land degradation. An integrative landscape process model of arid shrubland degradation is developed in which aeolian transport of material is the primary mechanism of degradation of arid shrublands.

2. MODEL HYPOTHESIS AND APPROACH

The model hypothesis to be tested explains the progressive devegetation of areas adjacent to sites of direct disturbance and destruction of islands of fertility in these areas. The inferred sequence can be visualized as:

(1) mobilization by wind of dust and plant litter, depleting the soils of nutrients in areas of direct disturbance.

(2) mechanical damage to and burial of plants by saltating sand in adjacent downwind areas.

(3) reduction of vegetation cover in adjacent areas, leading to an expanding area

in which wind removes dust and litter material, depleting the soils of nutrients.

(4) dune formation in adjacent areas, which decreases near-surface water availability for young plants, increases temperature and albedo, and buries ecologically important cryptobiotic crust and other bacterial communities.

(5) reduction of effective soil moisture and depletion of soil nutrients in areas of direct and indirect disturbance.

According to the model hypothesis, aeolian mobilization of dust, sand, and litter triggered by anthropogenic disturbance contributes to the destruction of islands of fertility by killing shrubs through burial and abrasion. Sand blown off of areas of direct disturbance may cover areas downwind several times the size of the initial disturbance. This interrupts nutrient-accumulation processes and allows the loss of soil resources by abiotic transport processes. The resulting reduction of vegetation cover, in turn, increases runoff and wind transport, reduces latent heat flux through evapotranspiration, and results in increased surface temperatures. These feedbacks can result in continuing reduction of vegetation cover and may contribute to regional climate change. The degradation process places arid shrublands in a landscape and process continuum between semiarid grasslands and Sahara-like hyper-arid barren lands.

In this study, soil samples and remote sensing data at two sites in the southwestern United States were collected in order to evaluate the depletion of soil nutrients by wind transport. At each site samples were collected from areas of severe direct disturbance and from adjacent areas both downwind and upwind. Sample populations from disturbed and undisturbed areas at each site were compared using t-tests to determine if depletion had occurred. Once significant depletion of soil nutrients was

identified, depletion factors were calculated by assuming that undisturbed upwind areas are representative of the pre-disturbance state for all populations. Soil surveys (Bulloch and Neher, 1977; Tugel and Woodruff, 1978; Meek, 1990) in the field areas indicate no difference in soil classification or surface geological history over the area sampled.

3. METHODS

3.1 Preliminary Observations

3.1.1 Manix Basin, Southeastern California, USA

This study concentrates on an abandoned central-pivot agricultural field in the Manix Basin. From a series of Landsat MSS images, it is apparent that this field underwent two phases of cultivation: from 1979-1981 and from 1987-1990, or seven years total (Ray, 1995). It has been fallow since 1990, and there has been no significant shrub regrowth on the field. The *Larrea tridentata-Ambrosia dumosa* shrubland immediately downwind of the abandoned field is characterized by dunes (up to 1 m tall) in the lee of shrubs sometimes coalescing into sand sheets. Although total plant cover is not visibly lower in the area downwind compared to nearby undisturbed desert, *Ambrosia dumosa* individuals are typically dead and living *Larrea tridentata* exhibit dead lower branches and abrasion scars on the upwind side of living limbs. These features (dunes, plant and limb mortality, and abrasion scars) are absent in the community upwind of the abandoned field.

3.1.2 Jornada Basin, South-central New Mexico, USA

In the spring of 1991, a semi-circular plot of land on the Jornada LTER site was cleared and maintained clear of vegetation (Havstad, 1999). This 'scraped site' is situated in patchy *Scleropogon brevifolius-Hilaria mutica* grassland with scattered *Prosopis glandulosa* (mesquite) and *Yucca spp.* The soil is loamy fine sand and sandy loam of aeolian origin derived from Rio Grande floodplain sediments (Bulloch and Neher, 1977). The historical wind direction in the basin is to the northeast as indicated by the alignment nearby Holocene aeolian sand ridges.

Observations made in the summer of 1998 indicate that in the seven years since the site's establishment, a large area immediately downwind of the barren area has been adversely affected by sand blown off of the scraped site. The area affected by blown sand extends at least 200 m downwind of the initial disturbance (Figure 1-1). Burial and abrasion of the shrubs as well as the grasses in this area have led to a significant decrease in shrub cover and the formation of dunes in the lee of remaining mesquite. Grasses, once plentiful in the adjacent downwind area, are completely absent. This pattern is strikingly similar to that seen in the Manix Basin and argues that anthropogenic disturbance and wind-erodable soil are the major contributors to the degradation of arid shrublands and the destruction of islands of fertility, even in semiarid regions of the Chihuahuan Desert.

3.2 Image Acquisition

Data from the Jet Propulsion Laboratory's Airborne Visible Infrared Imaging Spectrometer (AVIRIS) were acquired on August 29, 1998, over the Manix Basin and on May 27, 1997, over the Jornada Basin. AVIRIS measures the total upwelling spectral radiance in the solar-reflected spectrum from 400 to 2500 nm at 10-nm intervals. These spectra are acquired at 20-m spatial resolution across a 10-km wide swath from a NASA ER-2 aircraft flying at 20-km altitude. AVIRIS measurements are spectrally, radiometrically, and spatially calibrated and converted to units of radiance ($\mu W/cm^2/nm/sr$). The imaged vegetation and soils exhibit small but characteristic molecular absorptions and scattering characteristics which AVIRIS is sensitive enough to detect.

3.3 Sample Collection

Soil samples were collected in order to test the depletion of soil nutrients by wind transport from areas of direct human disturbance and from adjacent, downwind areas relative to undisturbed upwind areas. Samples were collected by inserting a 5 cm diameter steel pipe into the ground to a depth of 5-cm and placing the contents of the pipe in a sealed plastic bag. Samples were collect along three 200-m transects at each site: upwind of the disturbances, on the disturbances themselves, and downwind of the disturbances. Sample locations along the transects were determined by a random number table. Transects were oriented perpendicular to the apparent average wind direction as

indicated from remote sensing images of sand blow-outs (Figure 1-1) or, in the case of the Jornada LTER, historical wind directions as evidenced by sand streaks and ridges from remote sensing images. For each sample, whether it was taken from beneath shrubs or was from the bare soil between shrubs was noted.

3.3.1 Manix

Soil samples were collected on February 17, 1999, from an abandoned central-pivot agricultural field that was last cultivated in 1989 (Ray, 1995). The three transects which were sampled were located 100 m upwind of the edge of the field, in the center of the field, and 100 m downwind of the edge of the field. Thirty samples were collected along each transect and two extra samples were collected in the upwind transect. For samples in the downwind transect, where soil has blown off of the field and accumulated in dunes and sand sheets downwind of shrubs, it was noted whether samples were taken from the fine-grained dunes or the coarser interdune areas was also noted.

3.3.2 Jornada

Soils samples were collected on June 20-21, 1999, from the scraped site located at 32°34'14"N, 106°45'30"W. The three transects were located 50 m upwind of the edge of the scraped site, in the center of the site, and 100 m downwind of the edge of the site. Twenty samples were collected from the upwind and scraped site transects, and thirty samples were collected from the downwind transect. All samples from downwind of the

scraped site are from dunes. Here, sand removed from the scraped site blankets the entire downwind area and has in some places mounded in mesquite coppice dunes.

3.4 Laboratory Analysis

In the laboratory, all samples were oven-dried overnight, sieved to less than 2 mm and analyzed for NO_2^-, NO_3^-, NH_4^+, water-extractable PO_4^{-3}, bicarbonate-extractable PO_4^{-3}, Cl^-, SO_4^{-2}, K^+, and Li^+. The sum of NH_4^+-N, NO_2^--N, and NO_3^--N is considered to be an index of total available N (N_{Avail}). Bicarbonate-extractable PO_4^{-3} is considered to be an index of plant-available P. Samples from the Manix Basin were also analyzed for Na^+, while samples from the Jornada Basin were analyzed for Mg^{+2} and Ca^{+2}. Methods used in this study are described in Schlesinger *et al.* (1996). Concentrations of all species were converted to, and are reported in, μg (species)/g soil.

3.5 Statistical Analysis

Samples were divided into populations and sub-populations: upwind of the field or scraped site (sub-populations: undershrub and intershrub), on the field or scraped site, and downwind of the field or scraped site (sub-populations: undershrub and intershrub; dune and interdune). For each population and sub-population, the mean (in μg (species)/g soil), standard deviation, and coefficient of variation (C.V. = standard deviation / mean) was calculated. *t*-tests (α=0.01), calculated assuming that population variance is not equal, were used to deduce significant differences between means, and to determine their

relative magnitude. The undershrub sub-populations were too small to be included in *t*-test comparisons, and for the Jornada samples intershrub population *t*-test results are identical to results from the whole transects and therefore are not reported or discussed. All Jornada samples in the downwind transect were from dune sands blown off the scraped site.

Pearson product-moment correlation coefficients were calculated for all species for all samples as a whole and for each transect. Correlations were tested for significance at $\alpha=0.01$ against the null hypothesis that $\rho=0$ according to the method described by Sokal and Rohlf (1981).

4. RESULTS

Remote sensing images from AVIRIS for both sites are shown in Figures 3-1A and 3-1B. Mean species concentrations and *t*-test results for all populations and sub-populations are given in Tables 3-1a and 3-1b. Significant Pearson product-moment correlation coefficients are given in Tables 3-2a and 3-2b.

4.1 Spatial information: Remote Sensing

As shown in Figure 3-1, areas of progressive indirect disturbance are visible downwind of areas of direct disturbance in remote sensing images. They appear in both sites as bright plumes issuing from the downwind edge of direct disturbances which are also apparent in the images.

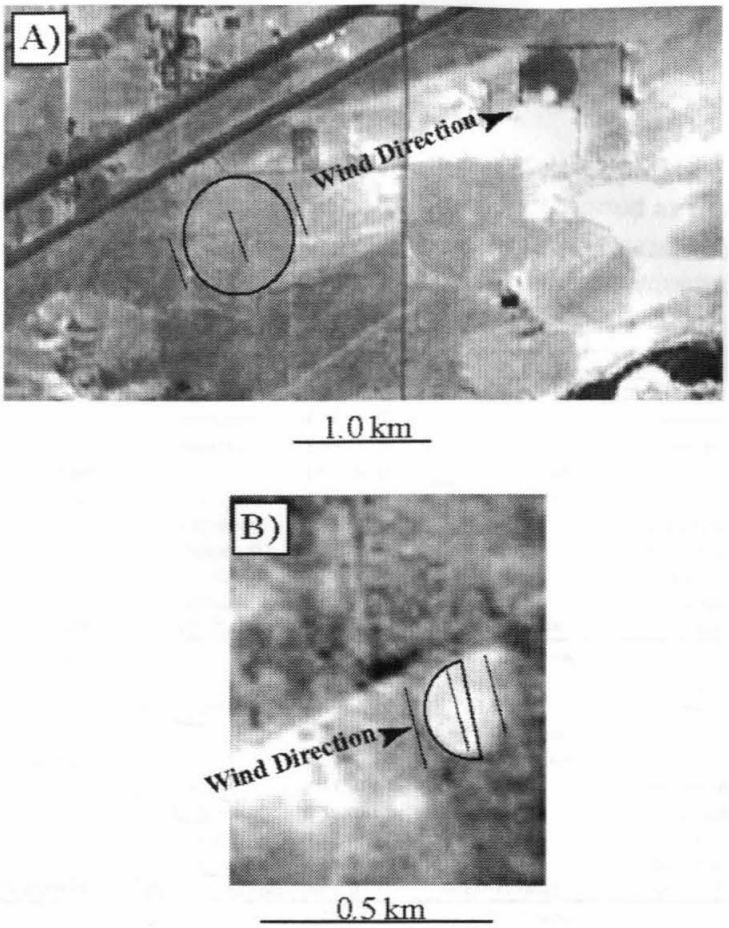

Figure 3-1. AVIRIS images of study sites.
A) AVIRIS image over set of central-pivot fields in the Manix Basin, southeastern California acquired August 28, 1997. The abandoned central-pivot agricultural field studied here is enclosed by the dark black line and the approximate locations of the sample transects are denoted by lighter lines. The redeposition of material eroded from the fields can be seen as brighter plumes downwind of the abandoned fields.
B) AVIRIS image over the scraped site, Jornada Basin, south-central New Mexico acquired May 27, 1997. The semi-circular scraped site is enclosed by the dark black, line and the approximate locations of the sample transects are denoted by lighter lines. The area downwind of the scraped site appears brighter than the surrounding desert due to sand blown off of the scraped site onto otherwise undisturbed desert.

Since its establishment in 1979, the sand blow-out associated with the abandoned agricultural field at Manix has expanded to several times the size of field itself. In Jornada, after only seven years since the initial disturbance at the scraped site, the sand blow-out associated with this feature is at least as large as the scraped site.

Table 3-1a. Means and *t*-test results for all populations and sub-populations for Manix samples. All numbers reported as μg/g soil. For *t*-test Results: U=Upwind, UIs=Upwind-intershrub, F=Field, D=Downwind, DIs=Downwind-intershrub, DId=Downwind-interdune, Dd=Downwind-dune.

Species	Population	Sub-population	Mean	C.V.	Species	Population	Sub-population	Mean	C.V.
N_{Avail}	*Upwind*		5.29	0.49	Cl	*Upwind*		3.92	0.38
		Intershrub	4.68	0.30			Intershrub	4.02	0.39
		Undershrub	7.63	0.60			Undershrub	3.53	0.33
	Field		14.1	0.57		*Field*		6.64	0.62
	Downwind		7.73	0.87		*Downwind*		4.41	0.54
		Intershrub	7.82	0.90			Intershrub	4.38	0.56
		Undershrub	6.71	0.24			Undershrub	4.74	0.41
		Dune	10.8	0.79			Dune	4.25	0.29
		Interdune	5.07	0.61			Interdune	4.54	0.68
t-test results		U<F>D, UIs<F>DIs, F>DId			***t-test results***		U<F>D, UIs<F>DIs, F>Dd		
Bicarb P	*Upwind*		3.35	0.23	SO_4	*Upwind*		6.27	0.37
		Intershrub	3.20	0.22			Intershrub	5.90	0.36
		Undershrub	3.99	0.19			Undershrub	7.76	0.34
	Field		4.29	0.34		*Field*		19.5	0.79
	Downwind		5.57	0.57		*Downwind*		7.73	0.43
		Intershrub	5.49	0.60			Intershrub	7.70	0.45
		Undershrub	6.59	0.32			Undershrub	8.13	0.29
		Dune	7.32	0.54			Dune	8.84	0.38
		Interdune	4.08	0.25			Interdune	6.78	0.46
t-test results		D>F>U, DIs>UIs<F, Dd>DId			***t-test results***		U<F>D, UIs<F>DIs, DId<F>Dd		
PO_4	*Upwind*		1.80	1.05	Na	*Upwind*		9.37	0.47
		Intershrub	1.47	0.90			Intershrub	9.60	0.48
		Undershrub	3.10	1.03			Undershrub	8.46	0.45
	Field		4.07	0.74		*Field*		28.3	1.29
	Downwind		5.12	0.73		*Downwind*		33.8	1.87
		Intershrub	5.09	0.76			Intershrub	36.3	1.79
		Undershrub	5.44	0.22			Undershrub	3.30	0.12
		Dune	7.52	0.54			Dune	28.1	2.70
		Interdune	3.06	0.52			Interdune	38.7	1.35
t-test results		D>U<F, DIs>UIs<F, F<Dd>DId			***t-test results***		U<F, UIs<F, F=Dd		
Mg	*Upwind*		n/a	n/a	K	*Upwind*		193	0.23
		Intershrub	n/a	n/a			Intershrub	193	0.23
		Undershrub	n/a	n/a			Undershrub	191	0.25
	Field		n/a	n/a		*Field*		258	0.40
	Downwind		n/a	n/a		*Downwind*		170	0.35
		Intershrub	n/a	n/a			Intershrub	167	0.35
		Undershrub	n/a	n/a			Undershrub	200	0.37
		Dune	n/a	n/a			Dune	155	0.48
		Interdune	n/a	n/a			Interdune	183	0.22
t-test results		n/a			***t-test results***		U<F>D, UIs<F>DIs, DId<F>Dd		
Ca	*Upwind*		n/a	n/a	Li	*Upwind*		0.40	0.30
		Intershrub	n/a	n/a			Intershrub	0.42	0.29
		Undershrub	n/a	n/a			Undershrub	0.32	0.19
	Field		n/a	n/a		*Field*		0.42	0.29
	Downwind		n/a	n/a		*Downwind*		0.38	0.44
		Intershrub	n/a	n/a			Intershrub	0.39	0.44
		Undershrub	n/a	n/a			Undershrub	0.28	0.27
		Dune	n/a	n/a			Dune	0.33	0.41
		Interdune	n/a	n/a			Interdune	0.43	0.43
t-test results		n/a			***t-test results***		none		

Table 3-1b. Means and *t*-test results for all populations and sub-populations for Jornada samples. All numbers reported as μg/g soil. For *t*-test Results: U=Upwind, UIs=Upwind-intershrub, S=Scraped Site, D=Downwind, DIs=Downwind-intershrub.

Species	Population	Sub-population	Mean	C.V.	Species	Population	Sub-population	Mean	C.V.
NA_{vail}	*Upwind*		35.7	0.94	Cl	*Upwind*		2.72	0.90
		Intershrub	29.9	1.34			Intershrub	2.44	0.94
		Undershrub	68.7	0.77			Undershrub	4.27	0.74
	Scraped Site		4.07	0.41		*Scraped Site*		3.80	1.34
	Downwind		6.59	0.98		*Downwind*		2.34	0.61
		Intershrub	5.83	0.97			Intershrub	2.37	0.62
		Undershrub	11.5	1.12			Undershrub	2.09	0.66
t-test results		D<U>S			***t-test results***		none		
Bicarb P	*Upwind*		11.2	0.63	SO_4	*Upwind*		9.05	1.84
		Intershrub	10.6	0.66			Intershrub	8.61	2.06
		Undershrub	14.8	0.50			Undershrub	11.5	0.92
	Scraped Site		2.36	0.66		*Scraped Site*		2.51	0.45
	Downwind		4.29	0.57		*Downwind*		1.67	0.69
		Intershrub	3.98	0.43			Intershrub	1.54	0.61
		Undershrub	6.32	0.83			Undershrub	2.57	0.81
t-test results		U>D>S			***t-test results***		S>D		
PO_4	*Upwind*		9.12	0.95	Na	*Upwind*		n/a	n/a
		Intershrub	7.94	0.89			Intershrub	n/a	n/a
		Undershrub	15.8	0.97			Undershrub	n/a	n/a
	Scraped Site		0.70	2.71		*Scraped Site*		n/a	n/a
	Downwind		3.05	0.46		*Downwind*		n/a	n/a
		Intershrub	2.85	0.35			Intershrub	n/a	n/a
		Undershrub	4.38	0.65			Undershrub	n/a	n/a
t-test results		U>D>S			***t-test results***		n/a		
Mg	*Upwind*		120	0.35	K	*Upwind*		337	0.22
		Intershrub	119	0.37			Intershrub	327	0.20
		Undershrub	122	0.20			Undershrub	390	0.30
	Scraped Site		98.7	0.34		*Scraped Site*		235	0.25
	Downwind		76.8	0.47		*Downwind*		215	0.28
		Intershrub	77.5	0.49			Intershrub	209	0.25
		Undershrub	72.6	0.40			Undershrub	251	0.40
t-test results		U>D			***t-test results***		D<U>S		
Ca	*Upwind*		1215	0.32	Li	*Upwind*		0.41	0.27
		Intershrub	1232	0.31			Intershrub	0.42	0.27
		Undershrub	1117	0.43			Undershrub	0.38	0.34
	Scraped Site		1490	0.34		*Scraped Site*		0.47	0.23
	Downwind		768	0.30		*Downwind*		0.33	0.27
		Intershrub	780	0.30			Intershrub	0.34	0.25
		Undershrub	694	0.25			Undershrub	0.31	0.43
t-test results		S>D<U			***t-test results***		S>D<U		

Table 3-2a. Significant (α=0.01) Pearson product-moment correlation coefficients for all species, by transect, for Manix samples.

		N_{total}	Bicarb P	PO_4	Mg^{+2}	Ca	Cl	SO_4	Na	K	Li
All Samples	N_{total}	1.00									
	Bicarb P	0.36	1.00								
	PO_4	0.35	0.68	1.00							
	Mg^{+2}	n/a	n/a	n/a	n/a						
	Ca	n/a	n/a	n/a	n/a	n/a					
	Cl	0.65	--	--	n/a	n/a	1.00				
	SO_4	0.73	--	--	n/a	n/a	0.80	1.00			
	Na	--	--	--	n/a	n/a	0.39	0.36	1.00		
	K	--	--	--	n/a	n/a	--	0.35	--	1.00	
	Li	--	--	-0.37	n/a	n/a	--	--	0.47	--	1.00
Upwind Transect	N_{total}	1.00									
	Bicarb P	--	1.00								
	PO_4	0.63	--	1.00							
	Mg^{+2}	n/a	n/a	n/a	n/a						
	Ca	n/a	n/a	n/a	n/a	n/a					
	Cl	--	--	--	n/a	n/a	1.00				
	SO_4	0.48	--	--	n/a	n/a	--	1.00			
	Na	--	--	--	n/a	n/a	--	--	1.00		
	K	0.41	--	--	n/a	n/a	--	0.62	--	1.00	
	Li	--	--	--	n/a	n/a	--	--	--	0.65	1.00
Field Transect	N_{total}	1.00									
	Bicarb P	--	1.00								
	PO_4	--	--	1.00							
	Mg^{+2}	n/a	n/a	n/a	n/a						
	Ca	n/a	n/a	n/a	n/a	n/a					
	Cl	0.77	--	--	n/a	n/a	1.00				
	SO_4	0.74	--	--	n/a	n/a	0.82	1.00			
	Na	0.65	--	--	n/a	n/a	0.63	0.69	1.00		
	K	--	--	0.69	n/a	n/a	--	--	--	1.00	
	Li	--	--	-0.53	n/a	n/a	--	--	0.64	--	1.00
Downwind Transect	N_{total}	1.00									
	Bicarb P	0.73	1.00								
	PO_4	0.85	0.79	1.00							
	Mg^{+2}	n/a	n/a	n/a	n/a						
	Ca	n/a	n/a	n/a	n/a	n/a					
	Cl	--	--	--	n/a	n/a	1.00				
	SO_4	0.56	0.61	0.58	n/a	n/a	--	1.00			
	Na	--	--	--	n/a	n/a	--	--	1.00		
	K	-0.44	--	--	n/a	n/a	--	--	0.50	1.00	
	Li	-0.39	--	--	n/a	n/a	--	--	0.53	0.58	1.00

Table 3-2b. Significant (α=0.01) Pearson product-moment correlation coefficients for all species, by transect, for Jornada samples.

		N_{Avail}	Bicarb P	PO_4^{-3}	Mg^{+2}	Ca^{+2}	Cl	SO_4	Na	K^+	Li
All Samples	N_{Avail}	1.00									
	Bicarb P	0.72	1.00								
	PO_4	0.84	0.83	1.00							
	Mg^{+2}	0.35	0.47	--	1.00						
	Ca	--	--	--	0.66	1.00					
	Cl	--	--	--	--	--	1.00				
	SO_4	0.56	0.75	0.76	--	--	--	1.00			
	Na	n/a	n/a	n/a	n/a	n/a	n/a	n/a	n/a		
	K^+	--	0.46	--	0.75	0.65	--	--	n/a	1.00	
	Li	--	--	--	0.64	0.73	--	--	n/a	0.42	1.00
Upwind Transect	N_{Avail}	1.00									
	Bicarb P	0.67	1.00								
	PO_4	0.82	0.87	1.00							
	Mg^{+2}	--	--	--	1.00						
	Ca	--	--	--	--	1.00					
	Cl	--	--	--	--	--	1.00				
	SO_4	--	0.87	0.82	--	--	--	1.00			
	Na	n/a	n/a	n/a	n/a	n/a	n/a	n/a	n/a		
	K^+	--	0.70	0.57	--	--	--	--	n/a	1.00	
	Li	--	--	--	0.68	0.66	--	--	n/a	--	1.00
Scraped Site Transect	N_{Avail}	1.00									
	Bicarb P	--	1.00								
	PO_4	--	0.98	1.00							
	Mg^{+2}	0.73	--	--	1.00						
	Ca	--	--	--	--	1.00					
	Cl	--	--	--	--	--	1.00				
	SO_4	--	--	--	--	--	--	1.00			
	Na	n/a	n/a	n/a	n/a	n/a	n/a	n/a	n/a		
	K^+	0.61	--	--	--	0.60	--	--	n/a	1.00	
	Li	--	--	--	--	0.84	--	--	n/a	--	1.00
Downwind Transect	N_{Avail}	1.00									
	Bicarb P	0.86	1.00								
	PO_4	0.57	0.57	1.00							
	Mg^{+2}	0.68	0.74	--	1.00						
	Ca	0.63	0.59	--	0.83	1.00					
	Cl	--	--	--	--	--	1.00				
	SO_4	0.92	0.85	0.68	0.70	0.67	--	1.00			
	Na	n/a	n/a	n/a	n/a	n/a	n/a	n/a	n/a		
	K^+	0.85	0.89	0.59	0.78	0.73	--	0.87	n/a	1.00	
	Li	0.48	0.53	--	0.55	0.60	--	0.53	n/a	0.55	1.00

4.2 Available Nitrogen (N_{Avail})

4.2.1 Manix

Samples from the abandoned field show the highest concentrations of N_{Avail}. Mean N_{Avail} concentration on the downwind transect is higher than the mean concentration on the upwind transect with 95% confidence. In the downwind transect, samples from dunes have higher mean N_{Avail} concentrations than samples from the interdune areas with 95% confidence. Samples from intershrub areas in both the upwind and downwind transects have lower mean N_{Avail} concentrations than samples from the abandoned field. The elevated nitrogen content on the abandoned field is likely due to the application and persistence of chemical fertilizer to the site.

Plant available P and N_{Avail} are significantly correlated in both the upwind and downwind transects. They are not correlated in the field transect.

4.2.2 Jornada

Results from *t*-test comparisons of means indicate that N_{Avail} is lowest on the scraped site, intermediate for the downwind transect, and highest on the upwind transect. Mean N_{Avail} concentrations from Jornada samples are much higher than those from the Manix Basin despite the fact that these soils have never been fertilized.

Plant available P and N_{Avail} are significantly correlated in both the upwind and downwind transects. They are not correlated in the scraped site transect.

4.3 Phosphorus

4.3.1 Manix

Concentrations of bicarbonate-extractable PO_4^{-3} and water-extractable PO_4^{-3} are significantly correlated (ρ=0.68, significant at α=0.01) for all samples. The regression of water-extractable PO_4^{-3} against bicarbonate-extractable PO_4^{-3} for all samples yields: PO_4^{-3} = -0.8 + 1.0*(bicarbonate-extractable PO_4^{-3}) with r^2= 0.47 and the slope of the regression line significant at α=0.01. The near-zero intercept and slope of unity for this regression suggest that water extraction of PO_4^{-3} provides a reliable measure of plant-available P in these soils.

Results from *t*-test comparisons of means indicate that plant-available P is more concentrated downwind, especially in dunes, than on the field itself, and that it is least concentrated in the upwind site. That plant-available P is more concentrated in the intershrub spaces in the downwind transect relative to those in the upwind transect reflects the fact that relatively small shrub canopies can give rise to relatively large phosphorus-enriched dunes. The elevated phosphorus content on the abandoned field is likely due to the application and persistence of P-containing chemical fertilizer on the site.

4.3.2 Jornada

Concentrations of bicarbonate-extractable PO_4^{-3} and water-extractable PO_4^{-3} are significantly correlated (ρ=0.83, significant at α=0.01) for all samples. The regression of water-extractable PO_4^{-3} against bicarbonate-extractable PO_4^{-3} for all samples yields: water-extractable PO_4^{-3} = -1.25 + 0.86*(bicarbonate-extractable PO_4^{-3}) with r^2= 0.69 and the slope of the regression line significant at α=0.01. Since the slope of this regression line is significantly below 1.0, water extraction of PO_4^{-3} in these soils does not provide a reliable means to measure plant-available P. However, high correlation coefficients between water extractable PO_4^{-3} and bicarbonate-extractable PO_4^{-3} indicates that water extractable PO_4^{-3} is a good index of plant-available P.

Results from t-test comparisons of means indicate that plant-available P is lowest on the scraped site, intermediate for the downwind transect, and highest on the upwind transect. Mean plant-available P concentrations from Jornada samples are much higher than those form the Manix Basin.

4.4 Other Species: Cl-, SO4-2, Mg+2, Ca+2, K+, Na+, Li+

4.4.1 Manix

Mean Cl^-, SO_4^{-2}, Na^+, and K^+ concentrations were all significantly higher in the field transect than the other two transects. The differences of the means from samples taken in the field and those from the upwind transect were 2.72, 13.2, 18.9, and 65 μg/g

for Cl^-, SO_4^{-2}, Na^+, and K^+, respectively. Mean concentrations of these ions were also significantly higher in samples taken from the field transect than those taken from the dunes in the downwind transect or the intershrub areas in the upwind transect. Mean Na^+ and SO_4^{-2} concentrations are higher on the downwind transect compared to the upwind transect with 95% confidence.

Chloride and SO_4^{-2} concentrations are also correlated with 95% confidence in samples from the downwind and field transects. Sodium concentrations are significantly correlated with Cl^- and SO_4^{-2} on samples from the field, but not significantly correlated in the other transects. For all three ions, concentrations in samples from intershrub areas in either the upwind or downwind transects (or both) are lower than those from the abandoned field. Chloride, SO_4^{-2}, and Na^+ concentrations are also significantly correlated with N_{Avail} in samples from the abandoned field.

Potassium concentrations are higher in the abandoned field than on the other transects. Concentrations from the abandoned field are also higher than in intershrub areas of the upwind and downwind transects. Potassium concentrations are significantly correlated with Na+ concentrations in the downwind transect.

Lithium concentrations were very low in all samples, and *t* tests between transects for lithium did not yield any significant relationships at the 99% confidence level. Significant correlations of Li^+ with Na^+ and K^+ were obtained in samples from the downwind transect.

4.4.2 Jornada

There is no obvious pattern of enrichment of Cl^-, SO_4^{-2}, Mg^{+2}, Ca^{+2}, K^+, and Li^+ in samples from any transect. Mean Ca^{+2}, SO_4^{-2}, and Li^+ concentrations are significantly higher on the scraped site relative to the downwind transect, possibly indicating that deflation of the scraped site has excavated $CaCO_3$ or $CaSO_4 \cdot 2H_2O$ illuvial horizons in these soils. The mean concentration of SO_4^{-2} on the upwind transect is higher than those on the scraped site and downwind with 95% confidence. Mean concentrations of Mg^{+2}, Ca^{+2}, and K^+ are lower on the downwind transect than the upwind transect.

Chloride and SO_4^{-2} concentrations are not significantly correlated with any other species on the scraped site and Cl^- concentrations are not significantly correlated with any other species on any other transect. This result is expected since the scraped site has never been irrigated.

In samples from the downwind transect, every measured species except PO_4^{-3} and Cl^- is significantly correlated with every other.

5. DISCUSSION

5.1 Salinization

The elevated concentrations of Cl^-, SO_4^{-2}, Na^+, and K^+ in the abandoned field in the Manix Basin compared to the upwind transect strongly suggest that salt has accumulated in the upper 5-cm of soil due to evaporation of irrigation water from the

field. That these ions are also significantly correlated with NO_3^- and N_{Avail} on the field suggests that these chemical perturbations are related, namely through cultivation.

Assuming that this field was cultivated for 7 years total, and that concentrations of these species in the upwind transect represent concentrations in the field prior to cultivation, Cl^-, SO_4^{-2}, Na^+, and K^+ accumulated at average rates of 0.4, 1.9, 2.7, and 9.3 μg/g year, or approximately 9.9, 30, 29, 4.9%/year, respectively. This is a dramatic addition of ions to the soil, which may limit the usability of these areas for extended agriculture.

5.2 Fertilization

The elevated concentration of available nitrogen in samples taken from the abandoned agricultural field at Manix is a clear indication that fertilizer was applied while this field was in active use. Plant-available P concentrations are also significantly higher in the field than in the upwind samples, indicating the addition of P-containing fertilizer. Concentrations of these nutrients are elevated after approximately 10 years of disuse, indicating the persistence of plant-available nutrients in this ecosystem.

Despite elevated N and P in the abandoned agricultural field at Manix, the absence of shrubs indicates that recolonization of fields by native shrubs is not simply related to nutrient content of the soils. Other factors such as soil compaction, wind erosion, or weather in the first few years after abandonment may account for the lack of vegetation on these fields. The presence in the Basin of other abandoned fields with total plant covers (*A. polycarpa*) higher than in undisturbed desert suggests that some

partially stochastic factor, such as weather, may control the regrowth of vegetation on abandoned fields.

In an experiment aimed at restoring Mojave Desert farmland by seeding native plants in order to reduce dust emissions, Grantz *et al.* (1998) found that by furrowing across the wind and direct seeding, they could establish *Atriplex canescens* in areas without deep sand. However, "this revegetation was achieved in an anomalous year with above average and late rainfall that eliminated early competition from annual species and later fostered abundant shrub growth. This success was not reproducible in more normal years, when minimal disturbance protocols such as broadcasting of seed on the untilled soil surface were as effective and less costly" (p. 1209). Thus, natural germination and regrowth of native perennial vegetation on abandoned fields may be rare, explaining the lack of cover on the field studied here. Bowers (1987) has suggested that allogenic factors affecting germination are also responsible for the establishment of winter annuals in the Mojave Desert. The importance of germination conditions, and in particular the timing and duration of precipitation, highlight the dramatic role of interannual variability and long-term regional climate on the response of this ecosystem to human disturbance.

5.3 Material Transport

The AVIRIS image in Figure 3-1B shows that in the samples from the Jornada Basin, the downwind soils were all derived from the scraped site. In addition, digging through the mantle of sand derived from the scraped site, the old pre-disturbance surface is apparent. In contrast to Manix, where dunes tend to be discreet objects in the lee of

shrubs separated by islands of the original surface, at Jornada, material blown from the scraped site has completely blanketed the adjacent downwind area. Surface soils upwind are richer in N_{Avail} and plant-available P than those from downwind, indicating an 80% net loss of available N and a 70% net loss of plant-available P from the soils blown off the scraped site. In addition, the scraped site itself lost nearly 94% of its N_{Avail} and nearly 79% of its plant-available P if the soils from the upwind transect are considered representative of the original condition throughout the study site. The loss of N and P from the surface soils dramatically impacts germination conditions for seeds in this area, and combined with other local environmental conditions—principally sand blasting from the scraped site—will reduce the establishment of new shrubs or grasses in these areas.

On the abandoned field in the Manix Basin, the addition of fertilizer for agriculture as well as other ions in irrigation waters provides an opportunity to probe the fate of material removed from the field by wind; field observations and remote sensing images (Figure 3-1) suggest that sand has blown off the agricultural field onto adjacent, downwind areas.

Significantly elevated concentrations of N_{Avail} (α=0.05) and plant-available P (α=0.01) on the field and the downwind transect relative to the upwind transect support this claim. Fertilizer, spread originally on the field for agriculture, has been spread across the landscape as the surface soil from the field has been eroded and transported by wind. Significantly elevated concentrations of Na^+ and SO_4^{-2} (α=0.05) on the downwind transect at Manix relative to the upwind transect suggest that salt species, added inadvertently during irrigation, have been spread with the moving sands.

Anthropogenic additions of soil nutrients and salt species to the abandoned field

at Manix provides us with the ability to examine the fate of soil removed from the field. Inferences may also be made about the texture of the mobilized soil. At the scraped site in the Jornada Basin, there have been no significant additions of chemical tracers (*i.e.*, fertilizer or salts) to the soil. Thus, the issue of whether soil blown off the scraped site is depleted of nutrients by winnowing and preferential removal of plant nutrients on dust particles available for long-range transport by wind suspension may be addressed. This signal is not apparent in the N_{Avail} and plant-available P data from Manix, possibly because the natural nitrogen and phosphorous concentrations were overwhelmed by fertilizer additions.

Leys and McTainsh (1994) and Larney *et al.* (1998) have suggested that soil nutrients and other chemical species are concentrated on small dust-sized particles in soils, and that wind erosion preferentially removes these particles, thereby depleting the soil of nutrients. The removal of material from the field onto downwind areas therefore may alter not only the soil chemistry, but the soil texture as well. In surface soils with a significant contribution of material eroded from a nearby disturbance, reduced clay content is thus expected due to this process of winnowing. At Jornada, mean Mg^{+2}, Ca^{+2}, K^{+}, and Li^{+} concentrations upwind of the scraped site are higher than downwind concentrations. Samples from the abandoned agricultural field at Manix also exhibit patterns suggestive of winnowing: Cl^{-}, SO_4^{-2}, and K^{+} display increased concentrations on the field relative to the material in the dunes. As long as all of the material in the dunes originated on the field, the observed difference in concentration indicates a net loss of these species, and the particles that carry them, by emission processes.

6. IMPLICATIONS FOR BIOGEOCHEMICAL DESERTIFICATION IN ARID SHRUBLANDS

A decade ago, Schlesinger et al. (1990) suggested a model for the degradation of semiarid grasslands. In their view, long-term grazing of grasslands leads to spatial and temporal heterogeneity of soil resources that promotes the invasion of shrubs. The presence of shrubs, in turn, enforces the localization of soil resources in islands of fertility by concentrating organic material below shrub canopies while intershrub spaces lose fertility through erosion and gaseous emissions.

The model hypothesis presented here that direct anthropogenic disturbance of arid shrublands that results in destruction of soil crusts and vegetation cover can lead to indirect disturbance of adjacent areas by initiating the disintegration of islands of fertility. The model hypothesis of degradation in arid shrublands states that aeolian mobilization of dust, sand, and litter triggered by anthropogenic disturbance contributes to the destruction of islands of fertility by killing shrubs through burial and abrasion. This interrupts nutrient-accumulation processes and allows the loss of soil resources by abiotic transport processes. The resulting reduction of vegetation cover, in turn, increases runoff and wind transport, reduces latent heat flux through evapotranspiration, and results in increased surface temperatures. These feedbacks can result in continuing reduction of vegetation cover and may contribute to regional climate change. The degradation process places arid shrublands in a landscape and process continuum between semiarid grasslands and Sahara-like hyper-arid barren lands.

The results presented here strongly support the model hypothesis of the

progressive degradation of arid shrublands associated with direct disturbance of the stable surface. In particular, they provide direct evidence that soil nutrients are depleted by wind erosion and redeposition. Removing the vegetation from the scraped site at Jornada has initiated a dramatic loss of nutrients from this ecosystem.

In addition, the scraped site provides an excellent example of the physical effects of degradation as ongoing saltation and aerosol fluxes remain higher here than anywhere else in the Jornada Basin (Gillette, 1999). Mesquite bushes growing near the scraped site exhibit severe branch abrasion and leaf stripping by wind. Grasses, once abundant, are now entirely absent. Regrowth of vegetation on the scraped site as well as in downwind areas is therefore limited by both the relatively low nutrient concentrations and the physical effects of blowing sand.

The results of this study also highlight the roles and interactions of climate and physical processes in initiating and propagating desertification in areas adjacent to direct disturbances. Elevated concentrations of available N and P on and adjacent to the abandoned fields in the Manix Basin have not contributed to vegetation regrowth. Indeed, sand blowing from the abandoned field has severely damaged the native vegetation and killed many individual plants. Human additions of N and P to this environment may not become significant until a period of increased available moisture. In the meantime, sand blowing off of the field will continue to denude vegetation downwind.

The removal of soil nutrients by wind from disturbed areas in deserts has important implications for human activities in arid regions. Areas adjacent to anthropogenic disturbances that remove vegetation cover, as well as the direct disturbances themselves, therefore, can be expected to become less fertile with time,

leading to progressive, expanding degradation and decreases in vegetation cover. Desertification of this sort can have serious environmental, agricultural, industrial, health, and safety consequences in arid lands as blowing sand destroys machinery and crops, covers roads, contributes to dust storms, and liberates airborne allergens and even pathogens. When informed by process models, remote monitoring tools may be used to identify areas at risk of runaway degradation before large areas are adversely affected.

Landscape processes necessarily exist in the context of regional climate and can either be supported or hindered by climatic conditions and changes, a fact that makes ultimate control of the extent of degradation climate-related. However, losses of plant cover can cause regional warming while aerosol production due to dust emission may contribute to global cooling. As a result, anthropogenic landscape change can contribute to regional climate changes and human activities in deserts are simultaneously subject to regional climate conditions and impacts upon them.

The vulnerability of arid lands to degradation argues for development of linked degradation process models and monitoring strategies in order to minimize environmental damage and to promote sustainable management of human activities in arid lands. This is particularly true in the face of global and regional socioeconomic factors which may compromise remediation strategies or promote inexpensive, but damaging, land-use practices.

CHAPTER 4

DISTRIBUTION OF VEGETATION IN WIND-DOMINATED LANDSCAPES: IMPLICATIONS FOR WIND EROSION MODELING AND LANDSCAPE PROCESSES

(*This chapter is in press in Journal of Geophysical Research-Atmospheres.*)

1. INTRODUCTION

Wind plays an important role in the evolution of arid and semiarid landscapes. While this is obvious in sand seas and sand dunes common in deserts, wind erosion is also a major component of landscape degradation (Ayoub, 1998; Bach, 1998; Barth, 1999; Çevik and Berkman, 1985; Darkoh, 1987; El-Baz *et al.*, 1985; Khalaf, 1989; Kishk, 1985; Leys and McTainsh, 1996; Luk, 1983; Wilshire, 1980; Zhao, 1985). Wind erosion tends to enforce the concentration of soil resources in islands of fertility (Schlesinger *et al.*, 1990). It is thus important to understand the detailed mechanisms by which wind interacts with the land surface.

By combining well-known relations between wind stress and saltation sand flux for sand sheets with relations between sand flux and dust emission by sandblasting, wind erosion models have been constructed which have been partly successful in predicting atmospheric mineral dust concentrations (Gillette and Passi, 1988; Marticorena *et al.*, 1997; Shao and Leslie, 1997). However, the effects of vegetation are not directly

included in these models. The effects of vegetation have been successfully modeled by approximating the form and spatial distribution of shrubs as solid hemispherical roughness regularly distributed elements on the soil (Musick and Gillette, 1990; Stockton and Gillette, 1990). The effect of randomly placed small vegetation patches has been modeled by considering vegetation primarily to cause a change in aerodynamic roughness length (Marticorena and Bergametti, 1995). However, for some vegetation, random placement is not observed and these models do not apply. For example, Phinn *et al.* (1996) have demonstrated systematic spatial patterns in Chihuahuan desert mesquite dunelands. For improved models of dust emission, we must understand the role of vegetation in mediating the interaction between the wind and the soil.

Recent research shows that desert areas dominated by mesquite (*Prosopis glandulosa*) plants, which have the same total vegetation biomass as other desert shrublands produce more dust by a ratio of about 4:1 to 8:1 (Gillette and Monger, 2000). Ground-based observations and investigations of aerial photographs led Dale A. Gillette (NOAA, Research Triangle Park, NC) to suggest that mesquite-dominated areas possess significantly elongated areas of bare soil (Figure 4-1). Further observations pointed to a possibility that these elongated areas of bare soil were preferentially oriented. Here, a "street" is defined in an anisotropic landscape with patchy vegetation as a patch of bare soil the width of which is much less than the length. Many streets may exist in a landscape, and streets can exhibit one or more preferred orientations. If such streets exist, and are preferentially oriented in the direction of the strongest winds, they may explain the high mass flux rates observed at mesquite sites compared to sites dominated by other kinds of vegetation.

Figure 4-1. Low-altitude oblique aerial photograph take of Fort Bliss, NM (Courtesy of H. C. Monger, New Mexico State University). At this site, which is approximately 100 km from the Jornada Long Term Ecological Research site, mesquite bushes are the principal vegetation in coppice dunelands. Notice the elongated "street" through the middle of the photograph.

The existence of streets in mesquite shrublands is a potentially important diagnostic feature for elevated dust production. The purpose of this study is three-fold: (1) using both field mapping and high spatial resolution aerial photographs, the existence of streets in mesquite dunelands are confirmed, (2) two image processing techniques that are able to identify the presence and orientation of streets and can be used generally to identify landscapes with streets are developed, and (3) the implications of streets for the evolution of arid and semiarid environments are addressed.

2. EXPERIMENTAL METHODS

2.1 Experimental Sites

The Jornada LTER site has 15 vegetation monitoring sites which represent the four dominant vegetation types in the basin: mesquite, creosote, tarbush, playa grasses, and non-playa grasses. The three net primary production monitoring sites dominated by mesquite plants (M-Nort, M-Rabb, and M-Well) were used for this study. Soils at these sites belong to the Onite-Pajarito association and Onite-Pintura complex which are principally comprised of sandy loam overlain by loamy sand (Bulloch and Neher, 1977).

2.2 Mapping and description of street length versus wind direction

Detailed vegetation maps were constructed at M-Nort, M-Rabb, and M-Well. Each of these sites possesses different vegetation coverage densities. Field mapping used a square grid with points every 0.5 meters. The grids used at M-Nort and M-Well were 50 m by 50 m and that used at M-Rabb was 50 m by 45 m. A cover map was produced which identified three plant categories found at each point of the grid: Mesquite, Perennials, and Yucca. These three categories (predominantly mesquite) covered all the plant types at the two sites. A fourth category was bare soil. The field maps were digitized and condensed into two categories: plant and bare soil.

The digitized maps were used to generate probability distributions for the length of bare soil area versus wind direction. For every grid point on the map, the length of

bare soil was measured at 12-degree compass intervals. This street length versus direction for each point on the grid allowed calculation of the probability distribution of street length versus direction.

Probability distributions of street length versus direction for the three sites were used to compute expected street length (integral of street length times probability of street length for all street lengths) versus wind direction for the three mesquite sites. The expected street length versus direction for the three sites was used to create plots for each site wherein the expected street length was extended from a central hub along its direction. By using 32 different directions at 12-degree intervals, a two-dimensional bare soil "rose" was drawn similar to a wind rose diagram (e.g., Figure 4-4). A rose diagram is a polar plot of some quantity—the expected street length, in this case—versus compass angle.

2.3 Image acquisition and processing

2.3.1 Digital Orthophoto Quads

Digital orthophoto-quads (DOQs) were obtained from the USGS and were chosen to include the three mesquite NPP sites. DOQs have a ground resolution of 1.0 m and are produced by digitizing USGS orthophoto quads. The aerial photographs that are the source data for these images were acquired in October, 1996. The 200 by 200 m subimages containing the mesquite NPP-monitoring sites were extracted from original images, and the red spectral band was used for all subsequent processing (Figure 4-2).

Digital number (DN) values in these images range from zero to 255 and

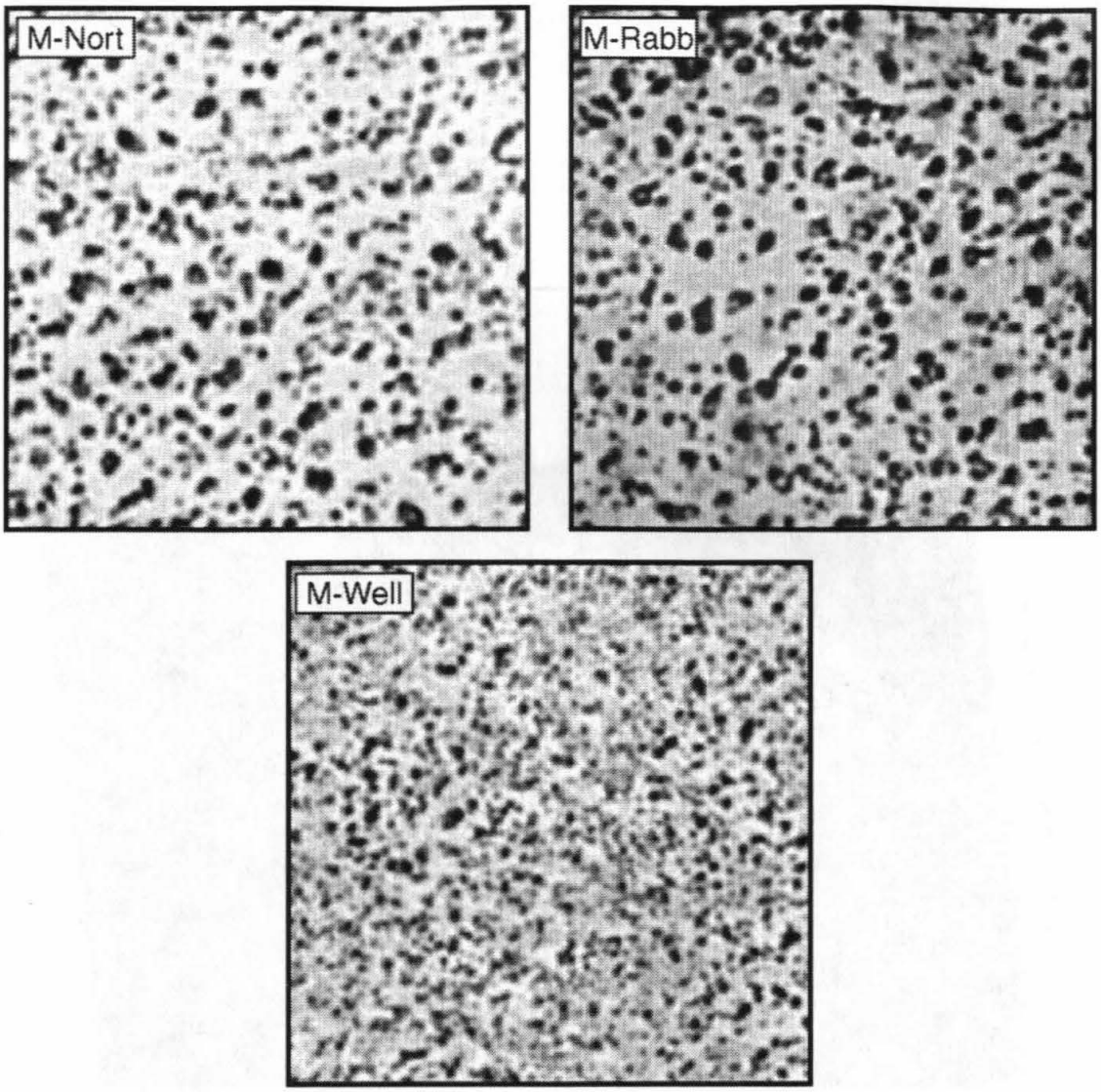

Figure 4-2. Images of the three mesquite dunelands sites used in this study. Images have 1-m resolution and are taken from United States Geological Survey Digital Orthophoto Quadrangles. Each image is 200 by 200 m and north is up. M-Nort and M-Rabb display large shrubs with large intershrub spacing while M-Well has smaller shrubs closer together.

discriminate between green vegetation (low DN values at red wavelengths) and bare soil (high DN values at red wavelengths). Since mesquite shrubs are generally larger than 1 m in diameter and are spaced more than 1 m apart, the resolution of the DOQs is smaller than the scale of spatial variability on the ground. This allowed identification of individual shrubs in the images and to apply two spatial analysis techniques to explore

the distribution of individual mesquite shrubs at each of the test sites.

2.3.2 Fourier Transform Analysis

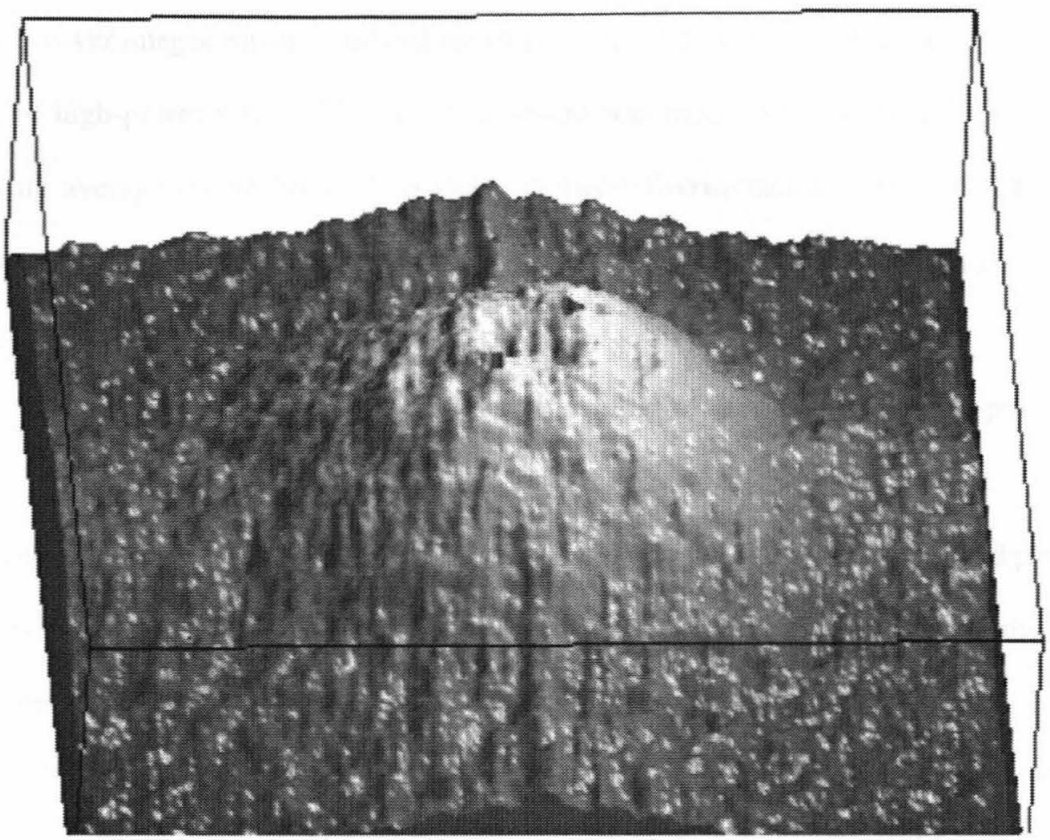

Figure 4-3. A smoothed (7 x 7) FT power image of the M-Nort site with power on the z-axis. The ring of high-power surrounding the center of the Fourier transform image was used to derive information of wavelength versus compass direction.

Two-dimensional Fourier transforms (FT) were performed on each of the mesquite-site subimages (Figure 4-2) using the fast-FT procedure in the Interactive Data Language (IDL version 5.3 for Unix). A log-power image was produced by calculating for each cell in the two-dimensional FT images:

$$log - power = \log_{10} \sqrt{(real)^2 + (imaginary)^2}, \qquad (1)$$

where *real* is the real portion of the FT spectrum for each cell and *imaginary* is the imaginary portion of the FT spectrum for each cell.

The resulting log-power images were characterized by a ring of high-power peaks, surrounding a strong, central zero-frequency peak. The zero-frequency offset peak in the power images was masked out for all subsequent processing steps leaving only the ring of high-power peaks. The resulting image was then smoothed by a 7 by 7 pixel moving average kernel filter. This step enhanced discrimination of the ring of high-power peaks and allowed identification of areas within it with relatively high power (Figure 4-3).

At a series of compass angles from the center of the image, the most powerful point in the high-power ring was found and its frequency was determined. These frequencies were then converted to wavelengths in normal spatial coordinates and plotted versus compass angle. These plots showed very little correlation with field results, and wavelengths were two to three times greater than actual average shrub spacing.

Therefore, a second approach was taken in order to highlight the angles at which the greatest degree of periodicity exists. In this approach, the most powerful point in the high-power ring was found for a series of compass angles from the center of the image, and its frequency and power was determined. The power was then re-scaled to the range of the expectation length from field mapping and was plotted versus compass angle. This approach does not allow for quantitative analysis of intershrub distances, but does allow identification of compass directions most likely to be aligned with streets.

2.3.3 Geostatistical Analysis

Unidirectional semivariograms were calculated for each image for compass angles between 90° and 270° with 2-degree intervals at lag distances from 0 to 50 m using the equation:

$$\gamma(h) = \frac{1}{2n}\sum_{i,j}(V_{t(i,j)+\boldsymbol{h}} - V_{t(i,j)})^2 \qquad (2)$$

where $\boldsymbol{h}$ is a vector with length equal to lag distance and compass direction between 90° and 270°, $\gamma(\boldsymbol{h})$ is the semivariance at $\boldsymbol{h}$, i is the east-west spatial coordinate, j is the north-south spatial coordinate, n is the total number of pixels considered, $V_{t(i,j)+\boldsymbol{h}}$ is the value of pixel at $(i,j)+\boldsymbol{h}$, and $V_{t(i,j)}$ is the value of the pixel at (i,j). Every point less than h from the edge of an image was used to calculate the semivariograms. Omnidirectional semivariograms were calculated by averaging unidirectional semivariograms over 180°. Since average shrub-shrub distance must be equal to the average distance between soil patches, no attempt was made to separate these two signals using semivariogram analysis. This is a general limitation of semivariance analysis.

3. RESULTS

3.1 Field Mapping Results

The field mapping at each site yielded two principal types of information: vegetation cover and estimates of expected street lengths as a function of compass angle. Vegetation cover at the three sites was 25.4%, 21.4%, and 15.7% for M-Nort, M-Rabb,

Table 4-1. The degree of development of streets and direction of street elongation using various methods. Elongation is the ratio of maximum length to minimum length for field mapping and semivariogram techniques.

		M-Nort	M-Rabb		M-Well
Field Mapping	Average width of soil patch (m)	11.7	10.3		9.38
	Direction of Elongation	45°	295°	25°	90°
	Elongation	1.33	1.48	1.18	1.25
Semivariogram Analysis	Average shrub-shrub distance (m)	15.5	13.2		10
	Direction of Elongation	78°	294° to 44°		n/a
	Elongation	1.42	1.17		1.00
FT Analysis	Direction of Elongation	40°	310°	27°	99°

and M-Well, respectively. These values for vegetative cover are low, but are reasonable for the mesquite coppice dunelands represented by each of these sites. The large amount of bare soil in these landscapes with vegetative cover concentrated in large, widely separated plants (Figure 4-2) suggests a high degree of soil nutrient heterogeneity. As a result, abiotic transport processes are likely to be more important in the distribution of soil resources than biotic transport processes (Schlesinger *et al.*, 1990). The observed larger mesquite plants and intershrub spacing at the M-Nort and M-Rabb sites relative to the M-Well site suggests that the concentration of soil resources in islands of fertility would be better developed at M-Nort and M-Rabb. Therefore, a preferred direction of streets would be better developed at these sites compared to M-Well.

Graphs of expected street length versus direction support this supposition, with M-Nort and M-Rabb displaying several dominant directions of elongation of bare soil areas between shrubs. M-Well, on the other hand, shows shorter average street lengths

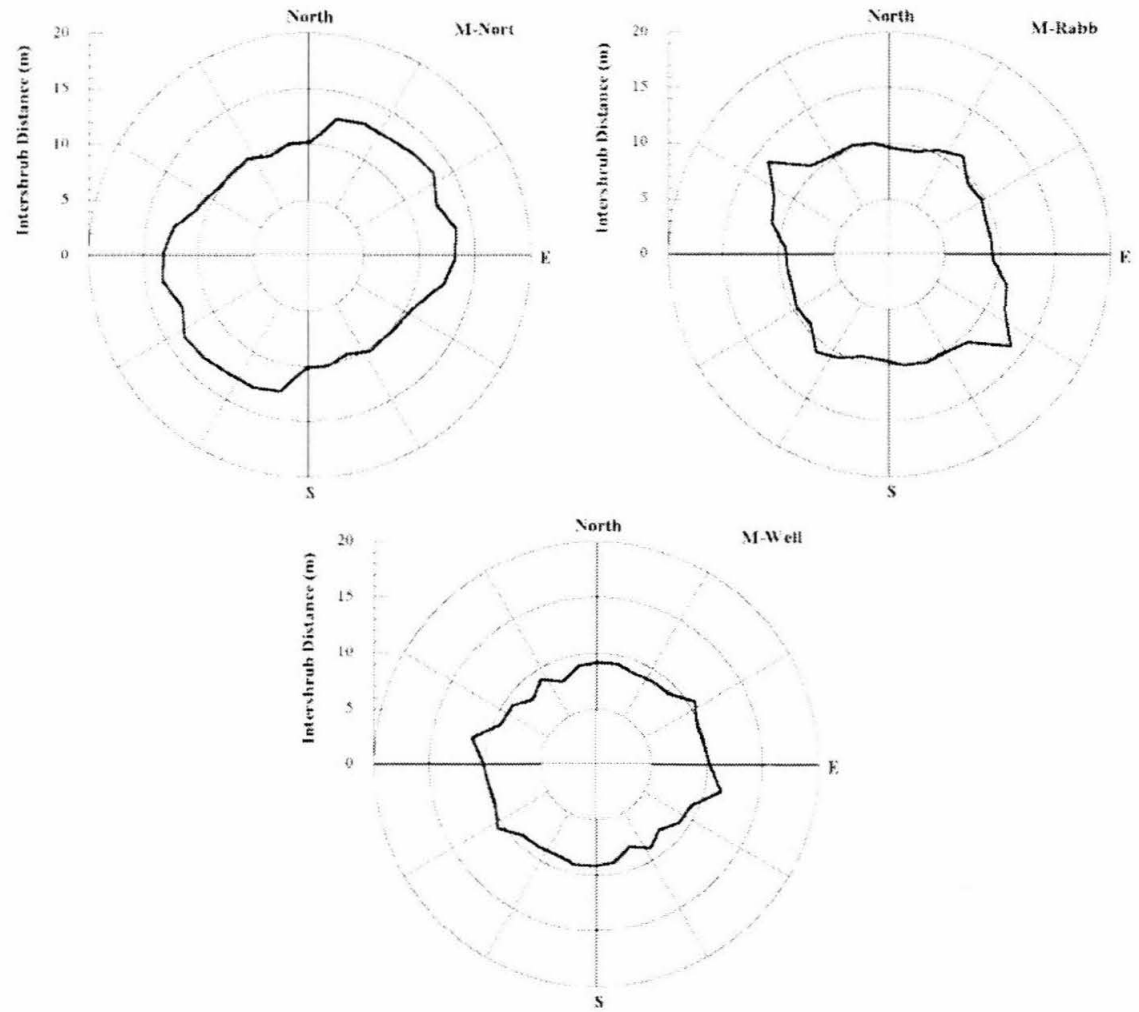

Figure 4-4. Expected street lengths versus compass direction from field mapping of M-Nort, M-Rabb, and M-Well.

with a poorly developed radial pattern (Figure 4-4). One index of the degree of development of streets at each site is "elongation"—the ratio of the maximum expected street length to the minimum expected street length (Table 4-1). Several points are clear. First, streets at M-Nort are better developed than at any other site. Second, streets at M-Rabb are less well-developed than those at M-Nort and there are two directions of elongation observed at this site. Third, streets at M-Well are the least well-developed and show weak east-west orientation.

Helm and Breed (1999) have reported that the majority of erosive winds blow principally towards the east-northeast or west-southwest at a site within 10 km of and on

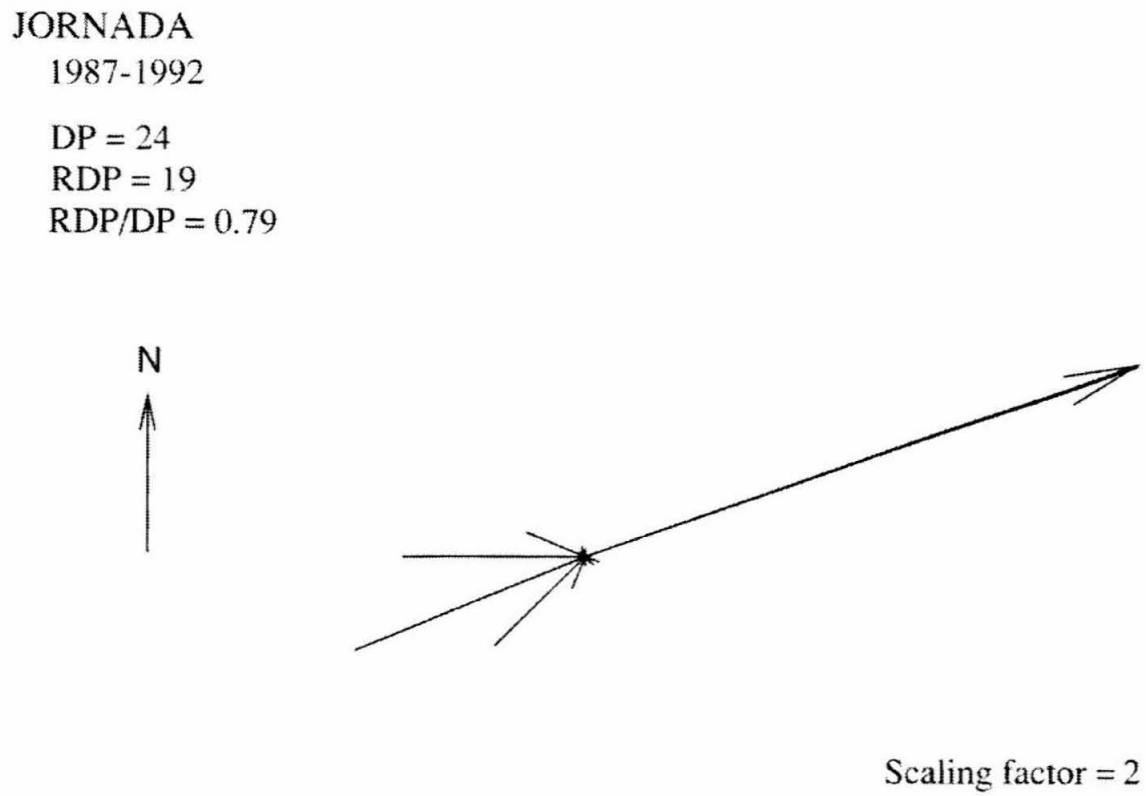

Figure 4-5. Sandrose for Jornada site. The sandrose is a circular histogram showing mean magnitude and upwind direction of the wind field. The length of the arms are proportional to the potential amount of sand drift from the upwind direction. The length of the resultant arm (arrow) is proportional to the potential net amount of sand moved toward the downwind direction. The lengths of the arms are derived using a weighting equation that applies only to wind speeds above threshold wind speed. The scaling factor is a linear reduction value used to scale the sandrose to the plotting area. DP, drift potential (sand moving capability of the wind from all directions); RDP, resultant drift potential (net sand-moving capability toward the resultant direction); RDP/DP, an index of directional variability of the wind field (1.00 = no variability). Figure from Helm and Breed (1999).

the same kind of topography as M-Nort, M-Rabb, and M-Well (Figure 4-5). Erosive winds are defined as winds with speeds greater than the wind erosion threshold. Field mapping results (Figure 4-4) from M-Nort indicate that streets are oriented with the dominant wind direction. At M-Rabb, one of the street directions is aligned with dominant direction of erosive winds, although this street orientation is less well developed than at M-Nort. At M-Rabb there is also a street direction aligned nearly perpendicular to the street direction at M-Nort.

3.2 Fourier Transform Analysis

The initial approach to FT analysis of the DOQ images at each of the sites (wavelength versus compass direction) bore little resemblance to field mapping results. The alternative approach, wherein peak power is plotted as a function of each compass angle, showed the same directions of elongation as were identified by the field mapping results (Figure 4-6, Table 4-1). Unfortunately, this approach is not able to yield

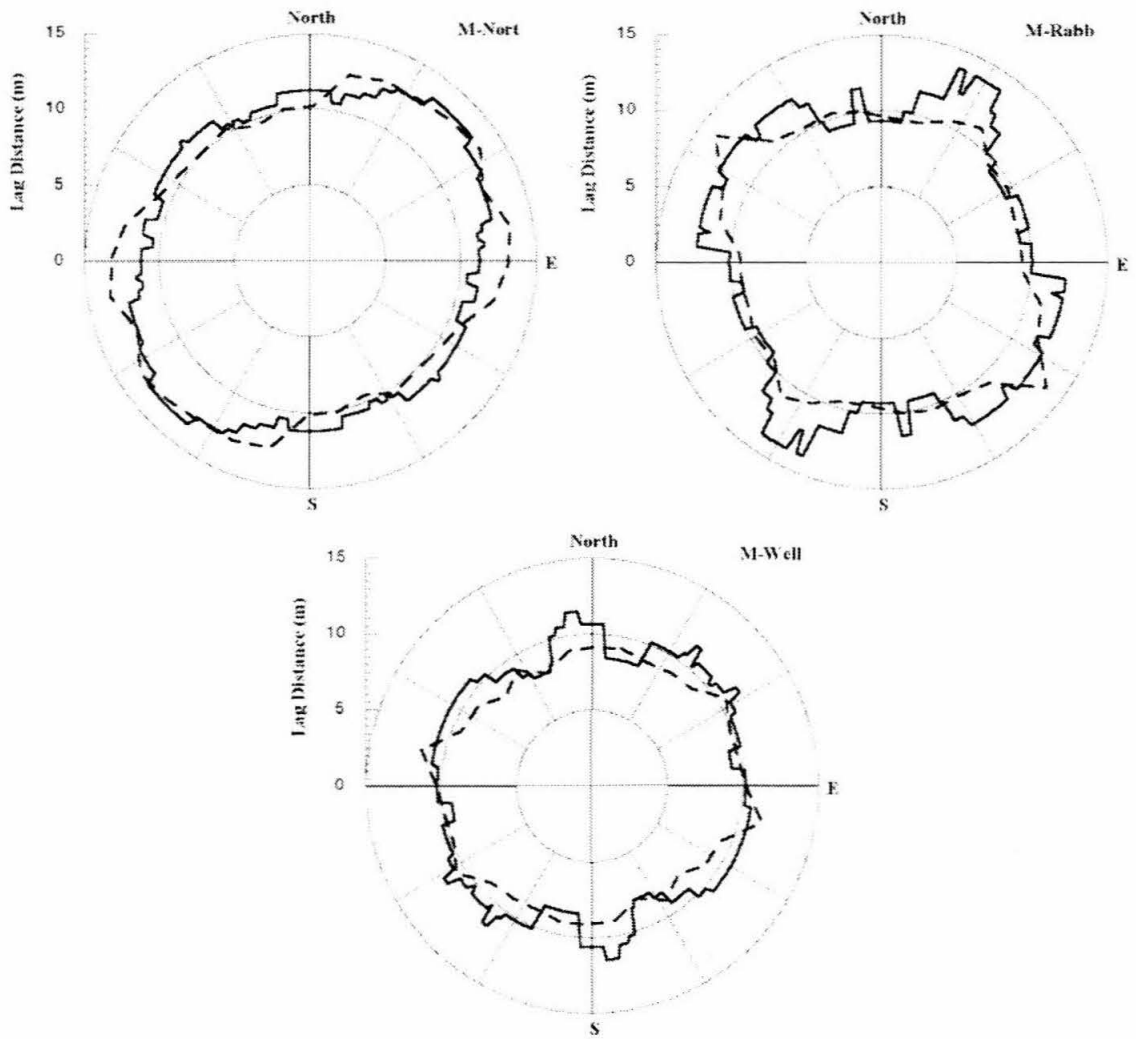

Figure 4-6. Total power times wavelength versus compass direction from Fourier transform analysis of images of M-Nort, M-Rabb, and M-Well, rescaled to the range of expected street length for each site. Dashed line is expected street length versus compass direction from field mapping.

quantitative information about the degree of elongation in these directions.

The reason for the success of the alternative approach to FT analysis in identifying preferred directions of elongation is not clear. It implies that the directions along which streets are preferentially oriented have a stronger periodicity than other directions. Non-random processes must be acting in these directions to enforce the observed periodicity. Wind is the most obvious process that may explain this phenomenon. I hypothesize that streets have a characteristic length and are superimposed on a landscape with more or less random shrub placement.

3.3 Geostatistical Analysis

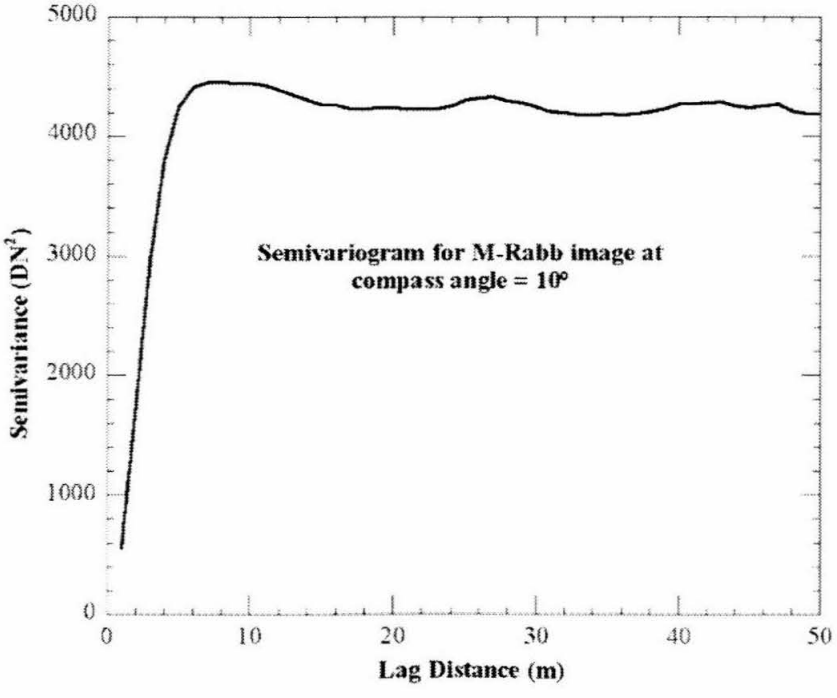

Figure 4-7. A sample unidirectional semivariogram from the M-Rabb site at 10° compass angle. Note the global maximum near a lag distance of 8 m and the sinusoidal "sill".

Unidirectional semivariograms calculated using Equation (2) do not exhibit typical behavior with a well-defined range and a flat sill. Rather, the regular dispersion of the mesquite shrubs gives the sills a weak sinusoidal shape after a very sharp rise to a local maximum (Figure 4-7) (see similar analyses in Phinn *et al.*, 1996; Schlesinger *et al.*, 1996). This is likely a manifestation of the "hole effect" which "reflects a tendency for high values to be symmetrically surrounded by low values, and vice-versa" (p. 55, Chilês and Delfiner, 1999). The hole effect is not present in omnidirectional semivariograms, indicating that the periodicity of shrub placement averages out over all directions and beyond some distance shrubs are randomly distributed. However, like unidirectional

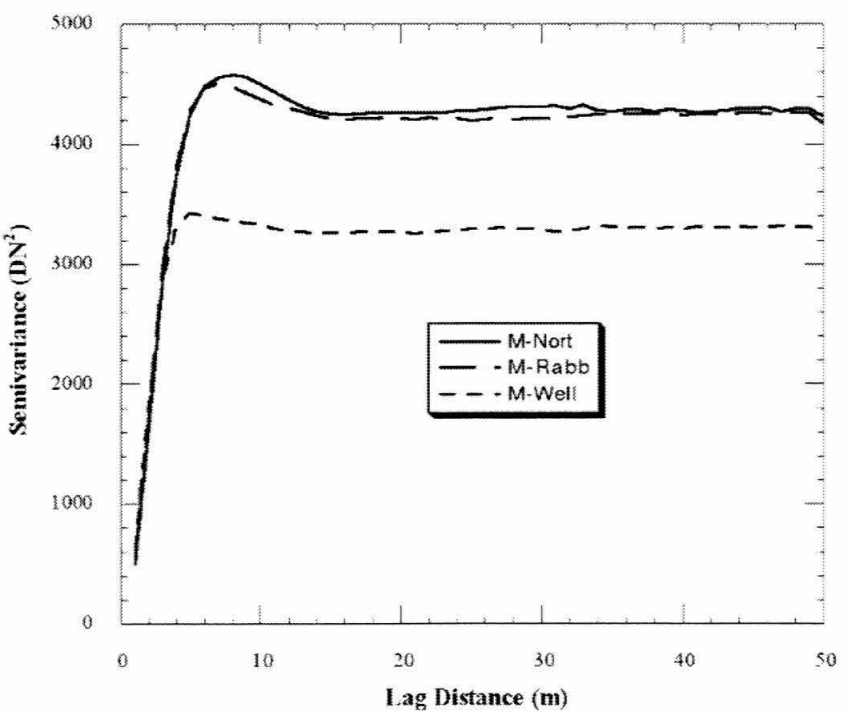

Figure 4-8. Omnidirectional semivariogram calculated from images of M-Nort, M-Rabb, and W-Well. Note that the sill is flat compared to unidirectional semivariograms (Figure 4-7). The location of the maximum for each semivariogram is equal to one-half the average intershrub spacing at each site.

semivariograms, omnidirectional semivariograms do exhibit a sharp rise to a global maximum (Figure 4-8).

The maxima in both omnidirectional and unidirectional semivariograms is due to the fact that soil and vegetation form discrete patches in the landscape. Since soil and shrubs display quite different DNs in the images, for distances equal to the average distance between the center of a shrub and the center of the soil patches around it, semivariance will be relatively high. As a result, the location of the maxima in both omnidirectional and unidirectional semivariograms is interpreted as one-half the average distance between the center of each shrub and the center of its closest neighbors (in a certain direction, for unidirectional semivariograms). Multiplying the lag distance at which this maximum appears by two therefore yields average distance between the center of each shrub in the images and the center of its neighbors. Plots of the average shrub-shrub distance versus compass angle give an indication of the development of streets at each of the sites and display a reasonable correlation with field results, especially at M-Nort (Figure 4-9). The shrub-shrub distances derived from omnidirectional semivariograms are larger than the distances between shrubs obtained from the field results (Table 4-1). This is simply because the field results and semivariogram results are measuring slightly different things: shrub-shrub distances from the semivariograms include the average width of the shrubs while expected street lengths from field mapping do not. The difference between these two therefore will yield average shrub width, assuming that shrubs themselves are roughly circular. M-Nort displays the largest average shrub width (3.8 m), M-Rabb has an intermediate average shrub width (2.3 m), and M-Well displays the smallest average shrub width (0.62 m). This result is consistent

with visual inspection of the DOQ subimages at each site (Figure 4-2) and supports the idea that islands of fertility are better developed at M-Nort and M-Rabb than at M-Well.

Analysis of the preferred direction of elongation of shrub-shrub distances and elongation in that direction (Table 4-1) shows that results from the semivariogram analysis are consistent with both the field mapping results and the FT analysis results. Semivariogram analysis was not able to identify two discreet street orientations at M-

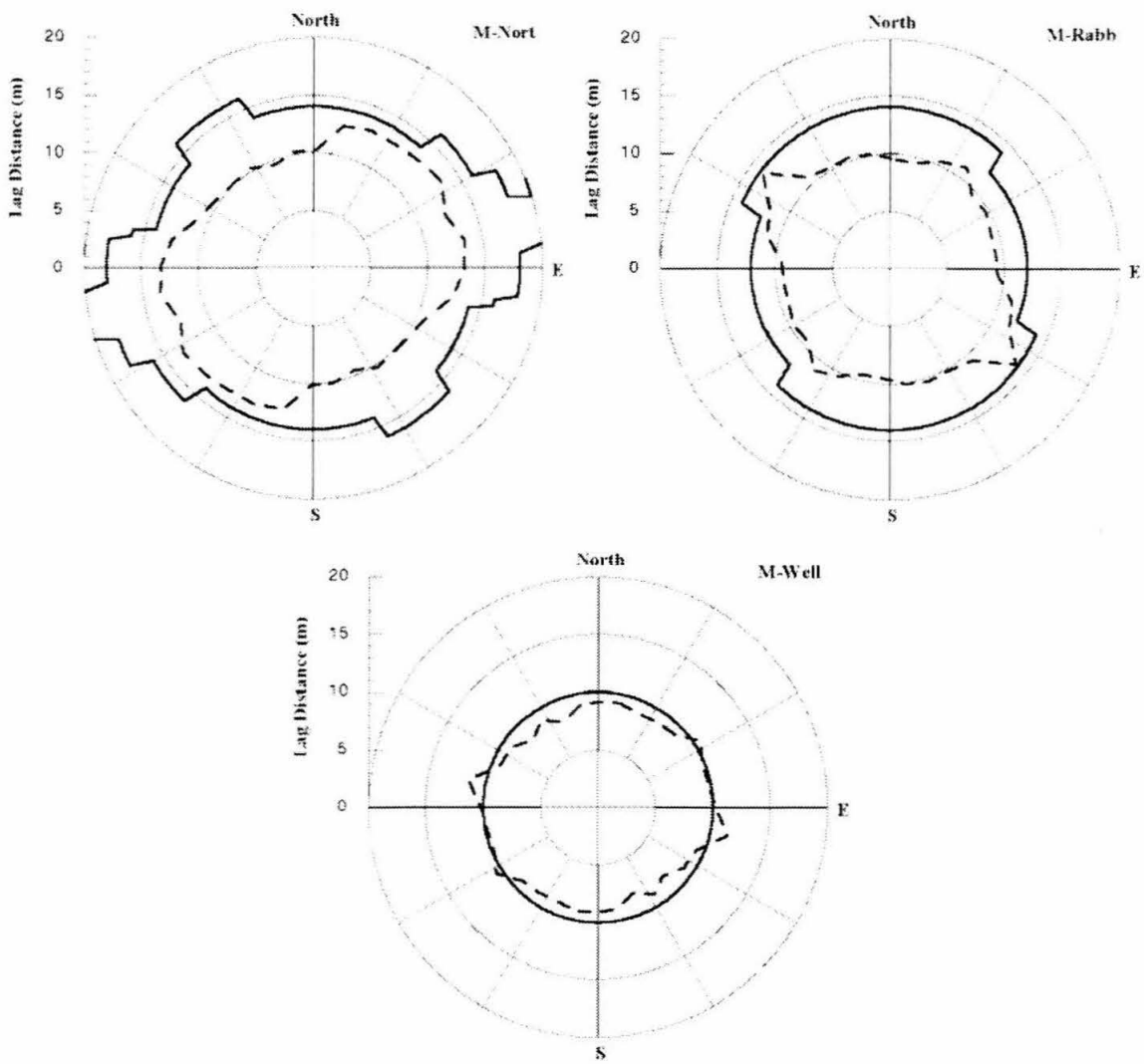

Figure 4-9. Shrub-shrub distance versus compass direction from unidirectional semivariogram analysis of images of M-Nort, M-Rabb, and M-Well. Dashed line is expected street length versus compass direction from field mapping.

Rabb, identifying instead a broad region of elongation between the two directions identified by the field mapping results. In addition, semivariogram analysis was not able to identify a preferred direction of elongation at M-Well. Nonetheless, semivariogram analysis of DOQ images at each of the sites confirmed the assessment of the degree of development of streets at each of the sites. Street development is most prominent at M-Nort which has the highest elongation ratio, it is intermediate at M-Rabb, and streets are poorly developed at M-Well, which has the lowest elongation ratio (~1).

4. DISCUSSION

4.1 The length and spacing of streets

Field mapping as well as FT and geostatistical analysis of DOQs from two of the three mesquite duneland sites suggest the existence of streets. At the third site, M-Well, islands of fertility are poorly developed and there does not appear to be any preferred direction of elongation. Relative to field mapping, the elongations from FT and semivariogram analysis give a poor indication of the characteristics of streets.

There are at least two different distributions of mesquite which might explain elongation of intershrub spaces at preferred directions. In the first distribution (Case I), every soil patch is slightly elongate and has approximately the same size (Figure 4-10). Alternatively, consider a landscape in which soil patches are typically not elongate and all have the same size. In this second type of mesquite distribution, several consecutive shrubs in one direction are "missing", forming a street, with the effect that the average soil patch is elongate (Case II). In this case, for a regular array of plants, it can be shown

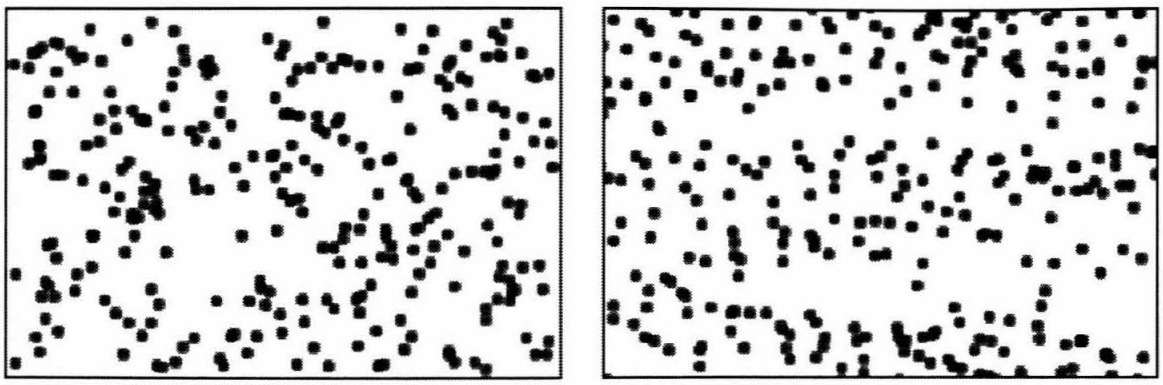

Figure 4-10. Two possibilities to explain the observed elongation of intershrub distances from field, FT, and geostatistical analyses. Case I: shrubs are uniformly distributed with average intershrub distance greater in horizontal direction. Case II: streets exist as a few long areas of bare soil interspersed in areas where mesquite have intershrub distances near the average.

that:

$$Average\ Elongation = \frac{1}{1 - ac(n-1)}, \tag{3}$$

where a is average intershrub spacing without streets, c is the concentration of streets expressed as streets per meter in the street-ward direction, and n is an integer that expresses the length of the streets measured in units of a. A measure of street density with units of streets per plant is defined as $C=ac$, which must be between 0 and 1. Equation (3) is subject to the constraint that $C < (n\text{-}1)^{-1}$ to avoid having a negative number of plants.

Equation (3) allows correlation of the elongation in a particular direction with the expected concentration of streets along that direction. For example, if streets are three times as long as the average intershrub spacing of 10 m ($n=3$, $a=10m$), then for an average elongation of 1.5 the concentration of streets must be 0.0167 m^{-1}. In other words, streets are separated from each other in the street-ward direction by 60 m in this case.

Previous field and laboratory experiments allow evaluation of the two possible cases for distributions of mesquite at Jornada (Case I and Case II). Wind tunnel experiments by Minvielle *et al.* (1999) simulated mesquite bushes arranged so that streets were present. Measured turbulent intensities show the existence of a wake for distances approaching an order of magnitude greater than the height of the simulated mesquite bushes. Thus, downwind of the simulated mesquite bushes, there is a zone of protection that lowers winds for distances of up to an order of magnitude greater than the height of the bush. In the streets, there is no zone of protection.

Gillette and Monger (2000) have shown that desert areas dominated by mesquite having the same biomass as other shrubland areas produce more dust by a ratio of about 4:1 to 8:1. Minvielle *et al.*'s (1999) laboratory simulations show that this observed increase in dust production could not result from Case I, where street-ward shrub spacing has to be at least ten times the average shrub height. For reasonable elongations (1.5) and mesquite dune heights (2 m), average shrub spacing would have to be approximately 20 m. This average distance between shrubs is greater than that from field and geostatistical analysis of mesquite sites at Jornada. Furthermore, in a field experiment, Gillette and Chen (2000) have reported that sand fluxes show a monotonic increase as the upwind distance from the shelter of vegetation increases. This supports Case II, where dust production is enhanced by a few large-fetch areas. Finally, field results indicate that very long streets (32 to 64 m) are much more probable in street-ward directions compared to cross-street directions (Figure 4-11). Streets exist in mesquite dunelands as a few long (relative to average shrub spacing) areas of bare soil interspersed in areas where mesquite have more average distances between shrubs.

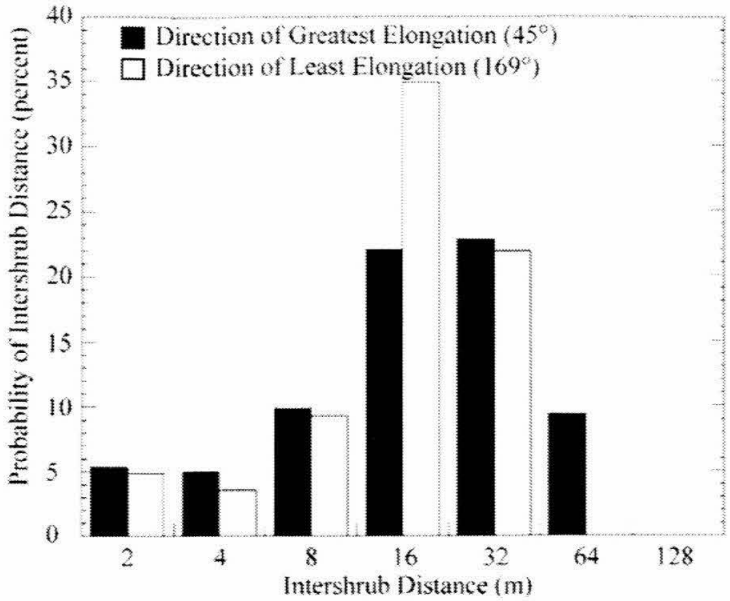

Figure 4-11. Probability of areas of continuous bare soil with length given on the x-axis at the M-Nort site for the direction of greatest and least elongation. Probability of intershub spaces at 169° for distances longer than 32 m is zero.

4.2 Implications for wind erosion modeling

Semivariogram and FT analysis of 1-m DOQs may be used to identify areas where streets exist and the principal street orientations. Thus, they provide important information for wind erosion modeling in arid and semiarid areas, because areas with streets are likely to exhibit increased wind erosion relative to areas without streets with the same vegetation biomass. All current mathematical models of wind erosion which take vegetation into account assume homogenous distribution of plants (see, for example, Wolfe and Nickling, 1993). Areas with streets are markedly anisotropic and exhibit increased wind erosion and dust production. New methods to estimate wind erosion must be developed which take this anisotropy into account.

4.3 Implications for landscape processes

Desertification has been defined as the loss or spatial redistribution of net primary productivity in arid and semiarid lands (Schlesinger *et al.*, 1990). The islands of fertility, centered around large perennial shrubs, that result from desertification processes are enforced by abiotic transport in degraded lands. Recent work by Schlesinger *et al.* (1999) has shown that increased water erosion can lead to increased losses of plant-available N and enforcement of islands of fertility in degraded semiarid landscapes. Klausmeir (1999) has shown that water erosion can produce inhomogenous vegetation distributions, and therefore islands of fertility, even in very low relief landscapes. This work on streets in mesquite dunelands indicates that wind, also, plays a role in the enforcement of islands of fertility and may be an important factor in landscape evolution as homogenous distributions of soil resources in grasslands are supplanted by heterogeneous distributions in shrublands.

In particular, the alignment of streets at both the N-Nort and M-Rabb sites with the prevailing direction of erosive winds indicates that wind itself played a vital role in the evolution of this landscape as it made the transition from grassland to shrubland in the last 150 years (Buffington and Herbel, 1965). I hypothesize that as the landscape became increasingly infested with woody shrubs, areas between shrubs became the sites of wind erosion. As the most erosive winds typically blow from one principal direction at Jornada, areas of bare soil that were aligned with the prevailing wind (proto-streets) saw a number of effects that more protected areas did not. These effects include:

(1) Increased saltation of sand grains and sand-blasting of plants in the proto-streets leading to increased mortality of plants in these areas, particularly seedlings and grasses with little effect on the wind profile,

(2) Increased plant evapotranspiration, and therefore greater water stress, of plants in the proto-streets leading to suppressed growth of plants in these areas,

(3) Increased winnowing of fine particles in the proto-streets leading to decreased water-holding capacity and nutrient availability in these areas (see Chapter 2), and

(4) Depletion of the seed bank in proto-streets as light, wind-movable seeds were progressively blown out of these areas.

The combined effect of the increased wind activity in the proto-streets suppressed vegetation in these areas, leading to the establishment of mature streets which remain areas of increased wind erosion and dust production. The effect of wind in the development of landscape structure would be greatest in areas with fine-grained soils susceptible to wind erosion. Grassland to shrubland transitions in landscapes with wind-stable soils are not as likely to develop streets, because winnowing of fines and sand blasting would be smaller (see Chapter 2).

Mature streets, even if they are not aligned with the prevailing wind direction such as one of the street directions at M-Rabb, are self-enforcing phenomena. When the wind does blow in the direction of a street, it is the site of increased wind erosion, even if it is not oriented with the prevailing wind. A few storms a year with winds aligned with a street, combined with other elements of inter-shrub competition for soil resources, may

be all that is needed to prevent new plants from growing in established streets. Thus, once a fabric of streets is established, it is likely to be a permanent feature in the landscape.

Even in landscapes with wind-erodible soils, street development may not be ensured. At the M-Well site, little street development is seen though this site underwent grassland to shrubland conversion at approximately the same time as the other sites (Buffington and Herbel, 1965). This may be due to the fact that this site is underlain by a thick, impermeable caliche layer which may have been exposed by wind erosion near the time of mesquite establishment. The resulting shallow rooting zone therefore is less amenable to deep-rooted mesquite and inhibits their growth. This may explain the larger number of smaller mesquite at this site, because the close spacing of mesquite at this site is likely due to the shallow rooting zone instead of wind effects. The close spacing of mesquites at this site also may help explain the absence of well-developed streets. In order for streets to develop, bare areas at least ten times the average shrub height are required. At M-Well, however, mesquite are closely spaced and thus street development is inhibited. This analysis suggests that water availability is more important than wind-related stresses in determining vegetation distribution.

Schlesinger *et al.* (1990) suggested that the development of shrub-centered islands of fertility associated with the degradation of semiarid grasslands was accompanied by a net loss of nutrients as the transition from grassland to shrubland occurred. This has been verified by Schlesinger *et al.* (1996) in a subsequent paper with detailed soil analyses in a variety of arid shrubland and semiarid grassland environments. In ongoing work on the role of surface runoff, Schlesinger *et al.* (2000) have concluded that loss of soil nutrients

by hillslope runoff cannot, by itself, account for the depletion of soil fertility associated with desertification in the Chihuahuan Desert.

Alternatively, wind erosion may prove to be a mechanism to explain widespread nutrient loss in degraded arid and semiarid environments. The elevated dust emission observed in mesquite shrublands may contribute to the observed and postulated loss of nutrients from these landscapes (Schlesinger *et al.*, 1996; Schlesinger *et al.*, 1990). N and P are concentrated on wind-erodible particles which are removed permanently by wind erosion (Larney *et al.*, 1998; Leys and McTainsh, 1994). Soil N and P concentrations at nearby site in the Jornada Basin are included in Chapter 3. These results suggest a five-fold net loss of available N and a three-fold net loss of plant-available P from a site free of vegetation during the eight years, indicating that wind erosion impacts soil fertility in actively deflating areas. Further work should be pursued to address the role of wind in removing nutrients from degraded landscapes and as well as the role of wind in enforcing islands of fertility in shrublands.

5. CONCLUSIONS

The existence of streets in areas of mesquite shrubs is a potentially important factor enhancing dust production. The purpose of this study was to: (1) confirm the existence of streets in mesquite dunelands, (2) develop image processing techniques that are able to identify the presence and orientation of streets and can be used generally to identify landscapes with streets, and (3) address the implications of the existence of streets for the evolution of arid and semiarid environments.

Through the use of field mapping as well as FT and semivariogram analysis,show that mesquite dunelands in the Chihuahuan Desert of southern New Mexico, USA, have inhomogenous shrub distributions. Streets exist in these landscapes but may be better developed in some areas compared to others. Soils in the streets are not protected from winds blowing down the streets and may therefore produce more dust than if vegetation were more evenly distributed. This may partially explain discrepancies between observed and predicted atmospheric dust concentrations. New models to incorporate the existence of streets are required if models of dust flux are to be realistic for these landscapes. The existence of streets also implies that wind plays a major role in the evolution of vegetated arid and semiarid landscapes with wind-erodible soils. Wind enforces islands of fertility centered around individual shrubs, prohibits vegetation growth between shrubs, and may provide an explanation for reduced soil fertility observed in shrublands. Further work is required to clarify the role of wind erosion in the degradation of semiarid landscapes undergoing grassland to shrubland conversion.

PART II

REMOTE MONITORING

After process modeling, remote monitoring forms the next step in promoting sustainable land use in arid and semiarid environments. Remote sensing is a time- and cost-efficient method for surveying and identifying the world's vast and fragile drylands. In Part II, remote sensing tools for dryland monitoring are evaluated. Chapter 5 is dedicated to establishing practical limits on the retrieval of vegetation information from hyperspectral remote sensing data in arid and semiarid environments. The potential utility of hyperspectral remote sensing in enhancing multispectral (Landsat-class) remote sensing is also discussed. In Chapter 6, the prospects for and challenges of using remote sensing in effective dryland monitoring are discussed.

CHAPTER 5

PRACTICAL LIMITS ON HYPERSPECTRAL VEGETATION DISCRIMINATION IN ARID AND SEMIARID ENVIRONMENTS

(*Much of this chapter is in press in Remote Sensing of Environment.*)

1. INTRODUCTION

Concerns over global land use and land cover change are rising as we strive to understand the impact of human activities on our planet. Remote sensing, using current or anticipated technology, is widely viewed as a time- and cost-efficient way to proceed with large-scale monitoring (Hall *et al.*, 1995). Indeed, remote sensing techniques and technologies are likely to afford the best opportunities to detect regional- or global-scale environmental change. However, the low vegetation cover of arid regions poses a significant obstacle to the fulfillment of this goal. With high hopes for these technologies, it is important to understand their limits.

In this paper the limits of multiple endmember spectral mixture analysis (MESMA) in soil and vegetation parameter retrievals are explored. MESMA is a modified spectral mixture analysis (SMA) approach in which many mixture models are calculated for each pixel in an image (Roberts *et al.*, 1998; Roberts *et al.*, 1997a). The basic SMA method estimates the proportion of each ground pixel's area that belongs to different cover types (Adams *et al.*, 1993; Gillespie *et al.*, 1990; Settle and Drake, 1993;

Shimabukuro and Smith, 1991; Smith *et al.*, 1990). SMA is based on the assumption that the spectra of materials in an instrumental instantaneous field of view (IFOV) combine linearly, with proportions given by their relative abundances. A combined spectrum thus can be deconvolved into a linear mixture of its "spectral endmembers"—spectra of distinct materials in the IFOV. The weighting coefficients of each spectral endmember, which must sum to one, are then interpreted as the relative area occupied by each material in a pixel.

SMA is particularly amenable for use with imaging spectrometry data where the number of useful bands is much higher than the number of model endmembers. Roberts *et al.* (1998; 1997b; 1993) have used linear mixture analysis of AVIRIS data to map green vegetation, nonphotosynthetic vegetation (NPV), and soils at the Jasper Ridge Biological Preserve and in the Santa Monica Mountains, CA. García-Haro *et al.* (1996) have applied SMA to high spectral resolution field spectroscopy in the detection of vegetation, finding it to be less sensitive to soil background than the normalized difference vegetation index (NDVI). Painter *et al.* (1998) have applied SMA to AVIRIS data acquired over snow-covered areas in the Sierra Nevada to estimate snow grain size. Most of these studies have used a least squares approach to estimate the fraction of each ground pixel belonging to each endmember.

The unique capabilities of imaging spectrometers have proven useful for SMA in a variety of different land-cover types with significant plant cover. In contrast, the quantitative detection of sparse vegetation in remote sensing imagery, and hence in many arid and semiarid areas worldwide, remains problematic. Few investigators have used hyperspectral data for the quantitative detection of vegetation at low covers (see for

example, Chen *et al.*, 1998; Elvidge *et al.*, 1993). Previous work by the current authors to retrieve vegetation type and cover from AVIRIS imagery met with only limited success (Okin *et al.*, 1998; Okin *et al.*, 1999). In order to determine the causes of our earlier difficulties, and to determine the limitations of SMA in arid regions, the current study was undertaken.

Quantitative retrieval of vegetation type, cover, biomass, or leaf area index (LAI) in areas of low cover is affected by several factors:

1) A large soil background in arid and semiarid regions, where soils can be bright and mineralogically heterogeneous, masks the spectral contribution of plants (Escafadel and Huete, 1991; Huete and Jackson, 1988; Huete *et al.*, 1985; Smith *et al.*, 1990).
2) There is the potential of nonlinear mixing in arid and semi-arid regions due to multiple scattering of light rays (Huete, 1988; Ray and Murray, 1996; Roberts *et al.*, 1993). Nonlinear mixing is likely to lead to an overestimation of green vegetation cover and an underestimation of shade.
3) Evolutionary adaptations to the harsh desert environment make desert plants spectrally dissimilar from their humid counterparts, in many cases lacking a strong red edge, exhibiting reduced leaf absorption in the visible, and displaying strong wax absorptions around 1720 nm (Billings and Morris, 1951; Ehleringer, 1981; Ehleringer and Björkman, 1976; Ehleringer and Björkman, 1978; Ehleringer and Mooney, 1978; Gates *et al.*, 1965; Mooney *et al.*, 1977; Ray, 1995).
4) Spectral variability within shrubs of the same species can be high in arid

and semiarid regions, as reported by Franklin *et al.* (1993) and Duncan *et al.* (1993). Rapid movement of many desert shrubs through phenological changes in response to small amounts of spatially-discontinuous precipitation can contribute to this effect.

5) Desert shrubs often display open canopies which contribute to poor correlations with leaf area index (LAI) (Hurcom and Harrison, 1998). Roberts *et al.* (1990) have also suggested that canopy structure can affect plant reflectance, particularly in the near infrared.

In this study I investigate whether, and at what level, MESMA of AVIRIS-derived reflectance can be expected to yield accurate estimates of vegetation type, vegetation cover, or soil surface type in regions with low vegetation covers (0 to 50%). In order to do this, I simulate noise-free and noise-degraded AVIRIS spectra of various soil, vegetation cover, and vegetation type classes, and neglect many other sources of error in real applications. Noise is modeled using the 1998 AVIRIS signal-to-noise ratio (SNR) which is greater than any other imaging spectrometer currently or soon to be deployed, including Earth Observer-1 (EO-1) Hyperion, Australian Resource Information and Environment Satellite-1 (ARIES-1), and Naval EarthMap Observer (NEMO) Coastal Ocean Imaging Spectrometer (COIS) data. This approach comprises a realistic best-case scenario in which many problems typical of remote sensing in areas of low cover or desert areas are minimized. In particular, several real-world limitations on remote sensing are absent: intra-species spectral variability, nonlinear mixing, lighting and topographic effects, uncertainty related to apparent surface reflectance retrievals, and noise in field or image endmembers. MESMA of full range (350 to 2500 nm) reflectance

derived from hyperspectral remote sensing data cannot retrieve vegetation type reliably at the low areal vegetation cover that normally characterize arid regions. However, vegetation cover and soil types may be mapped with greater reliably.

Having established limits on linear spectral unmixing in areas of low cover through spectral simulations, real AVIRIS data from the Mojave Desert, California, are evaluated. However, MESMA of AVIRIS-derived apparent surface reflectance is capable of mapping soil surface types even when vegetation parameters cannot be reasonably retrieved.

2. METHODS

2.1 Field Spectroscopy

Field reflectance spectra of soils and vegetation were collected in the Manix Basin on May 2, 1998, two days after an AVIRIS overflight. Field spectra were collected from 350 nm to 2500 nm using an ASD Full Range portable spectroradiometer (Analytical Spectral Devices, Inc., Boulder, Colorado). Spectra were acquired from 0.25 to 0.5 meters (nadir-looking) above targets with an 8% field of view, and divided by the near-simultaneous (<2 minutes) spectrum of a 100% reflective Spectralon panel (Labsphere, North Sutton, New Hampshire) to yield reflectance. Reflectance spectra were collected of soils, individual shrubs of dominant species (*L. tridentata, A. dumosa,* and *A. polycarpa*) and over small areas for grasses and non-photosynthetic vegetation (NPV) (typically in an approximately 5-m radius circle). Ten individual spectra were averaged

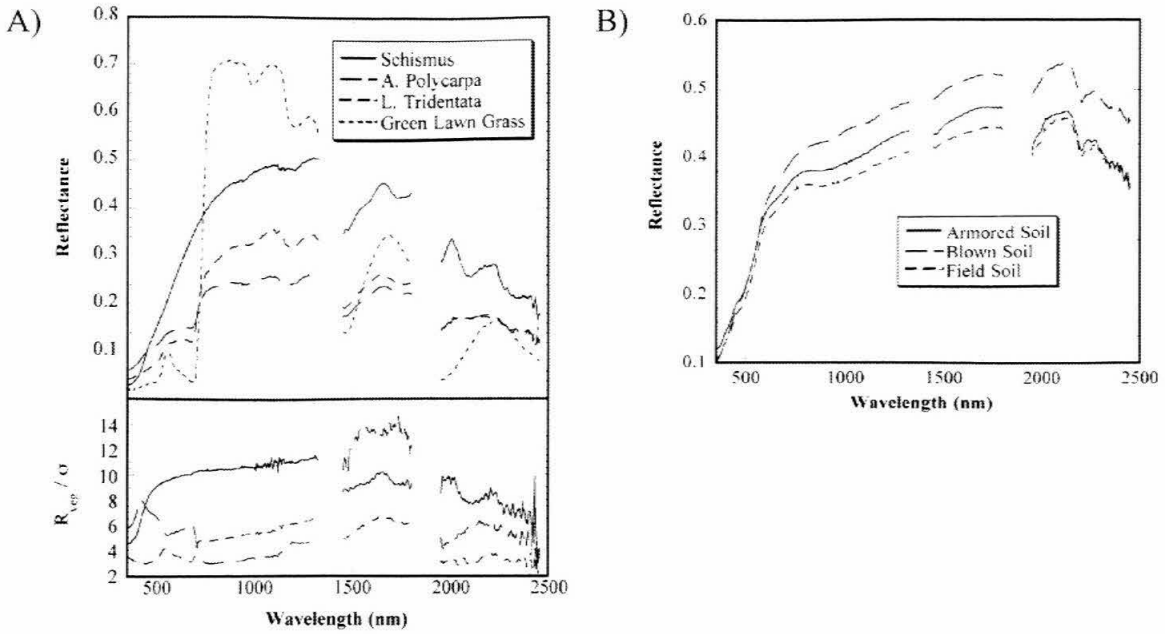

Figure 5-1. Field reflectance spectra of soils and vegetation collected in the Manix Basin on May 2, 1998, two days after the AVIRIS overflight. Field spectra were collected using an ASD Full Range portable spectroradiometer (Analytical Spectral Devices, Inc., Boulder, Colorado). Spectra were acquired from 0.25 to 0.5 meters (nadir-looking) above targets with an 8% field of view, and divided by the near-simultaneously (<2 minutes) spectrum of a 100% reflective Spectralon panel (Labsphere, North Sutton, New Hampshire) to yield reflectance. Ten spectra were averaged together for each shrub, NPV, grass, and soil. Senesced *Schismus* grass was used for this study. The quantity R_{veg}/σ is a signal-to-effect ratio which gives an indication of the intra-species spectral heterogeneity on the same scale as the signal-to-noise ratio.

together for each shrub, NPV, grass, and soil averaged spectra. Spectra of soils from other dates were used to supplement the spectral database. Averaged spectra were convolved to AVIRIS bands, and incorporated into a spectral library with 185 total averaged spectra (54 vegetation/NPV spectra and 131 soil spectra) from six sites. Representative spectra are shown in Figure 5-1.

2.2 Spectral Simulations

Representative field reflectance spectra of three abundant vegetation types in the Manix Basin (senesced *Schismus* grass, *A.* polycarpa, and L. *tridentata*) plus a

reflectance spectrum of green lawn grass from the USGS Digital Spectral Library (Clark *et al.*, 1993) were chosen as vegetation endmembers for spectral simulations. The lawn grass spectrum was chosen as it is representative of green vegetation, which is typically not found in the Mojave Desert. Representative spectra of three different common soil surface classes (blown quartz sand, armored deltaic deposits, and semi-armored soils from abandoned fields) were chosen as soil endmembers. The desert vegetation and soil spectra used as endmembers in spectral simulations were chosen from the spectral library using the method outlined by Gardner (1997) and Roberts *et al.* (1998) to determine their representation of the other spectra in their class. The endmembers used for spectral simulations are shown in Figure 5-1. The armored and field soils have very similar spectra due to their nearly identical surface appearance and related origins. The armored soil is a deflated deltaic deposit covered by a gravel lag, whereas the field soil is from an abandoned field located on deflated deltaic deposits where the deflationary lag has largely re-established since abandonment. The blown soil is from an area downwind of an abandoned field where sand, removed from the field by wind, has been deposited.

The four vegetation endmembers were each combined linearly with each of the three soil endmembers in varying proportions (representing from 0% to 50% vegetation cover in 2% increments) according to the equation:

$$R_S(\lambda) = f_{veg}R_{veg}(\lambda) + (1 - f_{veg})R_{soil}(\lambda), \quad (1)$$

where $R_s(\lambda)$ is the simulated reflectance spectrum of a given with specified cover on a given soil, f_{veg} is the fraction of vegetation, $R_{veg}(\lambda)$ is the reflectance spectrum of the vegetation endmember, and $R_{soil}(\lambda)$ is the reflectance spectrum of the soil endmember.

There were a total of 312 simulated spectra.

Signal-chain noise was modeled in the resulting spectra by adding to each band the reported 1998 AVIRIS signal-to-noise (Figure 5-2) (Green *et al.*, 1999) multiplied by a standard-normal random number:

$$R_{SN}(\lambda) = R_S(\lambda)\left(1 + \frac{N(0,1)}{SNR(\lambda)}\right), \tag{2}$$

where $R_{SN}(\lambda)$ is the simulated, noise-degraded spectrum, SNR(λ) is the signal-to-noise ratio, and N(0,1) is a random number generated from a normal distribution with a mean of zero and a standard deviation of one. A total of 16 complete sets of noise-degraded spectra were generated so that each spectrum in each set had its own unique noise vector.

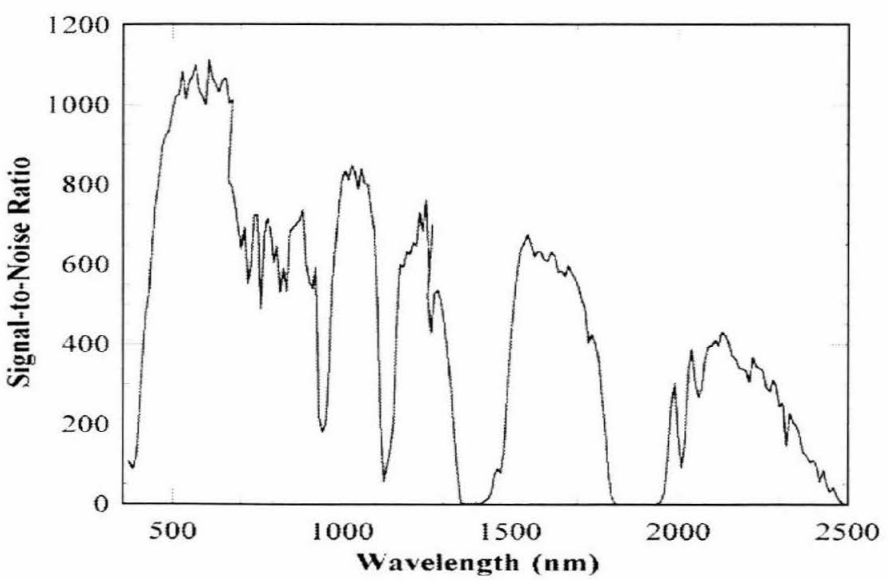

Figure 5-2. 1998 AVIRIS signal to noise ratio (SNR) used in spectral simulations (from,Green *et al.*, 1999).

2.3 Spectral mixture analysis of Simulated Spectra

Each of the noise-degraded simulated spectra was modeled by each of the non-degraded simulated spectra by minimizing root-mean-squared error (RMS) for a simplified SMA equation:

$$R_{SN}(\lambda) = f_{model} R_S(\lambda) + \varepsilon(\lambda), \tag{3}$$

where $-0.01 \leq f_{model} \leq 1.01$ and $\varepsilon(\lambda)$ is an error term. Interval limits slightly less than zero and slightly greater than one were used to accommodate a small amount of noise in the modeling. RMS is given by:

$$RMS = \frac{\left(\sum_{j=1}^{m} \left(\varepsilon_j \right)^2 \right)^{0.5}}{m}, \tag{4}$$

where ε_j are the error terms for each of the m spectral bands considered. In this study, a reduced set of 197 of the AVIRIS bands that covered the full AVIRIS spectral range were used. The full AVIRIS range was used in this study in order to allow simultaneous retrieval of vegetation and soil parameters. However, bands that span the deep atmospheric water absorptions at approximately 1400 nm and 1900 nm were not used.

In many cases, a noise-degraded spectrum was equally well modeled by two or more spectra. The spectra, $R_S(\lambda)$, which best modeled each noise-degraded spectrum, $R_{SN}(\lambda)$, with the lowest RMS was recorded. Cases in which RMS was greater than 2.5%, or in which residuals deviated from zero in the same direction for more than seven consecutive bands, were not considered. A RMS error of 2.5% was used as the

maximum error cutoff because the vast majority of spectra were modeled by at least one model within this limit.

Several categories of modeling errors were considered for the analysis of spectral simulation results:

1) Was each spectrum modeled by other spectra with the same vegetation type?
2) Was each spectrum modeled by other spectra within 10% of the modeled spectra, regardless of vegetation type?
3) Was each spectrum modeled by other spectra with the same soil type?

Since the spectra, genesis, and surface appearance of the armored soil and the field soil (Figure 5-1) were so similar, an additional potential error was considered:

4) Was each spectrum modeled by other spectra with the same or similar soil type?

The total number of times all spectra were modeled correctly according to each of the categories above was recorded. Spectra were also divided into vegetation cover classes (2-10%, 12-20%, 22-30%, 32-40%, and 42-50%) and the total number of times spectra in each cover class were modeled correctly was recorded. These were then divided by the total number of times all spectra were modeled and result was subtracted from one. The resulting metrics are interpreted as error probabilities. For example, consider the case where all simulated spectra with 22% to 30% *Schismus* were modeled a total of 100 times by spectra other than themselves. If only 25 of the spectra that modeled the *Schismus* spectra were themselves *Schismus* spectra (with other soils or other covers), then the error probability would be 75%.

The simulations carried out here represent a best-case scenario in which confusions due to intra-species spectral variability, nonlinear mixing, lighting and topographic effects, uncertainty related to apparent surface reflectance retrievals, and noise in field or image reference endmembers are absent.

In order to explore the effects of these other sources of variability on modeling success, each noise-degraded simulated spectrum in a set was modeled by all other noise-degraded spectra in a set. Although this approach does not directly address issues like non-linear mixing and intra-species or intra-soil spectral variability, it roughly simulates the effect of adding a modest amount of uncertainty to a spectral library. In practice, many types of uncertainty cannot be treated mathematically in the same way as instrumental noise. However, by adding noise to both the modeled spectra and the spectral endmembers, the magnitude of the effect expected from other sources of variability can be determined. If the addition of this modest amount of uncertainty compromises the ability to retrieve relevant information using SMA of hyperspectral data, much larger sources of uncertainty can certainly be expected to do so as well.

2.4 AVIRIS Image Preprocessing

AVIRIS data were acquired over the Manix Basin on April 30, 1998. AVIRIS measures the total upwelling spectral radiance in 224 bands from 400 to 2500 nm in 20-m ground pixels from a NASA ER-2 aircraft flying at 20-km altitude. The northern lobe of the Manix Basin (Figure 5-3), the focus of this study, was covered by flight 980430 run 10 scene 3. The data were radiometrically calibrated at the AVIRIS data facility (Jet

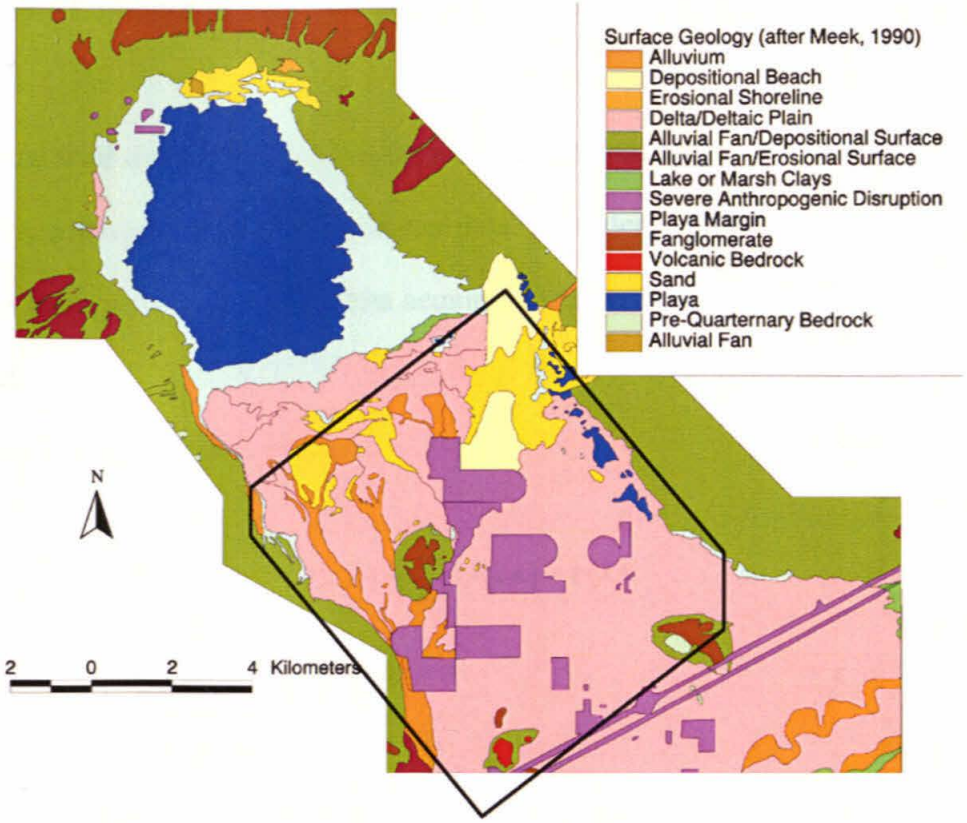

Figure 5-3. The surface geology of the northern (Coyote) lobe of the Manix Basin (After Meek, 1990). The outlined area is the location of the AVIRIS flight used in this study (flight 980430 run 10 scene 3).

Propulsion Laboratory, Pasadena, California). Apparent surface reflectance was retrieved using a technique developed by Green *et al.* (Green *et al.*, 1993; Green *et al.*, 1996; Roberts *et al.*, 1998; Roberts *et al.*, 1997b). The reflectance spectrum from a gravel parking lot in the AVIRIS scene was used to calibrate the apparent surface reflectance spectra of the entire scene. The AVIRIS image and its products were rectified using a nearest-neighbor triangulation method that employed 107 ground-control points chosen in the image and in a series of 1-m resolution USGS digital orthophotos.

2.5 Multiple Endmember Spectral Mixture Analysis (MESMA)

How well do spectral simulation results represent the success we might expect using SMA with real imaging spectrometer data? In order to probe this question, a SMA technique was applied to AVIRIS data acquired over the Manix Basin, a Mojave Desert shrubland.

The basic SMA equations are:

$$R_p(\lambda) = \sum_{i=1}^{n} f_i R_i(\lambda) + \varepsilon(\lambda), \tag{5}$$

$$\sum_{i=1}^{n} f_i = 1, \tag{6}$$

where $-0.1 \leq f_i \leq 1.01$, $\varepsilon(\lambda)$ is the difference between the actual and modeled reflectance, $R_p(\lambda)$ is the apparent surface reflectance of a pixel in an image, $R_i(\lambda)$ are the reflectance spectra of spectral endmembers in an n-endmember model, and f_i are weighting coefficients, interpreted as fractions of the pixel made up of endmembers i=1,2...n. RMS error is given by Equation 4.

MESMA is simply a SMA approach in which many mixture models are analyzed in order to produce the best fit (Gardner, 1997; Roberts *et al.*, 1998; Roberts *et al.*, 1997a). In the MESMA approach, a spectral library is defined which contains the spectra of plausible ground components. A set of mixture models with n ($n \geq 2$) endmembers from the library is defined, with shade always present as one endmember in the model.

Each model is fit to every pixel in a remote sensing image, and a valid fit is

restricted to a maximum preset RMS error and an additional constraint that not more than seven contiguous bands in the residual spectrum may deviate from zero in the same direction. 2.5% maximum RMS error was used in this study because the vast majority of pixels were modeled by at least one model within these limits. Increasing the maximum RMS had little impact on the number of unmodeled pixels in the image. The model that fits each pixel with the lowest RMS is recorded along with the endmember fractions for that model.

MESMA requires an extensive library of field, laboratory, and/or image spectra, where each plausible ground component is represented at least once. Including more than one spectrum of a ground component allows for the spectral variability often found in desert vegetation, thus partially overcoming a difficulty problem that is prevalent in arid region remote sensing (this study and Franklin *et al.*, 1993). However, there is a trade-off between having a small enough library that all models may be run on an standard computer in a reasonable amount of time, and having a library large enough to incorporate sufficient spectral variability in ground targets. Indeed, incorporating sufficient intra- and inter-species spectral variability in the spectral library to enable retrieval of vegetation type may be impossible given finite field and computation time. Furthermore, MESMA is a linear SMA technique and therefore not capable of dealing with nonlinear mixing effects other than those captured by the spectral library.

This study employs MESMA to retrieve soil type only because vegetation covers in the Manix Basin are lower than can be expected to yield reliable vegetation type and cover retrievals (Table 2-1, see Section 3.1). Nonetheless, vegetation spectra must be present in mixing models because the absence of the vegetation's contribution, even

when subtle, can confound soil type identification. In solving the mixing equations for each pixel and for each model, vegetation type and cover are always estimated, but these results should be considered unreliable. Soil retrievals, on the other hand, have much lower error probabilities and therefore can be considered reliable.

A total of 1,656 four-endmember models were used in MESMA modeling of apparent surface reflectance derived from the April 30, 1998, AVIRIS Manix Basin scene. The Supercomputing Visualization Workbench was used for planning and calculation of these model runs. Of these models, the one that modeled each pixel with the lowest RMS was chosen as the optimal model. Each four-endmember model consisted of shade + soil + shrub + grass or shade + soil + shrub1 + shrub2 spectra. Four-endmember models were chosen because in any given 20-m square in the Manix Basin, there will be at least two dominant types of vegetation (two shrub species or, more likely, a shrub species and a grass), soil, and shade. From ground observations, there are very few places in the basin that are bare soil (a two-endmember model). Because shrubs cover most of the basin, and high rainfall in the winter of 1998 promoted the growth of annual grasses, three-endmember (soil plus a single type of vegetation) areas are also rare. Five-endmember models and higher were excluded from consideration because they are computationally very expensive and they simply allow greater variability in vegetation which is not the purpose of this study. Instead, the intent was to use MESMA of AVIRIS data to map soil surface categories in the Basin.

Spectra used in four-endmember models were chosen from the library of field reflectance spectra to minimize computation time and to maximize spectral variability using the method outlined by Gardner (1997) and Roberts *et al.* (1998). In this library

analysis, each spectrum in the spectral library is modeled by every other spectrum in the library, coupled with shade, and constrained by the constraints that will be used in the final analysis. This approach allows spectra to be compared with one another, and redundant or unique spectra to be identified. Spectra were chosen that 1) modeled other spectra of the same type, 2) were not modeled by other spectra of the same type, and 3) were not confused with spectra of other types.

Thirty-six field spectra were chosen to be included in four-endmember models for this study. These spectra included two senesced *Schismus* grass spectra and one spectra of dead, herbaceous annuals (NPV), nine shrub spectra (two *A. dumosa*, two *A. polycarpa*, and five *L. tridentata* spectra) and 23 soil spectra (13 armored soil, six blown sand, and two soil spectra from abandoned fields in addition to two spectra from a nearby alluvial fan). The blown sand is spectrally bright and has smaller surface particle size than the other two soils.

3. RESULTS AND DISCUSSION

3.1 Spectral Simulations

The error probabilities when noise-degraded spectra are modeled by other noise-degraded spectra (Figure 5-5) are higher compared to those when noise-degraded spectra are modeled by non-degraded spectra (Figure 5-4). Thus, there is a dramatic effect in introducing even modest uncertainty to spectral endmembers.

How does this uncertainty compare quantitatively to others sources of error? The

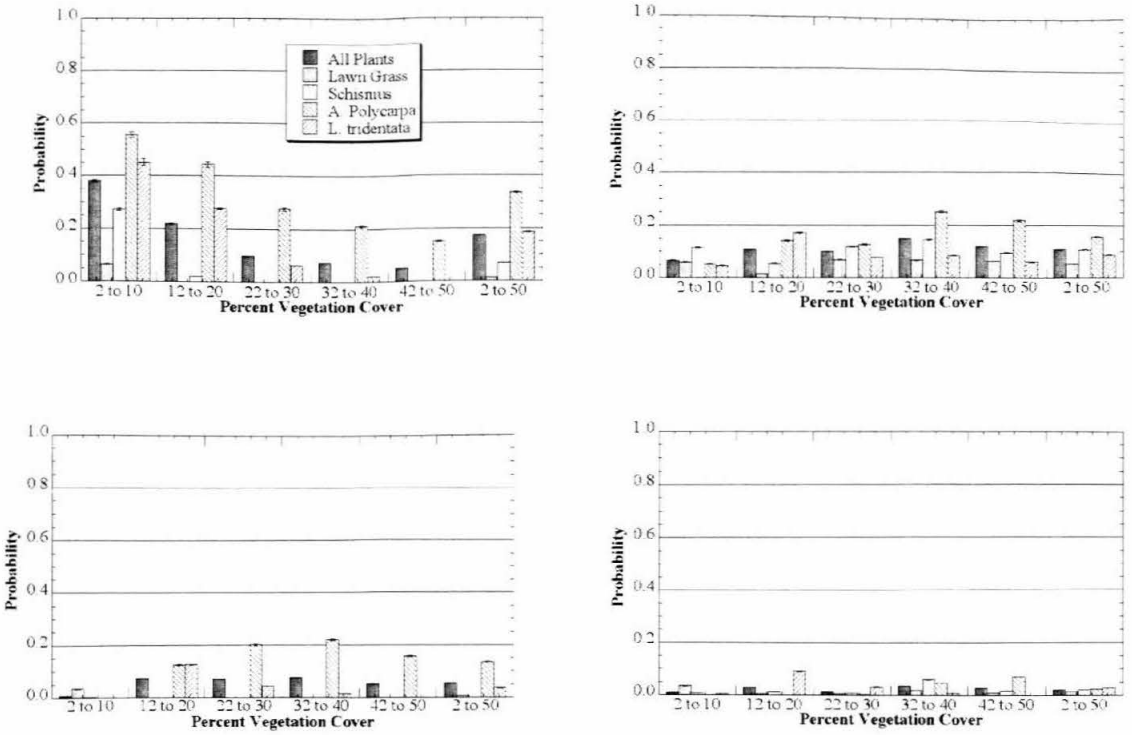

Figure 5-4. Error probabilities by vegetation type and cover class when noise-degraded spectra were modeled by noise-free endmembers. (A) Probability of modeling spectra with incorrect vegetation type. (B) Probability of modeling spectra with endmember cover greater than ±10% from that of the modeled spectrum. (C) Probability of modeling spectra with incorrect soil. (D) Probability of modeling spectra with dissimilar soil type. The "All Plants" category is an average of error probabilities for each species.

quantity R_{veg}/σ, where σ is the standard deviation of the 10 spectra averaged to produce R_{veg}, plotted in Figure 5-1 gives an indication of the intra-species spectral heterogeneity. Standard deviation is highly dependent on the samples that are used to calculate it and may not be representative of the population. The σ's represented here do not represent a comprehensive survey of the plant spectra for an entire population, but do provide a clear indication of the magnitude of R_{veg}/σ. R_{veg}/σ is a signal-to-effect ratio (SER) analogous to SNR, where here the "noise" is not instrument noise but intra-species spectral variability. R_{veg}/σ varies between 2 and 14, while the 1998 AVIRIS SNR varies between 300 and 1200 except in the deep atmospheric water bands (Figure 5-2). Asner *et al.* (1998) have reported intra-species spectral variability in reflectance spectra of many plants and litter

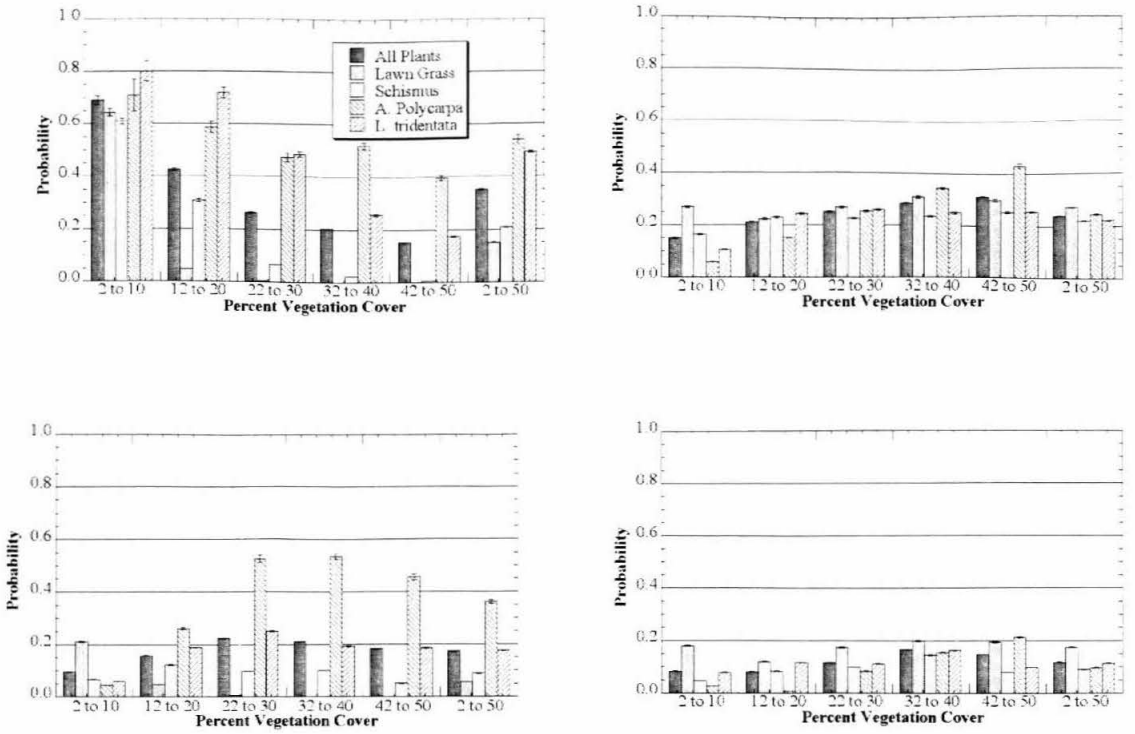

Figure 5-5. Error probabilities by vegetation type and cover class when noise-degraded spectra were modeled by noisy-degraded endmembers. (A) Probability of modeling spectra with incorrect vegetation type. (B) Probability of modeling spectra with endmember cover greater than ±10% from that of the modeled spectrum. (C) Probability of modeling spectra with incorrect soil. (D) Probability of modeling spectra with dissimilar soil type. The "All Plants" category is an average of error probabilities for each species.

types with SER values on order 10 for visible and near-infrared multispectral channels. Results from Asner's (1998) canopy-scale radiative transfer models of vegetation suggest that small changes in LAI, stem-area index, leaf angle, and the ratio of living material to litter can contribute to inter-canopy variability and therefore intra-species variability. For example, a 10% decrease in living material in a plant with 100% living material can increase near-infrared (NIR: approximately 800 to 1550 nm) reflectance from approximately 0.25 to approximately 0.30, a SER of 5 where the effect is not due to variability in reflectance but potential intra-species variability given by a change in living material. It is important to note that the change in these spectra is wavelength-dependent and nonlinear: the reflectance spectrum of a canopy with 90% living material cannot

simply be expressed as the reflectance spectrum of a canopy with 100% living material times a scalar. Intra-species variability has a magnitude much greater than instrumental noise and therefore is more likely to confound linear SMA.

Non-linear mixing is likely to further complicate the analysis if the spectra in the library were collected from areas with a different substrate than in the image. For example, Ray and Murray (1996), document an extreme case in which *Larrea tridentata* canopies occurred on a bright background, yet the library spectra were collected on a black background. The multiple scattering effect resulted in one-half the reflectance spectrum, equivalent to an SER of approximately 2. While this extreme is unlikely to occur often, it illustrates that intra-specific and multiple scattering effects are likely to be larger than the effects of instrumental noise.

Clearly, confusion due to intra-species variability and nonlinear mixing in vegetation is much more likely than that due to instrumental noise. Hence, the calculated error probabilities for cases where noisy spectra are modeled by noisy endmembers may be considered to yield a lower bound on the reliability of spectral unmixing of hyperspectral reflectance data by full-range field reflectance spectra.

3.1.1 Vegetation Retrievals

The error probabilities in Figure 5-4 clearly indicate that even in the best case the probability of incorrectly identifying vegetation types can be high (>50%), and errors are highly dependent on vegetation type as well as the amount of cover (Figure 5-4A). Errors were made in modeling green lawn grass less than 10% of the time and only for covers less than 10%, while errors occurred in recognizing *A. polycarpa* no less than 15%

of the time.

As has been suggested by Sabol *et al.* (1992) for soils in a shade-vegetation mixture, the spectral contrast of endmembers has a major influence on their detectability. The vegetation considered here may be grouped into two categories. Green lawn grass and senesced *Schismus* grass are "spectrally determinate" vegetation, while *A. polycarpa* and *L. tridentata* are "spectrally indeterminate" vegetation. The spectrally determinate vegetation both have high spectral contrast. The green lawn grass spectrum has a strong red edge and deep absorption bands due to water (Gao and Goetz, 1990). Unlike the green lawn grass spectrum, the spectrum of senesced *Schismus* grass has no red-edge, but does have strong absorption bands due to cellulose and lignin in the short-wave infrared-1 (SWIR1: approximately 1550 to 1900 nm) and short-wave infrared-2 (SWIR2: approximately 1900 to 2400 nm) regions (Elvidge, 1990). The spectrally indeterminate vegetation, on the other hand, lack deep chlorophyll absorptions around 420 nm and 680 nm (Gates *et al.*, 1965), a strong red edge, deep water absorption bands in the near-infrared, and the clear cellulose and lignin absorption bands in SWIR1 and SWIR2. Theus, spectrally indeterminate vegetation displays the same lack of spectral contrast shown by many other desert shrubs even during the growing season (Billings and Morris, 1951; Mooney *et al.*, 1977). Thus, vegetation remote sensing in arid and semiarid regions is faced with an inherent difficulty due to the low spectral contrast common among arid zone species.

When noise-degraded spectra are modeled by other noise-degraded spectra, errors in vegetation type retrievals for all desert plants remain above 30% at less than 20% cover, and error probabilities for *A. polycarpa* and *L. tridentata* type retrievals are greater

than 25% at less than 40% cover (Figure 5-5A).

The increase in the error probabilities in Figure 5-4A over Figure 5-5A indicates that adding even modest uncertainty to endmembers will influence how well vegetation type is modeled. Our ability to correctly identify species as a function of vegetation cover and spectral contras may be expressed assuming that a 30% rate of species-misidentification is unacceptable. For example, green lawn grass cannot be mapped at covers below 10%, senesced *Schismus* grass, below 20% cover, *L. tridentata*, below 30% cover, and *A. polycarpa*, below 40% cover. Thus, the ability to retrieve vegetation information using SMA of hyperspectral data at low covers is compromised by modest amounts of uncertainty. Note also that other sources of uncertainty in real-world applications of mixture analysis to hyperspectral data are much larger, and may further reduce the reliability of vegetation retrievals.

The probability of modeling errors in the retrieval of vegetation cover is significantly lower than the probability of error in retrieval of vegetation type (Figure 5-4B). With the exception of *A. polycarpa*, the probability of error in estimating vegetation cover within 10% of the modeled vegetation cover is lower than 10% and decreases with increasing cover.

Cover estimations also suffer from the additional uncertainty of modeling noisy spectra with noisy endmembers. With the exception of *A. polycarpa*, error probabilities of modeling spectra with greater than a 10% difference in cover remain below 25%. However, vegetation cover estimates are likely to be as vulnerable to additional sources of uncertainty and variability as vegetation type retrievals.

Thus, in arid and semi-arid regions with covers below at least 30%, SMA is

unable to reliably model vegetation type. Total surface cover can be estimated within 10% of the correct value, but only under the near-optimal conditions of the simulations. Spectrally determinate vegetation may be reliably retrieved at lower covers and areas of relatively high cover may be modeled correctly regardless of vegetation type. However, in an image with both spectrally determinate and indeterminate vegetation and a variety of vegetation covers, some of the data will be reliably modeled, while the rest will not. Without *a priori* knowledge of which is which, all vegetation type retrievals must be treated with care.

3.1.2 Soil Retrievals

In contrast to the errors in modeling vegetation type, errors in modeling soil type are much less likely, with error probabilities lower than 20% for most cases (Figure 5-4C). The probability of modeling a spectrum with the wrong soil type increases with increasing vegetation cover. This is due to the decreasing dominance of the soil spectrum. Given the similarity of two of the soil types—armored soil and field soil—the probability of modeling spectra with a dissimilar soil type drops even further (Figure 5-4D). When noise-degraded spectra are modeled by other noise-degraded spectra, errors in the retrieval of the same or similar soil types (Figures 5-5C and 5-5D) increase, but remain low compared to vegetation type retrievals of desert plants.

In cases where *A. polycarpa* is mixed with soils, error probabilities exhibit a counterintuitive increase for both percent cover and soil type retrieval. This effect is not present in Figure 5-4D where the armored and field soils are classed together. The field soil spectrum is the darkest soil spectrum at all wavelengths. Since f_{model} is constrained to

be less than 1.01, the field soil cannot model the armored soil. Thus, the presence of *A. polycarpa* must be leading to confusion between the armored and field soils by allowing *A. polycarpa*-field soil spectra to be modeled by armored soil spectra with lower covers.

Thus, the spectrum of *A. polycarpa* "couples" with the spectrum of the field soil to appear more like the armored soil spectrum without vegetation. The spectrum of *A. polycarpa* lacks strong water absorption bands near 940 nm and 1140 nm, is relatively flat in the NIR and SWIR2 regions, and has the smallest red-edge of all the spectra used in this study with high reflectance in the visible. These features make the spectrum of *A. polycarpa* look more like the soil spectra than any other vegetation spectrum considered here. It also has lower reflectance in SWIR2 relative to SWIR1. Thus, the *A. polycarpa* spectrum, when mixed with the field soil to represent moderate covers, decreases the SWIR2 reflectance of the combined spectrum at a rate greater than the decrease in the SWIR1 reflectance. The result is a spectral curve similar to that of the armored soil, but with a reduced reflectance at all wavelengths. Spectral coupling is also seen, to lesser degrees, with the senesced *Schismus* grass.

Both vegetation cover estimates and soil type retrievals are sensitive to spectral coupling. Thus, while vegetation cover estimates from SMA of hyperspectral data are more reliable than vegetation type retrievals and are not in error more than 25% of the time, they must be treated with care. The effect of coupling on soil type determinations is also strong, though overall error probabilities are low. If similarities in soil types are considered in order to class them into broader soil categories, these errors in soil type retrievals are minimized, and coupling effects are negated.

It is important to note that the accuracy of soil type retrievals is dependent on

vegetation type, independent of coupling effects. This suggests that retrievals of soil type must still consider vegetation type and cover in mixing models. The absence of the vegetation's contribution to pixel reflectance, even when subtle, could confound correct soil type identification.

Soil type retrievals, while adversely affected by the addition of greater uncertainty to the models, appear robust in cases where soil spectra are significantly different. While spectral variability within a soil type will play a role in reducing the accuracy of soil type retrievals, this effect will be smaller than it is for vegetation type retrievals. Soils within a given type and geographic area typically have smaller relative variations than vegetation types because soils do not undergo phenological change and the spectra of soil surfaces are not affected by canopy-scale effects (leaf-size, geometry, canopy structure, *etc.*). Thus, I conclude that soil type retrievals may be considered reliable in most cases where vegetation is at least less than 50%. The determination of soil surface properties is the proper domain for SMA in arid areas of low cover.

Each application of SMA results will have its own accuracy requirements. The results presented here may be used as guidelines for decisions on which analytical technique is to be used depending on information and accuracy requirements, or to inform accuracy assessment once minimum-RMS SMA has been employed.

3.2 MESMA of AVIRIS data

As a real-world application of the spectral simulation results, I used MESMA of AVIRIS data acquired over an arid shrubland to highlight the limitations and

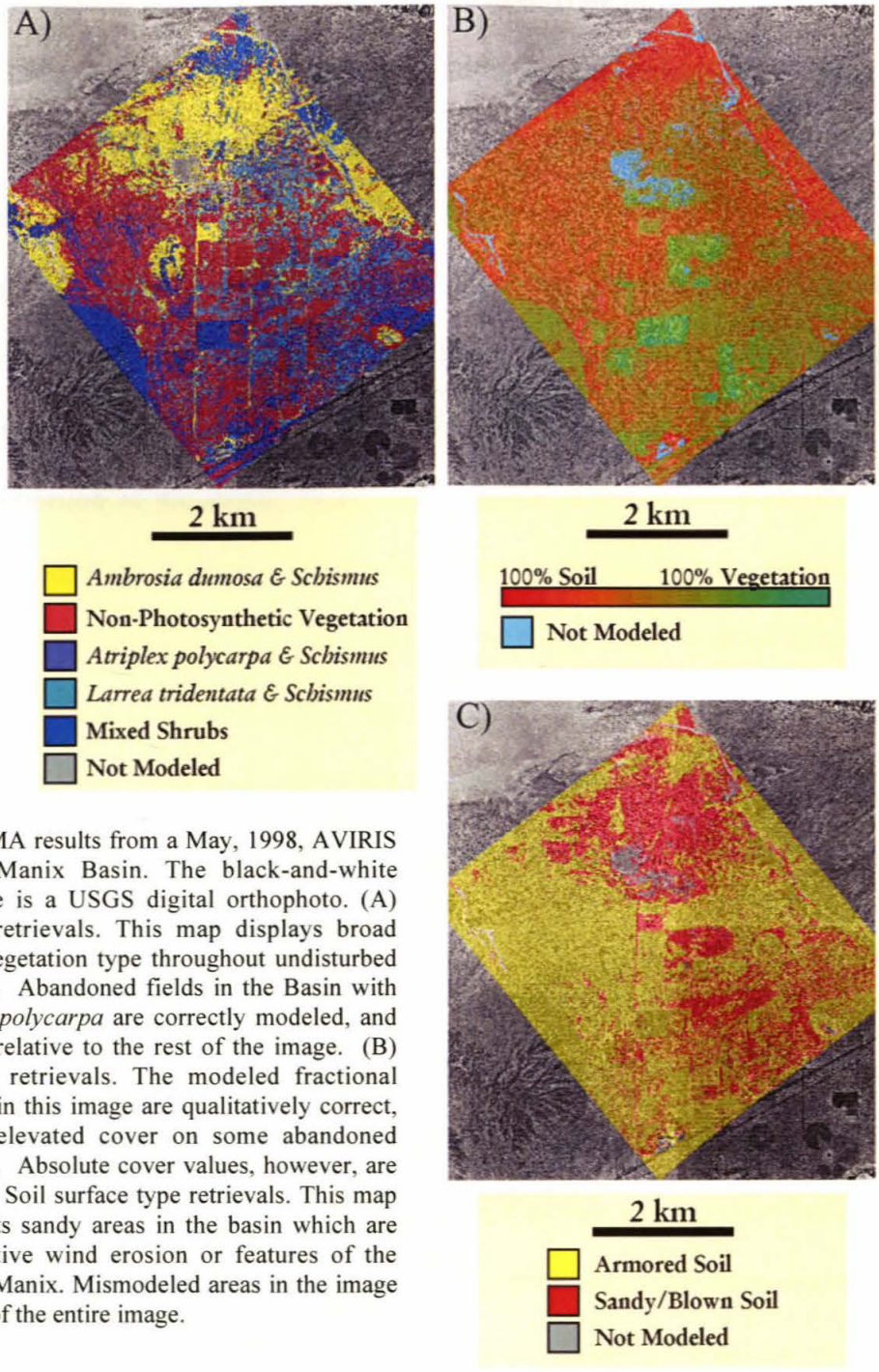

Figure 5-6. MESMA results from a May, 1998, AVIRIS scene from the Manix Basin. The black-and-white background image is a USGS digital orthophoto. (A) Vegetation type retrievals. This map displays broad mismodeling of vegetation type throughout undisturbed areas of the basin. Abandoned fields in the Basin with high covers of *A. polycarpa* are correctly modeled, and have high covers relative to the rest of the image. (B) Vegetation cover retrievals. The modeled fractional vegetation covers in this image are qualitatively correct, highlighting the elevated cover on some abandoned fields in the Basin. Absolute cover values, however, are overestimated. (C) Soil surface type retrievals. This map correctly highlights sandy areas in the basin which are either sites of active wind erosion or features of the ancient paleolake Manix. Mismodeled areas in the image are less than 10% of the entire image.

opportunities in arid region applications of SMA. MESMA results are depicted in Figures 5-6A through 5-6C.

Figures 5-6A and 5-6B depict vegetation type and vegetation cover retrievals, respectively. Lessons may be learned from these results. In Figure 5-6A, the largest area

is modeled by "Non-Photosynthetic Vegetation" which is a mixture of NPV and senesced *Schismus* grass. While these two components are ubiquitous in the Basin, *L. tridentata* is the dominant perennial and should have been recognized in more of the image when mixed with senesced *Schismus* grass. The spectral library incorporated more *L. tridentata* spectra than any other shrub in order to capture its spectral variability and increase its chances of being correctly modeled. Clearly, this approach only met with limited success. Furthermore, nowhere in the field is *A. dumosa* dominant, though it models a large proportion of the image. In particular, pixels in the northern part of the image which are modeled by *A. dumosa* are also modeled by the sandy soil. This could be an example of spectral coupling where the spectrum of the soil and vegetation in this area mix within the pixel to create a combined spectrum that appears as a different shrub altogether. Finally, *A. polycarpa* is the dominant perennial shrub only in areas that have been dramatically disturbed by human activity. The area of *A. polycarpa* identified on the southeastern fan is, therefore, inaccurate.

Vegetation modeling results were not without some success, however. Abandoned fields tend to have either high covers of *A. polycarpa* (as much as 30%) or an absence of perennial vegetation and moderate covers of annual grasses in wet years. The high covers of *A. polycarpa* are above the rough 30% vegetation cover threshold for reliability and are modeled correctly. The fields without perennial vegetation cover are also modeled correctly, possibly because of their spectral simplicity. The mixed success of vegetation type retrievals from AVIRIS imagery illustrates a principal pitfall in SMA of hyperspectral reflectance data from arid regions. Some areas, due to their cover or vegetation type, will be modeled correctly while others will not. As before, without

detailed *a priori* knowledge of the spatial arrangement of vegetation cover and type, all vegetation type retrievals must be considered ambiguous. With detailed *a priori* knowledge of the spatial arrangement of vegetation cover and type, the application of remote sensing to determine these parameters is redundant.

Vegetation cover estimates in Figure 5-6B were more successful than vegetation type retrievals. These results highlight the greater vegetation cover found on abandoned fields and disturbed areas dominated by *A. polycarpa*. However, the cover estimates also suggest high vegetation cover on abandoned fields that are known from field observations to lack perennial shrub cover. While these fields do have some annual grass cover, it is likely less than the 60% to 70% cover retrieved by spectral unmixing.

By and large, the vegetation cover estimates from MESMA (Figure 5-6B) are greater than the perennial shrub cover in Table 2-1. This may be due to the fact that no attempt was made in field estimates to incorporate annuals, and the winter of 1998 was a very wet El Niño year. The 20% to 40% covers estimated in some undisturbed areas and the 60% to 80% cover in abandoned fields are high but realistic for a wet year with relatively high grass covers.

Vegetation type retrievals may be used to place bounds on the confidence in interpreting vegetation cover retrievals. If there is sufficient spectral contrast between vegetation types and soil, vegetation cover can be reliably estimated. Spectral simulations presented here allow estimation of a threshold below which the presence of spectrally determinate vegetation cannot be estimated reliably. For green vegetation, this threshold is about 10%. For spectrally indeterminate vegetation types, cover cannot be estimated reliably at covers below 50%. In an image, one type of spectrally indeterminate

vegetation is likely to be modeled as some other spectrally indeterminate vegetation type. Therefore, areas of high uncertainty can be identified in an image. Cases in which there is very low cover for a spectrally determinate plant or relatively higher cover for a spectrally indeterminate plant are truly ambiguous.

In contrast to vegetation type retrievals, Figure 5-6C gives an accurate description of surface soil types at the time that this AVIRIS image was acquired. Comparison of the northern half of the image with the surficial geology (Figure 5-3) shows that MESMA was able to accurately map the sand and sandy-beach deposits. The areas modeled as "Sandy/Blown Soil" in the southern part of the image have a different origin. These are areas downwind of abandoned agricultural fields, roads, housing developments and other anthropogenic disturbances where sand has blown off the areas of direct disturbance onto adjacent, undisturbed areas.

However, modeling of soil surfaces in Figure 5-6C was not perfect. For example, one area in the middle of the image remained unmodeled. Ground observations indicate that this area should have modeled as Sandy/Blown Soil. This area is the brightest area in the entire image and the soil present here likely has reflectance higher than any of the blown soils in the spectral library. Since fractions greater than one were not allowed in the modeling of these spectra, a slightly darker soil cannot model a brighter soil, even if they could be expressed as scalar multiples of each other. One of the small playas in the northern part of the image was overlooked, which is not surprising as there were no spectra of this soil in the library. Other small playas on the northeastern edge of the image were modeled, but as armored soils. The alluvial fans in the image, which are located on the northeastern and southeastern edges of the image, were also misidentified

as armored soil. Despite these modeling errors (< 10% of the modeled image), MESMA is able to provide a reliable map of armored and sandy areas within the Manix Basin. Improvements in accuracy could be obtained by incorporating missing spectra—such as the bright sand and spectra from the small playas—into the library.

It is interesting to note that the abandoned fields in the image were modeled as armored soils and not by the spectra of field soils that were in the spectral library. These spectra are quite similar, suggesting that the deflationary armor that has been re-established on the abandoned fields makes these soil surfaces indistinguishable from their undisturbed cousins.

The MESMA results highlight the inaccuracy of vegetation type retrievals under low-cover conditions. In light of the spectral simulation results, the inability of MESMA to reliably map vegetation type in the Manix Basin arid shrubland with low cover is hardly surprising. This failure results from fundamental limitations of the basic SMA approach when the soil dominates the reflectance and when vegetation does not display typical green vegetation spectra. The dominance of the soil signature, on the other hand, provides an opportunity to map soil surface characteristics with MESMA of hyperspectral data.

Vegetation cover is modeled more reliably than vegetation type in arid regions, with the threshold of reliability lower for spectrally determinate vegetation than for spectrally indeterminate vegetation. Unlike simple SMA approaches, MESMA estimates shrub and grass cover, not the cover of green vegetation. Since shrubs in arid regions are spectrally dissimilar to green vegetation and are also spectrally dissimilar to one another, MESMA is better suited for estimation of vegetation cover in arid and semiarid regions

than simple unmixing.

The MESMA approach to mixture analysis is simply an extension of the simple SMA approach with many models calculated for each pixel of an image instead of just one. Thus, the inability of MESMA to reliably identify vegetation type in areas of low cover strongly implies that the basic SMA approach will also be unreliable. The effectiveness of MESMA in obtaining reasonable estimates of vegetation cover and soil surface type, on the other hand, suggests that the basic SMA approach to obtaining these parameters will be significantly more reliable. In using SMA for vegetation cover retrievals in arid and semiarid environments, however, it is of the utmost importance to use vegetation spectra from arid regions. Since vegetation in the world's deserts is spectrally dissimilar to typical green vegetation, mixture modeling using only green vegetation spectra will lead to significant underestimations of cover.

4. CONCLUSIONS AND IMPLICATIONS

In areas of low vegetation cover, MESMA of imaging spectrometer data using full-range field reflectance spectra is not able to provide reliable retrievals of vegetation type, when covers are below at least 30%. For spectrally determinate vegetation, cover may be estimated with high reliability while spectrally indeterminate vegetation is likely to yield very unreliably estimates. Low vegetation covers provide for the dominance of the soil spectral signature, providing an opportunity to retrieve soil type from spectral mixture models. These results circumscribe the applicability of MESMA to hyperspectral data, and therefore have important consequences for the use of current and planned

imaging spectrometers for arid regions. The principal import of these results is that the use of MESMA with hyperspectral reflectance data leads to unreliable vegetation type retrievals in arid areas.

This study has highlighted sources of ambiguity that are not currently recognized in hyperspectral data analysis. Several phenomena contribute to low reliability in vegetation type retrievals. Spectrally indeterminate vegetation types, characterized by low spectral contrast, are common in arid and semiarid regions and are difficult to model correctly, even at relatively high covers. Coupling of vegetation and soil spectra to cause confusion with other spectra can confound vegetation soil type retrievals. In practice, intra-species spectral variability and nonlinear mixing can account for uncertainties in spectral endmembers much larger than that due to instrumental noise modeled here. There are methods for partially compensating for these sources of uncertainty. Uncertainties of soil surface type may be reduced by classing similar soil types together. Spectral variability may be partially accommodated by including many spectra of the same vegetation or soil type into MESMA mixture models. Albedo effects may be eliminated by normalizing spectra or using their derivatives.

It is the landscape and vegetation structures themselves that contribute to the difficulty of hyperspectral remote sensing in arid regions. Arid environments are characterized by low cover globally. In addition, the ecological adaptations that make desert plants able to survive high heat and low water availability can make them spectrally indeterminate. Thus, the results of this study indicate that hyperspectral remote sensing is not a panacea for effective global monitoring of arid regions. Indeed, in contrast to the author's original expectations that the plant signature in hyperspectral

remote sensing would be the telltale sign of land degradation, the vegetation signature is by and large too faint amid a dominant, bright soil background to yield reliable and useful information. Changes in the spectral signature of the soil associated with land degradation, however, is identifiable with hyperspectral data and may serve as a fingerprint of desertification in low cover arid areas.

Given the limitations of SMA of hyperspectral data in the retrieval of vegetation cover and type, it is difficult to see how subtle vegetation biophysical and foliar chemistry parameters can reasonably be retrieved in low cover areas. I believe that no technique will be able to sufficiently compensate for all of the wide range of instrumental, atmospheric, and natural sources of uncertainty in order to fulfill this goal in arid regions. Noise will always be present in remotely sensed data. Reflectance retrievals from imaging spectrometer data are not perfect. Spectral variability and nonlinear mixing are a fact of life in arid and semiarid remote sensing. Some arid vegetation types are spectrally indeterminate. The reflectance of an entire pixel is the composites of the spectra of its constituent parts which may couple, thus causing confusion.

Remote sensing techniques and technologies have serious practical limits based on fundamental properties of instrumentation and the ubiquitous heterogeneity and vagaries of nature. New technologies and techniques need to be developed that address these limits in a realistic manner and applications of presently-available tools must be interpreted in line with their limitations. Although other classification techniques will also have to contend with sources of error intrinsic in remote sensing of arid regions, it is possible that another technique will be more robust under low-cover conditions than

SMA. For example, Drake *et al.* (1999) have suggested that mixture modeling is much more susceptible to noise than spectral matching.

The author will gladly make the data used in this study available for investigators wishing to evaluate other methods for vegetation mapping in an arid shrubland.

5. FUTURE WORK

Remote sensing techniques and technologies afford the best opportunities for detection of regional- or global-scale environmental change. Multispectral imagers such as the Landsat-class sensors provide spectral information in a limited number of broad spectral bands at medium spatial resolution with wide areal coverage. They are thus a potentially rich source of information about the global and regional state of the Earth's biosphere. Hyperspectral imagers, in contrast, provide high spectral resolution data over small areas and are well-suited for detailed studies on small scales. The complementary capabilities of hyperspectral imagers may be leveraged to enhance large-scale multispectral monitoring. This is particularly important in arid areas where traditional remote sensing techniques have proven problematic (Chapter and Huete, 1988; Huete and Jackson, 1987; Huete *et al.*, 1985) and where widespread land degradation and wind erosion create the need for affordable remote monitoring.

To date, little work has proceeded in examining the synergy between hyperspectral and multispectral datasets. Opportunities to add value to multispectral data

through the use of hyperspectral data may be provided by coordinated data acquisition. Several NASA initiatives allow simultaneous or near-simultaneous acquisition of hyper- and multispectral data: (1) NASA's New Millennium Earth Observer 1 (EO-1) platform supports both a multispectral imager and a hyperspectral instrument; (2) Landsat 7, with its multispectral Enhanced Thematic Mapper Plus (ETM+), will match within one minute the ground track of EO-1 and will thus provide near-simultaneous data; (3) the hyperspectral Airborne Visible Infrared Imaging Spectrometer (AVIRIS) can be tasked to underfly nearly any spaceborne multispectral imager.

In this chapter, it was shown that SMA of AVIRIS-derived surface reflectance images obtained over arid areas is capable of identifying wind-driven land degradation associated with human activities, as well as soils that are naturally vulnerable to degradation. In arid regions globally, wind erosion is a principal mechanism of land degradation. Agricultural activities, roads, utility corridors, ORV recreation, military maneuvers, firewood collection, and urban/suburban development all increase the vulnerability of the landscape to wind erosion by destroying sparse vegetation cover and disturbing fragile soil crusts (Campbell, 1972; El-Baz *et al.*, 1985; Fryrear, 1981; Grantz *et al.*, 1998; Hyers and Marcus, 1981; Khalaf and Al-Ajmi, 1993; Leys and McTainsh, 1994; Lovich and Bainbridge, 1999; Sharifi *et al.*, 1999; Zha and Gao, 1997). The soil and vegetation changes that accompany arid land degradation are the consequences of fundamental landscape processes. Insofar as these changes are detectable by remote sensing, remote sensing techniques can be valuable management tools and can enable identification of areas at risk of degradation before long-term or large-scale damage to the landscape has occurred.

In a pilot study in Appendix A, simulated multispectral bands are used to help define useful and simple multispectral indices for the entire constellation of past and present Landsat-class sensors to monitor areas at heightened risk of wind erosion. Having identified the most useful index for Landsat TM/ETM+, a real Landsat TM scene is used in combination with AVIRIS SMA results to identify sandy and wind erodible areas in much larger area than that covered by the AVIRIS data. This type of approach may help identify synergies between hyperspectral and multispectral remote monitoring data and may enhance the practical use of multispectral data in hard-to-sense arid areas.

CHAPTER 6

THE ROLE OF OPTICAL REMOTE SENSING IN DRYLAND MONITORING

1. INTRODUCTION

Arid and semiarid lands are found on every continent of the globe and among arid areas susceptible to land degradation, a large proportion are already degraded to some extent (Figure 6-1). At the same time, there are few institutions—at the global, regional, or local levels—with a mandate to gather reliable information about the extent of desertification or formulate reasonable avoidance or remediation plans. Thus, the risk of environmental degradation in arid and semiarid regions can be compounded by the lack political or economic will which then paves the way for insufficient land use oversight and greater degradation.

One of the greatest threats to drylands and their inhabitants is a lack of information. With their relatively large funding for basic and applied sciences as well as global monitoring assets, affluent nations are in a special position to expedite the provision of this badly needed information to individuals and organizations throughout the globe. The purpose of Chapters 2 through 4 was to partially fill the gap in our

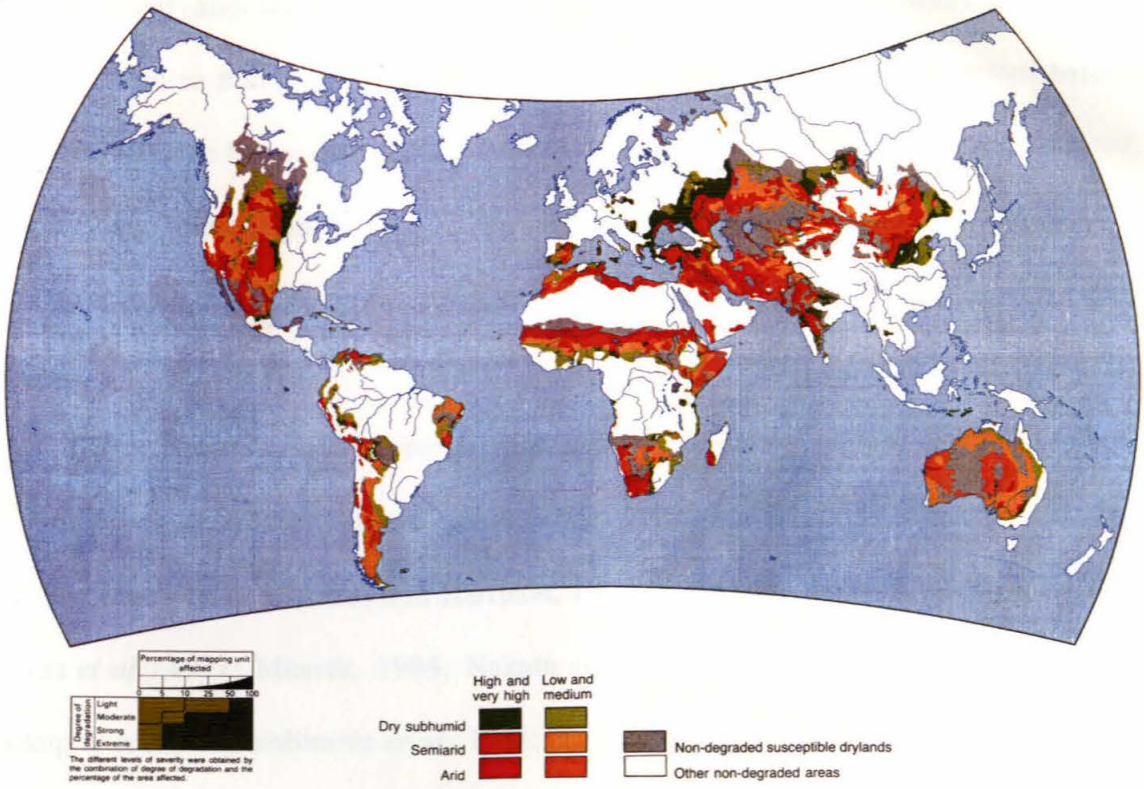

Figure 6-1. Soil degradation severity in susceptible drylands (from United Nations Environmental Programme, 1992).

process knowledge by providing and testing a new model for the role of wind erosion in arid land degradation.

Timely, relevant, and reliable information concerning the extent and risk of desertification is also extremely useful to institutions interested in stemming desertification. Individual land users, non-governmental organizations (NGOs), and government officials require two types of knowledge to address land degradation when it occurs. First, reliable information concerning the extent of desertification and its environmental causes are required to determine the severity of the problem and to map its advance. The prospects for the provision of this information by remote sensing is the subject of this chapter. Second, a means of forecasting desertification based on both

environmental and socioeconomic data is required to identify areas at risk of desertification so that avoidance or remediation strategies may be implemented before long-term damage has occurred. A proposed method for integrating both environmental and socioeconomic data for desertification forecasting that is analogous to leading economic indicators is proposed in Chapter 7 and outlined in greater detail in Appendix B.

Remote monitoring has long been suggested as a time- and cost-efficient method for monitoring desertification (see among others, Bowden *et al.*, 1974; Eve, 1995; Hudak and Wessman, 1998; Hurcom and Harrison, 1998; Kaushalya, 1992; Minor *et al.*, 1999; Mouat *et al.*, 1997; Musick, 1984; Nakata *et al.*, 1976; Pickup and Chewings, 1994; Pickup *et al.*, 1993; Robinove *et al.*, 1981; Smith *et al.*, 1990; Tsoar and Karnieli, 1996; Verstraete and Pinty, 1991; Warren and Hutchinson, 1984). The thought has been that satellite remote sensing data could provide data in near-real time over a very large area and on a continuous basis. This would allow continual monitoring of the temporal changes in degraded or at risk landscapes.

Unambiguous process indicators which can be detected with high confidence are required for effective remote monitoring of desert areas. Unfortunately, quantitative multitemporal arid region optical remote sensing is extremely difficult. My conclusion from the discussion in Chapters 5 is that despite its great promise, optical remote sensing is not capable of providing some types of information pertinent to desertification monitoring such as plant community composition. On the other hand, currently available optical remote sensing data and analysis techniques can provide other types of process-relevant information such as vegetation cover and soil surface type. The purpose of this

chapter is to identify methods and requirements for deriving process-relevant environmental information from optical remote sensing data. Here, I argue for an integrated view of the use of remote monitoring where both the processes of desertification and the practical uses of remote sensing data are incorporated.

Of course, non-optical means of remote sensing may also be used to provide information about the world's drylands. Estimates of vegetation type, biomass, or greening from radar, for example, may help identify the relative proportions of shrub and grass cover in degraded arid shrublands. Radar may also be used to estimate soil roughness, and therefore threshold wind velocities. Day-night thermal infrared imaging of arid areas may serve as an index of vegetation cover or soil moisture. These methods are outside the scope of this thesis. However, development of non-optical remote sensing methods may supplement optical data and should continue apace.

1.1 Remote Sensing Monitorables—Desertification vs. its Causes

How can remote sensing be used to monitor desertification and its causes? First, the theoretical limits and capabilities of remote sensing must be addressed, and this is the subject of this section. Second, the real-world possibilities and reasonable expectations for application of remote sensing data to desertification monitoring must be explored. This is the subject of Section 2.

From a theoretical point of view, remote sensing data may be used in two different ways to support desertification monitoring. These two "monitorables" are:

1) The land degradation itself and its manifestations in terms of vegetation and

soil, and

2) The causes and conditions for degradation along certain pathways.

The difference between these two monitorables is the focus of the analysis of remote sensing data. The first monitorable focuses on desertification itself and requires not only a general definition of desertification, but also a specific idea of how land degradation manifests in a particular instance. The second monitorable focuses on the causes of degradation and is more generally applicable because it does not require detailed knowledge of the manifestation of desertification, but instead allows for monitoring of the universal causes and conditions of desertification. While processes of desertification cannot themselves be observed, the situations and phenomena which trigger or support these processes may be. Thus, monitoring the causes and conditions for desertification can be a proxy for monitoring the processes themselves.

In the Manix Basin, the simplest way to monitor the manifestation of desertification would be to identify and monitor the sand blow-outs prevalent on the floor of the Basin. This approach is extremely useful for detailed case studies. However, this approach is not generally applicable. For example, in the Manix Basin, this approach only works on the basin floor. Were land degradation of another sort to occur on the nearby alluvial fans (such as gully erosion) or in a neighboring basin (such as salinization), it would be missed completely. Despite this, monitoring the manifestation of desertification may provide a simple and affordable way to address certain specific problems.

Monitoring the causes and conditions of desertification is a much more general approach and is preferable under most circumstances. Like monitoring the

manifestations of desertification, it requires a definition such as "the reduction or redistribution of net primary productivity" used in this thesis. However, it does not require detailed knowledge of the manifestation of this definition in every case. Instead, factors that effect the amount and distribution of NPP are monitored. In the Manix Basin, this approach would take the form of monitoring vegetation cover, vegetation type, vegetation greenness, soil surface characteristics, and human activities in the basin. The growth of areas that are windblown sand would indicate that vegetation is adversely affected, which would be seen as changes in vegetation cover, greenness, or type. A detailed process model is required to predict how the causes result in land degradation. Specifically, what is required is knowledge of *how* each of the monitored characteristics affects the landscape characteristic that is tied to the definition of desertification. Provided that a suitable process model exists, monitoring the causes of desertification is a general way in which monitoring desertification may proceed. Furthermore, since causes precede effects, monitoring the causes of desertification provides the ability to forecast desertification and to possibly circumvent it.

1.2 Remote Monitoring as a Planning/Management Tool

Monitoring degradation and its manifestations provide *post facto* monitoring of the extent of degradation, while monitoring the causes and conditions for degradation provides information about the risk of desertification and may allow us to identify areas at heightened risk of desertification before real damage occurs. In both capacities, remote sensing of lands that have succumbed to desertification or are threatened by it may be

used as a planning and management tool for these lands.

In the Manix Basin for example, monitoring desertification itself would help to identify areas in need of remediation or help to judge the success of remediation strategies. Monitoring the causes of desertification, such as disturbance of soil crusts and removal of vegetation which lead to wind erosion, would provide information that may be used by land managers to identify and develop avoidance strategies, such as building wind breaks or planting cover crops during fallow seasons.

1.3 Process-Relevant Observation and Monitoring- An Integrated Approach

Remote monitoring of desertification requires a generally applicable remote sensing strategy that is not dependent on the detailed local manifestations of desertification but may be implemented for local case-studies. It is thus preferable to monitor the causes and not the consequences of desertification. This approach requires use of consistent process models to bring meaning to observed landscape variables.

This view argues for an integrated approach to the use of remote sensing in dryland monitoring in which the processes of desertification circumscribe the use of remotely sensed data in light of its practical limits. This approach may be clarified by considering several questions which must be answered for any process-relevant remote monitoring study:

1) What are the relevant processes of desertification and what process models exist?
2) What environmental variables control the processes of desertification?

3) What process indicators can be unambiguously detected with remote sensing data?

4) What remote sensing data are best suited for retrieval of these environmental variables and what analysis techniques can yield high-confidence spatial information?

The answers to these questions are, for the most part, generally applicable to the world's drylands, but can be tailored to special circumstances or to detailed case studies.

The processes of desertification are necessarily tied to a definition of desertification. Although this thesis focuses on wind erosion, any process that enforces abiotic redistribution of nutrients and the reduction or redistribution of NPP—such as water erosion, rain splash, or salinization—is a process of desertification.

Consideration of the processes of desertification necessarily leads to identification of environmental variables which drive these processes. In terms of wind erosion, these variables would be: grain-size distribution, armoring, biological or chemical crusting, soil nutrient concentrations, plant structure (height, width, porosity, basal area, frontal areal, above-ground biomass), plant number density, vegetation community composition, and vegetation cover by species.

Once the process-related environmental variables that control desertification are determined, the remote sensing techniques for retrieval of this information can be identified. At this point, consideration of remote desertification monitoring must be tempered by the reality of the limitations of remote sensing data for provision of process-relevant information. In the following section, the final questions concerning which process indicators can be unambiguously detected as well as the data and analysis

techniques for their detection will be considered.

2. REMOTE SENSING DATA REQUIREMENTS: REASONABLE EXPECTATIONS

Unfortunately, much of the needed information cannot be retrieved from current remote sensing platforms. As was shown in Chapter 5, vegetation community type can not be reliably retrieved from even the best hyperspectral data at covers below about 30% under near-ideal conditions. The inconsistencies and vagaries of nature, especially in arid and semiarid regions, conspire against retrieval of much of the desired information. Currently no good method exists for retrieval of vegetation structure variables from optical remote sensing data (see, Franklin and Turner, 1992) though radar remote sensing may be able to supplement this data. As was also shown in Chapter 5, soil characteristics can be retrieved with greater reliability than vegetation characteristics in arid and semiarid regions; however, currently no method exists for retrieval of grain-size distribution or plant nutrient concentrations from optical remote sensing data. Some success has been obtained in retrieving soil mineralogy from optical data (see, for example, Vane and Goetz, 1988, 1993).

Of course, as remote sensing data quality improves and new analysis techniques are developed, the list of unambiguous process indicators that can be detected with high confidence will grow. In this section, I will discuss possible uses for remote sensing data in desertification monitoring. The discussion will be organized around three elements of sensor design—spatial, spectral, and temporal resolution—and the leverage that each can

give in providing process-relevant environmental information.

2.1 Spatial Issues—Large Pixels or Small?

Schlesinger *et al.* (1996) have noted that in degraded arid and semiarid lands, a principal change that occurs is a change of the scale of heterogeneity. As semiarid lands degrade from relatively homogenous grasslands to heterogeneous shrublands, the scale of spatial variability increases. The use of spatial statistics on soil samples in the Jornada Basin allowed Schlesinger *et al.* (1996) to identify this change in scale. This effect is also clearly seen in remote sensing images (Phinn *et al.*, 1996) and recently Hudak and Wessman (Hudak and Wessman, 1998) have used textural analysis of high-resolution aerial photographs to characterize woody plant encroachment in a South African savanna.

In order for textural analysis or spatial statistics to work, pixel size must be smaller than the scale of variability of at least one of the dominant landscape types—grasslands or shrublands. If pixel size is greater than the scale of variability then the differences between landscape elements such as soil and plants will average out and sub-pixel spatial information is lost. If pixel size is significantly smaller than the scale of heterogeneity (plant or inter-plant dimension), on the other hand, spatial statistics may be used to probe the distribution of vegetation or soil in the landscape. This was the technique used in Chapter 4 to verify the presence of streets in wind-dominated mesquite dunelands. These facts argue for pixel sizes that are uniformly smaller than the scale of variability on the ground.

All current and near-future spaceborne optical remote sensors fall into one of

three categories: panchromatic sensors, multispectral sensors, or hyperspectral sensors. Panchromatic sensors have one band in the visible spectrum. Because of this, these sensors can provide data with a very large number of pixels per line which translates to a high spatial resolution. Panchromatic sensors are therefore very useful in providing textural information because their pixel size may be smaller than the scale of heterogeneity on the surface while maintaining reasonable data rates. Very wide-band observation in the visible, and possibly in the short-wavelength near infrared, will allow discrimination of vegetation and soil (see Chapter 4) or observation of shadows cast by ground elements. Either vegetation/soil discrimination or shadow observation on a very fine scale allows textural analysis of many types.

2.2 Spectral issues—Hyperspectral or Multispectral?

Multispectral sensors collect data in a few broad spectral bands which cover important regions of the reflected solar spectrum (about 300 to 2500 nm). Because these sensors provide data in multiple bands, the total number of pixels per line for these sensors is less than that for panchromatic sensors. Therefore, spatial resolution is usually poorer for spaceborne multispectral sensors than for panchromatic sensors, although large swath widths are typically considered desirable. In addition, multispectral sensors lack the several narrow bands in the VNIR water absorption region which are required to model atmospheric water vapor and thereby calculate apparent surface reflectance. As a result, no *ab initio* method exists for converting calibrated multispectral radiance data to reflectance data (see Chapter 5). Reflectance is the quantity with real physical meaning

that is required for many types of data analysis such as spectral mixture analysis (SMA) or band matching.

Hyperspectral sensors, also called imaging spectrometers, provide data in a large number of narrow, contiguous bands that cover the entire reflected solar spectrum. Because these sensors provide data in a large number of bands, the total number of pixels per line for these sensors is greatly reduced compared to panchromatic or multispectral sensors. As a result, these sensors typically provide data in very narrow swaths (such as the NM-EO1 Hyperion instrument) or with large pixel sizes (such as the MODIS instrument). Hyperspectral data covers the VNIR water absorption region and therefore atmospheric water vapor and apparent surface reflectance can be retrieved (see Chapter 5 as well as Gao and Goetz, 1990; Green *et al.*, 1993; Roberts *et al.*, 1993).

Hyperspectral sensors, with their very high spectral resolution, have seemed to some a panacea, with the ability to retrieve information about minerals, soils, vegetation and the atmosphere (Vane and Goetz, 1993). The thought has been that the very low repeat times associated with small swaths would be more than compensated because hyperspectral data would tell all about the surface that one would want to know. Despite these early high hopes for hyperspectral remote sensing, it has proven less useful than originally thought.

In Chapter 5, hyperspectral simulations are used to demonstrate practical limits on spectral mixture analysis of hyperspectral data. The lesson from that chapter is that in arid and semiarid environments with low plant covers, even the best hyperspectral sensor under unrealistically optimal conditions cannot provide reliable retrievals of vegetation or community type. Real-world spectral variability and nonlinear mixing makes this picture

even more bleak. Despite this, fractional vegetation cover and soil surface type can be reliably retrieved from hyperspectral remote sensing.

Multispectral data has been used for a wide variety of landscape ecological applications. Since reflectance retrieval is not possible with these data, the typical use of multispectral data is with vegetation indices (band ratios) wherein atmospheric scattering, lighting effects, and sensor characteristics are obviated. In arid and semiarid environments, this approach is not effective (see Appendix A for a more complete discussion and references). Nonetheless, in Appendix A, I show that multispectral (Landsat) data is capable, in some circumstances, of identifying important process-relevant features such as soil surface texture, though not through band ratios. This was only possible by using soil retrievals from multiple endmember spectral mixture analysis of hyperspectral data. Appendix A suggests the compatibility of multi- and hyperspectral data in addressing regional problems such as wind erosion. It shows how a small hyperspectral subset of a large multispectral image can be used to quantitatively leverage the entire multispectral image.

Hyperspectral data do provide a method for determining vegetation cover and soil surface type, but the small scale of these images makes the data of limited usefulness. Multispectral data can provide soil information over a much larger scale, but requires a method to calibrate soil indices. Multispectral vegetation indices are functionally useless in arid and semiarid environments.

In order to facilitate regional monitoring of both soils and vegetation, both multispectral and hyperspectral imagers are required. For large-scale monitoring, a Landsat ETM+-like multispectral sensor with several bands in the visible, near, and

short-wave infrared with a spatial resolution, similar to ETM+ (30 m), may be used. In order to provide a way to retrieve surface reflectance from the multispectral imager and to train its observations by methods similar to that use in Appendix A, the multispectral data must be paired with a hyperspectral data with nearly identical resolution. The hyperspectral data may spatially subset multispectral data.

2.3 Temporal Issues—Toward Multitemporal Monitoring

When considering the temporal aspects of sensor design, it is useful to identify the timescales of the principal phenomena to be imaged. In arid and semiarid regions, there are three timescales on which landscape change occurs.

The landscape change with the fastest time constant is the nearly immediate greening of the landscape after a rain event. For example, Garcia-Pichel and Belnap (1996) have reported that cyanobacterial crusts, common in arid and semiarid environments, initiate photosynthetic activity within minutes of exposure to water. This is partially responsible for the change in appearance of these crusts after rainfall. Vegetation also responds on times ranging from minutes to hours after rain in some arid areas.

While some vegetation responds to individual precipitation events, arid and semiarid landscapes as a whole are largely controlled by seasonal changes in temperature and precipitation. Vegetation in the Chihuahuan Desert, for example, responds to two rainfall regimes: winter/spring precipitation and summer monsoonal precipitation. Thus, two distinct "greenings" occur in this landscape, as C_3 shrubs respond to winter/spring

precipitation and C_4 grasses respond to the summer monsoon rains. In contrast, vegetation in the Mojave Desert only displays one greening in the winter and early spring as the shrubs respond to winter rains. This environment lacks a summer monsoon and therefore does not support large grassland communities.

Finally, vegetation can vary interannually in response to changing climatic conditions or on decadal timescales in response to human disturbance or recovery. For example, over the past 150 years, the Jornada Basin has changed from a grass-dominated landscape to a shrub-dominated landscape (Buffington and Herbel, 1965). Droughts lasting a few years to decades can also have dramatic impacts on a vegetation community (see, for example, Muhs and Maat, 1993; Schultz and Ostler, 1993).

Changes in the soil typically occur on the annual to decadal timescale as well. For example, the appearance and growth of the sand blow-outs observed in the Manix Basin (see Chapter 3) can only be observed on annual timescales. While much of this erosion may happen in just a few large events each year, the cumulative effects are not seen on seasonal timescales. Soil development, or the formation of desert pavement, occurs on the timescale of centuries to millennia.

What do these various timescales mean for the design of a spaceborne sensor optimized to observe and monitor landscape changes in the world's arid and semiarid environments? First, changes in vegetation that occur on the minute to hour timescale cannot be effectively observed using remote sensing techniques, and these are probably meaningless to desertification anyhow. To do this would require observation repeat times of minutes which is highly unrealistic. Much more realistic, however, is observation of landscape changes that occur on timescales from seasonal to decadal.

These inter-seasonal observations are particularly important in monitoring areas with both grasslands and shrublands, such as the Sonoran and Chihuahuan Deserts, the Sahel, and much of Southern Africa.

Any remote sensing platform aimed at monitoring arid lands should provide data with repeat observations such that these landscape changes can be observed in reasonable detail. Since the greenings associated with seasonal rains in arid and semiarid environments last several months, a minimum repeat time for observation of these phenomena would have to be on the scale of a month. In order to track the progress of vegetation greenings and to account for missed observations due to cloud cover, however, repeat times on the order of two weeks will provide adequate observation of landscape changes from inter-seasonal vegetation changes to drought monitoring to decadal-scale desertification.

2.4 Integrative Issues—Possible Data Sources

In order to provide useful process-relevant data about the state of vegetation and soils in arid and semiarid environments, and thereby to provide monitoring capability, the combined used of panchromatic, hyperspectral, and multispectral data is optimal. However, with upcoming spaceborne remote sensors, no great need exists to design and deploy a desertification monitoring-optimized system. While it is optimal for all data to be collected from a single platform, perhaps this is asking too much. Within the next several years, a suite of remote sensing data products will be available which, when used together, should provide data to proceed with desertification monitoring globally.

Currently, no satellite has characteristics which makes it ideal for arid region remote monitoring. However, combined use of data from different multispectral (Landsat-class), hyperspectral, and very high resolution panchromatic instruments currently or soon to be available can fulfill many monitoring needs. For example, the New Millennium Earth Observing-1 (NM-EO1) satellite, which is due for launch October 17, 2000, and has the Landsat-class Advanced Land Imager (ALI) and the 220-band Hyperion imager, will come close to providing hyper-and multispectral requirements for arid region remote monitoring. In the private sector, Orbimage, Inc., plans to launch in 2001 Orbview-4. This platform has panchromatic (1-m resolution), multispectral (4-m resolution), and hyperspectral (8-m resolution) imagers but also has a very small swath width (8 km). Data from this platform will be useful in providing information about small areas, but will not provide regional monitoring capability. However, since high-resolution data for textural analysis may not be required as frequently as multispectral data, the small swath widths may be acceptable. Thus, the possibility exists for Orbview-4 or similar next-generation imagery be used for local and regional monitoring or to enhance Landsat imagery for regional to global desertification monitoring.

Unfortunately, current remote sensing analysis tools and techniques for working in arid and semiarid regions are inadequate for measuring many important landscape features. As discussed at length in Chapter 5, arid region remote sensing is fraught with difficulties and traditional techniques do not perform well in these areas. If remote sensing is to provide process-relevant information which is of use to land managers, new techniques must be developed.

3. NEAR-TERM PROSPECTS FOR IMPROVED REMOTE MONITORING TECHNIQUES

Two things are required to obtain process-relevant from remote sensing data: the data itself and the tools to analyze it. The appropriate data for the task was discussed in the previous section. The appropriate tools to analyze remote sensing data form arid and semiarid regions will be discussed here.

The purpose of this section is to highlight several near-term prospects for improvement of dryland remote monitoring techniques. In Chapter 5 it was concluded that in deserts vegetation community monitoring is unreliable at low covers. As a result, it is reasonable to address and improve the prospects for monitoring soils in arid and semiarid areas. It is particularly important to focus on soil properties which can effect desert vegetation either directly or indirectly. Nonetheless, the ability to accurately determine vegetation type and cover from remote sensing data remains a worthwhile goal because desertification typically manifests as a change in the landscape's vegetative state.

3.1 Concentrating on the Soil

The principal lesson from Chapter 5 of this thesis is that vegetation in arid and semiarid regions is inherently difficult to observe, even under optimal conditions. The near-term development of hyperspectral data analysis tools should focus on soil properties. At first, this may seem an ineffective way to monitor desertification which is often defined in terms of plant productivity. Note, however, that Schlesinger *et al.* (1990;

1996) use soil properties to define desertification. Furthermore, vegetation and net primary productivity are, in part, dependent on soil properties. Thus, when data analysis is carried out in the context of a process model such as the one constructed in Chapters 2 and 3, observed changes in soil properties can be tied to changes in the vegetation community. Soil surface properties which can be retrieved from hyperspectral data can yield important information concerning the vegetation. The soil properties which would be most useful for desertification monitoring have already been listed in Section 1.4 of this chapter. Many methods already exist for retrieval of mineralogical information from soils. Here avenues of exploration for other parameters will be discussed.

3.1.1 Grain-size Distribution

The grain-size distribution of surface soils is of the utmost importance for monitoring desertification, especially in areas prone to wind erosion. In addition to vegetation parameters, this soil parameter can largely control wind erosion in arid and semiarid environments. Painter *et al.* (1998) have effectively used radiative transfer modeling to obtain snow grain sizes from hyperspectral imagery. This approach works in snow-covered environments due to the extremely simple mineralogy of snow. Most soils contain a variety of minerals. However, mature sands which are most prone to mobilization by wind often have a simple mineralogy dominated by quartz grains. The Painter *et al.* (1998) method for retrieval of grain size should be attempted in aeolian environments in order to retrieve grain-size data in arid and semiarid environments. The availability of this type of information would allow estimation of threshold friction velocity for wind erosion and therefore the vulnerability to wind erosion.

3.1.2 Soil Armoring

According to the "born at the top" model of desert pavement formation, the clasts which armor the soil are exposed to the surface throughout the development of the pavement (McFadden *et al.*, 1987; Wells *et al.*, 1995). As a result, the armoring clasts can develop desert varnish on their upper surfaces which is often obvious in the field. The presence of desert pavement is indicative of a stable surface and protection against wind and water erosion. Stable surfaces, therefore, may be identified through the distinct spectral characteristics of the desert varnish on pavement clasts. Hyperspectral tools (such as SMA) which can identify the presence or absence of desert pavements may be able to provide information on the stability of arid lands and their vulnerability to disturbance.

3.1.3 Soil Nutrient Concentrations

Currently, no method exists for determining nutrient concentrations in the soil using optical remote sensing. This availability of this information on a regional scale would obviously be of great importance in monitoring desertification. Monitoring nutrient concentrations in the soil is essential to assess the viability of the vegetation community. However, in the absence of prominent and unique spectral signatures of the target nutrients, another method must be employed to determine soil nutrient concentrations. One approach is to obtain a large number of soil samples coincident with and within a hyperspectral image. Multiple regression of nutrient concentrations against pixel reflectance (in one to several bands) may provide an empirical relation which may

be used to predict nutrient concentrations elsewhere.

3.2 Possibilities for Retrieval of Vegetation Information

3.2.1 Two-Step MESMA

A principal difficulty in obtaining vegetation information, and especially species information, is intra-species spectral variability. The MESMA approach allows for some intra-species spectral variability by incorporating several spectra of each species in the spectral library. However, the potential range of spectral variability is so great that many spectra may have to be incorporated into the spectral library. Under the basic MESMA approach, this translates to an extremely large number of mixture models to run on each image and a very large amount of computing time. In short, trying to accommodate the degree of spectral variability observed in the field in the basic MESMA approach quickly becomes computationally unrealistic.

This trouble may be bypassed partially by instituting a two-step MESMA process. The first step of the processing would be a basic MESMA analysis with a limited number of vegetation spectral endmembers and enough soil endmembers to adequately retrieve the desired soil surface information. This was the technique used in Chapter 5 where it was established that MESMA of AVIRIS data is capable of retrieving information about soil surface types in arid and semiarid regions.

Once the soil fractional cover and the soil spectrum for each pixel has been retrieved in this way, the soil contribution to each pixel's reflectance can be removed leaving a component that is, ideally, due only to vegetation. This secondary "vegetation

image", may then be unmixed by MESMA using a library that contains only vegetation spectra. Since these spectra do not need to be mixed with soils, as this component was removed, the total number of models which must be run for each pixel is greatly reduced. As a result, the vegetation-only spectral library can contain a large number of spectra of each species type, thus accommodating significant spectral variability without geometric increases in computation time.

This two-step MESMA process is a sub-set of the basic MESMA approach. In particular, it simply reduces the total number of models that need to be run on each pixel by eliminating in the first step models that include soils which are not likely present in each pixel.

The creation of a "vegetation image" in the first step of the two-step MESMA may have other ancillary benefits. In particular, it may allow more reliable calculation of traditional vegetation indices. This possibility arises because one of the most often-cited problems with the use of vegetation indices in arid and semiarid areas is that the dominant soil signature can dramatically affect index values independent of changes in vegetation component of the spectrum (Huete and Jackson, 1987; Huete *et al.*, 1985; Huete *et al.*, 1984). Thus, using a vegetation image, this problem may be obviated. However, it does not deal with the fact that arid region vegetation typically lacks the strong red-edge which is exploited by vegetation indices (see Chapter 5). Thus, calculation of vegetation indices from a vegetation image may still result in values which are difficult to correlate with process-relevant vegetation parameters. While this method cannot provide estimates of vegetation cover, it may enable temporal monitoring of vegetation greening and senescence.

3.2.2 The Use of Spatial Information

Encoded in all remote sensing imagery is not only spectral information, but spatial information as well. This fact is so intuitively obvious that it is often overlooked. We see image spatial coherence—the resolution of pixels in an image into regions much larger than a single pixel—when we look at an image. Lack of spatial coherence manifests as noise in an image and its presence often suggests problems in acquisition or analysis of an image. Furthermore, spatial coherence conforms to our typical idea of the way in which landscapes exist—with soils and plant communities in an area being more or less similar to their neighbors.

This spatial information, and in particular spatial coherence, may be able to be leveraged to enhance our analysis of remote sensing imagery. For example, image pixels that are larger than the scale of variability on the ground may allow leverage of landscape characteristics that vary slowly and smoothly.

Consider for example, a long north-south basin. In the north, a medium-sized shrub (Shrub A) grows with low cover, while in the south a different medium sized shrub grows (Shrub B), also with low cover. The transition between the Shrub A-dominated part of the basin and the Shrub B-dominated occurs smoothly.

In this case, it is useful to have pixels several times larger than the inter-shrub spacing of either Shrubs A or B. Since the transition occurs smoothly and slowly, a pixel in the basin may be expected to be very similar to its adjacent pixels. Some degree of spatial coherence is then expected when, say, MESMA is used to map the distributions of Shrubs A and B. If, in the presence of non-linear mixing, spectral variability, and

instrument noise, this coherence is not borne out by the analysis, a further constraint of spatial coherence may be imposed on the mixture modeling to provide a better fit. Forcing adjacent pixels to be modeled in a similar way may allow the correct modeling of the vegetation of this basin.

This approach has not, to the author's knowledge, been tried. A major reason for this is that it requires that all pixels in a scene be unmixed simultaneously. This is enormously costly in terms of computation and until recently, has been out of reach for most serious researchers. Nonetheless, with the increasing availability of high-performance computing resources, adding spatial constraints to remote imagery analysis will likely provide significant increases in our ability to tease out valuable information.

3.2.3 The Use of Temporal Information

Vegetation in dryland environments can undergo very dramatic phenological changes which are accompanied by changes in the vegetation's spectral signature. This "spectral phenology" may be leveraged in remote sensing analysis to identify different types of vegetation in arid and semiarid landscapes.

For example, grasses in the Chihuahuan Desert summer are green but are senesced at all other times of the year. Shrubs, on the other hand, tend to remain green throughout the year. Thus, the presence of grass in remote sensing imagery may be detected by the ingrowth of its spectral signature during the summer. This technique has been used by Eve (1995) with AVHRR data to discriminate between grass- and shrub-dominated Chihuahuan landscapes.

One of the major manifestations of the desertification of semiarid lands

worldwide is the colonization of grasslands by woody vegetation. Thus, the ability to detect and discriminate grasses and woody vegetation would provide a valuable tool for desertification monitoring. In light of the difficulty of retrieving vegetation information from hyperspectral imagery under optimal conditions, the use of temporal information in to constrain landscape classification has a dramatic potential for the provision of process-relevant desertification monitoring information to land managers.

4. SUMMARY

Arid and semiarid environments around the globe are facing dramatic degradation. At the same time no political or financial institution exists with the authority or mandate to monitor this degradation. In other words, the world's drylands are suffering from a terminal lack of information. As a result, there is little hope to combat global.

Optical remote sensing is not a perfect tool to supply this information. It suffers from real limitations in terms of the information that it can provide. Nonetheless, degradation of arid and semiarid lands is fundamentally a spatial phenomenon and the time-dependent processes involved in desertification are largely important due to their spatial extent. Optical remote sensing is a tool with promise to provide timely information about the state of the world's drylands in a time- and cost-effective manner.

The preferable method for monitoring desertification is to monitor the causes and conditions of desertification and not the manifestation of desertification itself. This not only allows the general application of a monitoring strategy, but also raises the possibility

of monitoring areas at heightened risk of desertification before real damage is done.

Monitoring the causes of desertification requires the use of a process model which then guides the choice of which landscape variables are most relevant. Once the monitoring scheme is thus determined, remote sensing acquisition and analysis tools need to be employed. Currently, there is no single spaceborne platform which is ideally suited for arid region remote monitoring. Likewise, data analysis tools are currently insufficient for providing process-relevant information to land managers.

Nonetheless, exploration of the spatial, spectral, and temporal issues in dryland remote monitoring can suggest the appropriate use of remote sensing data. Effective monitoring can take advantage of 1) a high-resolution panchromatic imager, 2) a medium-resolution Landsat-like multispectral imager, and 3) a medium-resolution hyperspectral imager. In order to obtain useful temporal information, the repeat observation time must be approximately two weeks.

Much of the required data is currently or will soon be available. Thus, new techniques need to be developed to retrieve process-relevant information from existing optical sensors. Since the likely optimal use of hyperspectral imagery for monitoring purposes is to inform multispectral data analysis, high-quality hyperspectral analysis tools need to be created for use in arid and semiarid environments. Near-term strategies which may prove useful are: 1) concentration on the soil signature, 2) two-step MESMA processing, 3) the use of spatial information, and 4) the use of temporal information. Development of high-performance hyperspectral imagery analysis tools has the potential to enable the provision of process-relevant information to land managers worldwide. The availability of this information will be a valuable tool in the identification of areas at

heightened risk of desertification.

PART III

TOWARD SUSTAINABLE LAND USE

IN ARID AND SEMIARID ENVIRONMENTS

Advances in the understanding of the processes of desertification and its monitoring using remote sensing made in Parts I and II are only part of the goal of this thesis. Chapter 7 clearly identifies obstacles on the road to sustainable land use in arid and semiarid areas and outlines approaches to overcoming them. In particular, future work on wind-driven desertification process modeling and remote monitoring of desertification are outlined. An integrative approach to forecasting desertification combining both socioeconomic and environmental factors is also proposed.

CHAPTER 7

OBSTACLES ON THE ROAD TO SUSTAINABILITY

Throughout this thesis, I have discussed process modeling and remote monitoring results which enhance the basic scientific knowledge of desertification and its observation. Nonetheless, obstacles on the road to sustainability in arid and semiarid environments still exist. The basic susceptibility of the world's drylands to degradation remains compounded by a serious lack of information about (1) the causes and processes of desertification, and (2) about the extent of desertification as well as how to effectively monitor it. Therefore, as a global society we lack the knowledge necessary to combat desertification effectively. Finally, we lack the ability to forecast desertification. The purpose of this chapter is to identify such obstacles more precisely and to outline approaches to overcoming them.

1. WIND-DRIVEN DESERTIFICATION: PROCESS MODELING

Part I of this thesis has provided significant new insight about the role of wind erosion as a desertification process. In particular, I have proposed and tested a preliminary model of wind-driven desertification (Chapters 2 and 3) as well as shown that wind itself influences vegetation distribution in degraded lands so as to permit

enhanced wind erosion (Chapter 4). These chapters show that mobilized sand is a key environmental factor in initiating and propagating local desertification. In addition, the analyses in Chapter 5 and Appendix A indicate that mobilized sand is a phenomenon that can be effectively identified from space, thus highlighting its importance in desertification monitoring and forecasting. In Appendix C, I suggest that the El Niño Southern Oscillation (ENSO) can be used as a leading indicator of the frequency of wind erosion events at a site in the arid southwest. Despite this progress, much work remains in understanding the role of wind in desertification. The following sections address three specific questions in process modeling of wind-driven desertification: wind vs. water in dryland degradation, the role of climate, the role of disturbance. Appendix D elaborates on these questions and proposes a set of new experiments to directly address them.

1.1 The Role of Wind vs. Water in Dryland Degradation

Since the publication by Schlesinger *et al.* (1990) of a general model of the degradation of arid lands, desertification has been defined as the reduction or redistribution of net primary productivity in arid and semiarid environments which is accompanied by a similar reduction and spatial redistribution of soil resources. Both the action of water and wind in redistributing and removing nutrients are often cited as possible mechanisms for this reorganization of soil resources (Schlesinger *et al.*, 1996; Schlesinger *et al.*, 1990). At issue is the question of which abiotic process is responsible for (1) the net loss of nutrients from the landscape, and (2) the reorganization of nutrients, soil particles, and organic particles within the landscape.

A great deal of work has been carried out examining the role of water in nutrient reduction and enforcement islands of fertility in degraded rangelands. However, in a recent paper, Schlesinger *et al.* (2000) have concluded that water erosion cannot, by itself, account for the depletion of soil fertility associated with desertification in the Chihuahuan desert. In the Manix Basin, it is clear that wind, not water, is responsible for shrubland degradation.

Thus, it is important to examine in more depth the role of wind in the degradation of arid and semiarid shrublands. Understanding the causes and conditions of wind erosion in arid and semiarid lands is vital to our understanding of local, regional, and global ecological systems as well as our ability to estimate consequences of human activities on these lands. The process model presented in Chapter 2 and validated in Chapter 3 is a first step in understanding the role of wind as a desertification process. However, no study to date has addressed in a large-scale experiment at multiple sites the magnitude and effect of wind erosion in natural arid and semiarid lands. Until this question is addressed, the importance of wind erosion in landscape dynamics, desertification, and global change will remain ill-defined. As a next step, the analysis and experiments presented in Appendix D will help define climate and vegetation thresholds that control wind erosion in arid and semiarid grasslands. This and other work, therefore, will help clarify the role of wind in triggering and propagating desertification.

1.2 The Role of Climate

Global anthropogenic climate change is likely to effect arid and semiarid regions

all over the world (Muhs and Maat, 1993). General circulation models (GCMs) predict that increases in atmospheric greenhouse concentrations will tend to make the world's drylands hotter, generally less amenable to agriculture, and drier due to increased evapotranspiration (Forman *et al.*, 1992; Hansen *et al.*, 1988; Rind, 1990, Adams, 1990 #556). Simulations also show that greenhouse gas-induced warming may reduce soil moisture in arid and semiarid areas (Rind, 1990; Washington and Meehl, 1984) due to a decrease in the ratio of precipitation to evapotranspiration. The increased frequency of droughts under this scenario is likely to trigger landscape changes in modern arid and semiarid environments (Forman *et al.*, 1992; Rosenzweig and Hillel, 1993). There is a high probability that global anthropogenic climate change will have serious effects on the American Great Plains and Southwest. Paleoclimatic studies here suggest that increased aeolian activity in the past, including actual dunes, has been associated with hotter and dryer conditions (Forman *et al.*, 1992; Madole, 1994; Morrison, 1991; Stokes and Swinehart, 1997; Woodhouse and Overpeck, 1998).

Understanding the role of wind as a landscape process is vital not only in understanding the present degradation of arid and semiarid lands currently observed globally, but also in understanding the environmental history of the American Southwest and the Great Plains. Here, since the last ice age, several episodes of aridification have occurred with large mobile sand belts covering much of the western Great Plains (Forman *et al.*, 1992; Madole, 1994; Morrison, 1991; Stokes and Swinehart, 1997; Woodhouse and Overpeck, 1998). The Great American Dust Bowl in the first half of the 20th century was, in part, a remobilization of these dunes driven by a relatively short period of drought (10-20 years) (Rosenzweig and Hillel, 1993). The potential for wind

erosion throughout the western U.S. clearly remains extremely high and as the Dust Bowl episode illustrates, decadal-scale drought can have dramatic consequences for geomorphic landscape processes (Forman *et al.*, 1992; Rosenzweig and Hillel, 1993) and dust emission (Gillette and Hanson, 1989).

There has, of course, been much discussion about the relative importance of human versus climate drivers of arid land degradation and wind erosion, but both can have a dramatic impact on a landscape. Despite this, little information exists on the role of climate change in inducing desertification or on the mechanisms through which it is likely to act. Again, the experiments discussed in Appendix D will help identify climate thresholds at which dryland environments become highly susceptible to desertification.

1.3 The Role of Disturbance

As suggested in Chapters 2 and 3, removal of vegetation and destruction of the soil crust in arid areas can enhance wind erosion and initiate local desertification. Likewise, at the Jornada LTER site, grazing has initiated dramatic changes in vegetation and an increase in wind and water erosion. The types of disturbance seen at the Manix Basin and in the Jornada, however, are severe. At some lower level of disturbance, these effects will be less pronounced and at some level of disturbance, land degradation processes may not be triggered at all.

The role of disturbance in initiating desertification remains an open question. In particular, disturbance regime—below which no large-scale landscape changes occur and above which processes of desertification are initiated—need to be identified for dryland

environments. The principal question which needs to be asked is, "at what level of disturbance does desertification occur?" Of course, the type of disturbance can greatly impact the response of a desert landscape, and natural disturbances may have much different consequences than human disturbances.

Little research has been done in identifying desertification thresholds or in determining the relative effects of landscape- or climate-state and disturbance type. The experiments proposed in Appendix D provide a method for separating the effects of climate, landscape state, and severity of disturbance in initiating wind erosion in semiarid grasslands. In particular, they will help tease apart the climatic and anthropogenic drivers of desertification by simulating a range of disturbances at sites along a bioclimatic transect and identifying thresholds at which landscape change (vegetation change or wind erosion) becomes highly probable. Further research of this types is required to identify disturbance thresholds and the factors that control them.

2. REMOTE MONITORING OF DESERTIFICATION

In Chapter 6, I proposed an integrated view of the use and potential role of remote sensing in dryland monitoring. According to this view, both the processes of desertification and the practical uses of remote sensing data are incorporated to provide reasonable expectations for the use of remote monitoring of desertification. I concluded that a balanced, affordable suite of optical remote sensing data—high-resolution panchromatic data, regional multispectral data, and targeted hyperspectral data—are required for effective optical monitoring of the causes of desertification. Thus, it is clear

that improving the understanding of desertification processes is a critical first step to providing tools and techniques for remote monitoring of desertification. Process models can suggest the relevant metrics for study from spaceborne remote sensing instruments.

At the same time, quantitative remote sensing in arid and semiarid regions is much more difficult than originally expected. For example, in Chapter 5, I show that species identification in arid and semiarid regions is unreliable. However, by concentrating on the soil signature, valuable information may be obtained. In Chapter 4, I show that high-resolution panchromatic imagery can be used to predict enhanced wind erosion in shrublands. In Chapter 5, I show that soil texture is monitorable using hyperspectral remote sensing techniques. In Appendix A, I show that multispectral data can identify sandy soils in some cases. These successes are important because of their relation to the process model of wind-driven desertification developed in Chapters 2 and 3 where the presence of wind-erodible soils plays a major role in the initiation and propagation of desertification.

Because no organization currently has a global mandate to monitor desertification, monitoring will have to be carried out by local and regional interested institutions and organizations. These groups will become an important constituency for U.S., foreign, or international satellite systems because they will require high-quality satellite data. These groups will also require high-quality process models to proceed with remote observation and monitoring because they must be informed by field-tested process models in order to guide these observations and to put them in their proper context.

Although the scientific community's process models of desertification are not yet

perfect, remote monitoring of desertification remains the most time-and cost-efficient way to provide timely and affordable information about the world's drylands. Whether monitoring occurs at a local, regional, or global scale, it must proceed promptly using the best process and remote sensing data available. With so much of the world's drylands degraded or at risk of desertification, the potential environmental and humanitarian disasters that could ensue in the upcoming decades justifies development and deployment of effective desertification remote sensing strategies.

3. FORECASTING DESERTIFICATION

A large proportion of the world's arid and semiarid areas are either degraded or at risk of degradation. Since desertification is often extremely costly, or even impossible, to reverse, careful attention must be paid to the areas at risk of desertification. If possible, areas at heightened or immanent risk of desertification must be identified so that policy and management structures can be put in place before widescale landscape damage occurs.

Clearly landscape structure, soil, and climate can influence an area's risk for desertification, but the pressures which will influence at-risk areas are not solely environmental. Humans also act on the landscape and their behaviors reflect socioeconomic factors. Thus, both environmental and socioeconomic drivers must be taken into account in order to identify areas at heightened risk of desertification.

The potential response of large groups of people under socioeconomic pressures can be extremely difficult to forecast. However, we are not left without hope. There is a

practical index which is used in perhaps an even more challenging human circumstance. Leading economic indicators (LEIs) are widely accepted economic indices used to forecast the near-term behavior of the United States economy. The U.S. LEI calculated by The Conference Board, and used by the U.S. Department of Commerce, incorporates ten different types of data such as the S&P 500 Index, money supply, building permits for new private houses and an index of consumer expectations (see http://www.tcb-indicators.org/index.htm for more information). The marketplace, it turns out, is an arena where the collective behavior of many individuals may be forecast by aggregating diverse economic data into a single equation with predictive ability. This capability exists even in the absence of a full mechanistic understanding of the myriad cause and effect relationships.

What is required for forecasting desertification is an LEI-like scheme—Leading desertification indicators (LDIs)—in which both environmental and socioeconomic considerations are aggregated to provide some estimation of an area's risk of desertification. Leading climate indicators have already been suggested to forecast food production shortfalls to enhance regional food security (Broad and Agrawala, 2000).

An added complication exists in developing leading indicators of desertification that does not exist for LEIs. The intrinsic susceptibility of landscapes to desertification needs to be taken into account in addition to the factors that influence them. For example, semiarid grasslands in southern New Mexico are more susceptible to environmental change than similar grasslands in central New Mexico. Thus, even given identical environmental (*e.g.*, climate change) and socioeconomic conditions (*e.g.*, population growth or grazing pressure), the two grasslands may not respond in the same

way. As a result, LDIs will have to be regionally specific, and evaluation of an LDI for central New Mexico will have to be slightly different than the evaluation of an LDI for southern New Mexico. Likewise, assessment of desertification risk in the American Southwest will be different from its assessment in the Sahel.

What is an LDI? An LDI is a map of the projected risk of desertification for drylands at scales from local to global. In an LDI, every point on the map would have a value, calculated from the most recently available data, which reflects the risk of desertification. The value of the LDI at every point on the map is a function of diverse environmental, socioeconomic, or political factors. Although the equation for the LDI may take many forms, a simple combination of functions is suggested:

$$LDI = f(S, F_i),$$

where S reflects the intrinsic susceptibility of the landscape to desertification and each F_i is a function, incorporating one type of environmental or socioeconomic data, that reflects a projected effect on the susceptibility to degradation.

As a simple, qualitative example of an LDI, consider the U. S. states that share a border with Mexico. At the time of the ratification of the North American Free Trade Agreement (NAFTA), there was a great deal of discussion of the potential environmental effects of this treaty on the southwestern United States. Abundant information already exists suggesting that arid and semiarid areas in the Southwest are highly susceptible to degradation (see, among others, Chapters 2-4, Brown *et al.*, 1997; Buffington and Herbel, 1965; Schlesinger *et al.*, 1990). In addition, counties along the U.S.-Mexico border are experiencing some of the fastest population growth rates in the country (J. Peach, *personal communication*). Finally, the analysis of the relationship between ENSO and

wind erosion in Appendix C indicates that in some years with unusually hot and dry weather, the landscape is particularly vulnerable to wind erosion. These factors—intrinsic susceptibility to land degradation, high population growth, and vulnerability to climatic fluctuations—taken together, suggest that drylands in the southwestern states are at high-risk of desertification. This example shows how the combination of both environmental and socioeconomic data may be used to forecast desertification. While this type of analysis is crude, it is much better than nothing in providing concrete data which may then be used to inform policy and management decisions.

A great deal of work will have to go into development of effective quantitative LDIs. This effort will have to be employed in retrospective analysis of several well-defined case studies. Different forms of the LDI equation will have to be tested and new coincident or lagging indicators of desertification developed. Despite the significant work required in the development of LDIs, the semi-empirical approach of incorporating a variety of environmental and socioeconomic data provides hope for reliable forecasting of desertification.

The principal goal in LDI desertification forecasting is to help promote sustainable land use even when a detailed mechanistic understanding of the processes is unavailable. Information about the susceptibility of his lands to desertification may help an Australian rancher decide which paddocks should be used during an especially dry year. Nationwide desertification risk data may help the United States Secretary of Agriculture determine a subsidy for cattle in different regions. Or, in the NAFTA case above, regional desertification risk data may inform arguments in matters of international policy.

In short, land use decisions based on desertification risk information may help individual land owners, local and national governments, corporations, and transnational institutions avoiding the most serious impacts from land use. As discussed in Chapter 1, this is important not only for maintaining the standard of living of ranchers and farmers in the richest nations in the world. It is increasingly necessary for developing nations to conserve ecological resources if they are to participate fully in the global market economy.

4. CONCLUSION

This thesis has been presented in three parts reflecting its threefold purpose: (I) to develop and test a process model of wind-driven desertification, (II) to evaluate next-generation process-relevant remote monitoring strategies for use in arid and semiarid regions, and (III) to identify elements of effective management for the world's drylands.

In Part I of the thesis, the processes of desertification were considered. A new process model of wind-driven desertification was developed and tested in the field and the role of wind in dryland landscape development was considered and a new phenomenon— street development—was identified in degraded areas with wind-erodible soils.

In Part II, remote sensing tools for dryland monitoring were evaluated. I established practical limits on the retrieval of vegetation information from hyperspectral remote sensing data in arid and semiarid environments and showed that soil identification could be retrieved using hyperspectral remote sensing. In addition, the prospects for and

challenges to using remote sensing in effective dryland monitoring were discussed and an integrated view of remote monitoring wherein it is intimately tied with process modeling was argued. The principal combined conclusion of Parts I and II is that mobilized sand is a key process-related environmental factor that both indicates desertification and can be monitored using currently-available remote sensing tools.

Parts I and II therefore represent a significant step forward in our understanding of desertification and how to monitor it. Nonetheless, significant obstacles still exist on the road to sustainable land use in arid and semiarid areas. In Part III, this chapter, some of these obstacles are identified and approaches to overcoming them are outlined. Finally, a scheme for forecasting desertification that includes both socioeconomic and environmental considerations is proposed and an initial approach to creation of this leading index is outlined.

APPENDIX A

HYPERSPECTRAL ENHANCEMENT OF MULTISPECTRAL INDICES: POTENTIAL USE FOR MAPPING WIND-ERODIBLE SOILS IN AN ARID SHRUBLAND

1. INTRODUCTION

The purpose of this appendix is to identify multispectral indices sensitive to the presence of sandy soil surfaces. This is a pilot study to determine whether and how well a small amount of hyperspectral data can be used to enhance the use of multispectral data. With several combined hyperspectral/multispectral data acquisition strategies currently or soon-to-be available, this type of approach may determine the future synergistic use of these two complementary data types.

Hyperspectral AVIRIS data are used to simulate Landsat Extended Thematic Mapper Plus (ETM+) and Multispectral Scanner (MSS) bands. With the exception of ETM+'s visible-near infrared panchromatic band, Landsat Thematic Mapper (TM) bands are approximately equivalent to the newer ETM+ bands. These simulations are aimed at identifying useful and simple multispectral indices for the entire constellation of past and

present Landsat-class sensors to monitor areas at heightened risk of wind erosion. Having identified the most useful index for Landsat TM/ETM+, a real Landsat TM scene is used in combination with AVIRIS SMA results to identify sandy and wind erodible areas in much larger area than that covered by the AVIRIS data. I conclude that, in some circumstances, a small amount of hyperspectral data may be used to enhance the use of a much larger multispectral dataset. Further work remains to solidify the potential hybrid use of multispectral and hyperspectral data.

2. METHODS

2.1 MESMA of AVIRIS Data

MESMA of AVIRIS data is discussed at length in Chapter 5. This appendix employs MESMA to retrieve only soil type because vegetation cover in the Manix Basin is lower than can be expected to yield reliable vegetation type retrievals (see Chapter 5). Nonetheless, vegetation spectra must be present in mixing models because the absence of the vegetation's contribution, even when subtle, can effect soil type identification. In solving the mixing equations for each pixel and for each model, vegetation type and cover are always estimated, but these results are considered unreliable. Soil retrievals, on the other hand, have much lower error probabilities and therefore are considered reliable.

2.2 Simulation of Multispectral Data

Simulated Landsat TM/ETM+ and MSS reflectance data were created by

Table A-1. Landsat MSS and TM/ETM+ Bands and 1998 AVIRIS bands averaged together for simulations.

	Landsat Sensor Bandpass (nm)	1998 AVIRIS Bands Averaged
MSS Band 1	400 to 500	14 to 23
MSS Band 2	600 to 700	24 to 35
MSS Band 3	700 to 800	36 to 46
MSS Band 4	800 to 1100	47 to 77
TM/ETM+ Band 1	450 to 515	10 to 15
TM/ETM+ Band 2	525 to 605	17 to 25
TM/ETM+ Band 3	630 to 690	28 to 35
TM/ETM+ Band 4	775 to 900	45 to 57
TM/ETM+ Band 5	1550 to 1750	127 to 146
TM/ETM+ Band 7	2090 to 2350	183 to 208
ETM+ Panchromatic	520 to 900	17 to 57

averaging the AVIRIS-derived apparent surface reflectance bands that fall within each multispectral band passes (Table A-1). The units for the simulated multispectral data are thus percent reflectance. No attempt was made to resample the resultant images to Landsat resolutions (80 m for MSS, 30 m for optical TM/ETM+ multispectral bands, and 18.5 m for the ETM+ visible panchromatic band). As a result, simulated MSS and TM/ETM+ reflectance images were exactly coregistered with the SMA results.

2.3 Choice and Evaluation of Candidate Indices

Multispectral indices are formulae that employ pixel values from one or more multispectral bands. They may be complicated multiband functions or they may be relatively simple as is the case here for indices where index value equals the DN for a single band or equals the sum of DN values for two bands. Several potential indices for both TM/ETM+ and MSS were considered for the same pixels that were modeled as "Sandy/Blown Soil" using MESMA (Figure 5-6C) using only multispectral indices. In

addition to individual TM/ETM+ and MSS bands, the sum of MSS bands two and three as well as the sum of TM/ETM+ bands five and eight (panchromatic band) were considered as possible indices of the presence of sand. This resulted in 14 indices.

Index images were calculated for each candidate index. Pixels in each index image were then divided into two populations: those modeled by one of the blown sand endmembers in MESMA analysis and those that were not. One-hundred pixels were chosen at random from each of these populations and the Student's t-statistic for the null hypothesis that the two groups had the same means was calculated. The resulting probabilities of making Type II (false positive) errors are known as p-values. This procedure was repeated ten times for each index image and the average p-values were calculated. The p-values give an indication of the ability to discriminate between those pixels modeled by blown sand and those that were not for each multispectral index.

In order to identify, using multispectral bands only, those pixels that were likely to have sandy soils, a threshold index approach was used. The threshold index approach identifies pixels for which the value of an index exceeds some threshold:

$$\text{Threshold Index} = \begin{cases} 1 & \textit{index value} \geq \textit{threshold} \\ 0 & \textit{index value} < \textit{threshold} \end{cases} \tag{4}$$

where *index value* is the numerical value calculated for an index and a pixel. To find the value of *threshold*, a goodness-of-fit parameter was defined as:

$$Fit = B - S - I, \tag{5}$$

where B is the number of pixels identified by MESMA as sandy and by a threshold index, S is the number of pixels identified only by MESMA as sandy, and I is the number of

pixels identified only by a threshold index. In this way, threshold values are defined as the value for a multispectral index above which sand is likely to have been modeled using MESMA and is found by maximizing *Fit*. For each candidate index, the value of *Fit* was calculated at several threshold values and the optimal threshold value was determined.

3. RESULTS AND DISCUSSION

3.1 MESMA Modeling Results

MESMA soil surface retrievals provide an accurate picture of surface soil types at the time that this AVIRIS image was acquired (Figure 5-6C). MESMA soil retrievals are discussed in Chapter 5 in some depth. Most important for this discussion, however, is the fact that MESMA does not model some sandy soils because of a spectrally very bright sandy soil in the spectral library. Such bright, unmodeled soils occur in the northern part of the AVIRIS image. Thus, while much of the AVIRIS image was modeled correctly, a few areas failed to be modeled because they were too bright. Due to the brightness of these soils in all bands, and especially in short-wavelength infrared, these areas will be identified as sandy by the threshold indices.

3.2 Multispectral Simulations and Spectral Indices

The ability of each index to discriminate between areas that were modeled as sandy and those that were not is shown as p-values in 2. Values below 0.01 (99%

Table A-2. Comparisons of proposed index values for pixels modeled by sand and pixels not modeled by sand. T-test p-values indicate separability of sandy and non-sandy pixels for each candidate index.

Candidate Index	Mean ± σ for Sandy SMA Pixels	Mean ± σ for Non-sandy SMA Pixels	Average t-test p-value for ten 100-pixel subsamples
MSS Band 1	23 ± 2	22 ± 2	0.2241
MSS Band 2	31 ± 2	30 ± 3	0.0422
MSS Band 3	37 ± 2	35 ± 3	5.09E-06
MSS Band 4	41 ± 2	38 ± 3	7.09E-08
MSS Band 2 + Band 3	67 ± 4	64 ± 5	0.0089
ETM+ Band 1	17 ± 2	16 ± 2	0.1848
ETM+ Band 2	25 ± 3	24 ± 3	0.0888
ETM+ Band 3	32 ± 2	30 ± 3	0.0012
ETM+ Band 4	39 ± 2	37 ± 3	4.32E-08
ETM+ Band 5	46 ± 3	43 ± 4	2.25E-07
ETM+ Band 7	36 ± 4	35 ± 4	0.0036
ETM+ Panchromatic	34 ± 2	32 ± 3	0.0003
ETM+ Band 5 + Pan	79 ± 5	75 ± 6	3.76E-06

Table A-3. Fit parameter values for threshold values obtained from average of means and by maximizing fit parameter value for selected proposed indices.

Candidate Index	Optimal threshold value	*Fit* parameter
MSS Band 3	36.9	-31,404
MSS Band 4	40.5	-10,438
MSS Band 2 + Band 3	68.3	-40,411
ETM+ Band 3	32.3	-47,919
ETM+ Band 4	39.1	-17,983
ETM+ Band 5	45.5	-19,556
ETM+ Panchromatic	33.9	-36,093
ETM+ Band 5 + Pan	79.4	-22,908

confidence) indicate a statistically significant discriminatory ability. Nine candidate indices were identified which appeared able to discriminate between non-sandy and sandy areas: MSS bands 3, 4, and band 2 + band 3, and TM/ETM+ bands 3, 4, 5, 7, pan (ETM+ only) and band 5 + pan (ETM+ only). Optimal threshold values for each index

were determined by maximizing *Fit* (Table A-3 and Figure A-1).

Optimal threshold values for each index were all very close to the mean index value for those pixels identified as sand by MESMA. Values of *Fit* were all negative, indicating that more pixels were identified as sandy either by MESMA or the index, but not both, than were identified by both MESMA and the index. This is principally due to the inability of the threshold indices to identify the diffuse area of blowing sand in the southeastern portion of the image and MESMA's underestimation of the extent of the sandy area in the northern part of the image (see Chapter 5 and Figure A-1).

The relative inability of the multispectral threshold indices to identify the diffuse areas of blowing sand in the image indicates that SMA is a more sensitive technique for identification of sand than the simple threshold index approach. On the other hand, the absence of a very bright sand spectral endmember in the spectral library caused MESMA to fail to identify the bright sandy soils in the northern part of the basin. Thus, multispectral index results may be used to supplement SMA results in areas that were not modeled with the given spectral library.

The candidate indices are successful because sand-sized particles scatter light more efficiently than larger particles (Hapke, 1981). Thus, the cover of saltation-sized particles in areas of sand blow-outs reflect more light at all wavelengths than the gravel lag that covers the surface in undisturbed areas. In addition, since vegetation cover decreases pixel reflectance in all bands compared to sandy soils, lower cover results in higher reflectance. Lack of vegetation cover increases a soil's susceptibility to wind erosion (see among others, Wolfe and Nickling, 1993).

Green vegetation is also an efficient light scatterer in the near-infrared. This is the

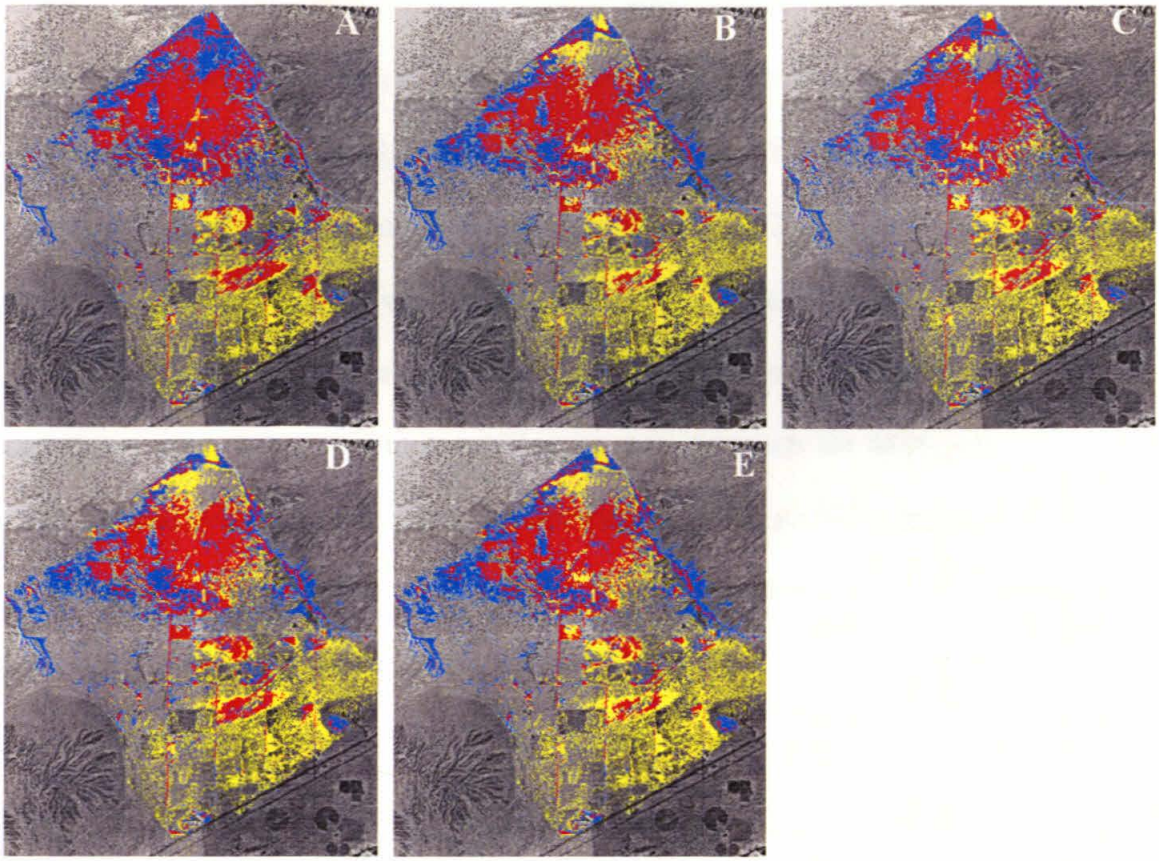

Figure A-1. Comparison of MESMA and multispectral indicators of sandy areas in the Manix Basin. Optimal threshold values (Table 6-2) were used for each index to identify those pixels with sandy surface soils. Yellow: Sandy areas identified only by MESMA. Blue: Sandy areas identified only by multispectral index. Red: Sandy areas identified by both MESMA and multispectral index. A) TM/ETM+ band 5 index compared to MESMA results. B) TM/ETM+ panchromatic band index compared to MESMA results. C) TM/ETM+ band 5 plus panchromatic band index compared to MESMA results. D) MSS band 3 index compared to MESMA results. E) MSS band 2 + band 3 index compared to MESMA results.

origin of the vegetation red-edge and the basis of the widely-used Normalized Difference Vegetation Index (NDVI). As a result, multispectral threshold indices which employ bands in the near-infrared (NIR) are susceptible to errors in which areas of high vegetation cover are confused with sandy areas. Thus, MSS band 4 as well as TM/ETM+ bands 4 and 8 (panchromatic) are not advisable for use in multispectral indices aimed at identification of sandy areas. MSS band 3, with bandpass from 700 to 800 nm, is partially in the NIR and will be sensitive to the limb of the vegetation red-edge. Nonetheless, it is less sensitive to vegetation than true NIR bands, and provides much better discrimination

between pixels with sandy soils and those with other cover (Table A-2). The sensitivity of MSS band 3 to vegetation can be partially overcome by summing it with MSS band 2 which is less sensitive to vegetation, but also less sensitive to the presence of sand. Nonetheless, absorption by iron minerals in the MSS band 2 and band 3 region (Hunt *et al.*, 1971) may cause underestimation of sandy areas for soils with high iron content.

Of the 14 original multispectral threshold indices considered as candidates for identifying sandy areas in remote sensing images, one each for MSS and TM/ETM+ yields the best overlap with MESMA results while avoiding probable confusion with high vegetation cover. For Landsat MSS, the sum of bands 2 and 3 works best as an indicator of sand while band 5 works best for Landsat TM/ETM+.

Critical to this application of multispectral indices is the threshold value chosen above which a pixel is identified as sandy. Hyperspectral apparent surface reflectance data were used to determine the optimal threshold value that gives the best overlap between hyperspectral MESMA results and multispectral threshold index results. The numerical values determined in this study for optimal threshold values are in units of percent reflectance, and are therefore not transferable to other studies in which uncalibrated or non-reflectance units are used. Nonetheless, the method developed here, namely maximization of the *Fit* parameter to find the optimal threshold value, is transferable to studies that do not use reflectance images. So long as no processing steps, sensor attributes, or atmospheric processes change the position of the maximum of *Fit*, the method presented here will yield results that provide the best match between SMA and multispectral index results. Furthermore, acquisition of hyperspectral and multispectral data must be as nearly coincident as possible. Changes in the vegetation or

soil with time are likely to lead to the choice of inappropriate optimal threshold values.

Additive and multiplicative atmospheric scattering and absorption effects will not affect the position of the maximum of *Fit* when plotted against threshold value, nor will offset and gain effects from remote sensing sensors. Thus, the proposed multispectral threshold indices may be used with raw DN from Landsat-class sensors. This is particularly important for older Landsat sensors (including MSS) which are no longer calibrated and in which detectors may have drifted. Image striping resulting from poor cross-calibration of detectors, which can lead to inconsistent DNs within an image may be partially compensated by equalizing the mean and standard deviation of each set of lines.

Finally, although SMA of hyperspectral data are used here to identify sandy areas, any raster or vector dataset that provides this information may be used. This is particularly important for older multispectral data that have little or no temporal overlap with hyperspectral data. So long as pixels in a multispectral image can be located in a reliable raster or vector dataset that provides information about soil surface texture, the method outlined here is applicable and may be used to identify critical threshold values for the detection of sand.

3.3 Application to a Landsat TM Scene

In order to test the method developed in this study, a Landsat TM scene which covered the Manix Basin as well as a large area of the Mojave desert was coregistered with an AVIRIS scene. No other processing steps were applied to the Landsat data. This

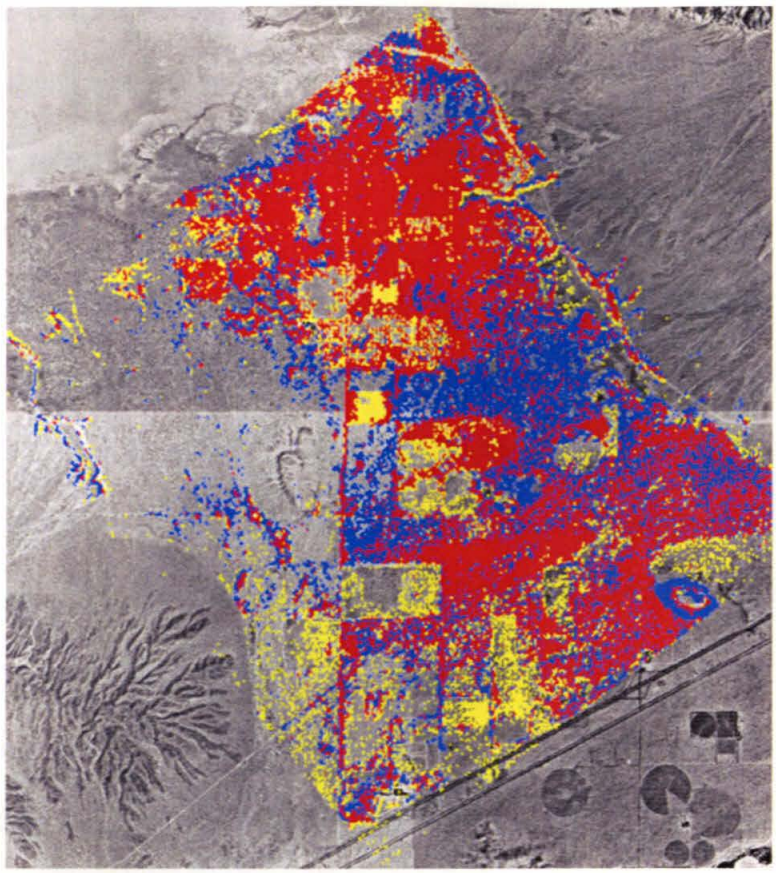

Figure A-2. Comparison of MESMA and Landsat TM band 5 indicators of sandy areas in the Manix Basin. Optimal threshold value for this Landsat TM band 5 threshold index was 217. Yellow: Sandy areas identified only by MESMA. Blue: Sandy areas identified only by multispectral index. Red: Sandy areas identified by both MESMA and multispectral index.

scene was acquired on June 14, 1998, one and one-half months after the AVIRIS data, so vegetation and soil conditions should be nearly identical for the area of overlap. Landsat TM band 5 was used in this portion of the study since simulated Landsat bands indicated that it would provide the best identification of sandy soils.

The pixels in the TM image were classified as sandy or non-sandy soils based on the AVIRIS MESMA results. As with the simulated Landsat data, a Student's *t*-test was used to verify that the TM band 5 values for these two populations have different means. The average p-value was 1.7×10^{-4}, indicating that the means for these two populations were significantly different.

Next, the optimal threshold was found by maximizing *Fit* in Equation (5). The optimal threshold value was found to be 217 with a *Fit* value of 874. Finally, those pixels with TM band 5 values greater than or equal to the threshold were identified in the full TM scene.

In the area of overlap between the TM scene and the AVIRIS image (Figure A-2), the TM band 5 threshold index identifies a larger number of pixels as sandy than the TM/ETM+ band 5 data simulated by the AVIRIS data (Figure A-1A). In particular, on the eastern side of the AVIRIS image, the TM band 5 threshold index was able to identify a diffuse area of sand that was overlooked by the simulated TM/ETM+ band 5 threshold index. However, some of the eastern portion of the image which was not identified by MESMA as being sandy is identified as such by the TM band 5 threshold index. These discrepancies may be due to the larger pixel size in the TM image compared to the simulated TM/ETM+ data which had AVIRIS-sized pixels. Despite the slight discrepancies the TM band 5 threshold index can be used in an actual TM scene to identify sandy areas susceptible to wind erosion.

When applied to the entire TM scene, the band 5 threshold index identifies areas in the Mojave desert known to be active aeolian environments (Figure A-3). For example, many playas are identified in the image as being sandy. Playa areas are not only spectrally bright, which leads to their identification by the index, but are often areas of dramatic wind erosion (Gillette *et al.*, 1997; Lancaster and Baas, 1998). In addition, the index identifies the area around Harper Lake as an area of potential wind erosion. Bowden *et al.* (1974) and Nakata *et al.* (1976) identified this area, as well as parts of the

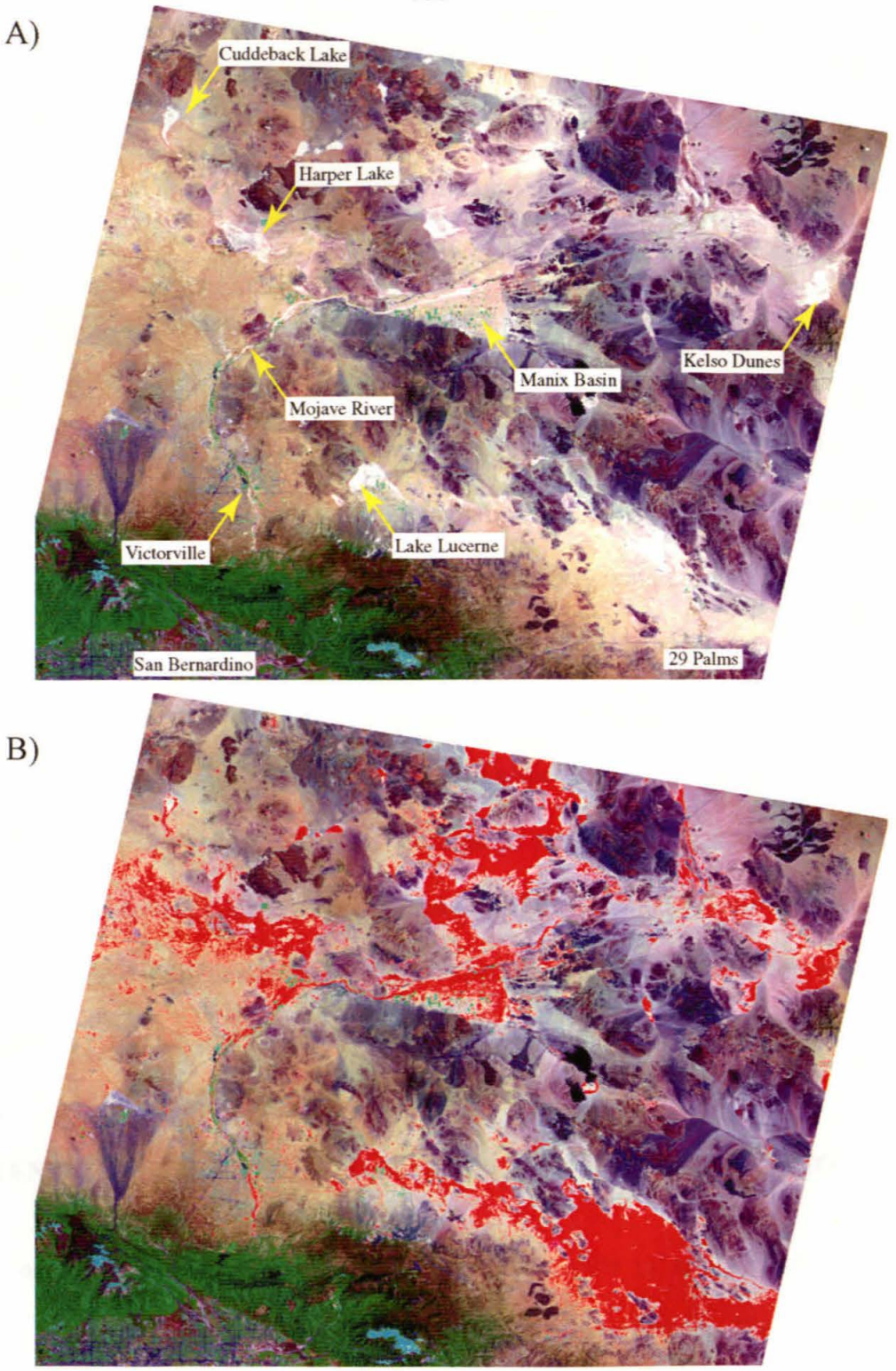

Figure A-3. Landsat TM band 5 threshold index of sandy surface soils for the June 14, 1998, TM image. A) False-color image with TM bands 5:4:2 as red:green:blue. B) Sandy pixels (in red) overlain on top of false color image. Areas identified as sandy in this image correspond to well-known areas of sandy, wind-erodible soils.

Mojave River near Victorville as the origins of sand plumes in an ERTS-1 image from 1973. The TM band 5 threshold index identifies the Manix Basin/Afton Canyon/Kelso Dune system as being highly wind erodible which is in agreement with published studies (Chapter 2 and Evans, 1962; Meek, 1989; Sharp, 1966). The area between Lucerne Valley and Twentynine Palms is identified as being highly wind erodible. This is in good agreement with visual inspection of this area in false-color at full resolution. The area north of the Manix Basin is within the Fort Irwin Military Reservation. While this area is not open for ground inspection, a recent overflight of the area by the author on a commercial jetliner confirms that it is very sandy and highly wind eroded.

The method presented here employs hyperspectral MESMA results to identify multispectral indices of sand or wind erosion and to find critical threshold values for these indices. This approach makes use of very high spectral resolution AVIRIS data in a small area to identify process-relevant features in relatively low spectral resolution Landsat data that covers a large area. Application of this method to both simulated and real multispectral data indicates that it can be successful in the identification of areas at risk of wind degradation in arid shrublands.

4. POTENTIAL APPLICATION TO STUDIES OF LAND DEGRADATION

The appearance and movement of sand blow-outs in arid environments are important as they signify the triggering of land degradation processes. Blowing sand has serious consequences for landscapes undergoing degradation (see Chapters 2 and 3). Aeolian removal and transport of dust, sand, and litter are the primary mechanisms of degradation, killing plants by burial and abrasion, interrupting natural processes of

nutrient accumulation, and allowing the loss of soil resources by abiotic transport.

Remote sensing tools that provide reliable information about relevant ground features such as sand blow-outs are an important element of change detection and landscape forecasting. This is particularly important in the Earth's vast and fragile arid and semiarid areas that are undergoing unprecedented land use pressures. Land degradation in these environments is typically irremediable and where possible, remediation techniques are rarely employed (Dregne and Chou, 1992). Thus it is vitally important to identify degraded areas or areas at risk of land degradation before it occurs. Remote sensing of soil surfaces can contribute this vital information. MESMA has proven an effective tool in identifying ground signatures relevant to arid and semiarid landscape health. Multispectral indices, when enhanced by MESMA results, are able to identify sandy areas in arid regions and thus provide hope for identifying degraded areas or areas susceptible to wind erosion over large areas. Sand blow-outs are active degradation features. Information on their temporal and spatial extent is valuable for land managers and can contribute to informed land-use decisions, potentially avoiding land use that can lead to land degradation in this or similar arid shrublands globally. Repeated analysis in subsequent years could track the progress of desertification or the effectiveness of remediation attempts. This information could be used to improve the process model or identify useful remediation strategies.

APPENDIX B

IDENTIFYING AREAS AT RISK OF DESERTIFICATION: THE LEADING DESERTIFICATION INDICATOR CONCEPT

1. INTRODUCTION

Arid and semiarid areas cover approximately thirty percent of the Earth's land surface and can be found on every continent of the globe. These vast drylands are fragile environments in which degradation can be irremediable. At the same time, many deserts around the world are facing unprecedented land-use pressures. It is thus imperative to identify areas at risk of desertification before permanent damage is done.

The principal goal in this sort of desertification forecasting is to help promote sustainable land use. For example, information about the susceptibility of his lands to desertification may help an Australian rancher decided which paddocks should be used during an especially dry year. Or, a nationwide assessment of desertification risk may help the United States Secretary of Agriculture determine a subsidy for cattle in different regions.

In short, land use decisions based on desertification risk information may help individual landowners, local and national governments, corporations, and transnational

institutions avoiding the most serious impacts from land use. As discussed in Chapter 1, this is important for maintaining the standard of living of all citizens of the world. It will become increasingly necessary for developing nations to conserve ecological resources if they are to participate fully in the global market economy.

The goal of this appendix is to outline a concept by which process-relevant remote monitoring can be combined with climatological and socioeconomic data to identify areas at heightened risk of desertification before damage occurs. This approach respects the fact that both climate and human land use can cause desertification, though it does not place any particular weight on either cause.

What good can come of such an exercise? Surely land-use decisions worldwide are based on short-term economic utility and besides, a global map of desertification risk is bound to be caught up in a quagmire of politicization.

Both of these objections have real merit. It is true that a data product is only as good as its uses, and if there is no sincere interest in identifying areas at risk of desertification then attempts to do so are useless. However, as global population increases along with the demands we place on the land to provide sustenance, the sustainability of environmental resources will gain greater importance.

Although there is currently no significant call for a means of desertification forecasting, the availability of such information can be expected to promote the development of interested constituencies. Just as in the recent cases of the ozone hole, water pollution, acid rain, and global warming, the provision of useful information is an essential step in promoting national or global dialog on large-scale environmental issues.

The issue of politicization of a global map of desertification risk is also

significant. Many of the factors which can affect land use—whether economic, diplomatic, or demographic—are political in nature. The North American Free Trade Agreement is a very good example of the politicization of environmental issues. Before ratification of this treaty, nay-sayers cited the specter of widespread environmental degradation as on of the sure outcomes of free trade. Supporters, on the other hand, suggested that the improvement of economic conditions in Mexico would lead to tightening of environmental controls. It is not yet clear which camp has proven correct and opinions on the impact of the treaty remain, in large part, speculative.

The uncertainty is a major pitfall for any scheme which attempts to use socioeconomic data, diplomatic ties, or governmental attitudes to identify risk. The idea of a "leading desertification indicator" (LDI) concept, which will be outlined here, is to rely as much on hard scientific data as possible. As more speculative considerations are included, the LDI becomes more speculative but the index may remain useful to a different constituency. The result is a tiered LDI system with one tier (Tier I) based solely on low-uncertainty scientific data or analysis and subsequent tier (Tiers II and III) including more speculative data or analysis. This approach allows transparency in terms of the speculative inputs and therefore provides a built-in mechanism for determining the usefulness of the LDI for a particular application. Managing the uncertainty of the LDI approach is discussed in Section 3 of this appendix.

2. THE LEADING DESERTIFICATION INDICATOR CONCEPT

The LDI is a map of the projected risk of desertification for drylands at scales

from global to local. In a real or prototype LDI, every point on the map would have a value, calculated from the most recently available data, which reflects the risk of desertification. The value of the LDI at every point on the map is a function of diverse environmental, socioeconomic, or political factors. Although the equation for the LDI may take many forms, here a simple linear combination of functions is suggested as a first cut:

$$LDI = S + \sum f_i ,$$

where S reflects the intrinsic environmental susceptibility of the landscape to desertification and each f_i is a function, incorporating one type of environmental or socioeconomic data, with either positive or negative values. A negative value for f_i represents a decreased desertification risk and a positive value for f_i represents an increased desertification risk.

The purpose here is not to suggest what the values of an LDI should be, nor how particular data can be converted into LDI values. Instead, the LDI concept will be painted in broad strokes that point to its most important features and potential sources of data with the knowledge that implementation of the concept will require a great deal of additional work.

It is important to consider the timescale of desertification when considering how to construct the LDI. In most cases worldwide, desertification occurs on the timescale of 10 to 100 years. Thus, it must be the goal of the LDI to project the risk of desertification on this same timescale.

The hierarchical approach to the LDI allows analysis at a variety of scales which become the levels of the hierarchy: the entire Earth, geopolitical regions, individual

nations, and local divisions within nations. At each level the inputs to the LDI are greater and the maps are more detailed. This approach allows the incorporation of information which may not be available for all areas of the globe. For example, nations such as the United States routinely collect enormous amounts of environmental, climate, and socioeconomic data. LDI maps of the US therefore may be reasonably expected to be more detailed than maps of, say, the Sudan where decades of civil war, poverty, and drought have made collection of these data impossible. In particular, this approach—allowing values of f_i vary around zero—means that the LDI equation does not need to be modified to reflect different amounts of available information. If a type of information is unavailable, the f function that reflects that information is simply set to zero.

Each level of the hierarchy refers to the level below it for its basic unit of analysis and inherits information from the level above it. For example, on the level of the geopolitical region, the basic analysis units are the individual nations within the region as well as the entire region as a whole. LDI maps at this scale inherit the data from the global map and then modify it based on the geopolitical inputs.

The LDI map on the global "Information Level" is thus the root for LDI maps on all other levels. It is the most purely scientific and also defines the basic mapping scale for all levels but the local.

2.1 Global Information Level

The LDI map at the Global Information Level depicts the basic susceptibility of the world's drylands to degradation. The map on this scale will be based on both present

climate information and projected climate changes.

The first step in the production of the global LDI map is the determination of which areas are susceptible to desertification at all. This may be done simply by identifying and masking out from all subsequent analysis those areas which are either too dry to be exploited in any fashion (*e.g.*, the Sahara Desert) or which are too humid to be subject to desertification at all (*e.g.*, the Amazon Basin). The World Atlas of Desertification (United Nations Environmental Programme, 1992) already provides a map of susceptible drylands (see Figures 6-1).

Determination of the risk of desertification at this level could be determined by global climate models (GCMs). This method would determine risk based on the difference between the present climate and the future climate projected at decadal intervals. In particular, changes in potential evapotranspiration (which is temperature dependent) and precipitation will be used to assign LDI values at this level. For example, in reliable GCM models and a projection of doubled atmospheric CO_2 concentrations, an area might be predicted to see increased evapotranspiration and decreased precipitation. This aridification would suggest a high risk of desertification for this region while another region which becomes more humid would have a lower risk of desertification. Of course, using GCMs to predict a region's vulnerability to climate change requires reliable GCM forecasts. This capability does not yet exist, but is an extremely active area of research. It is reasonable to suggest, therefore, that once reliable GCM forecasts are available, they be included in the LDI.

Global climate modeling implies a fundamental model cell size. This size, often around 1° x 1°, becomes the core granularity of the LDI maps on the global, geopolitical,

and national scales. The scale of the LDI map on the local scale may be smaller, however, based on the incorporation of finer-scale data there.

2.2 Geopolitical Information Level

The LDI map on the level of the Geopolitical region modifies the Global Information Level LDI map by considering specific conditions within geopolitical regions. The drylands of North America, therefore, would be treated differently from drylands in Northern Africa. At this level, the possible effect of international treaties, trade agreements, or similar trans-national arrangements on drylands within a region are of principal importance. As already discussed with the NAFTA agreement, the effect of treaties and the like on the environment can be controversial. The inputs at this level, therefore, are highly speculative.

2.3 National Information Level

The LDI map on the National Information Level modifies the Geopolitical Information Level LDI map by considering specific climate, political, economic, and demographic conditions within a single nation. The data incorporated at this level is scientific, socioeconomic, and political. Maps produced at this level may therefore be somewhat speculative, depending on which information is incorporated.

What sort of information is to be included at this Information Level?

1) Climate trends, *e.g.*, observed warming in certain areas, the effect of global

teleconnections on certain areas.

2) Population trends, *e.g.*, demographic patterns within a country, areas of dramatic population changes, average acreage per household.
3) Economic trends, *e.g.*, commodity prices, the number of new business permits per county, total number of non-farm vs. farm jobs.
4) Political trends, *e.g.*, government programs promoting rural development in certain areas, tax policies which promote poor land use practices, government attitudes toward agriculture, grazing, mining, and preservation.

As an example from the United States, Balling (1991) and Balling *et al.* (1998) have reported a significant warming trend in the Sonoran Desert. At the same time, the Southwest is among the fastest growing areas in the US. Simultaneously, the current tax code provides tax breaks to landowners who keep livestock, regardless of the cost to their land. Thus, the Sonora Desert area is at high risk of desertification based on National Information Level considerations only. These considerations must then be convolved with considerations from the Global and Geopolitical Information Levels in order to determine the overall, absolute desertification risk for this area. If, for example, this area is at low risk of desertification based on projected climate, then the absolute desertification risk is lower than if the area is at high risk of desertification based on projected climate.

2.3 Local Information Level

The LDI map on the Local Information Level modifies the National Information Level LDI map by considering environmental and socioeconomic conditions within a single state or county. It is at this level that detailed geographic information comes into play, and it is here that satellite remote monitoring may play a role in desertification risk assessment.

Types of environmental information which may be included at this level are:

1) Physical: presence of sandy soils, slopes, paleolakes, or desert pavements.
2) Biological: vegetation cover, vegetation type, shrub to grass ratio, the presence of cryptobiotic crusts.
3) Hydrological: distance to the watertable, source and timing of precipitation.

Socioeconomic data may also be included such as land-use trends, planned road or dam building, rural population, trends in sales of fertilizer, irrigation equipment, or fencing equipment.

3. MANAGING UNCERTAINTY AND SUITING USERS

The three principal types of data which are to be incorporated into the LDI maps at different levels are scientific data (including climate trends and landscape variables), socioeconomic data (including economic and population trends), and projections based on international political considerations. Each of these three types of LDI inputs carries

its own usefulness and degree of uncertainty. Scientific environmental data is the least speculative type of input and also the most widely useful. Individual landowners, state and national policymakers, and international organization can all use this information to make land-use decisions.

Socioeconomic data is often collected objectively, but the impact of various socioeconomic variables on environmental variables can be highly speculative. Thus, these data are more speculative than scientific environmental data. It is also useful to fewer user groups. The individual landowner, for example, may not care that the population in his county is increasing when it comes to making decisions about how to use his land. The collective nature of socioeconomic data, however, is quite useful to policymakers.

International political analysis is a highly speculative art and may only be useful to a select group. Again, an individual landowner may not care that NAFTA may cause environmental degradation in a neighboring country, and national policymakers may also decide that this is not pertinent to their land-use policy decisions. International organizations such as the UN or the Pan-American Conference, however, may determine that the affect of international trade agreements effects environmental security or international convention negotiations.

Thus, three different tier of LDI are proposed, each with a different degree of uncertainty as well as a different target user group:

Tier I LDI includes only scientific climate or environmental data. Tier I LDIs are therefore available at the Global, National, and Local Information Levels. The most significant use of a Tier I LDI will be at the Local Information Level where it will enable

informed land-use decisions by individual landowners or local land-use policymakers. An added feature of the Tier I LDI is that it does not rely on socioeconomic data because, even in the most advanced countries, socioeconomic data is collected infrequently. Scientific data, on the other hand, is much easier to collect and compile. This provides a robustness and consistency to the Tier I LDI in that it can be calculated for most of the globe and with some regularity.

Tier II LDI includes Tier I data as well as socioeconomic data and are therefore also available at the Global, National, or Local Information Levels. The most significant use of a Tier II LDI will be at the National Level where state and federal governing bodies may use the information to make broad policy decisions.

Tier III LDI includes data from Tiers I and II as well as international political analysis and therefore are available at all Information Levels. The most significant use of a Tier III LDI will be at the Global or Geopolitical Levels where international organizations and transnational corporations may use the information.

Dividing the LDI concept into these three tiers allows the LDI to be customized to a user's specific need. Clearly the concerns of an Arizona lettuce farmer are not the same as an Ethiopian diplomat negotiating a treaty to combat desertification. The flexibility of the LDI concept allows for both of these perspectives to be honored. The hierarchical approach of different Information Levels provides information at an appropriate level of detail for various uses. The three tiers of LDI, likewise, provides the relevant type of information for different users.

4. THE ROLE OF SATELLITE REMOTE MONITORING

Scientific environmental data form the core of the LDI approach and is incorporated at all levels and tiers. Some of these data may come from climate observations or models, as in the basic susceptibility map of the Global Information Level. Other data may come from detailed field mapping and yet other data may come from remote monitoring. However, the determination of LDI values at each Information Level must be an ongoing process so that a current LDI map provides the best information presently available. Outdated LDI maps will not do anyone any good.

This fact argues for a highly efficient mode of scientific data collection. As discussed in Chapter 6, satellite remote monitoring has the potential to be such a method. In addition, the location of the sensor outside of the atmosphere frees the data collection from political boundaries, harsh landscapes, and armed conflict. Thus, the role of satellite remote monitoring in the development and calculation of the LDI is clear: to make detailed, timely, and process-relevant information about the state of the world's drylands available and affordable.

The greatest use of remote monitoring data is at the Local Information Level where it can be used to provide detailed information about the distribution of factors that contribute to or hinder desertification. In particular, it can be used as an integrated tool to identify environmental variables that are related to desertification through a process model. Thus LDI maps at the Local Information Level may have a granularity much smaller than that of the basic susceptibility map inherited from the Global Information Level. Maps at the Local level, indeed, must have a granularity equal to the pixel size at

which the detailed environmental information is provided. Since many current and future sensors have resolutions of 20 to 30 m, these maps may be quite detailed indeed. In addition, much of the information that goes into calculation desertification risk in these maps is passed down from the Global, Geopolitical, and National levels.

5. CONCLUSION

The world's drylands are at risk. Increasing land-use pressures and changing climate conditions are contributing to the irremediable degradation of these lands. The LDI concept provides a way to identify areas at heightened risk of desertification. This information has great potential for use in land-use decision making and policy implementation in order to avoid destructive land-use practices in the most vulnerable areas.

While still only a concept, the LDI approach has great power. It allows integration of information from many disciplines at many levels to be incorporated into a map of the risk of desertification with tremendous local detail. The incorporation of scientific data, and particularly remote monitoring data, in the LDI provides process-relevance and detail. The use of this scientific data also provides acknowledgment of the fact that climate and environmental variables play an important role in desertification globally. The incorporation of socioeconomic data and political analysis, on the other hand, honors the reality that human beings on this planet are partially responsible for desertification and vulnerable with regard to its effects.

The environment is the lowest rung on the ladder to peace and prosperity.

Therefore, any tool that promotes sustainable land use, in the long run, will contribute to global and regional political and economic stability. Thus, in addition to promoting sustainable land use, use of a scheme to forecast and possibly avoid environmental degradation such as the LDI concepts will help engender global security.

APPENDIX C

CORRELATION BETWEEN ENSO ANOMALY AND WIND EROSION IN THE MANIX BASIN

Arid and semiarid lands can be extremely fragile in their response to anthropogenic disturbance. Once disturbed the degradation can be irremediable on human timescales and with limited financial resources. Thus, the ability to forecast desertification would be of great use for land managers, government planners, and interested institutions and organizations.

As discussed in Chapter 8, land degradation in arid and semiarid environments depends on a combination of environmental as well as socioeconomic factors. The predictive force of using socioeconomic factors to forecast desertification needs to be explored further and one scheme for doing so—the Leading Desertification Indicator—is discussed at length in Appendix B. In the meantime, the use of purely environmental factors to forecast desertification can be probed in simpler ways.

The El Niño-Southern Oscillation (ENSO) is one environmental factor which potentially may be used to help forecast desertification, at least in the American

Southwest. ENSO has been shown to affect climate, and therefore vegetation, in the southwestern US (Li and Kafatos, 2000; Lucero, 1998). In particular, when the equatorial Pacific is in the El Niño state (a positive ENSO anomaly), the southwestern states experience more precipitation, lower temperatures, and an increase in vegetation cover compared to the average climate and vegetation state. On the other hand, when the equatorial Pacific is in the La Niña state (a negative ENSO anomaly), the southwestern states experience less precipitation, higher temperatures, and a decrease in vegetation cover.

Since vegetation cover suppresses wind erosion (see Chapters 2 and 3 as well as Appendix D for further discussion), it is reasonable to expect that wind erosion in the southwestern states will be correlated with ENSO anomaly. In particular, one would expect greater observed wind erosion during La Niña years relative to El Niño years.

In order to probe this relationship, I compiled data for the observed January ENSO anomaly for the period 1973 to 1999. In addition, I compiled data for the Sand Mobility Index (SMI) (Lancaster, 1988; Lancaster and Helm, 2000) at the Daggett Airport in the Manix Basin and the observed number of dust events at the airport using the method of Bach *et al.* (1996). The SMI is defined as:

$$SMI = \frac{W}{P/PE}, \tag{1}$$

where W is the percentage of time that the wind speed is above some threshold (5.5 m/s at 6.1 m height used here and in Bach *et al.* (1996)), P is the measured annual precipitation, and PE is the potential evapotranspiration calculated using the Thornwaite method (Thornwaite and Mather, 1957).

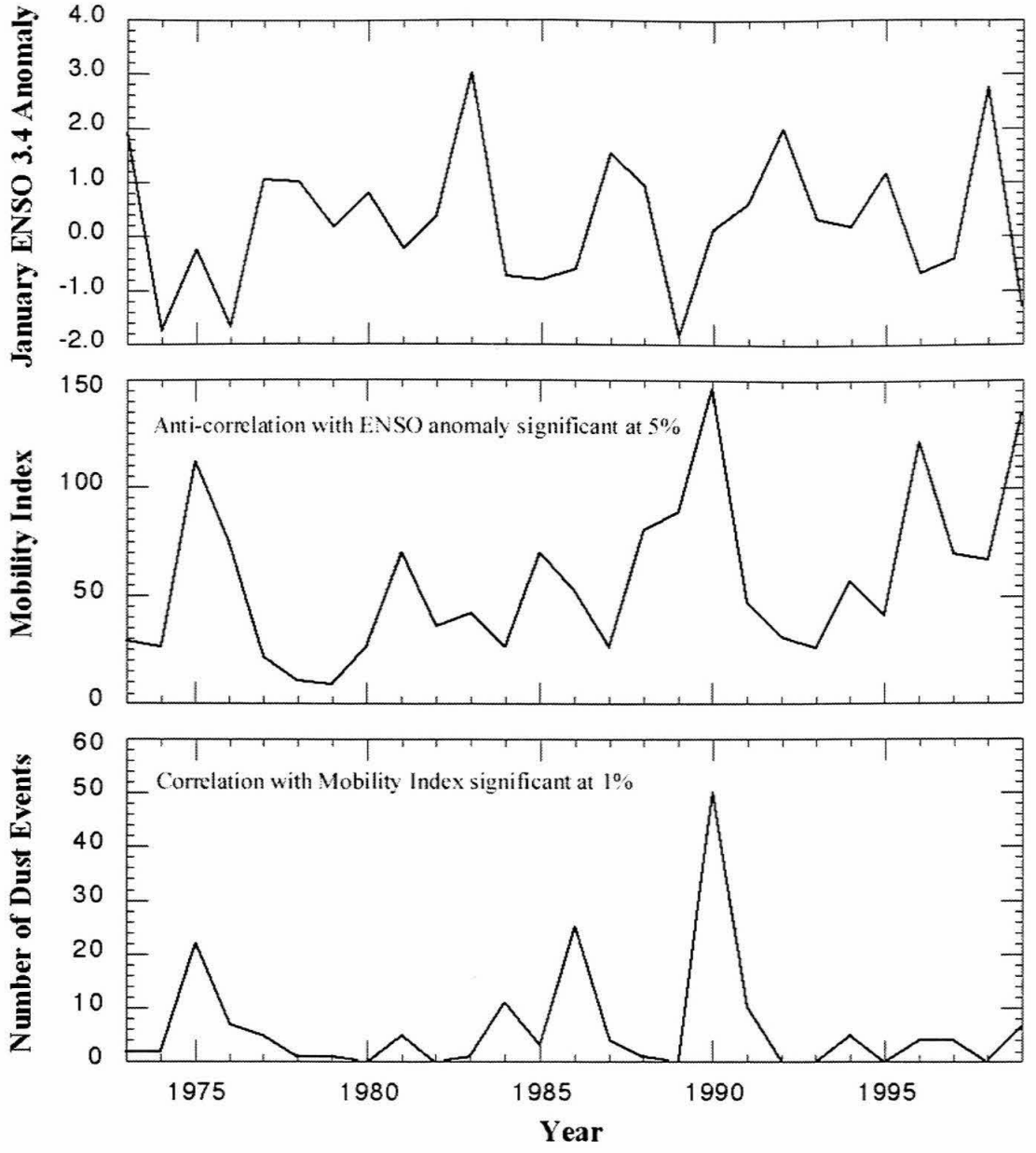

Figure C-1. Statistically significant (95% confidence) anti-correlation between January ENSO 3.4 Anomaly and Sand Mobility Index (Lancaster, 1988). Correlation between the Sand Mobility Index and number of dust events at this site is also significant (99% confidence).

As expected, my results indicate a statistically significant (95% confidence) anti-correlation between the January 3.4 ENSO anomaly and the Sand Mobility Index and the observed number of dust events at Daggett (Figure C-1). In addition, there was also a statistically significant (99% confidence) positive correlation between the computed

values of the Sand Mobility Index and the observed number of dust events at Daggett, confirming the findings of Lancaster (1998) and Lancaster and Helm (2000) that the Index is correlated with wind erosion events. Furthermore, the four peaks in observed dust events in 1981, 1984, 1986, and 1990 are confirmed by Ray (1995) who deduced large wind erosion events in 1981, 1984, sometime between 1985 and 1988, and in 1990 by estimating the area of sand blow-outs downwind of abandoned central-pivot fields in the Manix Basin.

These results indicate that the ENSO anomaly can be used to predict years of heightened wind erosion, and therefore years at which areas within the Southwest are likely to be at heightened risk for wind-driven desertification. As the phenomenology of ENSO and other semi-regular climate fluctuations improve, the ability to predict these oscillations will also improve (Kerr, 1999). Improved ability to forecast the ENSO anomaly using climate models may help improve the lead-time for forecasting times of particular susceptibility to wind erosion.

Thus, observation or prediction of the ENSO anomaly may be a useful data input for land managers so that the most harmful land use activities may be minimized in years and seasons with the highest potential for wind erosion.

APPENDIX D

DUST EMISSION AND NUTRIENT LOSSES FROM SEMIARID GRASSLANDS: RELATION TO CLIMATE CHANGE AND DESERTIFICATION

1. INTRODUCTION

Arid and semiarid areas clearly are susceptible to wind erosion. However, current models of wind erosion may still be improved, due to the complex nature of the phenomenon and the fact that our mathematical understanding of wind erosion relationships comes in large part from well constrained but non-representative wind tunnel studies. While necessary for understanding the dynamics of wind and its interaction with the Earth's surface, wind tunnel studies nonetheless tend to oversimplify wind, soil, and vegetation conditions. Natural environments are complex places, with complex interactions of the biotic and abiotic elements of wind erosion.

The purpose of this appendix is two-fold. First, this appendix will identify problems that remain in understanding the role of wind erosion as it relates to natural ecosystems and human disturbance. This will be accomplished by summarizing the state-of-the-art in wind erosion research and highlighting questions that remain in predicting wind erosion and nutrient losses by wind. The second purpose of this appendix is to

delineate a series of experiments that will help fill gaps in our knowledge of the mechanisms of wind erosion and which will help us evaluate its importance under different environmental and land use conditions. These experiments have been proposed to the NSF in response to a cross-site LTER research opportunity. In particular, I will suggest a set of measurements to address the vulnerability of arid and semiarid environments to aeolian land degradation by looking at the rates of removal and redistribution of nutrients from arid and semiarid landscapes by wind at three sites in the National Science Foundation's (NSF) Long Term Ecological Research (LTER) network that represent a bioclimatic gradient. This would be the first-ever cross-site study that measures the magnitude of wind erosion and nutrient removal by wind at various levels of aridity. The bioclimatic transect would allow probing of the relationship between wind transport and the vegetation/climatic determinants of wind erosion.

2. DOES WIND EROSION MATTER?

Since the publication by Schlesinger *et al.* (1990) of a general model of the degradation of arid lands, desertification has been thought of as the reduction or redistribution of net primary productivity in arid and semiarid environments which is accompanied by a similar reduction and spatial redistribution of soil resources. In the Chihuahuan Desert, where much of the work supporting this view of desertification has been carried out, the establishment of islands of fertility in once-homogenous landscapes and overall losses of soil nutrients have been the principal manifestations of desertification. As environments undergo the transition from grasslands to shrublands, it

is inferred that abiotic transport processes become more important than biotic processes in the distribution of nutrients. Both water and wind are often cited as possible mechanisms for the reorganization and loss of soil resources (Schlesinger *et al.*, 1996; Schlesinger *et al.*, 1990). At issue is the question of which abiotic process is responsible for (1) the net loss of nutrients from the landscape, and (2) the reorganization of nutrients, soil particles, and organic particles within the landscape. A great deal of work has proceeded examining the role of water in nutrient reduction and enforcement islands of fertility in degraded rangelands. By contrast, few studies have examined the complementary role of wind in promoting the reduction and spatial redistribution of nutrients in degrading arid and semiarid landscapes.

Recent research by Schlesinger *et al.* (1999; 1996) has supported the reduction and spatial redistribution of plant-available N in desert environments undergoing the conversion from grasslands to shrublands as well as the role of water in promoting degradation. However, in a recent paper, Schlesinger *et al.* (2000) have concluded that water erosion cannot, by itself, account for the depletion of soil fertility associated with desertification in the Chihuahuan desert. It is nonetheless a primary mechanism for the movement of material (mineral particles, organic particles, and dissolved nutrients) in arid and semiarid environments.

If water is not the sole agent of soil degradation in arid lands, it is high time to seriously examine the role of wind in the degradation of arid and semiarid shrublands. Several recent studies have supported the view that wind erosion is a principal mechanism for reduction of soil fertility in arid and semiarid lands, and that wind may play an important role in shaping an environment as it undergoes transition from

grassland to shrubland (see Chapters 2, 3, and 4, and Larney *et al.*, 1998; Leys and McTainsh, 1994). Furthermore, model calculations show that wind may account for much greater amount of soil erosion than water under slightly windier climatic conditions than present (Figure D-1). Much of this work has focussed on highly disturbed or agricultural lands. Few studies have evaluated the role of wind in the removal or redistribution of soil resources in landscapes undisturbed by humans. As one example, Coppinger *et al.* (1991) have used bomb-test ^{137}Cs to show that wind may be significant factor in transporting soils from between shrubs to under them in a sagebrush scrub landscape in Wyoming.

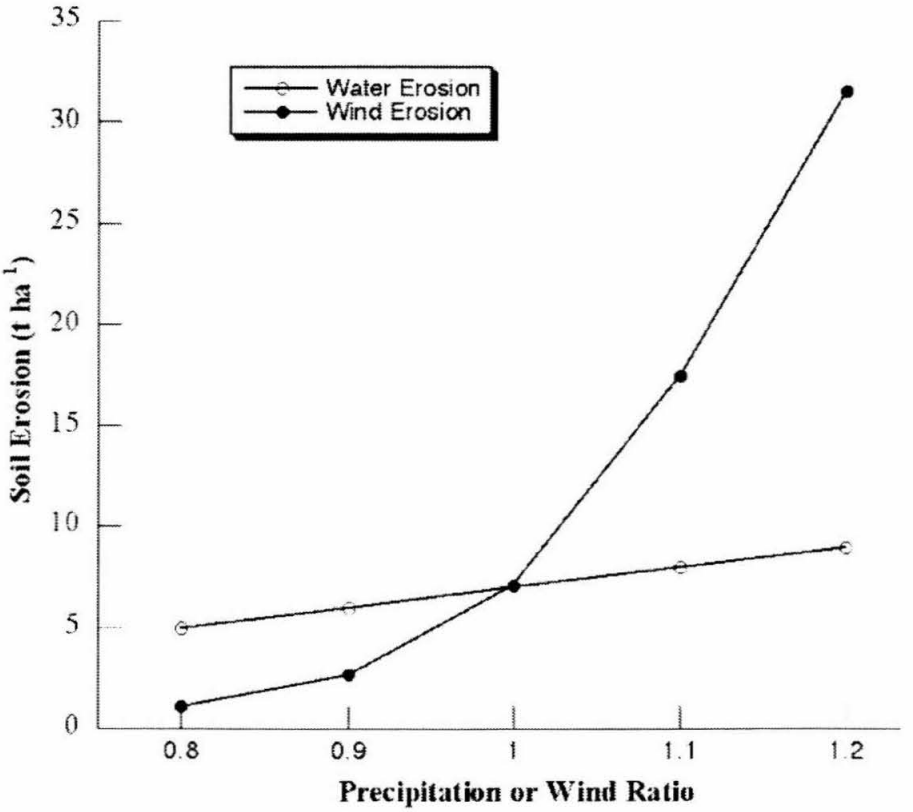

Figure D-1. Sensitivity of soil erosion in the US corn belt to climate change as estimated using EPIC (From Gregory *et al.* Managed Production Systems. In *The Terrestrial Biosphere and Global Change: Implications for Natural and Managed Ecosystems* 229-270 (Cambridge University Press, 1999)). For water erosion, temperature, CO2, and wind speed were held at current values, while precipitation volume (expressed as ratio to current volumes) was varied. For wind erosion, temperature, CO2, and precipitation volume were held at current values, while wind speed (expressed as ratio to current speeds) was varied. Each point represents the 100-year average of 100 randomly selected sites.

Thus, understanding the causes and conditions of wind erosion in arid and semiarid lands is vital to our understanding of local, regional, and global ecological systems as well as our ability to estimate consequences of human activities on these lands. No study to date has addressed the magnitude and effect of wind erosion in natural arid and semiarid lands using a large-scale experiment at multiple sites. Until this question is addressed, the importance of wind erosion in landscape dynamics, desertification, and global change will remain ill-defined.

3. THE STATE OF THE ART

The purpose of this section is to highlight in detail known parameters which effect wind erosion, to show how they are related to one another, and to identify areas where our knowledge is incomplete. This section is divided into three parts. In the first, general relations for wind flow and wind erosion are discussed. In the second, soil characteristics that influence wind erosion are discussed, and in the third, the role of vegetation in suppressing wind erosion is discussed. The very important roles of climate and human disturbance will be considered separately in following sections.

3.1 General Wind Erosion Relations

Although wind speed and direction affect wind erosion, landscape structure (both soils and vegetation) controls the wind profile, shear stress partitioning on the surface, and wind erodibility. As a first-order example of the way that landscape structure affects

wind profile, consider the Bagnold equation (Chapter 2, Equation (3)). For surfaces without roughness elements, the Bagnold equation has the form:

$$u(z) = \frac{u_*}{0.4} \ln\left(\frac{z}{z_o}\right), \tag{1}$$

where $u(z)$ is the wind speed at height, z, u_* is the wind shear velocity (also called the friction velocity), and z_o, is a parameter known as the aerodynamic roughness height (Bagnold, 1941). For surfaces with roughness elements such as vegetation or rocks, the Bagnold equation takes another form (Owen, 1964):

$$u(z) = \frac{u_*}{0.4} \ln\left(\frac{z-d}{Z_o}\right), \tag{2}$$

where Z_o is the roughness height, and d is a parameter known as the displacement height. Wolfe and Nickling (1993) point out that z_o in Equation (1) and Z_o in Equation (2) are not the same. Z_o is the roughness length defined primarily by the roughness elements and not merely the aerodynamic roughness of the soil, z_o. The displacement height represents the adjustment in measured height above the ground surface required to obtain the best fit of the logarithmic model. Displacement height has been interpreted as the mean level at which momentum is absorbed by the individual elements of a vegetation community (Wolfe and Nickling, 1993). The presence of roughness elements on a surface is of principal importance as it determines shear velocity, u_*. Shear velocity controls the amount of erosion that happens in any given soil due to a general relationship:

$$q \propto u_*^4, \tag{3}$$

where q is the horizontal mass flux due to wind erosion. The exact form of Equation (3) depends on a threshold friction velocity, u_{*t}, and soil characteristics. Horizontal mass flux, q, consists of those particles which are available for short-range transport. For a given soil, it is related to vertical mass flux, F_A, by:

$$F_A = kq, \tag{4}$$

where k is a dimensional constant with units of distance (Gillette, 1977; Gillette *et al.*, 1997).

When considering landscape processes, F_A is of principal importance because it represents vertical flux of those particles which are available for long-range transport. As discussed in Chapters 2 through 4, nutrients tend to be concentrated on the smaller particles which comprise F_A. Consideration of vertical flux is thus vital in understanding nutrient budgets of arid and semiarid environments where wind may account for a large proportion of nutrient loss from and redistribution within the landscape.

3.2 The Impact of Soil Characteristics on Wind Erosion

Soil texture and soil roughness are a major determinant of wind erodibility in arid and semiarid lands (Gillette, 1988; Gillette *et al.*, 1980). In particular the amount of fine particles (diameters less than about 90 μm) has a dramatic effect on the dust emitted from a soil surface for long-range transport during an erosion event (Leys and McTainsh, 1994). The coefficient k in Equation (4) is highly dependent on soil texture and is greatest for sandy loams, intermediate for loamy sands, and lowest for sands and clays. For example, studies by Gillette *et al.* (1980) have found regression relationships between

q and soil texture, including:

$$u_{*_t} = 390 - 3.3(\%\ \text{Sand}). \tag{5}$$

Furthermore, the presence of soil armors or cryptobiotic crusts in arid and semiarid environments can suppress dust emission by these soils (Belnap, 1995; Marticorena *et al.*, 1997b). Gillette (1988) also found that wind erosion depended on organic matter content, calcium carbonate composition, and physical surface state (smooth-loose, cloddy, and crusted). Gillette *et al.* (1980) also found that geomorphic history and location could influence wind erodibility. They found threshold shear velocities increase threshold shear velocities in the rank order: disturbed soils (except disturbed heavy clay soils) < sand dunes < alluvial and aeolian sand deposits < disturbed playa soils < skirts of playas < playa centers < and desert pavements (alluvial deposits).

The exact form of Equation (3) and values of k in Equation (4), therefore, depend on a wide variety of soil parameters. No relationship currently exists in the literature which allows for accurate calculation of either. Indeed, the study of wind erosion remains frustratingly empirical, with measurement parameters *in situ* often needed to make reasonable predictions of wind erosion.

3.3 The Role of Vegetation in Controlling Wind Erosion

The earliest attempts to model wind erosion of soils did not take vegetation into account. However, in the last 20 years, the realization that vegetation is an important determinant of wind erodibility in an area has increased along with the tools to analyze its

effects (Gillette and Stockton, 1989; Lancaster, 1988; Lancaster and Baas, 1998; Lancaster and Helm, 2000; Marshall, 1971; Musick and Gillette, 1990; Musick *et al.*, 1996; Wolfe and Nickling, 1993).

Both vegetation cover and vegetation structure are important in determining the protection supplied for a soil by vegetation. In particular, the height, width, shape, and permeability of vegetation canopies can influence the degree of protection from the wind by increasing apparent threshold wind velocity (Gillette and Stockton, 1989; Marshall, 1971; Musick and Gillette, 1990; Musick *et al.*, 1996). In order to quantify this relationship, Marshall (1971) suggested use of the "lateral cover", L_c, as a parameter which takes both vegetation density and shape into account:

$$L_c = \frac{L_a}{A}, \tag{2}$$

where L_a is the frontal-silhouette area of an individual plant (cm^2) and A is the average floor area per plant (cm^2). In bounded wind tunnel experiments, A is related to the total floor area, F, by $A = (F/N)$, where N is the total number of roughness elements. However, in field experiments, A is equal to $1/D$, where D is the plant density ($plants/m^2$). Marshall (1971) also showed how L_c could be used to predict the degree of protection against wind erosion provided by various amounts of vegetation cover in semiarid rangelands.

Due to partitioning of shear stress between that absorbed by plant canopies and that absorbed by the soil surface (leading to the mobilization of sediment), vegetation cover can increase threshold shear velocity. Threshold shear velocity, u_{*t}, can related to horizontal mass flux, q, by a more sophisticated version of Equation (3):

$$q \propto \begin{cases} \dfrac{\rho u_*^3}{g}\left(1 - \dfrac{u_{*_t}^2}{u_*^2}\right) & \text{for } u_* > u_{*_t} \\ 0 & \text{for } u_* < u_{*_t} \end{cases} \tag{6}$$

where ρ is the density of air (Owen, 1964; Shao and Raupach, 1993).

Musick and Gillette (1990) have shown that:

$$R = \frac{u_{*_t}}{u_{*_l}} < 1, \tag{7}$$

where R is the threshold friction velocity ratio, u_{*_t} is the threshold shear velocity with vegetation, and u_{*_l} is the threshold friction velocity for the same soil without vegetation. R varies positively and monotonically with $\mathrm{Log}(1/L_c)$. Furthermore, Raupach *et al.* (1993) have derived a relationship between R and L_c such that:

$$R = \left[\frac{1}{(1 - m\sigma L_c)(1 + m\beta L_c)}\right]^{1/2}, \tag{8}$$

where m is a constant ≤ 1, σ is the ratio of roughness-element basal area to frontal area, and β is the ratio of the drag coefficient for an isolated roughness element to the drag coefficient for the ground surface in the absence of roughness (Raupach *et al.*, 1993). Raupach *et al.* (1993) have suggested values of β = 100 and m = 0.5 for typical field conditions, although these can vary slightly for specific field conditions. For a given landscape, wind conditions and u_{*_l} are relatively constant. Equation (19), therefore, implies that decreases in cover or changes in vegetation structure will lead to increased saltation flux and dust emission.

3.4 Conclusion

With the exception of Equation (5) above, all of the relations discussed have been determined solely from physical arguments or derived from wind tunnel experiments. This knowledge lays the groundwork necessary for understanding aeolian processes in a much more complex natural setting. In particular, this knowledge provides us with several important elements on which we can build future field experiments. It provides, (1) an understanding of the basic parameters which need to be measured that may not be intuitively obvious, such as lateral cover, (2) mathematical relations to which real data may be compared, and (3) a preliminary understanding of the processes to guide actual design of the experiment. Nonetheless, purely physical arguments and laboratory experiments cannot substitute for field experiments in which conditions are not completely controlled. Natural elements of wind, soil, and vegetation all have major impacts on wind erosion. If we are to truly understand the role of wind erosion as a natural landscape and land degradation process, the theoretical and laboratory relations discussed here need be brought to bear on the future field experiments.

4. WHY CLIMATE MATTERS

In addition to landscape structure, climatic conditions can have a major impact on wind erosion. This relationship, however, is more complicated than the one between wind erosion and vegetation structure or soil characteristics. In particular, it is confounded by the fact that climate affects not only wind (speed, direction, and

variability), but vegetation and soils as well. Before the relationship between climate and wind erosion can be understood, therefore, the complicated relationships between landscape and structure must be understood. However, certain simple relationships hold which may inform our understanding of why climate matters in considering wind erosion and how climate changes may impact wind erosion in arid and semiarid environments.

4.1 Landscape Response to Regional Climate

There has been much discussion about the relative importance of human versus climate drivers of arid land degradation and wind erosion, but both can have a dramatic impact on a landscape (Brown *et al.*, 1997; Schlesinger *et al.*, 1990).

Global anthropogenic climate change is likely to effect arid and semiarid regions all over the world (Muhs and Maat, 1993). General circulation models (GCMs) predict that increases in atmospheric CO_2 concentrations will tend to make the world's drylands hotter and drier due to increased evapotranspiration (Rind, 1990). The increased frequency of droughts under this scenario is likely to trigger landscape changes in modern arid and semiarid environments (Forman *et al.*, 1992; Rosenzweig and Hillel, 1993). If the modern Kalahari is any measure, the decrease in the ratio of precipitation to potential evapotranspiration associated with drought will mobilize vegetation-stabilized dune areas. Here, changes in vegetation associated with droughts have a major effect on the mobility of linear dunes (Lancaster, 1988; Lancaster and Helm, 2000). There is a high probability that global anthropogenic climate change will have serious effects on the American Great Plains and Southwest. Paleoclimatic studies here suggest that increased

aeolian activity here in the past has been associated with hotter and dryer conditions (Forman *et al.*, 1992; Madole, 1994; Morrison, 1991; Stokes and Swinehart, 1997; Woodhouse and Overpeck, 1998).

Thus, understanding the role of wind as a landscape process is vital not only in understanding the present degradation of arid and semiarid lands observed globally, but also in understanding the environmental history of the American Southwest and the Great Plains. Here, since the last ice age, several episodes of aridification have occurred with large mobile sand belts covering much of the western Great Plains (Forman *et al.*, 1992; Madole, 1994; Morrison, 1991; Stokes and Swinehart, 1997; Woodhouse and Overpeck, 1998). The Great American Dust Bowl in the first half of the 20th century was, in part, a remobilization of these dunes driven by a relatively short period of drought (10-20 years) (Rosenzweig and Hillel, 1993). The potential for wind erosion throughout the western U.S. clearly remains extremely high and as the Dust Bowl illustrates, decadal-scale drought can have dramatic consequences for geomorphic landscape processes (Forman *et al.*, 1992; Rosenzweig and Hillel, 1993) and dust emission (Gillette and Hanson, 1989).

Vegetation type and cover are influenced by both precipitation and temperature. For example, Lancaster (1988) and Lancaster and Helm (2000) have suggested and tested a climatic sand mobility index on partially stabilized dunes and sand sheets. The effectiveness of this index is based on the fact that vegetation is sensitive to short-term climate regime. The index, M, is given by:

$$M = \frac{W}{(P/PE)}, \tag{9}$$

where W is the percent of time that the wind is above the threshold wind velocity, P is the

annual precipitation and PE is the annual potential evapotranspiration calculated using the Thornwaite method (Thornwaite and Mather, 1957). The quantity (P/PE) is known as the effective annual precipitation. Critical values of M are: <50, dunes inactive; 50-100, only crests of dunes active; 100-200, dunes active, but interdunes and lower dune slopes are vegetated; and >200, dunes fully active.

Climate change may either increase or decrease anthropogenic effects on a landscape. For example, during wetter than average years, the presence of annual grasses at covers greater than about 15% halts wind erosion, and increased soil moisture leads to higher threshold shear velocities (Brazel and Nickling, 1987; Lancaster and Baas, 1998). In drier than average years, threshold shear velocity may be lower due to decreased soil moisture, and annual cover is greatly reduced leading to accelerated degradation. Longer droughts will have a more lasting effect as perennial cover decreases in response to drought. For example, in the northern Mojave Desert, Schultz and Ostler (1993) have reported a dramatic decrease in total plant cover after only 4 years of drought.

Finally, precipitation and temperature can also affect the amount of wind erosion that occurs in an area. Precipitation is able to directly suppress wind erosion by giving the surface greater cohesion just after rain events or by promoting the formation of soil crusts (Helm and Breed, 1999). High temperatures can enhance wind erosion by increasing evapotranspiration which leads to less effective moisture to suppress wind erosion (Lancaster, 1988). In addition, certain processes associated with weather such as freezing and thawing and drought accompanied by frequent strong winds can break soil aggregates into small erodible units that decrease the initial wind speed for soil movement as well as the horizontal soil flux as a function of wind speed (Gillette, 1977).

4.2 Climate Response to Landscape Change

Landscape change itself may induce regional climate changes resulting in potential landscape-climate feedbacks. Some of the global feedbacks of desertification have recently been reviewed by Schlesinger and Pilmanis (1998). They conclude that losses of plant cover increase albedo and decrease latent heat flux in favor of sensible heat flux, resulting in regional temperature increases. This effect has also been suggested for the Middle East by Nasrallah and Balling (1995), who attribute much of the recent climatic warming in that region to the spread of desertification.

Wind erosion and dust emission are also important in a global context (Schlesinger and Pilmanis, 1998). Dust derived from erosion off of deserts is a major component of nutrient delivery to the oceans. Aeolian P and Fe have been shown to control net primary production in the world's oceans (Duce and Tindale, 1991; Talbot *et al.*, 1986) and thereby may influence oceanic uptake of CO_2 (Coale *et al.*, 1996; Martin, 1990). In addition, atmospheric dust has been shown to increase planetary albedo, partially counteracting global warming due to greenhouse gasses (Andreae, 1996). Increasing dust emissions due to human disturbance of desert shrublands offers a potential negative feedback between desertification and future global and regional climate warming (Tegen and Fung, 1995). Sahai (1998) has suggested that this effect has already been seen on a regional scale in India where temperature decreases have accompanied widespread land degradation due to increased atmospheric dust concentrations.

Desertification, therefore, may produce competing effects on the regional and global climate: regional warming due to decreased vegetation cover and global cooling due to reduction of atmospheric CO_2 or increased planetary albedo. Once again, until the role of wind erosion in desert environments, and in particular the relationship between wind erosion and desertification, is understood and until dust and nutrient fluxes from arid environments are quantified, the balance between regional warming and global cooling remains an open question.

5. THE ROLE OF DISTURBANCE

In *Soil and Vegetation Systems,* Trudgill (Ch. 8, 1988) discusses the effect of disturbance on stability and change of soil and vegetation systems. In the introduction to his chapter, he remarks that:

> soil and vegetation systems are used by man as a resource in many ways. In all cases the systems are being altered and influenced. It is therefore of crucial importance to try to evaluate what effects man has upon soil and vegetation systems. Primarily, the concern is with how far man can apply pressures to a system before the pressures cause an alteration to a new and different state. If it is clear that alteration is an inevitable consequence of a certain action, or group of actions, then value-judgments must be considered and a decision taken as to the desirability of the new state. Thus, the environmental scientist should be concerned with the evaluation of the resilience of natural systems and the identification of thresholds,

> which, if crossed, will lead to the occurrence of a non-returnable (irreversible) state. If these concepts are known it will be possible to evaluate the desirability of a state in terms of its stability in the face of the forces acting on it" (p. 134).

In the context of this thesis, this statement means that we must look closely at the role of disturbance and the possible consequences of disturbance in arid and semiarid environments. By and large, arid and semiarid environments are highly susceptible to change when disturbed as was shown in Chapter 2 and 3, and there are many examples of desertification in the literature from all over the globe. However, some environments are more susceptible to change than others. Trudgill (1988) suggests that the degree of resilience in various parts of a system is related to the amounts of energy which are flowing through the system: "stability cannot be given any general, objective definition but only definition in the face of forces action upon it. Given identical forces, the most stable system will be the one with the greatest amount of replenishing, input energy" (p. 137). In arid and semiarid regions, vegetation is the only autogenic factor that can control wind erosion, and therefore net primary production may serve as an index of stability. Thus, the Manix Basin, with low net primary production, has low stability with respect to wind erosion. A semiarid grassland with relatively high net primary production, on the other hand, is much more resistant to disturbance.

Of course, the degree of the disturbance also impacts a landscape's response. Diagramatically, this is shown in Figure D-2. In terms of wind erosion, a "stable" landscape is one in which disturbance either fails to initiate significant erosion, or the amount of erosion that comes as a consequence of disturbance is inconsequential in terms

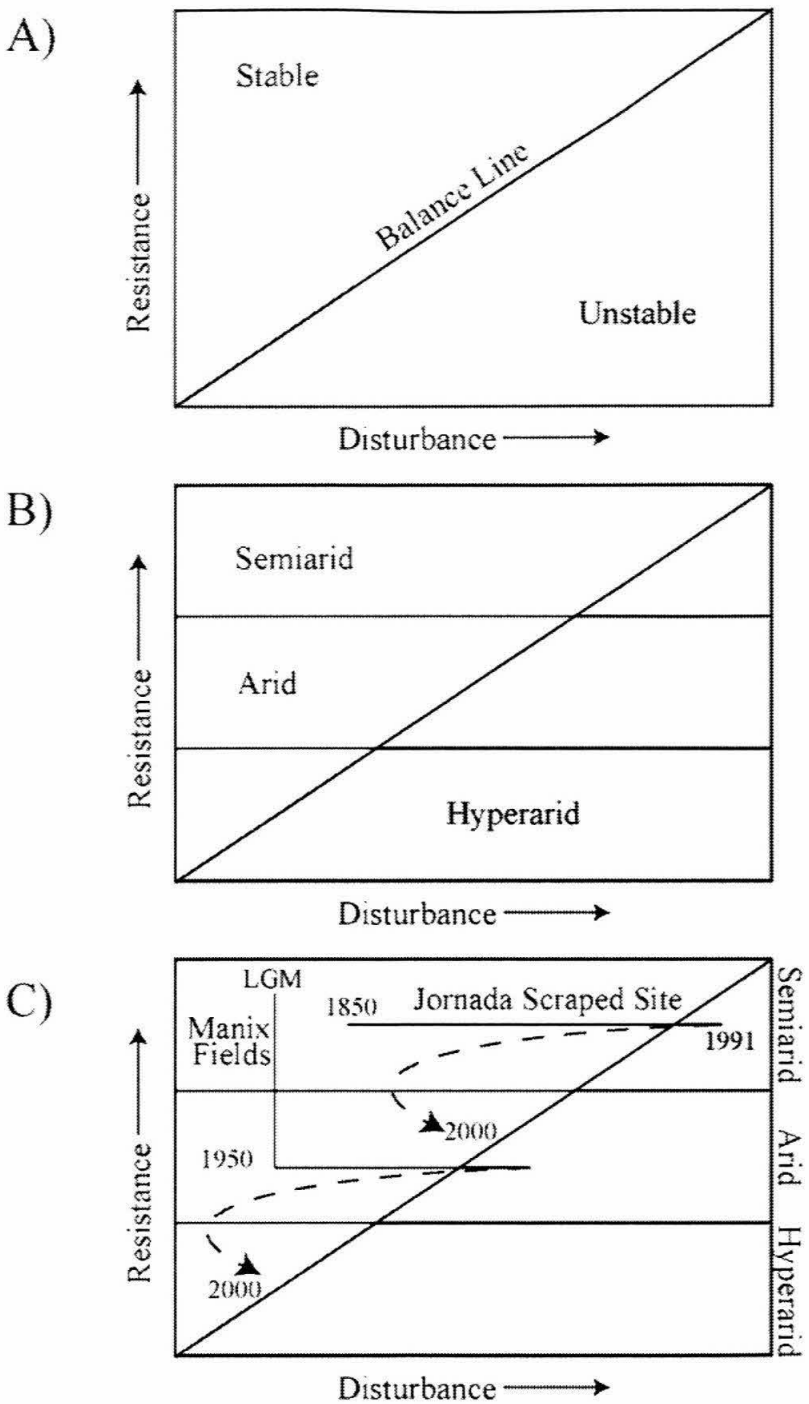

Figure D-2. Ecosystem stability in terms of inherent resistance and disturbance. **A)** A general case. **B)** The stability of dryland ecosystems with respect to disturbance. Resistance is determined by the amount of energy flowing through a system. Thus, semiarid environments are the most resistant and hyperarid environments are the least resistant. **C)** A responsive view of the interaction between resistance and intensity of anthropogenic disturbance. Here, disturbance that causes widespread landscape change affects the resistance of the landscape by changing the landscape structure itself. The trajectories of the Manix and Jornada Basins are illustrated and autogenic changes within the landscape in response to disturbance are shown as dashed lines.

of the nutrient reservoir in the soil. In "unstable" landscapes disturbance initiates wind erosion which then leads to further degradation of the soil and vegetation resources.

The "scraped site" at the Jornada LTER site in south-central New Mexico is a good example of the way in which disturbance may affect the landscape leading to increased and sustained wind erosion (See Chapter 3 for more details). Although this site was established as a part of a wind erosion study, it is not unlike land clearing that accompanies agriculture or other human activities.

In the spring of 1991, a semi-circular plot of land was cleared and maintained clear of vegetation (Havstad, 1999). This scraped site is situated in patchy *Scleropogon brevifolius-Hilaria mutica* grassland with scattered *Prosopis glandulosa* (mesquite) and *Yucca* spp. The soil is loamy fine sand and sandy loam of aeolian origin derived from Rio Grande floodplain sediments (Bulloch and Neher, 1977). Observations made in the summer of 1998 indicate that in the seven years since the site's establishment, a large area immediately downwind of the barren area has been adversely affected by sand blown off of the scraped site. Burial and abrasion of the shrubs as well as the grasses in this area have led to a significant decrease in plant cover and the formation of dunes in the lee of remaining mesquite bushes (Figure D-3). This pattern is strikingly similar to that seen in the Manix Basin and argues that anthropogenic disturbance and wind-erodable soil are major contributors to the degradation of arid shrublands and the destruction of islands of fertility, even in semiarid regions of the Chihuahuan Desert. The fact that no chemical additions have been made to the soils in this area indicates that the physical effects of blowing sand are primary in causing degradation in areas downwind of direct disturbance.

Figure D-3. A photograph of a sand dune and dead mesquite bush downwind of the Scrape Site at Jornada taken in the summer of 1998. The prevailing wind direction is from right to left (west to east) across this photograph and the Scrape Site itself is right of this photograph. The mesquite bush has been severely abraded, stripped of its leaves, and buried by the encroaching sand. Otherwise undisturbed, the area downwind of the Scrape Site has undergone dramatic change from a mixed grassland-shrubland to an area largely devoid of living plants.

The landscape change from a grassland to a shrubland that resulted from establishment of the scraped site therefore not only leads to increased wind erosion on the site itself but to sustained dust emissions from the area of indirect disturbance downwind of it. Gillette and Monger (2000) have reported that grasslands produce the least amount of dust of all the landscape types at Jornada. At the same time, mesquite dunelands produce more dust by a ratio of 4:1 to 8:1 compared to other landscapes with similar standing biomass. Thus, any disturbance that triggers the change to a mesquite duneland will dramatically influence dust emission and therefore nutrient losses from that landscape.

As another example of the role of disturbance on wind erosion, Fearnehough *et al.* (1998) have reported that anthropogenic activities have led to rapid accumulation of aeolian particles in stabilized dunes in arid northern China. This has significantly changed the surface environment. Increased moisture retention by a fine sand with significant aeolian dust resulted in decreased moisture penetration and led to subsequent

desiccation of deeper soils. This has led to vegetation changes, with planted deep-rooted, xerophytic shrubs declining from 12% to only 3% cover after 37 years. The shrubs were replaced by cryptobiotic crusts and later by shallow-rooted annual species, which increased from 0% to approximately 12% cover over the same period. They conclude that stabilized dunes may become increasingly vulnerable to deflation with the progressive decline in shrub cover associated with increased dust deposition.

6. PROPOSED EXPERIMENTS TO BETTER DELINEATE THE ROLE OF WIND EROSION

We do not yet have an adequate understanding of the role that wind erosion plays in either disturbed or undisturbed environments This is not just a question of how much wind erosion happens, but also a question of how do wind fluxes of nutrients and materials compare to the reservoirs and other biotic or abiotic fluxes. This information is vital in understanding landscape processes as a whole and the response of environments to direct or indirect anthropogenic disturbance.

The purpose of this section is to propose a next step for understanding the role of wind as a landscape process. In particular, I will suggest a set of measurements to assess the vulnerability of arid and semiarid environments to aeolian land degradation by looking at the rates of aeolian removal and redistribution of nutrients from arid and semiarid landscapes at three sites in the LTER network that constitute a bioclimatic gradient: the Jornada and Sevilleta LTER sites in New Mexico and the Shortgrass Steppe LTER site in Colorado. This would be the first-ever cross-site study that measures the

magnitude of wind erosion and nutrient removal by wind at various levels of aridity. The bioclimatic transect would allow probing of the relationship between wind transport and the vegetation/climatic determinants of wind erosion.

6.1 Bioclimatic Transect

Since the different geographical locations of each of the suggested LTER sites represent different levels of aridity (the Jornada LTER site is the most arid, while the Shortgrass Steppe LTER site is the least arid), we are able to use geographical position as a proxy for climatic condition. In this way, the role and magnitude of wind erosion at different levels of aridity may be investigated. Soil maps are given in Figure D-4.

6.1.1 Jornada LTER Site

The Jornada LTER site is located in south-central New Mexico in the Chihuahuan Desert. As previously discussed, it has undergone dramatic vegetation changes with many areas of grassland becoming shrublands in the last 150 years (Buffington and Herbel, 1965). At this site, study of this transition from grassland to shrubland has been the principal research theme. It is clear from much of this research that this landscape is vulnerable to desertification which may not be remediable on generational timescales of within economic feasibility (see for example, Schlesinger *et al.*, 1990; Whitford *et al.*, 1995). Disturbances in grasslands at this site have demonstrably initiated the transition to shrublands and the removal of soil resources (see Chapter 3 and Gillette and Chen, 2000).

Jornada LTER Site

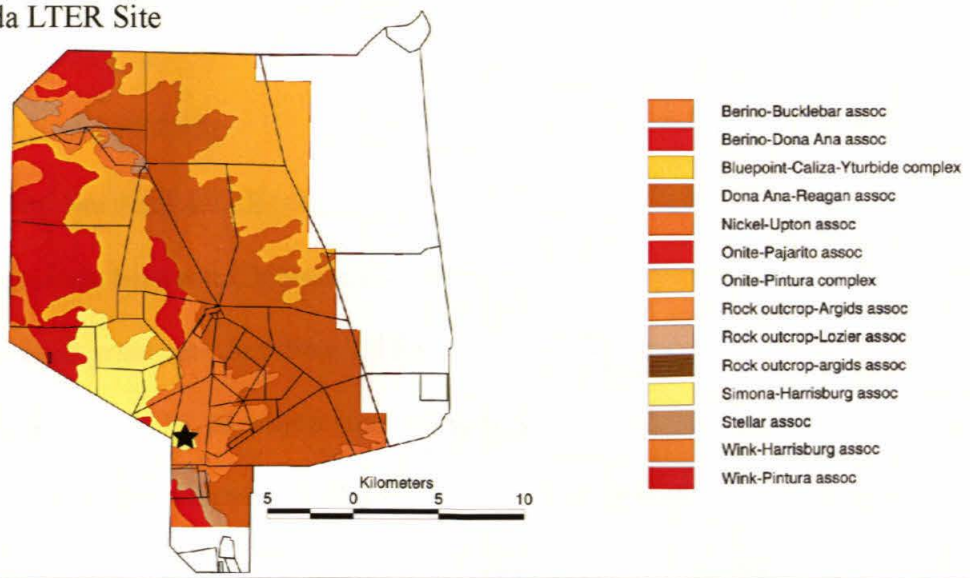

Sevilleta LTER Site

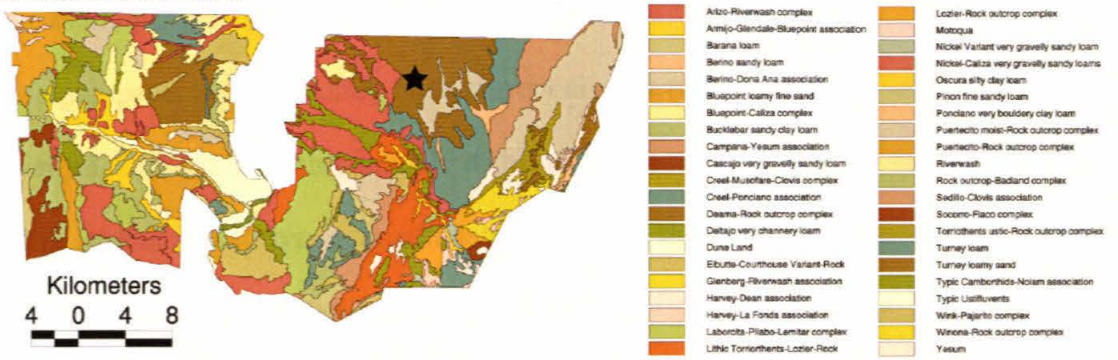

Shortgrass Steppe LTER site
(Central Plains Experimental
Range section)

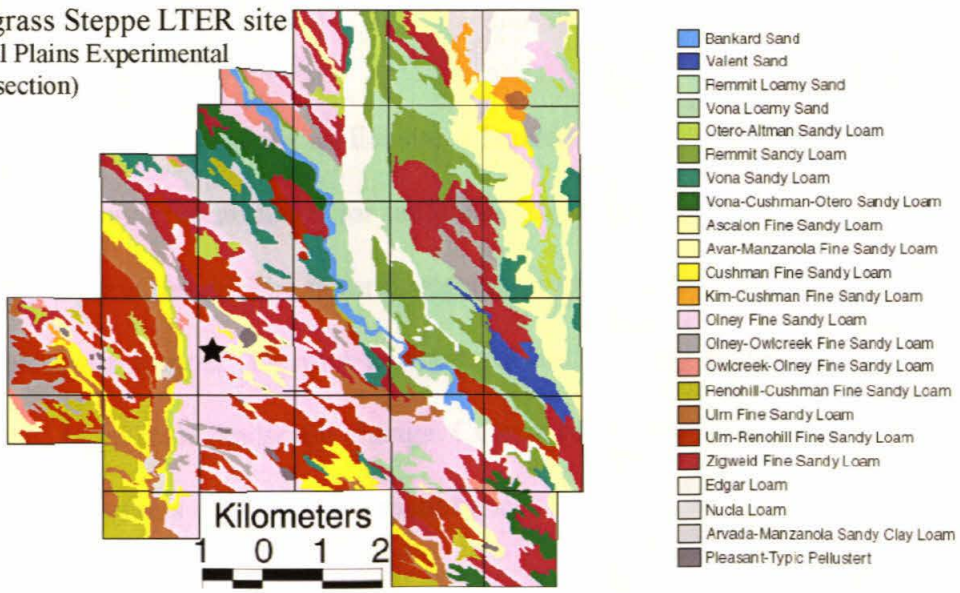

Figure D-4. Proposed localities for experimental treatments at each LTER site, indicated by a black star. Jornada LTER site: pasture fences are shown in black. The proposed treatment locality is approximately 2.5 km northwest of South Well. Sevilleta LTER site: the proposed treatment locality is within Mackenzie Flats in the Turney loamy sand. Shortgrass Steppe LTER Site: section boundaries are shown in black. The proposed treatment locality is approximately 2 km northeast of the Central Plains Experimental Range (CPER) LTER headquarters in the Olney fine sandy loam.

6.1.2 Sevilleta LTER Site

The Sevilleta LTER site is located in central New Mexico. This site includes a transition zone between Chihuahuan Desert shrubland and shortgrass steppe. A former Spanish land grant, the Sevilleta LTER site was heavily grazed by livestock from the mid-1800s until 1974, at which time it became the Sevilleta National Wildlife Refuge. All livestock were removed during 1974-1976, and have been excluded for the last 25 years. With somewhat greater annual precipitation than the Jornada LTER site, much of the Sevilleta's grassland vegetation has substantially recovered from the livestock's grazing impacts indicating that, in its current climate regime, it is less vulnerable than the Jornada LTER site to anthropogenic disturbance. Current research at this site is focused on the attributes and dynamics of ecotones among the desert, grassland, and woodland biomes found in central New Mexico.

6.1.3 Shortgrass Steppe LTER

The Shortgrass Steppe LTER site is located in northeastern Colorado. This site is a premier national research site for understanding geomorphic and ecosystem dynamics in shortgrass grasslands. The natural vegetation of the area is characteristic of much of the short grass steppe. Despite agricultural and grazing pressures, this site has not undergone large-scale landscape change. Current research at this site stresses the stability and resilience of this ecosystems to disturbance.

6.2 Disturbance and Scale

Dryland environments are shaped in part by allogenic factors such as climate and human activity which affect vegetation cover. Wind erosion, in turn, is partially a function of vegetation cover. To investigate wind erosion as a function of disturbance which changes vegetation cover, therefore, any successful experiment must create disturbances in grassland vegetation at each of the LTER sites at a range of intensity.

The principal result of such an experiment will be an increase in wind erosion with decreasing cover at each site. However, each of the sites will respond differently to disturbance. At the Jornada LTER site, which appears to be the most vulnerable to disturbance, the area of direct disturbance and the downwind area of indirect disturbance will likely undergo a transition to a shrubland which will sustained high erosion rates. At the Sevilleta LTER site, the downwind area may undergo a change in species composition. At the Shortgrass Steppe LTER site, the least vulnerable to disturbance, there will likely be little effect of vegetation disturbance besides an increase in dust emission. The response to disturbance at different levels of intensity at each site will be a function of their location on the bioclimatic transect and may be indicative of the landscape's response to larger-scale disturbance, be it anthropogenic or natural.

6.3 Timescales

The proposed study should focus on decadal to century-scale landscape processes rather than processes that occur on geological timescales. The reason for this is two-fold:

(1) the timescale of human activities in arid and semiarid environments, particularly in the Southwest, is on the order of 10-100 years, and (2) the onset of long-term climate change will be experienced by the affected landscapes first as a short-term change. It is only as the new climatic conditions become entrenched that longer-term landscape-shaping processes will become dominant.

For the three- to five-year duration of a field experiment which measures wind flux from natural and disturbed areas across a bioclimatic transect mineral weathering and input of nutrients from geological sources may be ignored. However, detrital plant matter, which is often itself mobilized by the wind, is likely to decompose and add to the total soil nutrient reservoir. Consideration of wind-mobile organic particles is therefore vital in understanding short-term landscape response to disturbance and the overall role of wind in arid and semiarid ecosystem dynamics.

6.4 Experimental Set-up and Required Measurements

In order to address the question of aeolian sediment and nutrient budgets at the Jornada, Sevilleta and Shortgrass Steppe LTER sites, several general categories of measurement are necessary: wind observations, dust flux observations, and laboratory determination of wind-transported sediment characteristics. Wind observations indicate the speed and direction of the wind as well as other important parameters for the grassland localities chosen for this study. Dust flux measurements will be carried out at several selective removal treatment sites to determine the effect of reducing cover on aeolian sediment and nutrient budgets.

6.4.1 Site Selection

The four principal determinants of dust emission that are pertinent for the proposed study are wind speed, vegetation cover (areal cover and lateral cover), vegetation type (grasses versus shrubs), and soil texture. Wind speed is an allogenic factor which cannot be controlled for in a landscape-scale experiment, but which is related to inter-site climate differences. Preliminary experimental sites have been identified at each LTER site (Figure D-4).

At each LTER site, one set of treatments will be established (Figure D-5) and flux from these sites will be measured dust. These must be chosen on the basis of the soil texture (sandy loam), vegetation (grasslands), and topography (flat areas large enough to accommodate the experiment with little interference from nearby hills).

6.4.2 Experimental Treatments at Each Locality

Once relatively homogenous (in terms of soil texture, landform, and vegetation cover) sampling localities are chosen at each LTER site, five different treatments must be made to the vegetation. At two (controls), no vegetation will be removed. The control sites provide a measure of background flux which may be subtracted from measured fluxes at partial-cover treatments to yield an estimate of the true elevation of dust flux with decreasing cover. At the three partial-cover treatment sites, cover will be reduced to roughly 75%, 50%, and 25% of original cover, respectively. At the last site, all vegetation will be removed.

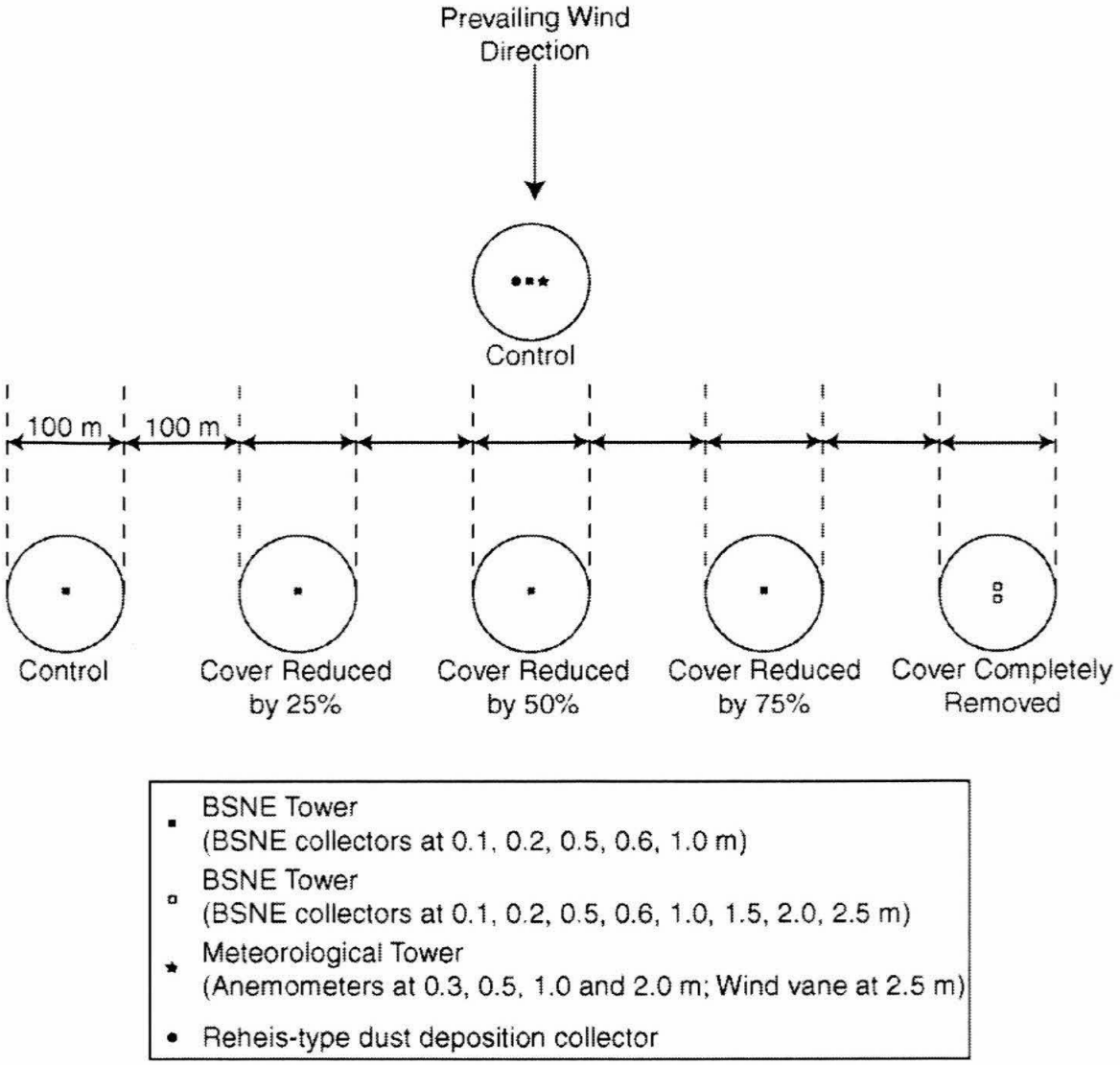

Figure D-5. Schematic of the experimental layout at each LTER site. Circles represent treatments, have diameters of 100 m, and are spaced 100 m apart perpendicular to the direction of the prevailing wind. Each treatment has at least one BSNE tower, but the treatment with no cover has two which allows calculation of vertical flux. A meteorological tower is located at the control site that is upwind of the vegetation treatments.

Vegetation removal may be carried out by removal of individual plants in such a way that the remaining vegetation is evenly distributed. Vegetation removal may proceed by clipping the grass at ground level and killing the grass root by application of a biodegradable herbicide (for example, Roundup®). This approach provides for minimum disturbance of the soil surface and minimizes the chance that vegetation will re-grow

during the course of the experiments.

Vegetation treatments must be large enough so that at the center where dust flux measurements will be made, wind conditions are in equilibrium with the correct level of cover. In addition, at treatments of this size, atmospheric dust concentrations will be largely at equilibrium with the true dust emission in partial-cover treatments. Furthermore, vegetation treatments must be arranged so that very little wind-borne material from one site contaminates flux measurements at other sites. Therefore, each treatment area must be at least 100-m radius circles, separated by 100 m, with the treatments all aligned perpendicular to the prevailing wind direction (Figure D-5). The prevailing wind at the Jornada and Sevilleta LTER sites is from the southwest while the prevailing wind at the Shortgrass Steppe LTER site is from the northwest. One control site must be several hundred meters upwind of the treatments to avoid contamination from treatment sites, while one control site must be in line with them.

Once vegetation treatments have been established, we will use the method suggested by Musick (1999) to estimate both total aerial coverage at each site (and the control), vegetation height, plant width. From these parameters, we can estimate lateral cover, L_c, which is related to the amount of protection a landscape experiences from wind erosion.

6.4.3 Measurements

At the end of each field season, we will have measured or calculated several parameters for each treatment at each LTER site:

(1) Wind-related vegetation parameters from the treatments, including: L_c, σ, D,

(2) Wind-related soil parameters from the treatments, including: soil texture, concentration of chemical species in surface soil,

(3) Wind speed and direction as a function of height and time: U,

(4) Shear velocity, roughness height, and zero-displacement height as a function of time: u_*, z_o, and d, respectively,

(5) Ratio of threshold shear velocity with vegetation cover to threshold shear velocity without vegetation cover: R,

(6) Horizontal, upward, and downward sediment fluxes as a function of time: q, F_A, and F_d, respectively, and

(7) Net gain/loss of sediment, net gain/loss of measured nutrients, turnover time with respect to wind erosion for soil nutrients, τ^j, and nutrient enrichment factor (E).

Our primary comparison of each of these parameters will be between treatments at each LTER site. This comparison yields information about the effect of decreasing cover in relatively constant environmental and climatic conditions. In particular, our principal expectation is an increase in both net sediment and net nutrient losses as a function of decreasing cover.

Since decreasing cover in relatively constant environmental and climatic conditions is typically associated with human-induced landscape change and grazing, this comparison will provide insight into the effect of wind on the overall soil nutrient budget in human-degraded landscapes. Furthermore, although temperature and precipitation can affect the wind erodibility of soils by affecting the amount of moisture in the soil during

wind events, this effect is likely smaller than the sheltering effect of vegetation. Thus, the intra-LTER site comparison of treatments will also yield valuable insight into the relation between short-term climate change (*i.e.*, drought) and wind erosion.

Our secondary comparison of each of these parameters will be between LTER sites for roughly equal amounts of cover. Since the localities for the treatments at each of the LTER sites are to be chosen so that soil texture and landform are as similar as possible, the effect of soil characteristics on wind erosion will be largely mediated. Instead, this comparison will show the effect of vegetation and climate on wind erosion and the role of wind in landscape change with long-term changes in climate regime. In particular, a major goal of both intra- and inter-site comparisons is determination of the threshold of absolute cover (or L_c) below which wind erosion and nutrient removal by wind increases to a significant amount.

This approach allows us to address a fundamental question on the role of wind in natural landscapes: what matters most in determining the magnitude of wind erosion in natural environments, total cover or climatic factors? If total cover, regardless of location along a bioclimatic transect, is the predominant factor in determining wind erosion, that has much different consequences for land management than if long-term climate is the predominant factor in determining wind erosion. Until this question has been answered, therefore, identification of areas on a regional scale in which wind erosion is a problem that cannot be effectively pursued. Furthermore, this approach allows us to determine a landscape's response to sustained disturbances of the size proposed here. This is likely a function of location along a bioclimatic transect and is a vital piece of information for scientists and land managers alike.

6.5 Aeolian Sediment and Nutrient Budgets

Consider any landscape in which wind may erode soils in conjunction with atmospheric dust deposition. For such a landscape, the following fundamental aeolian sediment budget will hold:

$$F_A - F_D = \text{Net Change of Sediment,} \tag{10}$$

where F_A is the dust emission from the landscape to the atmosphere and F_D is the atmospheric dust deposition, both in units of g/m^2/yr. For nutrient species on emitted or deposited dust particles, a further aeolian nutrient budget will hold:

$$C_A^i F_A - C_D^i F_D = \text{Net Change of Nutrient } i, \tag{11}$$

where C^i_A is the concentration of chemical species i on emitted dust particles, and C^i_D is the concentration of chemical species i on deposited dust particles. In this study for each LTER site at different levels of cover, we will quantify F_A, F_D, C^i_A, and C^i_D. Further, we may define an enrichment factor, E, which is given by:

$$E = \frac{C_A^i}{C_S^i}, \tag{12}$$

where C^i_S is the concentration of chemical species i in the bulk soil surface.

It is our expectation that both net loss of sediment and net loss of each nutrient considered will be decreasing functions with increasing cover. If this supposition is borne out by the data, we will have confirmed that wind does indeed play a greater role in

removing dust particles and soil nutrients at lower levels of plant cover. This is due to the fact that increasing cover increases the threshold velocity below which wind erosion does not occur. As a result, the fraction of time that the wind is above a certain threshold velocity for a certain cover will decrease with increasing cover Thus, with decreasing cover, F_A will increase while F_D is a local constant.

Relationships between net sediment loss versus cover will allow us to compare our results to previously published models and verify our technique. In addition, our plots of net nutrient loss versus cover will allow us to quantify the relationship between cover and nutrient loss at different climatic conditions represented by our three target LTER sites, and develop a regionalized model of nutrient removal by wind. Specifically, for each vegetation removal treatment at each LTER site, a metric of the importance of wind transport in the overall nutrient cycling of each landscape at a variety of vegetation covers must be computed. The turnover time is the appropriate metric:

$$\tau^i = \frac{C_S^i}{\text{Net Loss of Nutrient, } i}, \tag{13}$$

where τ^i is the turnover time with respect to wind erosion for nutrients i in the soil. For the Shortgrass Steppe LTER site with relatively high soil nutrient contents, τ^i should be high compared to values of τ^i for the Jornada LTER site with relatively low soil nutrient content.

The derived values of E for each site and treatment can also help us address whether wind plays a role in the redistribution of dust and nutrients *within* an ecosystem. Consider a cross-section through a grassland with incomplete cover. This cross-section may be divided into infinitesimal length elements, dx. The areas between individual

plants will be the loci of upward dust flux while plants themselves will be the loci of downward dust flux. The following relation must hold:

$$\int f_u dx - \int f_d dx = F_A, \tag{14}$$

where f_u is the upward dust flux from inter-plant areas, f_d is the downward dust flux from intra-plant areas, and F_A is the dust emission from the landscape to the atmosphere above an imaginary surface parallel to the soil and above the vegetation. The quantity, r, which gives the ratio between the total upward dust flux and the total downward dust flux in the inertial sublayer:

$$r = \frac{\int f_u dx}{\int f_d dx}, \tag{15}$$

must be greater than one for non-negative values of F_A. Fractional areal cover and r must be inversely related because with increasing cover $\int f_d dx$ will decrease while $\int f_u dx$ will increase. Furthermore, for large values of r, little redistribution of materials from inter-plant to intra-plant areas will occur, while for small values of r, a large amount of redistribution of materials will occur.

Within plant canopies, mean wind velocity must drop due to increased turbulence caused by the stems and leaves of the plant itself. Since smaller particles may be suspended in air masses with smaller mean wind velocities, turbulence within the plant canopy will lead to the preferential loss of larger particles from the air mass within the plant canopy. Shachak and Lovett (1998) have shown that large organic particles are more enriched in N and P than smaller mineral particles as they are largely made up of

fragments of plant material. However, both particle classes have higher concentrations of N and P than the bulk source soil. Thus, as the larger organic particles settle out of the air mass, the remaining dust will be relatively depleted in N and P. As the smaller mineral particles which are poorer in N and P are ejected from the plant canopy, they will rejoin the bulk air mass and can be removed from the system as part of F_A which is then nutrient-depleted. As a result, the enrichment of wind-borne material relative to the parent material, E, should decrease with decreasing r and therefore with increasing fractional areal cover. This analysis provides an indirect test for whether nutrients are redistributed within the landscape by the wind.

6.6 Redistribution of Nutrients Within the Landscape

Measuring dust flux allows us to address one aspect of the role of wind as a landscape process in arid and semiarid environments: net loss of nutrients from the environment at various levels of cover and climatic conditions. The other important aspect of both water and wind in the degradation of drylands is the redistribution of nutrients within the landscape, and particularly concentration of nutrients around individual plants to create islands of fertility. Rain splash has been implicated as one mechanism for the creation of physical islands of fertility in arid and semiarid areas (See for example, Wainwright *et al.*, 1999). However, few studies have yet been published which addresses the role of wind in the creation of islands of stability (See Shachak and Lovett, 1998).

As discussed in Section 5.5, within plant canopies, mean wind velocity drops due

to increased turbulence caused by the stems and leaves of the plant itself. Therefore, if shrubs remove wind-borne particles, the nutrient enrichment factor (E in Equation (12)) should decrease with increasing fractional areal cover. This analysis provides a direct test for whether nutrients are redistributed within the landscape by the wind.

We will also proceed with modeling the effect of vegetation on filtering particles out of the air. Since vegetation is composed of a network of branches, stems, and leaves, turbulence occurs within the shrub canopy. This may result in the deposition of entrained particles at the base of the plant. Since wind-entrained particles typically are enriched in plant nutrients, deposition of nutrient-rich particles within the plant canopy could potentially be a very strong enforcer of islands of fertility. Very little work has been done on this problem. Unpublished data of Dale Gillette (*personal communication*) shows dust concentrations within a plant canopy are greatly elevated compared to that outside the plant. This implies that the plant acts as a dust filter. Attempts must be made to model this effect in order to better understand the role of wind in creating physical islands of fertility.

6.7 Measuring Vertical Dust Flux, F_A

Measurements of vertical dust flux, F_A in g $(m^2\ s)^{-1}$, can be quite difficult and must be done indirectly. While several methods have been suggested to measure this quantity, Gillette (1977), Shao *et al.* (1993), and Gillette *et al.* (1997) have developed a relatively simple method for its estimation. Of principal importance in this model of vertical dust flux is Shao *et al.*'s (1993) observation that the ejection of dust particles by

saltation bombardment, as opposed to detachment of dust particles by aerodynamic forces, is the principal mechanism for the natural entrainment of dust by wind. Therefore, this model states that F_A is proportional to the surface vertical flux of kinetic energy of saltation grains. Likewise, the vertical flux of kinetic energy of saltating grains is proportional to the horizontal flux, q in g/(m s)$^{-1}$, of the saltating grains. Mathematically, Shao *et al.* (1993) expressed F_A as:

$$F_A = Km_d \frac{g}{\Psi} qf\left(\frac{V_H}{u_*}\right), \tag{16}$$

where K is a constant, m_d is the mass per particle, g is the acceleration due to gravity, Ψ is the binding energy, V_H is the horizontal particle velocity, $f(V_H/u_*)$ is a nondimensional function, and

$$q = \int_0^\infty CV(z)dz, \tag{17}$$

where C is the concentration of saltating particles, and $V(z)$ is the horizontal particle speed at height z. The quantity V_H/u_* has been shown to be roughly constant with a value of approximately 10 (Gillette *et al.*, 1997).

Shao *et al.*'s (1993) and Gillette *et al.*'s (1997) analyses thus suggest that:

$$F_A/q = k, \tag{18}$$

where k is a function only of the binding energy and mass per saltating particle. Mass per saltating particle reflects the size distribution of the saltating material; coarse sand would have higher mass per particle than fine sand. Binding energy could vary with differences

in the texture of the soil, chemical composition, clay mineralogy, and salt and organic matter content, as well as a variety of the physical properties of the source material including the size distribution of soil aggregates as affected by wetting, drying, freezing, thawing, and erosive processes such as sandblasting. Thus, while there is significant variability in reported values of k in the literature (See for example, Gillette, 1977; Gillette *et al.*, 1997), for most purposes, k should be constant for a specific soil and when averaged over several weeks and days.

Once a reliable value of k has been determined for an area, values of F_A can be easily determined from measured values of q.

6.7.1 Finding Horizontal Mass Flux, q

The horizontal mass flux, q, may determined by capturing wind-borne sediment at various heights using Big Spring Number Eight (BSNE) samplers (Fryrear, 1986). These samplers have been shown by Shao *et al.* (1993) to have efficiencies of approximately 90% for particles >50 μm.

Following the analysis of Gillette *et al.* (1997), the mass of airborne particles collected by a set of BSNE sampler is divided by the area of the sampler's inlet and the time of collection. This quantity is referred to as $Q(z)$, where z is the height above the ground. Values of $Q(z)$ are then fit to the equation:

$$Q(z) = c\,\mathrm{Exp}(az + bz^2), \tag{19}$$

where a, b, and c are fitting coefficients. Total horizontal flux is calculated by integration:

$$q = \int_0^{\infty} Q(z)\, dz. \tag{20}$$

6.7.2 Finding Values of k

Since the proportionality between F_A and q is soil-specific, k must be calibrated for a specific field condition if it, together with q, is to yield reasonable estimates of F_A. In order to do this, F_A must be calculated using another method. This method is a great deal more time consuming and expensive than the method summarized by Equation (18). As a result, it will be used simply to find reliable values of k, which will then be used to calculate the other values of F_A.

Conservation of mass implies that divergence of the horizontal flux gives the vertical flux at any point:

$$F_A(D) = \frac{\partial}{\partial x} q(D), \tag{21}$$

where $q(D)$ is the horizontal mass flux of particles of diameter D and x is the distance upwind. F_A is a function of particle diameter due to faster settling velocities of larger, and heavier, particles. However, by integrating:

$$F_A = \int_0^{D_{\max}} F_A(D)\, dD, \tag{22}$$

where D_{max} is the maximum particle size of interest, the horizontal mass flux for particles with diameters less than D_{max} may be determined. Since particles less than approximately 100 μm can be removed for long range transport (Leys and McTainsh, 1994), D_{max} may be set to 100 μm.

This method of calculating F_A requires detailed particle size analyses and assumes that the bulk of the fine dust mass ($< D_{max}$) is contained in a layer from the ground to the top of the BSNE collectors. It also requires two sets of BSNE samplers separated by a short distance (~10 m) with the line between them parallel to the wind. At sites where this method is used to calculate F_A, therefore, an additional set of BSNE collectors will be required and the collectors will have to be placed at heights greater than 1 m (the maximum height of BSNE collectors for determination of q).

6.8 Modeling Regional Effect of Wind on Landscapes

Wind erosion has effects on the Earth's biosphere from local to global scales. While it is vitally important to understand the fundamental processes that shape arid and semiarid environments, it is also necessary to generalize results so that the role of wind erosion may be understood on basin, watershed, state, regional or global scales. As the final phase of the proposed research, we will attempt to regionalize our understanding of wind erosion by producing maps of estimates of nutrient losses by wind and susceptibility to climate and anthropogenic landscape change.

Several papers in the past have developed wide-area wind erosion and dust emission maps (see for example, Gillette and Hanson, 1989; Gillette and Passi, 1988; Marticorena and Bergametti, 1995; Marticorena *et al.*, 1997a; Shao and Leslie, 1997). In particular, Gillette and Passi (1988) and Gillette and Kirby (1989) use a parameterized model of dust emission. This model may be slightly altered to yield estimates of nutrient losses by wind by multiplying the modeled dust emission by the estimated nutrient

contents relative to the nutrient concentration in the surface soil. However, the dust flux results from the proposed study may suggest re-parameterization of the Gillette and Passi (1988) model for semi-natural landscapes.

Much of the information on vegetation and soil parameters required to extend models of desertification could come from remotely sensed data. Unfortunately, remote sensing in arid and semiarid areas is particularly difficult and the data or techniques do not yet exist to make reliable estimates of cover, species type or vegetation structure, and soil grain-size characteristics (Chapter 5 and 8). Perhaps in five or ten years, these data and tools will exist, but until that time the results from the proposed study will provide baseline information for ecosystem monitoring over large scales.

7. CONCLUSION

While it is clear that wind is an important feature of arid and semiarid environments, few studies have evaluated the role of wind in the removal or redistribution of soil resources in natural landscapes. The types of measurements suggested here would address, for the first time ever in a large-scale experiment at multiple sites, the magnitude and effect of wind erosion in the nutrient budgets of desert landscapes. Understanding the role of wind in transporting soil nutrients requires evaluating its influence in several different semiarid climate regimes. Without this element, landscape-scale measurements cannot be extrapolated through time to shed light on how climate change will affect these landscapes, nor can they inform our understanding of how anthropogenic disturbance affects landscapes under different

climatic conditions.

The experiments suggested here address two fundamental questions on the role of wind in natural landscapes: (1) does total cover or climate control the magnitude of nutrient removal by wind in natural environments? and (2) how do aeolian nutrient losses compare with the surface soil reservoir and other observed nutrient losses? Vegetation removal treatments at different sites along a bioclimatic transect represent a powerful experimental examination of both of these questions. For example, if total cover, regardless of location along a bioclimatic transect, is the predominant factor in determining wind erosion, that has much different consequences for land management than if long-term climate is the predominant factor in determining wind erosion. Further, if nutrient turnover times with respect to wind erosion are very short or observed nutrient loss rates to wind are high compared to other observed losses, a major geomorphic process responsible for degradation of arid and semiarid environments will have been identified.

CITED REFERENCES

Adams, J.B., M.O. Smith, and A.R. Gillespie, 1993, *in* Pieters, and Englert, eds., Remote Geochemical Analysis: Elemental and Mineralogical Composition: Cambridge, Cambridge University Press, p. Ch. 7.

Adams, R.M., C. Rozenzweig, R.M. Peart, J.T. Rictchie, B.A. McCarl, J.D. Glyer, R.B. Curry, J.W. Jones, K.J. Boote, and L.H. Allen, Jr., 1990, Global climate change and U.S. agriculture: Nature, v. 345, p. 219.

Andreae, M.O., 1996, Raising dust in the greenhouse: Nature, v. 380, p. 389-390.

Avnimelech, Y., and J.R. McHenry, 1984, Enrichment of transported sediments with organic carbon, nutrients, and clay: Soil Science Society of America Journal, v. 48, p. 259-266.

Asner, G., 1998, Biophysical and biochemical sources of variability in canopy reflectance: Remote Sensing of Environment, v. 64, p. 234-253.

Asner, G., C. Wessman, D. Schimel, and S. Archer, 1998, Variability in leaf and litter optical properties: Implications for BRDF model inversions using AVHRR, MODIS, and MISR: Remote Sensing of Environment, v. 63, p. 243-257.

Ayoub, A., 1998, Extent, severity and causative factors of land degradation in the Sudan: Journal of Arid Environments, v. 38, p. 397-409.

Babu, S.C., and R. Hassan, 1995, International migration and environmental degradation-The case of Mozambican refugees and forest resources in Malawi: Journal of Environmental Management, v. 43, p. 233-247.

Bach, A.J., A.J. Brazel, and N. Lancaster, 1996, Temporal and spatial aspects of blowing dust in the Mojave and Colorado Deserts of southern California, 1973-1994: Physical Geography, v. 17, p. 329-353.

Bach, A.J., 1998, Assessing conditions leading to severe wind erosion in the Antelope Valley, California, 1990-1991: Professional Geographer, v. 50, p. 87-97.

Bagnold, R.A., 1941, The Physics of Blown Sand and Desert Dunes: New York, Methuen, 265 p.

Balling, R.C., J.M. Klopatek, M.L. Hildebrandt, C.K. Moritz, and C.J. Watts, 1998, Impacts of land degradation on historical temperature records from the Sonoran Desert: Climatic Change, v. 40, p. 669-681.

Balling, R.C., Jr., 1991, Impact of desertification on regional and global warming: Bulletin American Meteorological Society, v. 72, p. 232-234.

Barbier, E.B., 1997, The economic determinants of land degradation in developing countries: Philosophical Transactions of the Royal Society of London Series B-Biological Sciences, v. 352, p. 891-899.

Barth, H., 1999, Desertification in the Eastern Province of Saudi Arabia: Journal of Arid Environments, v. 43, p. 399-410.

Belnap, J., 1995, Surface disturbances: their role in accelerating desertification: Environmental Monitoring and Assessment, v. 37, p. 39-57.

Belnap, J., K.T. Harper, and S.D. Warren, 1993, Surface disturbance of cryptobiotic soil crusts: Nitrogenase activity, chlorophyll content, and chlorophyll degradation: Arid Soil Research and Rehabilitation, v. 8, p. 1-8.

Billings, W.D., and R.J. Morris, 1951, Reflection of visible and infrared radiation for leaves of different ecological groups: American Journal of Botany, v. 39, p. 327-331.

Biswas, R., 1998, Determinants of Foreign Direct Investment [Ph.D. thesis]: College Park, Maryland, University of Maryland.

Bongaarts, J., 1996, Population pressure and the food supply system in the developing world: Population and Development Review, v. 22, p. 483.

Bowden, L.W., L.R. Huning, C.F. Hutchinson, and C.W. Johnson, 1974, Satellite photograph presents first comprehensive view of local wind: the Santa Ana: Science, v. 184, p. 1077-1078.

Bowers, M.A., 1987, Precipitation and the relative abundances of desert winter annuals: A 6-year study in the northern Mohave Desert: Journal of Arid Environments, v. 12, p. 141-149.

Brady, N.C., and R.R. Weil, 1999, The Nature and Properties of Soils: Upper Saddle Ridge, New Jersey, Prentice-Hall.

Brazel, A.J., and W.G. Nickling, 1987, Dust storms and their relation to moisture in the Sonoran-Mojave Desert region of the south-western United States: Journal of Environmental Management, v. 24, p. 279-291.

Broad, K., and S. Agrawala, 2000, The Ethiopia food crisis-uses and limits of climate forecasts: Science, v. 289, p. 1693-1694.

Brown, J.H., T.J. Valone, and C.G. Curtin, 1997, Reorganization of an arid ecosystem in response to recent climate change: Proceedings of the National Academy of Science, v. 94, p. 9729-9733.

Buffington, L.C., and C.H. Herbel, 1965, Vegetational changes on a semidesert grassland range from 1858 to 1963: Ecological Monographs, v. 35, p. 139-164.

Bulloch, H.E., Jr., and R.E. Neher, 1977, Soil Survey of Dona Ana County Area, New Mexico: Washington, D. C., Soil Conservation Service, United States Department of Agriculture.

Buwalda, J.P., 1914, Pleistocene beds at Manix in the eastern Mohave Desert region: University of California Bulletin of the Department of Geology, v. 7, p. 443-464.

Campbell, C.E., 1972, Some environmental effects of rural subdividing in an arid area: A case study in Arizona: The Journal of Geography, v. 71, p. 147-154.

Carpenter, D.E., M.G. Barbour, and C.J. Bahre, 1986, Old field succession in Mojave Desert scrub: Madroño, v. 33, p. 111-122.

Carter, D.J., P.J. Findlater, and G.H. McTainsh, 1999, An economic solution to water repellency and wind erosion on light textured soils, *in* Conacher, A., ed., Commission on Land Degradation and Desertification: Perth, Australia, International Geographic Union, p. 6.

Çevik, B., and A. Berkman, 1985, Wind erosion control and sand dune stabilization practices implemented in the Great Konya Basin of Turkey, *in* El-Baz, F., El-Tayeb, I.A., and Hassan, M.H.A., eds., International Workshop on Sand Transport and Desertification in Arid Lands: Khartoum, Sudan, World Scientific, p. 375-388.

Chilês, J.-P., and P. Delfiner, 1999, Geostatistics: New York, John Wiley and Sons, Inc., 695 p.

Chen, Z., C.D. Elvidge, and D.P. Groeneveld, 1998, Monitoring seasonal dynamics of arid land vegetation using AVIRIS data: Remote Sensing of Environment, v. 65, p. 255-266.

Clark, R.N., G.A. Swayze, A.J. Gallagher, T.V.V. King, and W.M. Calvin, 1993, The U.S. Geological Survey, Digital Spectral Library: Version 1: 0.2 to 3.0 microns, USGS, p. 1340.

Clements, T., J.F. Mann, R.O. Stone, and J.L. Eymann, 1963, A study of windborne sand and dust in desert areas: Natick, Massachusetts, United States Army Natick Laboratories, Earth Sciences Division.

Coale, K.H., K.S. Johnson, S.E. Fitzwater, R.M. Gordon, S. Tanner, F.P. Chavez, L. Ferioli, C. Sakamoto, P. Rogers, F. Millero, P. Steinberg, P. Nightingale, D. Cooper, W.P. Cochlan, M.R. Landry, J. Constantinou, G. Rollwagen, A. Trasvina, and R. Kudela, 1996, A massive phytoplankton bloom induced by an ecosystem-scale iron fertilization experiment in the equatorial Pacific Ocean: Nature, v. 383, p. 495-501.

Coppinger, K.D., W.A. Reiners, I.C. Burke, and R.K. Olson, 1991, Net erosion on a sagebrush steppe landscape as determined by Cs-137 distribution: Soil Science Society of America Journal, v. 55, p. 254-258.

Darkoh, M.B.K., 1987, Combating desertification in the arid and semi-arid lands of Tanzania: Journal of Arid Environments, v. 12, p. 87-99.

Dohrenwend, J.C., W.B. Bull, L.D. McFadden, G.I. Smith, R.S.U. Smithe, and S.G. Wells, 1991, Quaternary geology of the Basin and Range province in California, *in* Morrison, R.B., ed., Quaternary Nonglacial Geology: Coterminous U.S., Volume K-2: Boulder, Colorado, Geological Society of America, p. 321-352.

Drake, N.A., S. Mackin, and J.J. Settle, 1999, Mapping vegetation, soils, and geology in semiarid shrublands using spectral matching and mixture modeling of SWIR AVIRIS imagery: Remote Sensing of Environment, v. 68, p. 12-25.

Dregne, H.E., 1995, Desertification control: A framework for action: Environmental Monitoring and Assessment, v. 37, p. 111-122.

Dregne, H.E., and N.-T. Chou, 1992, Global desertification dimensions and costs, *in* Dregne, H.E., ed., Degradation and Restoration of Arid Lands: Lubbock, Texas, Texas Tech University Press, p. 249-282.

Duce, R.A., and N.W. Tindale, 1991, Atmospheric transport of iron and its deposition in the ocean: Limnology and Oceanography, v. 36, p. 1715-1726.

Duncan, J., D. Stow, J. Franklin, and A. Hope, 1993, Assessing the relationship between spectral vegetation indices and shrub cover in the Jornada Basin, New Mexico: International Journal of Remote Sensing, v. 14, p. 3395-3416.

Ehleringer, J., 1981, Leaf absorptances of Mohave and Sonoran Desert plants: Oecologia, v. 49, p. 366-370.

Ehleringer, J., and O. Björkman, 1976, Leaf pubescence: effects on absorptance and photosynthesis in a desert shrub: Science, v. 192, p. 376-377.

Ehleringer, J.R., and H.A. Mooney, 1978, Leaf hairs: effects on physiological activity and adaptive value to a desert shrub: Oecologia, v. 37, p. 183-200.

Ehleringer, J.R., and O. Björkman, 1978, Pubescence and leaf spectral characteristics in a desert shrub, *Encilia farinosa*: Oecologia, v. 36, p. 151-162.

El-Baz, F., I.A. El-Tayeb, and M.H.A. Hassan, 1985, Sand Transport and Desertification in Arid Lands, *in* El-Baz, F., El-Tayeb, I.A., and Hassan, M.H.A., eds., International Workshop on Sand Transport and Desertification in Arid Lands: Khartoum, Sudan, World Scientific, p. 472.

Elvidge, C.D., 1990, Visible and near-infrared reflectance characteristics of dry plant materials: International Journal of Remote Sensing, v. 11, p. 1775-1795.

Elvidge, C.D., Z. Chen, and D.P. Groeneveld, 1993, Detection of trace quantities of green vegetation in 1990 AVIRIS data: Remote Sensing of Environment, v. 44, p. 271-279.

Escafadel, R., and A.R. Huete, 1991, Improvement in remote sensing of low vegetation cover in arid regions by correcting vegetation indices for soil "noise": C. R. Academie des Sciences Paris, v. 312, p. 1385-1391.

Evans, J.R., 1962, Falling and climbing sand dunes in the Cronese ("Cat") Mountain Area, San Bernardino County, California: Journal of Geology, v. 70, p. 107-113.

Evans, R.D., and J. Belnap, 1999, Long-term consequences of disturbance on nitrogen dynamics in an arid ecosystem: Ecology, v. 80, p. 150-160.

Eve, M.D., 1995, High Temporal Resolution Analysis of Land Degradation in the Northern Chihuahuan Desert Using Satellite Imagery [Ph.D. thesis]: Las Cruces, New Mexico, New Mexico State University.

Fearnehough, W., M.A. Fullen, D.J. Mitchell, I.C. Trueman, and J. Zhang, 1998, Aeolian deposition and its effect on soil and vegetation changes on stabilised desert dunes in northern China: Geomorphology, v. 23, p. 171-182.

Forman, S.L., A.F.H. Goetz, and R.H. Yuhas, 1992, Large-scale stabilized dunes on the High Plains of Colorado: Understanding the landscape response to Holocene climates with the aid of images from space: Geology, v. 20, p. 145-148.

Franklin, J., and D.L. Turner, 1992, The application of a geometric optical canopy reflectance model to semiarid shrub vegetation: IEEE Transactions on Geoscience and Remote Sensing, v. 30, p. 293-301.

Franklin, J., J. Duncan, and D.L. Turner, 1993, Reflectance of vegetation and soil in Chihuahuan desert plant communities from ground radiometry using SPOT wavebands: Remote Sensing of Environment, v. 46, p. 291-304.

Fryrear, D.W., 1981, Long-term effect of erosion and cropping on soil productivity, *in* Péwé, T.L., ed., Desert Dust: Origin, Characteristics, and Effect on Man, Volume Special Paper 186: Boulder, Colorado, Geological Society of America, p. 253-259.

Fryrear, D.W., 1986, A field dust sampler: Journal of Soil and Water Conservation, v. 41, p. 117-120.

Gao, B.-C., and A.F.H. Goetz, 1990, Column atmospheric water vapor and vegetation liquid water retrievals from airborne imaging spectrometer data: Journal of Geophysical Research, v. 95, p. 3549-3564.

García-Haro, F.J., M.A. Gilabert, and J. Meliám, 1996, Linear spectral mixture modelling to estimate vegetation amount from optical spectral data: International Journal of Remote Sensing, v. 17, p. 3373-3400.

Garcia-Pichel, F., and J. Belnap, 1996, The microenvironments and microscale productivity of cyanobacterial desert crusts: Journal of Phycology, v. 32, p. 774-782.

Gardner, M., 1997, Mapping Chaparral with AVIRIS Using Advanced Remote Sensing Techniques [M.A. Thesis]: Santa Barbara, CA, University of California, CA.

Gates, D.M., H.J. Keegan, J.C. Schleter, and V.R. Weidner, 1965, Spectral properties of plants: Applied Optics, v. 4, p. 11-20.

Gibbens, R.P., J.M. Tromble, J.T. Hennessy, and M. Cardenas, 1983, Soil movement in mesquite dunelands and former grasslands of southern New Mexico from 1933 to 1980: Journal of Range Management, v. 36, p. 145-148.

Gillespie, A.R., M.O. Smith, J.B. Adams, S.C. Willis, A.F. Fischer, III, and D.E. Sabol, Jr., 1990, Interpretation of residual images: Spectral mixture analysis of AVIRIS images, Owens Valley, California, *in* Green, R.O., ed., Second AVIRIS Workshop: Jet Propulsion Laboratory, Pasadena, California, Jet Propulsion Laboratory, p. 243-270.

Gillette, D.A., 1977, Fine particulate emissions due to wind erosion: Transactions of the American Society of Agricultural Engineers, v. 29, p. 890-897.

Gillette, D.A., 1988, Threshold friction velocities for dust production for agricultural soils: Journal of Geophysical Research, v. 93, p. 12645-12662.

Gillette, D.A., 1999, Personal Communication.

Gillette, D.A., and H.C. Monger, 2000, Constructing a model of wind erosion and dust emission for the Jornada del Muerto Basin, *in* LTER II, Schlesinger, W.H., ed.

Gillette, D.A., and K.J. Hanson, 1989, Spatial and temporal variability of dust production caused by wind erosion in the United States: Journal of Geophysical Research, v. 94, p. 2197-2206.

Gillette, D.A., and P.H. Stockton, 1989, The effect of nonerodible particles on wind erosion of erodible surfaces: Journal of Geophysical Research, v. 94, p. 12885-12893.

Gillette, D.A., and R. Passi, 1988, Modeling of dust emission caused by wind erosion: Journal of Geophysical Research, v. 93, p. 14223-14242.

Gillette, D.A., and W. Chen, 2000, Particle production and aeolian transport from a "supply-limited" source area in the Chihuahuan Desert: Journal of Geographical Research, v. Submitted.

Gillette, D.A., D.W. Fryrear, T.E. Gill, T. Ley, T.A. Cahill, and E.A. Gearhart, 1997, Relation of vertical flux of particles smaller than 10 μm to aeolian horizontal mass flux at Owens Lake: Journal of Geophysical Research, v. 102, p. 26009-26015.

Gillette, D.A., J. Adams, A. Endo, D. Smith, and R. Kihl, 1980, Threshold velocities for input of soil particles into the air by desert soils: Journal of Geographical Research, v. 85, p. 5621-5630.

Gleditsch, N.P., 1998, Armed conflict and the environment: A critique of the literature: Journal of Peace Research, v. 35, p. 381-400.

Grantz, D.A., D.L. Vaughn, R. Farber, B. Kim, M. Zeldin, T. Van Curen, and R. Campbell, 1998, Seeding native plants to restore desert farmland and mitigate fugitive dust and PM_{10}: Journal of Environmental Quality, v. 27, p. 1209-1218.

Greeley, R., and J.D. Iversen, 1985, Wind as a Geological Process on Earth, Mars, Venus and Titan: Cambridge, Cambridge University Press, 333 p.

Green, R., B. Pavri, J. Faust, and O. Williams, 1999, AVIRIS radiometric laboratory calibration, inflight validation, and a focused sensitivity analysis in 1998, *in* Green, R.O., ed., The 1999 AVIRIS Workshop, Volume JPL 99-17: Pasadena, CA, Jet Propulsion Laboratory, p. 161-176.

Green, R.O., D.A. Roberts, and J.E. Conel, 1996, Characterization and compensation of the atmosphere for the inversion of AVIRIS calibrated radiance to apparent surface reflectance, *in* Green, R.O., ed., Sixth Annual JPL Airborne Earth Science Workshop, Volume 1: Pasadena, CA, Jet Propulsion Laboratory, p. 135-146.

Green, R.O., J.E. Conel, and D.A. Roberts, 1993, Estimation of aerosol optical depth and additional atmospheric parameters for the calculation of apparent surface reflectance from radiance measured by the Airborne Visible/Infrared Imaging Spectrometer, *in* Green, R.O., ed., Fourth Annual JPL Airborne Geoscience Workshop, Volume 1: Pasadena, CA, Jet Propulsion Laboratory, p. 73-76.

Grepperud, S., 1996, Population pressure and land degradation: The case of Ethiopia: Journal of Environmental Economics and Management, v. 30, p. 18-33.

Hall, F.G., J.R. Townshend, and E.T. Engman, 1995, Status of remote-sensing algorithms for estimation of land-surface state parameters: Remote Sensing of Environment, v. 51, p. 138-156.

Hansen, J., I. Fung, A. Lacis, D. Rind, R. Ruedy, and G. Russell, 1988, Global climate changes as forecast by Goddard Institute for Space Studies three-dimensional model: Journal of Geophysical Research, v. 93, p. 9341-9364.

Hapke, B., 1981, Bidirectional reflectance spectroscopy. 1. theory: Journal of Geophysical Research, v. 86, p. 3039-3054.

Hauge, W., and T. Ellingsen, 1998, Beyond environmental scarcity: Causal pathways to conflict: Journal of Peace Research, v. 35, p. 299-317.

Havstad, K., 1999, Personal Communication.

Helm, P., and C.S. Breed, 1999, Instrumented field studies of sediment transport by wind, *in* Breed, C.S., and Reheis, M., eds., Desert Winds: Monitoring wind-related surface processes in Arizona, New Mexico, and California, Volume USGS Professional Paper 1598: Washington, DC, United States Government Printing Office, p. 30-51.

Hennessy, J.T., B. Kies, R.P. Gibbens, and J.M. Tromble, 1986, Soil sorting by forty-five years of wind erosion on a southern New Mexico Range: Soil Science Society of America Journal, v. 50, p. 391-394.

Homer-Dixon, T.F., 1999, Environment, Scarcity, and Conflict: Princeton, New Jersey, Princeton University Press, 253 p.

Hudak, A.T., and C.A. Wessman, 1998, Textural analysis of historical aerial photography to characterize woody plant encroachment in South African savanna: Remote Sensing of Environment, v. 66, p. 317-330.

Huete, A.R., 1988, A soil-adjusted vegetation index (SAVI): Remote Sensing of Environment, v. 25, p. 295-309.

Huete, A.R., and R.D. Jackson, 1987, Suitability of spectral indices for evaluating vegetation characteristics on arid rangelands: Remote Sensing of Environment, v. 23, p. 213-232.

Huete, A.R., and R.D. Jackson, 1988, Soil and atmosphere influences on the spectra of partial canopies: Remote Sensing of Environment, v. 25, p. 89-105.

Huete, A.R., D.F. Post, and R.D. Jackson, 1984, Soil spectral effects on 4-space vegetation discrimination: Remote Sensing of Environment, v. 15, p. 155-165.

Huete, A.R., R.D. Jackson, and D.F. Post, 1985, Spectral response of a plant canopy with different soil backgrounds: Remote Sensing of Environment, v. 17, p. 37-53.

Hunt, G.R., J.W. Salisbury, and C.J. Lenhoff, 1971, Visible and near-infrared spectra of minerals and rocks: III. oxides and hydroxides: Modern Geology, v. 2, p. 195-205.

Hurcom, S.J., and A.R. Harrison, 1998, The NDVI and spectral decomposition for semi-arid vegetation abundance estimation: International Journal of Remote Sensing, v. 19, p. 3109-3125.

Hyers, A.D., and M.G. Marcus, 1981, Land use and desert dust hazards in central Arizona, *in* Péwé, T.L., ed., Desert Dust: Origin, Characteristics, and Effect on Man, Volume Special Paper 186: Boulder, Colorado, Geological Society of America.

Kasusya, P., 1998, Combating desertification in northern Kenya (Samburu) through community action: a community case experience: Journal of Arid Environments, v. 39, p. 325-329.

Kerr, R.A., 1999, Big El Niños ride the back of slower climate change: Science, v. 283, p. 1108-1109.

Khalaf, F.I., 1989, Desertification and aeolian processes in the Kuwait Desert: Journal of Arid Environments, v. 16, p. 125-145.

Khalaf, F.I., and D. Al-Ajmi, 1993, Aeolian processes and sand encroachment problems in Kuwait: Geomorphology, v. 9, p. 111-134.

Khresat, S.A., Z. Rawajfih, and M. Mohammad, 1998, Land degradation in north-western Jordan: causes and processes: Journal of Arid Environments, v. 39, p. 623-629.

Kishk, M.A., 1985, Desert encroachment on the fringes of the Nile Valley, Egypt, *in* El-Baz, F., El-Tayeb, I.A., and Hassan, M.H.A., eds., International Workshop on Sand Transport and Desertification in Arid Lands: Khartoum, Sudan, World Scientific, p. 196-208.

Klausmeier, C.A., 1999, Regular and irregular patterns in semiarid vegetation: Science, v. 284, p. 1826-1828.

Koch, M., and F. El Baz, 1998, Identifying the effects of the Gulf War on the geomorphic features of Kuwait by remote sensing and GIS: Photogrammetric Engineering and Remote Sensing, v. 64, p. 739-747.

Lado, C., 1999, Environmental resources, population and sustainability: Evidence from Zimbabwe: Singapore Journal of Tropical Geography, v. 20, p. 148-168.

Lancaster, N., 1988, Development of linear dunes in the southwestern Kalahari, South Africa: Journal of Arid Environments, v. 14, p. 233-244.

Lancaster, N., and A. Baas, 1998, Influence of vegetation cover on sand transportation by wind: Field studies at Owens Lake, California: Earth Surface Processes and Landforms, v. 23, p. 69-82.

Lancaster, N., and P. Helm, 2000, A test of a climatic index of dune mobility using measurements from the southwestern United States: Earth Surface Processes and Landforms, v. 25, p. 197-207.

Lanz, T.J., 1996, Environmental degradation and social conflict in the Northern Highlands of Ethiopia: the case of Tigray and Wollo provinces: Africa Today, v. 43, p. 157-182.

Larney, F., M. Bullock, H. Janzen, B. Ellert, and E. Olson, 1998, Wind erosion effects on nutrient redistribution and soil productivity: Journal of Soil and Water Conservation, v. 53, p. 133-140.

Leathers, C.R., 1981, Plant components of desert dust in Arizona and their significance for man, *in* Péwé, T.L., ed., Desert Dust: Origin, Characteristics, and Effect on Man, Volume Special Paper 186: Boulder, Colorado, Geological Society of America, p. 191-206.

Leys, J., and G. McTainsh, 1994, Soil loss and nutrient decline by wind erosion- cause for concern: Australian Journal of Soil and Water Conservation, v. 7, p. 30-35.

Leys, J.F., and G.H. McTainsh, 1996, Sediment fluxes and particle grain-size characteristics of wind-eroded sediments in southeastern Australia: Earth Surface Processes and Landforms, v. 21, p. 661-671.

Li, Z.T., and M. Kafatos, 2000, Interannual variability of vegetation in the United States and its relation to El Niño/Southern Oscillation: Remote Sensing of Environment, v. 71, p. 239-247.

López, M.V., 1998, Wind erosion in agricultural soils: An example of limited supply of particles available for erosion: Catena, v. 33, p. 17-28.

Lovich, J., and D. Bainbridge, 1999, Anthropogenic degradation of the southern California desert ecosystem and prospects for natural recovery and restoration: Environmental Management, v. 24, p. 309-326.

Lucero, O.A., 1998, Effects of the southern oscillation on the probability for climatic categories of monthly rainfall, in a semi-arid region in the southern mid-latitudes: Atmospheric Research, v. 49, p. 337-348.

Luk, S.-H., 1983, Recent trends in desertification in the Maowusu Desert, China: Environmental Conservation, v. 10, p. 213-224.

Lyles, L., and J. Tatarko, 1986, Wind erosion effects on soil texture and organic matter: Journal of Soil and Water Conservation, v. 46, p. 191-193.

Mabbutt, J.A., and C. Floret, 1980, Case Studies on Desertification: United Kingdom, United Nations, Scientific and Cultural Organization.

Madole, R.F., 1994, Stratigraphic evidence of desertification in the west-central Great Plains within the past 1000 yr: Geology, v. 22, p. 483-486.

Marshall, J.K., 1971, Drag measurements in roughness arrays of varying density and distribution: Agricultural Meteorology, v. 8, p. 269-292.

Marticorena, B., and G. Bergametti, 1995, Modeling the atmospheric dust cycle: 1. Design of a soil-derived dust emission scheme: Journal of Geophysical Research, v. 100, p. 16415-16430.

Marticorena, B., G. Bergametti, B. Aumont, Y. Callot, C. N'Doumé, and M. Legrand, 1997, Modeling the atmospheric dust cycle: 2. Simulation of Saharan sources: Journal of geophysical Research, v. 102, p. 4387-4404.

Marticorena, B., G. Bergametti, D.A. Gillette, and J. Belnap, 1997b, Factors controlling threshold friction velocity in semiarid and arid areas of the United States: Journal of Geophysical Research, v. 102, p. 23277-23287.

Martin, J.H., 1990, Glacial-interglacial CO_2 change: The iron hypothesis: Paleoceanography, v. 5, p. 1-13.

McFadden, L.D., S.G. Wells, and M.J. Jercinovich, 1987, Influence of eolian and pedogenic processes on he origin and evolution of desert pavements: Geology, v. 15, p. 504-508.

Meek, N., 1989, Geomorphic and hydrologic implications of the rapid incision of Afton Canyon, Mojave Desert, California: Geology, v. 17, p. 7-10.

Meek, N., 1990, Late Quaternary Geochronology and Geomorphology of the Manix Basin, San Bernardino County, California [Ph.D. thesis]: Los Angeles, California, University of California at Los Angeles.

Minvielle, F.B., B. Marticorena, D.A. Gillette, R. Lawson, and R. Thompson, 1999, Study of roughness length for low roughness densities and several porosities: Research Triangle Park, NC, Fluid Modeling Facility, United States Environmental Protection Agency.

Mitchell, D.J., M.A. Fullen, I.C. Trueman, and W. Fearnehough, 1998, Sustainability of reclaimed desertified land in Ningxia, China: Journal of Arid Environments, v. 39, p. 239-251.

Mooney, H.A., J. Ehleringer, and O. Björkman, 1977, The energy balance of leaves of the evergreen desert shrub *Atriplex hymenelytra*: Oecologia, v. 29, p. 301-310.

Morrison, R.B., 1991, Quaternary Nonglacial Geology: Coterminous U.S., Volume K-2: Boulder, Colorado, Geological Society of America.

Morrison, R.B., 1991a, Quaternary geology of the southern Basin and Range Province, *in* Morrison, R.B., ed., Quaternary Nonglacial Geology: Coterminous U.S., Volume K-2: Boulder, Colorado, Geological Society of America, p. 353-371.

Morrison, R.B., 1991b, Quaternary stratigraphic, hydrologic, and climatic history of the Great Basin, with emphasis on Lakes Lahonton, Bonneville, and Tecopa, *in* Morrison, R.B., ed., Quaternary Nonglacial Geology: Coterminous U.S., Volume K-2: Boulder, Colorado, Geological Society of America, p. 283-320.

Muhs, D.R., and P.B. Maat, 1993, The potential response of eolian sands to greenhouse warming and precipitation reduction on the Great Plains of the USA: Journal of Arid Environments, v. 25, p. 351-361.

Musick, H.B., 1999, Field monitoring of vegetation characteristics related to surface changes in the Yuma Desert, Arizona, and at the Jornada Experimental Range in the Chihuahun Desert, New Mexico, *in* Breed, C.S., and Reheis, M., eds., Desert Winds: Monitoring wind-related surface processes in Arizona, New Mexico, and California, Volume USGS Professional Paper 1598: Washignton, DC, United States Government Printing Office, p. 71-84.

Musick, H.B., and D.A. Gillette, 1990, Field evaluation of relationships between a vegetation structural parameter and sheltering against wind erosion: Land Degradation and Rehabilitation, v. 2, p. 87-94.

Musick, H.B., S.M. Trujillo, and C.R. Truman, 1996, Wind-tunnel modelling of the influence of vegetation structure on saltation threshold: Earth Surface Processes and Landforms, v. 21, p. 589-605.

Nakata, J.K., H.G. Wilshire, and G.C. Barnes, 1976, Origin of Mojave Desert dust plumes photographed from space: Geology, v. 4, p. 644-648.

Nasrallah, H.A., and R.C. Balling, 1995, Impact of desertification on temperature trends in the Middle East: Environmental monitoring and assessment, v. 37, p. 265-271.

National Climate Data Center, 1993, Solar and Meteorological Surface Observation Network: 1961-1990, Volume III: Western United States, National Climate Data Center.

National Climate Data Center, 1997, U.S. Precipitation by State, California, Volume 1999, National Climate Data Center.

Okin, G.S., W.J. Okin, D.A. Roberts, and B.C. Murray, 1998, Multiple endmember spectral mixture analysis: application to an arid/semi-arid landscape, *in* Green, R.O., ed., 7th JPL Airborne Earth Science Workshop: AVIRIS, Volume 1: Jet Propulsion Laboratory, Pasadena, CA, Jet Propulsion Laboratory, Pasadena, CA, p. 291-300.

Okin, W.J., G.S. Okin, D.A. Roberts, and B. Murray, 1999, Multiple Endmember Spectral Mixture Analysis: Endmember choice in an arid shrubland, *in* Green, R.O., ed., The 1999 AVIRIS Workshop: Pasadena, California, Jet Propulsion Laboratory.

Owen, P.R., 1964, Saltation of uniform grains in air: Journal of Fluid Mechanics, v. 20, p. 225-242.

Painter, T.H., D.A. Roberts, R.O. Green, and J. Dozier, 1998, The effect of grain size on spectral mixture analysis of snow-covered area from AVIRIS data: Remote Sensing of Environment, v. 65, p. 320-332.

Paulsen, H.A., Jr., and F.N. Ares, 1962, Grazing values and management of black gramma and tobosa grasslands and associated shrub ranges of the Southwest, U.S. Forest Service.

Phinn, S., J. Frankling, A. Hope, D. Stow, and L. Huenneke, 1996, Biomass distribution mapping using airborne digital video imagery and spatial statistics in a semi-arid environment: Journal of Environmental Management, v. 47, p. 139-164.

Pinstrup-Andersen, P., and R. Pandya-Lorch, 1998, Food security and sustainable use of natural resources: A 2020 Vision: Ecological Economics, v. 26, p. 1-10.

Post, W.M., J. Pastor, P.J. Zinke, and A.G. Stangenberger, 1985, Global patterns of soil nitrogen storage: Nature, v. 317, p. 613-616.

Raupach, M.R., D.A. Gillette, and J.F. Leys, 1993, The effect of roughness elements on wind erosion threshold: Journal of Geophysical Research, v. 98, p. 3023-3029.

Ray, T.W., 1995, Remote Monitoring of Land Degradation in Arid/Semiarid Regions [Ph.D. thesis]: Pasadena, CA, California Institute of Technology.

Ray, T.W., and B.C. Murray, 1996, Nonlinear spectral mixing in desert vegetation: Remote Sensing of Environment, v. 55, p. 59-64.

Rind, D., 1990, Potential evapotranspiration and the likelihood of future drought: Journal of Geophysical Research, v. 95, p. 9983-10004.

Roberts, D.A., J.B. Adams, and M.O. Smith, 1990, Predicted distribution of visible and near-infrared radiant-flux above and below a transmittant leaf: Remote Sensing of Environment, v. 34, p. 1-17.

Roberts, D.A., M. Gardner, R. Church, S. Ustin, G. Scheer, and R.O. Green, 1998, Mapping chaparral in the Santa Monica Mountains using multiple endmember spectral mixture models: Remote Sensing of Environment, v. 65, p. 267-279.

Roberts, D.A., M. Gardner, R. Church, S.L. Ustin, and R.O. Green, 1997, Optimum strategies for mapping vegetation using multiple endmember spectral mixture models, SPIE Conference Imaging Spectrometry III, Volume 3118: San Diego, CA, p. 108-119.

Roberts, D.A., M.O. Smith, and J.B. Adams, 1993, Green vegetation, nonphotosynthetic vegetation, and soils in AVIRIS data: Remote Sensing of Environment, v. 44, p. 255-269.

Roberts, D.A., R.O. Green, and J.B. Adams, 1997b, Temporal and spatial patterns in vegetation and atmospheric properties from AVIRIS: Remote Sensing of Environment, v. 62, p. 223-240.

Rosenzweig, C., and D. Hillel, 1993, The Dust Bowl of the 1930s: Analog of greenhouse effect in the Great Plains: Journal of Environmental Quality, v. 22, p. 9-22.

Sabol, D.E., Jr. , J.B. Adams, and M.O. Smith, 1992, Quantitative subpixel spectral detection of targets in multispectral images: Journal of Geophysical Research, v. 97, p. 2659-2672.

Sahai, A.K., 1998, Climate change: A case study over India: Theoretical and Applied Climatology, v. 61, p. 9-18.

Schlesinger, W.H., A.D. Abrahams, A.J. Parsons, and J. Wainwright, 1999, Nutrient losses in runoff from grassland and shrubland habitats in Southern New Mexico: I. rainfall simulation experiments: Biogeochemistry, v. 45, p. 21-34.

Schlesinger, W.H., and A.M. Pilmanis, 1998, Plant-soil interactions in deserts: Biogeochemistry, v. 42, p. 169-187.

Schlesinger, W.H., J.A. Raikes, A.E. Hartley, and A.F. Cross, 1996, On the spatial pattern of soil nutrients in desert ecosystems: Ecology, v. 77, p. 364-374.

Schlesinger, W.H., J.F. Reynolds, G.L. Cunningham, L.F. Huenneke, W.M. Jarrell, R.A. Virginia, and W.G. Whitford, 1990, Biological feedbacks in global desertification: Science, v. 247, p. 1043-1048.

Schlesinger, W.H., T.J. Ward, and J. Anderson, 2000, Nutrient losses in runoff from grassland and shrubland habitats in southern New Mexico: II. Field plots: Biogeochemistry, v. 49, p. 69-86.

Schultz, B.W., and W.K. Ostler, 1993, Effects of prolonged drought on vegetation association in the Northern Mojave Desert, *in* Roundy, B.A., McAurthur, E.D., Haley, J.S., and Mann, D.K., eds., Wildland shrubs and arid land restoration symposium, Volume General Technical Report INT-GTR-315: Las Vegas, Nevada, U.S. Department of Agriculture, Forest Service, Intermountain Research Station, p. 228-235.

Settle, J.J., and N.A. Drake, 1993, Linear mixing and the estimation of ground cover proportions: International Journal of Remote Sensing, v. 14, p. 1159-1177.

Shachak, M., and G.M. Lovett, 1998, Atmospheric deposition to a desert ecosystem and its implications for management: Ecological Applications, v. 8, p. 455-463.

Shao, Y., and L.M. Leslie, 1997, Wind erosion prediction over the Australian continent: Journal of Geophysical Research, v. 102, p. 30091-30105.

Shao, Y., and M.R. Raupach, 1993, Effect of saltation bomardment on the entrainment of dust by wind: Journal of Geophysical Research, v. 98, p. 12719-12726.

Shao, Y., G.H. McTainsh, J.F. Leys, and M.R. Raupach, 1993, Efficiencies of sediment samplers for wind erosion measurement: Australian Journal of Soil Research, v. 31, p. 519-532.

Sharifi, M., A. Gibson, and P. Rundel, 1999, Phenological and physiological responses of heavily dusted creosote bush (*Larrea tridentata*) to summer irrigation in the Mojave Desert: Flora, v. 194, p. 369-378.

Sharp, R.P., 1966, Kelso Dunes, Mojave Desert, California: Geological Society of America Bulletin, v. 77, p. 1045-1074.

Shimabukuro, Y.E., and J.A. Smith, 1991, The least-squares mixing models to generate fraction images derived from remote sensing multispectral data: IEEE Transactions on Geoscience and Remote Sensing, v. N1, p. 16-20.

Smith, G.I., and F.A. Street-Perrott, 1983, Pluvial Lakes of the Western United States, *in* Wright, H.E., Jr., ed., Late Quaternary Environments of the United States, Volume 1: The Late Pleistocene: Minneapolis, Minnesota, University of Minnesota Press, p. 190-212.

Smith, M.O., S.L. Ustin, J.B. Adams, and A.R. Gillespie, 1990, Vegetation in deserts: I. a regional measure of abundance from multispectral images: Remote Sensing of Environment, v. 31, p. 1-26.

Sokal, R.R., and F.J. Rohlf, 1981, Biometry: Principles and Practice of Statistics in Biological Research: New York, W.H. Freeman and Company, 859 p.

Spitzer, H.A., 1993, Antelope Valley emergency soil erosion control: Land and Water, v. 1993, p. 20-24.

Stockton, P.H., and D.A. Gillette, 1990, Field Measurement of the sheltering effect of vegetation on erodible land surfaces: Land Degradation and Rehabilitation, v. 2, p. 77-85.

Stokes, S., and J.B. Swinehart, 1997, Middle- and late-Holocene dune reactivation in the Nebraska Sand Hills, USA: Holocene, v. 7, p. 263-272.

Stylinski, C., and E. Allen, 1999, Lack of native species recovery following severe exotic disturbance in southern Californian shrublands: Journal of Applied Ecology, v. 36, p. 544-554.

Talbot, R.W., R.C. Harriss, E.V. Browell, G.L. Gregory, D.I. Sebacher, and S.M. Beck, 1986, Distribution and geochemistry of aerosols in the tropical North Atlantic troposphere: Relationship to Saharan dust: Journal of Geophysical Research, v. 91, p. 5173-5182.

Talbot, W.J., 1947, Swartland and Sandveld. A survey of the land utilization and soil erosion in the Western Lowland of the Cape Province: Cape Town, South Africa, Oxford University Press, 79 p.

Tegen, I., and I. Fung, 1995, Contribution to the atmospheric mineral aerosol load from land surface modification: Journal of Geophysical Research, v. 100, p. 18707-18726.

Thomas, D., 1997, Science and the desertification debate: Journal of Arid Environments, v. 37, p. 599-608.

Thornwaite, C.W., and J.R. Mather, 1957, Instructions and tables for computing potential evapotranspiration and the water balance, Publications in Climatology, Volume 10: Centerton, New Jersey, Laboratory of Climatology Drexel Institute of Technology, p. 311.

Trudgill, S.T., 1988, Soil and Vegetation Systems: Oxford, Clarendon Press, 211 p.

Tugel, A.J., and G.A. Woodruff, 1978, Soil Survey of San Bernardino County, California: Mojave River Area: Washington, D. C., Soil Conservation Service, United States Department of Agriculture.

United Nations Environmental Programme, 1992, World Atlas of Desertification: London, Edward Arnold, 69 p.

Vane, G., 1993, Terrestrial imaging spectroscopy: current status, future trends: Remote Sensing of Environment, v. 44, p. 117-126.

Vane, G., and A.F.H. Goetz, 1988, Terrestrial imaging spectroscopy: Remote Sensing of Environment, v. 24, p. 1-29.

Vasek, F.C., H.B. Johnson, and D.H. Eslinger, 1975, Effects of pipeline construction on Creosote bush scrub vegetation of the Mojave Desert: Modroño, v. 23, p. 1-64.

Verstraete, M.M., and S.A. Schwartz, 1991, Desertification and global change: Vegetatio, v. 91, p. 3-13.

Wainwright, J., A.J. Parsons, and A.D. Abrahams, 1999, Rainfall energy under creosotebush: Journal of Arid Environments, v. 43, p. 111-120.

Walker, A.S., 1982, Deserts of China: American Scientist, v. 70, p. 366-376.

Warren, P.L., and C.F. Hutchinson, 1984, Indicators of rangeland change and their potential for remote sensing: Journal of Arid Environments, v. 7, p. 107-126.

Washington, W.M., and G.A. Meehl, 1984, Seasonal cycle experiment on the climatic sensitivity due to doubling of CO_2 with an atmospheric general circulation model coupled to a mixed-layer ocean model: Journal of Geophysical Research, v. 89, p. 9475-9503.

Wells, S.G., L.D. McFadden, J. Poths, and C.T. Olinger, 1995, Cosmogenic ^{3}He surface-exposure dating of stone pavements: implications for landscape evolution in deserts: Geology, v. 23, p. 613-616.

Westing, A.H., 1994, Population, desertification, and migration: Environmental Conservation, v. 21, p. 109-114.

Whitford, W.G., 1992, Biogeochemical consequences of desertification: American Chemical Society Symposium Series, v. 483, p. 352-259.

Whitford, W.G., G. Martinez-Turanzas, and E. Martinez-Meza, 1995, Persistence of desertified ecosystems: Explanations and implications: Environmental Monitoring and Assessment, v. 37, p. 319-322.

Williams, J.D., J.P. Dobrowolski, N.E. West, and D.A. Gillette, 1995, Microphytic crust influence on wind erosion: Transactions of the American Society of Agricultural Engineers, v. 38, p. 131-137.

Wilshire, H.G., 1980, Human Causes of Accelerated Wind Erosion in California's Deserts, *in* Coates, D.R., and Vitek, J.D., eds., Thresholds in Geomorphology: London, George, Allen and Unwin, p. 415-433.

Wolfe, S.A., and W.G. Nickling, 1993, The protective role of sparse vegetation in wind erosion: Progress in Physical Geography, v. 17, p. 50-68.

Woodhouse, C.A., and J.T. Overpeck, 1998, 2000 years of drought variability in the central United States: Bulletin of the American Meteorological Society, v. 79, p. 2693-2714.

Zha, Y., and J. Gao, 1997, Characteristics of desertification and its rehabilitation in China: Journal of Arid Environments, v. 37, p. 419-432.

Zhang, K.H., and Markusen, 1997, Vertical multinationals and host-country characteristics: Cambridge, Massachusetts, National Bureau of Economic Research, p. 22.

Zhao, S., 1985, Drifting sand hazard and its control in northwest arid China, *in* El-Baz, F., El-Tayeb, I.A., and Hassan, M.H.A., eds., International Workshop on Sand Transport and Desertification in Arid Lands: Khartoum, Sudan, World Scientific, p. 253-266.